ABSTRACT

Title of Document: TOPOLOGY CONTROL AND POINTING IN FREE SPACE OPTICAL NETWORKS

Yohan Shim, Doctor of Philosophy, 2007

Directed By: Associate Professor Steven A. Gabriel
Department of Civil and Environmental Engineering

Free space optical (FSO) communication provides functionalities that are different from fiber optic networks and omnidirectional radio-frequency (RF) wireless communications in that FSO is optical wireless (no infrastructure installation cost involving fibers) and is highly directional (no frequency interference). Moreover, its high-speed data transmission capability is an attractive solution to the first or last mile problem to bridge to current fiber optic network and is a preferable alternative to the low data rate directional point-to-point RF communications for inter-building wireless local area networks.

FSO networking depends critically on pointing, acquisition and tracking techniques for rapidly and precisely establishing and maintaining optical wireless links between network nodes (physical reconfiguration), and uses topology reconfiguration algorithms for optimizing network performance in terms of network cost and congestion (logical reconfiguration). The physical and logical reconfiguration process is called Topology Control and can allow FSO networks to offer quality of service by quickly responding to various traffic demands of network users and by efficiently managing network connectivity.

The overall objective of this thesis research is to develop a methodology for self-organized pointing along with the associated autonomous and precise pointing technique as well as heuristic optimization methods for Topology Control in bi-connected FSO ring networks, in which each network node has two FSO transceivers.

This research provides a unique, autonomous, and precise pointing method using global positioning systems (GPS) and local angular sensors (e.g., tilt sensors or inertial navigation systems), which is applicable to both mobile and static nodes in FSO networking and directional point-to-point RF communications with precise tracking. Through medium (264 meter) and short (40 meter) range pointing experiments using an outdoor testbed on the University of Maryland campus in College Park, sub-milliradian pointing accuracy is presented. The short range experiment involves an automatic pointing system implemented by real-time kinematic GPS, bi-axial tilt sensors, a helium-neon laser ($\lambda = 633$ nanometers) and a two-axis gimbal, which shows that the automatic pointing system is reliable.

In addition, this research develops fast and accurate heuristic methods for autonomous logical reconfiguration of bi-connected ring network topologies as well as a formal optimality gap measure tested on an extensive set of problems. The heuristics are polynomial time algorithms for a congestion minimization problem at the network layer and for a multiobjective stochastic optimization of network cost and congestion at both the physical and network layers.

TOPOLOGY CONTROL AND POINTING IN FREE SPACE OPTICAL NETWORKS

By

Yohan Shim

Dissertation submitted to the Faculty of the Graduate School of the
University of Maryland, College Park, in partial fulfillment
of the requirements for the degree of
Doctor of Philosophy
2007

Advisory Committee:
Associate Professor Steven A. Gabriel, Chair
Professor Christopher C. Davis
Research Professor Stuart D. Milner
Professor Gregory B. Baecher
Professor Gilmer L. Blankenship
Associate Professor Subramanian Raghavan

Dedication

This thesis is dedicated to God who gave me new hope when I had lost it, and to my late father and father-in-law who let me seek my own dream when I still had not yet found one. May their souls rest in peace beside You.

Acknowledgements

I deeply thank the many individuals and groups who have contributed directly or indirectly to the completion of my thesis research. The time spent in my doctoral studies was a wonderful opportunity as well as a great challenge for me. First, I would like to thank Dr. Steven Gabriel for his attention to my work and advice on my academic improvement.

I am grateful for the support of Dr. Stuart Milner and Dr. Christopher Davis, who encouraged me to accomplish as much as I could in my research, and provided the freedom to realize my idea. Also, I appreciate Dr. Davis for his kind and valuable feedback on my pointing experiment and this manuscript.

I thank Jaime Llorca, Juan Carlos Franco, and John Rzasa in the Center for Networking of Infrastructure Sensors and the Maryland Optics Group for their willing help in my research.

I wish to thank all of the faculty and staff of the Department of Civil and Environmental Engineering, whose kind help allowed me to overcome the many difficulties I experienced as a graduate student.

Also I thank my former colleagues, Dr. Sam-Ok Koo, Dr. Chang-Sun Yoo, Jun-Baek Kim, Kyung-Ryoon Oh, and Sang-Jong Lee at the Korea Aerospace Research Institute for their valuable assistance whenever I needed their help.

I appreciate my former professors, Dr. Kang-Woong Lee at Korea Aerospace University, South Korea, and Drs. Mark White and Carl D. Meyer at North Carolina State University for their references when I transferred to the University of Maryland, College Park.

The National Science Foundation has provided me support as a graduate research assistant throughout my doctoral studies, and I am grateful for their assistance.

Finally, I would like to thank my wife, Seung-Won (Elizabeth), and two beautiful sons, Eui-June (David) and Eui-Sun (Albert), and family in South Korea for their devotion and prayers.

Table of Contents

List of Tables

List of Figures

Chapter 1: Motivation and Objectives

Free Space Optical (FSO) communications has been recognized as a high-speed wireless bridging technology to current fiber optic networks (Davis et al., 2003), as well as a valuable technology in commercial and military backbone networks (Milner et al., 2003). FSO architectures include fixed and mobile base stations or nodes, and FSO communication systems involve direct line-of-sight, point-to-point links with high data rate (> 1 Gbps) optical transceivers through the atmosphere.

1.1 The Main Challenge in FSO Networks

An FSO network can be affected by frequent changes in its optical links. These changes are due to the dynamic performance of optical wireless links, which depend on the effect of node mobility and atmospheric obscuration (e.g., dense fog, dust, or snow) and sudden changes in traffic demands. Thus, an FSO network must be capable of autonomous physical and logical reconfiguration responding to degradation in one or more links; this is called *Topology Control* (Davis et al. 2003). This reconfiguration occurs both physically, by means of pointing, acquisition and tracking (PAT), and logically, by using autonomous reconfiguration algorithms. For example, Figure 1-1 shows how topology control works against a degradation problem. Because of a sudden change in link or traffic states, physical reconfiguration is necessary. Then, the reconfiguration algorithms yield an optimal topology which minimizes cost or congestion in the network. Subsequently, the PAT techniques create a new topology in accordance with the solution.

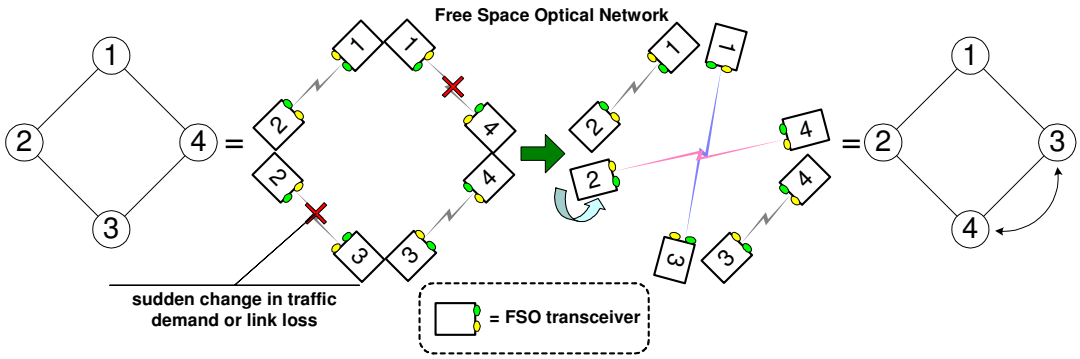

Figure 1-1. Degradation scenario and respective action taken by topology control. (Example of bi-connected ring network topology with directional optical links)

FSO transceivers – Hard to align their directional, narrow laser beams

To reduce the effect of atmospheric obscuration existing on the path to the receiver, the FSO transmitter concentrates its power (1mW to 100mW) in the form of a narrow laser beam. As it propagates toward the receiver at a remote site, the beam widens. The amount of spread is defined by the beam divergence angle. If the transmitted beam falls within the field-of-view (FOV) of the receiver, then the receiver can receive the beam properly, enabling successful pointing; otherwise, establishment of the link fails. The FOV is defined as a maximum acceptance angle for the incoming laser beam (Figure 1-2).

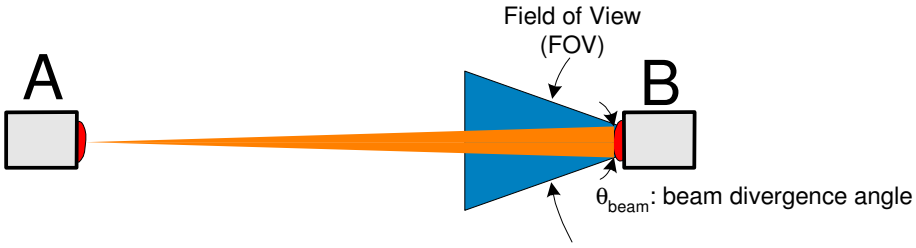

Figure 1-2. An example of proper pointing

Challenge in Physical Reconfiguration: Self-Organized Pointing

Since FSO communication networks include an optical link using a narrow, directional laser beam, it is essential to steer FSO transceivers precisely between two nodes as shown in Figure 1-3. This process is referred as "pointing". If the link is available, "acquisition" is complete. If either node is mobile, then the node is tracked by the other node to maintain the established link - "tracking". The tracking is achieved by estimating (predicting) the future position and velocity of the mobile node.

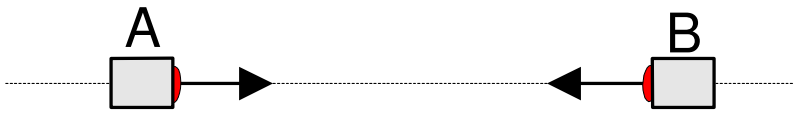

Figure 1-3. Pointing between FSO transceivers in nodes A and B

For an autonomous physical reconfiguration, the optical link between any two nodes in the network should be established without being guided or managed by an external source; thus, pointing must be self-organized. However, the self-organized pointing is a challenging problem because of the following reasons:

- Pointing requires microradian to milliradian accuracy.
- The pointing direction of laser beam is unknown (the hardest question about pointing).
- Nodes can be mobile; it requires tracking and locating them in a common navigation coordinate frame.
- Two pointing systems should operate independently to align their laser beams for a complete pointing.

- A local pointing system may be interoperable with another pointing system whose system components are different from those used at a local one.

Challenge in Logical Reconfiguration: Topology Optimization

In a logical reconfiguration, an optimal topology in an FSO network is determined by a graphical mapping of the configuration of its network elements (nodes and links). Given a cost matrix for each possible link (Figure 1-4 (b)) and the traffic matrix for all origin-destination nodes pair in the network (Figure 1-4 (c)), the mapping of the network elements is related to an optimization problem whose objective is finding an optimal topology minimizing overall cost (e.g., transmission power) or congestion (defined here as the sum of all loads across the network) (or both). Since the existence or utilization of a link (i, j) between two nodes i and j is represented by binary variables, the optimization problem is a mixed-integer linear program (MILP) which may have many feasible solutions, subsequently requiring a large amount of computer time to find global optima to the related Network Layer Topology Control Problem (Shim et al., 2005). Since, for example, there are $(n-1)!/2$ possible ring topologies for a bi-connected ring network topology with n nodes and $2^{n(n-1)}$ possible routings for each ring topology, enumeration of all topologies is not computationally attractive when a near-real time solution is required. Consequently, a fast heuristic approach providing near-optimal solutions is helpful for topology control.

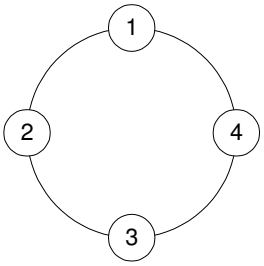

(a) Initial topology

node i \ node j	1	2	3	4
1	0	10	20	30
2	10	0	30	10
3	20	30	0	5
4	30	10	5	0

(b) Cost matrix

origin node \ destination node	1	2	3	4
1	0	5	20	30
3	10	0	10	10
3	10	20	0	15
4	5	30	10	0

(c) Traffic matrix

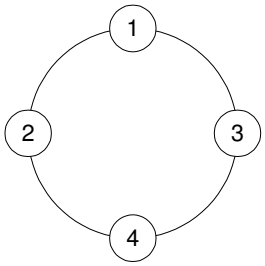

(d) Minimum cost topology

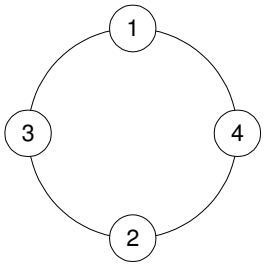

(e) Minimum congestion topology

Figure 1-4. Example of topology optimization

1.2 Research Focus and Achievements

The overall research objectives of this thesis are to provide the answers to the following two questions:

- How to quickly and precisely establish optical links between nodes (mobile or fixed) in the network? (Pointing)
- How to optimize network performance in terms of network cost and congestion in bi-connected FSO ring networks? (Topology Optimization)

These questions have been answered through the research described in this thesis. A methodology has been developed for self-organized pointing along with the associated autonomous and precise pointing technique for physical reconfiguration. The principal accomplishments of this work relative to the first question are:

- The generation of complete information as to where nodes are and as well as where they are heading in a common navigation coordinate frame using GPS.
- Representation of this information in a local body coordinate frame with 3-dimensional attitude angles of nodes (platforms) by using GPS and local angular sensors (e.g., tilt sensors, INS).
- Development of a method for precise measurement of the pointing direction (pointing vector) of an FSO transceiver and its directional, narrow laser beam.
- Development of an independent and interoperable pointing procedure to complete pointing between local and remote transceivers.
- The design of a precise pointing system and demonstration of its pointing accuracy with an automatic pointing system.

Answers for the second question have demanded the development of accurate heuristic methods for topology optimization in bi-connected ring networks. This work has included the solution of the following two problems:

- Network Layer Topology Control Problem (NLTCP)

Defined as a congestion minimization problem at the network layer (Shim et al., 2005). Its solution is a best ring topology with an optimal routing strategy responding to the given traffic demands between origin (source) and destination nodes pair in a ring network. The traffic demand in the network is given in the form of a traffic matrix (e.g., Figure 1-4 (c)).

- Multiobjective Optimization Problem (MOP)

  Defined by selecting a best ring topology which minimizes both physical layer cost and network layer congestion with uncertain traffic demands (Gabriel et al., 2006). The cost matrix (e.g., Figure 1-4 (b)) is generated by obscuration scenarios considering link distance and a cloud model (Gabriel et al., 2006). The uncertainty in the traffic patterns is represented by a set of probabilities (i.e., $\{p_1,..., p_K\}$) assigned to K traffic matrices (stochastic load).

The major accomplishments of the work relative to the second question are:

- Development of polynomial time heuristic algorithms for NLTCP and MOP which have been shown to be scalable algorithms for a wide range of test problems.
- Development of a theoretical bound for the optimality gap of both heuristics (for NLTCP and MOP) by which the upper bound on the optimality gap of a problem with a large number of nodes can be known without finding its global optimum.

1.3 GPS-based Autonomous Reconfiguration Scenario: Connection between Self-Organized Pointing and Topology Optimization

This dissertation combines hardware as well as software methods for reconfiguring ring topologies. To better connect these two research areas, we provide an example of autonomous reconfiguration for mobile nodes with the physical reconfiguration (by the self-organized pointing with GPS and local angular sensors) and the logical reconfiguration (by the heuristic algorithms for NLTCP and MOP).

First, assume that there are six nodes in a coverage area in which they can continuously track at least five common GPS satellites and a central node can move around the coverage area to collect all information necessary to the initial link establishment. This configuration is shown in Figure 1-5 with the autonomous reconfiguration described in the next sections.

Initial Link Establishment

For establishing initial links between all nodes, first, each node broadcasts its data packet to neighbor nodes as shown in Figure 1-5. The data packet includes each node's identification number (ID), navigation (NAV) information (orientation and position), and its traffic demand; it may also include ID and NAV information as well as information about received power (an estimate of link "cost") from its existing and potential neighbors. Then, a central node collects all packets from the mobile nodes, and generates a potential link table and input cost and traffic matrices as shown in Figure 1-6 with additional weather information from ground or satellite resources.

The information is displayed on the screen of an automatic vehicle location system (AVLS).

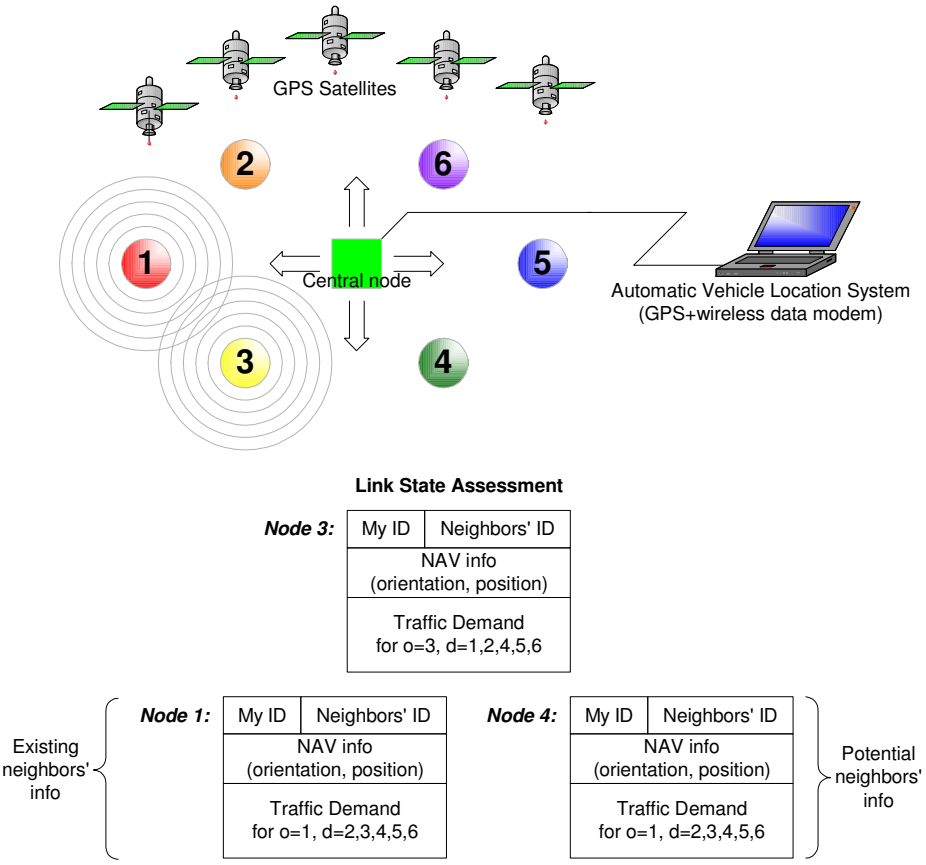

Figure 1-5. Centralized Topology Control

For a bi-connected ring network with n nodes, there exist $(n-1)!/2$ ring topologies. The heuristic algorithms for NLTCP and MOP provide topologies that are near-optimal in general but may be optimal in some cases and the associated routing tables; the heuristics are based on the shortest path (hop) routing scheme. For example, Figure 1-7 shows a ring network topology solution and its routing table from the heuristic for NLTCP or MOP. The routing table is made up of the sequence

of links from origin node to destination node on the ring network, and it contains the shortest hop routing direction for each traffic demand of origin-destination pairs.

Node	Neighbors
1	2, 3, 4, 5, 6
2	1, 3, 4, 5, 6
3	1, 2, 4, 5, 6
4	1, 2, 3, 5, 6
5	1, 2, 3, 4, 6
6	1, 2, 3, 4, 5

(a) Potential links

node i \ node j	1	2	3	4	5	6
1	0	c12	c13	c14	c15	c16
2	c21	0	c23	c24	c25	c26
3	c31	c32	0	c34	c35	c36
4	c41	c42	c43	0	c45	c46
5	c51	52	c53	c54	0	c56
6	c61	c62	c63	c64	c65	0

(b) Cost matrix

origin node \ destination node	1	2	3	4	5	6
1	0	r12	r13	r14	r15	r15
2	r21	0	r23	r24	r25	r26
3	r31	r32	0	r34	r35	r36
4	r41	r42	r43	0	r45	r46
5	r51	r53	r53	r54	0	r56
6	r61	r62	r63	r64	r65	0

(c) Traffic matrix

Figure 1-6. Node information and input matrices

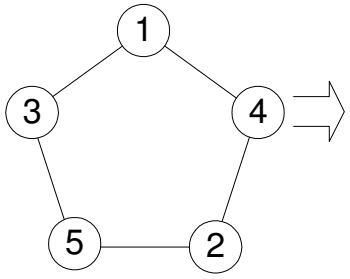

o	d	routing (sequence of links)	o	d	routing (sequence of links)
1	2	(1,4) → (4,2)	2	1	(2,4) → (4,1)
1	3	(1,3)	3	1	(3,1)
1	4	(1,4)	4	1	(4,1)
1	5	(1,3) → (3,5)	5	1	(5,3) → (3,1)
2	3	(2,5) → (5,3)	3	2	(3,5) → (5,2)
2	4	(2,4)	4	2	(4,2)
2	5	(2,5)	5	2	(5,2)
3	4	(3,1) → (1,4)	4	3	(4,1) → (1,3)
3	5	(3,5)	5	3	(5,3)
4	5	(4,2) → (2,5)	5	4	(5,2) → (2,4)

Figure 1-7. The shortest hop routing for a ring network topology with $n = 5$

Finally, the central node disseminates an initial link establishment command with its RF data transmitter or, if the distance between itself and nodes in the other side is too long, relays the command with an FSO transceiver. For example, the link command would be *1-3-4-5-6-2-1* (Figure 1-8). According to the link command, each node establishes its directional link with other nodes by the self-organized

pointing procedure and the autonomous and precise pointing method developed in Chapter 2.

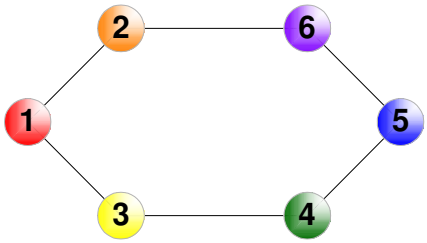

Figure 1-8. Link command

After the Initial Link Establishment: Consideration of mobile node dynamics

Forming a wireless backbone network with mobile nodes such as aircraft and unmanned air vehicle requires continuous tracking and control of their orientation and position. For this purpose, each node regularly updates (broadcasts) its navigation information (orientation and position). The navigation information is utilized to:

i) Compute fuel consumption for each mobile node, which subsequently estimates the probable flight time (i.e., how long the node can maintain its connectivity in the network). According to this estimation, it is possible to refuel or replace any node whose remaining amount of fuel is enough only for returning to an air base, thus efficiently maintaining network connectivity.

ii) Coordinate and reassign the mobile nodes for efficient use of network resources. For example, Figure 1-9 (a) shows the coordination of four mobile nodes in a coverage area. In a heavy traffic area, two nodes are assigned in Section A to manage the traffic to minimize network congestion. When heavy traffic is expected to occur in Section B, node 2 is reassigned to Section B to handle the traffic without adding a fifth node to the coverage area (Figure 1-9

(b)). GPS-based automatic vehicle tracking technology will speed up the coordination and reassignment. For directional communication, during the coordination and reassignment, link loss can be avoided by the GPS-based pointing technique developed in Chapter 2.

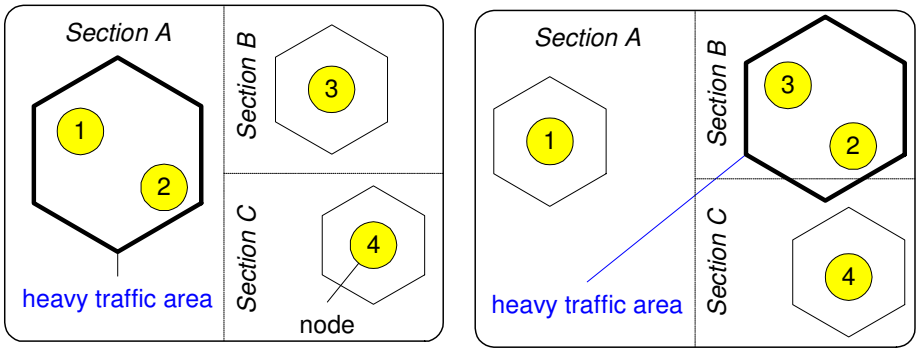

(a) Before the reassignment (b) After the reassignment

Figure 1-9. Efficient use of network resources by automatic vehicle tracking and control

Coordination and reassignment are decision problems related to network topology creation with priority. The decision problem is solved as the first-level in the topology optimization with the objective of minimizing cost (e.g., bit-error-rate, fuel, time), and then optimal routes are selected as the second-level problem with the objective of minimizing congestion as the NLTCP. The amount of fuel consumption and estimated time spent in the reassignment may be additional costs in the optimization model as shown in Figure 1-10. Those costs are also inputs to the heuristic for MOP which subsequently yields optimal topology and routes; then, the PAT techniques will create a new topology according to the optimal solutions. Figure 1-11 shows the overall process in Topology Control; the physical and logical

reconfiguration process will be repeated whenever the costs and traffic demands change.

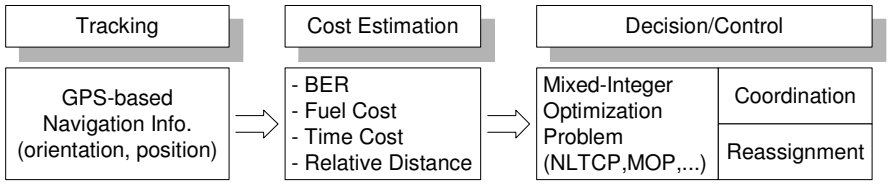

Figure 1-10. Diagram of mobile node control

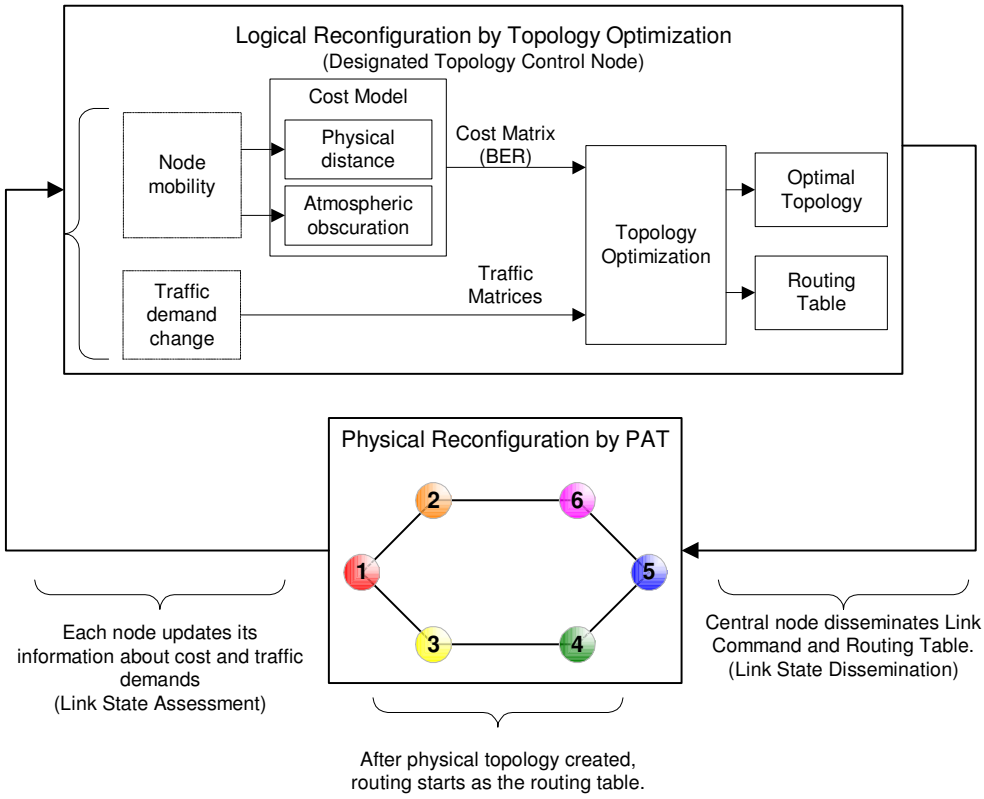

Figure 1-11. Diagram of the overall process in Topology Control

1.4 Overview of the Dissertation

The rest of the dissertation is organized as follows. Chapter 2 provides our unique methodology for self-organized pointing and the associated autonomous and precise pointing technique, error analysis of the method with computer simulation, and results of pointing experiments with an automatic pointing system implemented by the pointing method. The chapter considers various error sources affecting pointing accuracy and self-organized pointing methodology for mobile platforms. Chapter 3 provides a survey of literature in routing and topology control problems in fiber optic and free space optical networks. Next, the accuracy performance of our heuristic methods for FSO networking is presented with numerical results. The method is compared to simulated annealing and genetic algorithms, which helps in understanding their different characteristic and performance in congestion minimization problem. Then, an evaluation method that estimates the optimality gap without knowing a global solution for a ring network with a large number of nodes (more than 15) is presented. Finally, it is shown in an application example that our heuristic methods can be utilized as an evaluation tool for heuristics in the congestion minimization problems with ring topology. Lastly, Chapter 4 provides a summary of the major findings of the dissertation and suggestions for future work as well as a listing of the papers that have resulted from this research.

Chapter 2: Pointing

FSO communications has been recognized as a high-speed wireless bridging technology to current fiber optic networks (Davis et al., 2003), and a valuable technology in commercial and military backbone networks (Milner et al., 2003). However its bright prospects depend on the performance of pointing system, and autonomous reconfiguration algorithms dealing with the effects of node mobility and atmospheric obscuration.

Precise laser beam pointing requiring microradian to milliradian accuracy is a challenging problem unless both nodes are close to each other. In this case manual alignment is straightforward, and can be guided by the use of optical beacons, or image based pointing. However, if the link distance is more than a few kilometers, then these techniques become increasingly difficult to implement. Instead, we need complete information as to where nodes are (their position coordinates) as well as FSO transceiver angular pointing coordinates (pointing vectors). The use of various kinds of position and angular sensor devices is therefore natural in pointing systems, as described previously (Ho et al., 2006; Ho et al., 2004; Epple, 2006; Wilkerson et al., 2006; Yee et al., 1998); Table 2-1 compares the various sensor devices used in pointing systems.

Table 2-1. Comparison of pointing sensors

	Camera	GPS/INS	RTK GPS
Sensor output	2-D image	Position, Velocity, Acceleration, Time	Position, Velocity, Time
Components	- Lens - Image processing unit (or machine vision unit)	- GPS unit, - 3-axis gyros, - 3-axis accelerometers	- RTK GPS unit, - Wireless RF data Tx/Rx
Accuracy	Depending on - Pixel size, and - Quality of image	Depending on the cost; For example,	NovAtel RT-2 ($14,000) - Position accuracy: < 3 cm (within 10km from BASE)

	processing software (or machine vision S/W)	Honeywell H746G ($85,000) - Attitude accuracy: < 0.1~ 0.2 deg - Bias of gyro: 1 deg/hr - Range of rate: >600 deg/s - Range of accel: 21 g - Gyro type: FOG BEIsystron C-MIGITS III ($26,000) - Position accuracy: < 4.0 m - Heading accuracy: 1.5 mrad+1~3 deg/hr - Velocity accuracy: 0.1 m/s - Bias of gyro: 1~3 deg/hr - Range of rate: 1000 deg/s - Rage of accel: 8~15 g - Time accuracy: 1 μs - Output rate: 1~5 Hz	- Velocity accuracy: 0.03 m/s RMS - Time accuracy: 20 ns RMS - Range of velocity: 514 m/s - Range of accel: 4 g - Output rate: 1~20 Hz
Pointing /Tracking Area	Local	Global	Global

Previous authors (Ho et al., 2006; Ho et al., 2004) have described a coarse pointing system using a 180° field-of-view (FOV) fisheye camera and a 30° FOV regular camera. The omnidirectional fisheye camera first acquires the target (fixed or mobile node) of interest by image extraction. Next, the 30° FOV camera is rotated toward the target of interest based on a homographical computation. The rotation angles are used to generate a radial trifocal tensor, which is applied to estimate the movement of the FSO transceiver on the target (tracking). In this work a pointing error around 0.2° was reported.

Other authors (Epple, 2006; Wilkerson et al., 2006) describe low-cost and lightweight pointing system for mobile nodes such as aircraft or ground vehicle. Their pointing system (MOCT: Mobile Optical Communication Terminal) used both Differential GPS (DGPS) and inertial navigation system (INS) to measure a coarse pointing vector, as well as a camera to provide a fine pointing vector. However, due to the low accuracy of DGPS (5 *m*) and INS (3°), the coarse pointing error appeared as 0.79° (mean) in azimuth and 0.3° (mean) in elevation; the standard deviations of

the pointing error in azimuth and elevation were 1.25° and 0.2°, respectively. They employed an optical beacon in measuring a fine pointing vector. The camera on the MOCT continuously tracked the beacon on the ground, and the real-time image was used to compute the fine pointing vector. Their tracking system was based on an optical camera (17° FOV) and DGPS. During their tracking experiment, an aircraft regularly broadcast its error corrected position; then an optical ground station tracked the airplane by estimating the next position and velocity of the aircraft.

Yee et al. (1998) describe a method of pointing to a designated stellar target (e.g., star or satellite) with known position coordinates from a mobile platform (e.g., airplane, terrestrial vehicle, or ship). An INS mounted on a pointing instrument (e.g., telescope, antenna, sensor, laser, missile launcher, etc.) measures three dimensional attitude angles (roll, pitch, yaw); then the angular differences between the desired pointing angles to the target and the attitude angles from the INS provide pointing command signals as input to the pointing instrument. The pointing system utilizes GPS position updates to compensate for drift errors in the INS measurements.

Cohen et al. (1993) used four GPS antennas to measure attitude angles of an aircraft as shown in Figure 2-1. The lengths of baseline vectors 1, 2, and 3 were around 11 meters, 8 meters, and 11 meters, respectively; a baseline vector was defined as a vector between two GPS antennas. The heading was determined by baseline vector 2; elevation and roll were determined by baseline vector 1 and 3. High accuracy INS, Litton LN-93 (attitude accuracy: 0.05° in 95 %) were used as a

reference for comparing the attitude angles measured by the three baseline vectors. They reported that the heading accuracy was 0.1° and the elevation and roll accuracy was 0.2° during their flight test. "The purpose of the test flight is to provide a quantitative experimental basis for the kinematic accuracy performance evaluation of attitude determination using GPS (Cohen et al., 1993)" in aviation.

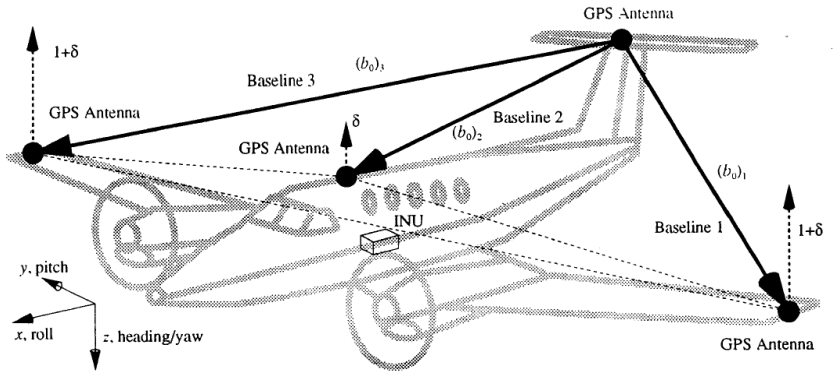

Figure 2-1. Aircraft attitude determination using multiple GPS antenna (Cohen et al., 1993)

The above pointing systems depend on optical devices (Ho et al., 2006; Ho et al., 2004; Epple, 2006; Wilkerson et al., 2006) or INS combined with GPS (Epple, 2006; Wilkerson et al., 2006; Yee et al., 1998); GPS or DGPS acts as a secondary device for providing position updates and correcting INS drift error, whose position accuracy is at the meter level. This research describes a precise pointing technique that is applicable to link initiation in FSO networking; the technique employs Real-Time Kinematic (RTK) GPS and local angular sensors (e.g., tilt sensors or INS). The RTK GPS provides centimeter level positioning accuracy (e.g., 2 cm for the NovAtel RT2W); it has been used in applications requiring precise location, navigation, and tracking (Cohen et al., 1993; Lachapelle et al., 1996; Buick, 2006). *Because the*

pointing technique utilizes highly accurate GPS to provide primary pointing information, it is distinct from previously described pointing systems (Ho et al., 2006; Ho et al., 2004; Epple, 2006; Wilkerson et al., 2006; Yee et al., 1998).

2.1 Design of Autonomous and Precise Pointing System using RTK GPS

2.1.1 A Methodology for Self-Organized Pointing

We have been developing a pointing technique that is applicable to link initiation in FSO networking. At link initiation, each node measures its position by stand-alone GPS or differential GPS (such as RTK GPS); GPS provides global positioning information. Then it broadcasts the position information through a wireless RF data transceiver.

In a centralized network (such as a ring network), a central node collects all position information from all nodes within the RF coverage. Next, it determines the best ring topology from the information, and sends out pointing commands to nodes telling each node where to connect. In a decentralized or distributed network, each node can make its own link decisions based on the GPS location information from its neighbor nodes. Since this pointing technique aims to achieve point-to-point interconnections between any two nodes, it can be applied to a centralized or decentralized networking.

Our pointing technique is based on measuring *i)* three dimensional attitude angles (roll, pitch, yaw) of an FSO transceiver mounted on a two-axis gimbal and *ii)*

pointing vector of the transceiver (i.e., where the FSO transceiver is directing its laser beam). The attitude angles and pointing vector are measured on the local tangent plane or navigation frame, such as East-North-Up (ENU) coordinates (Leick, 1995). As illustrated in Figure 2-2, our unique methodology for self-organized pointing procedure works as follows:

A Methodology for Self-Organized Pointing:

STEP 1) The precise position of two FSO transceivers at A and B is measured referenced to a local origin in ENU coordinates.

STEP 2) The displaced angles, θ_1 and θ_2, to the baseline $\overline{AB}$ are determined; they become a control input to the gimbal.

STEP 3) The FSO transceivers at A and B are aligned to be on the baseline $\overline{AB}$ ($|\overline{AB}|$: link distance); two transceivers point to each other (and become interconnected).

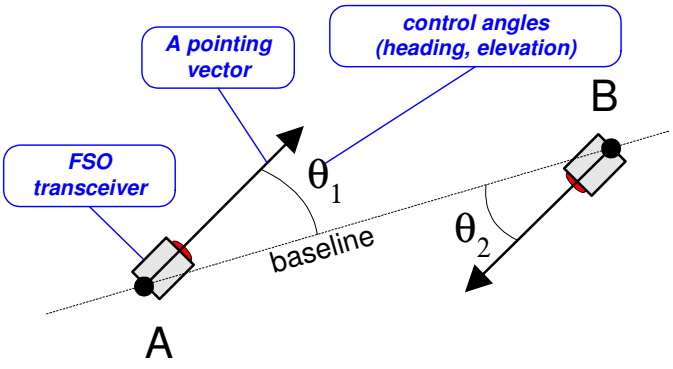

Figure 2-2. A pointing scenario

Once the baseline vector $\overrightarrow{AB}$ or $\overrightarrow{BA}$ is known in STEP 1, each pointing system at A

and B continues to STEP 2, independently. The only necessary information for the two pointing systems at A and B is each other's location; then the two systems operate independently to align their FSO transceivers on the baseline. By this scheme, we can interoperate with another pointing system placed at B (whose system components may be different from those used at A) only if we know the coordinates of B.

2.1.2 Method of Pointing Vector Measurement

A vector is defined by two points in a coordinate frame; if the coordinates of the two points are C_1 and C_2, respectively, then the vector is computed by the difference of the two coordinates, $C_2 - C_1$, which is the vector from C_1 to C_2. Likewise, knowing the pointing vector of an FSO transceiver requires measurement of two points on the path through which the laser beam of the transceiver passes (Figure 2-3).

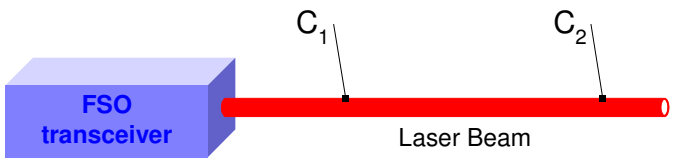

Figure 2-3. A pointing vector on the path of laser beam

Figure 2-4 illustrates our method for pointing vector measurement. Figure 2-4 (a) shows a GPS antenna mounted on FSO transceiver placed on a mobile platform which is stationary at a location C_1; then, the mobile platform moves forward in a

straight line to another location C_2 (For simplicity, it is assumed that the mobile platform is on a flat surface). C_1 and C_2 are RTK GPS coordinates for a GPS antenna mounted on the FSO transceiver, whose coordinates are $C_1 = [E_1, N_1, U_1]^T$ and $C_2 = [E_2, N_2, U_2]^T$. Therefore, the pointing vector between C_1 and C_2 is calculated as:

$$u = \frac{[E_2 - E_1, N_2 - N_1, U_2 - U_1]^T}{D}, \quad (1)$$

where $D = \left\| [E_2 - E_1, N_2 - N_1, U_2 - U_1]^T \right\|$ and $\|\bullet\|$ is the Euclidean vector norm. If the platform moves on a curved surface as shown in Figure 2-4 (c), then the pointing vector in the figure can be obtained by rotating the horizontal vector $[E_2 - E_1, N_2 - N_1, 0]^T$ by the pitch (or roll) angle from the local angular sensors (e.g., tilt sensors or INS). Figure 2-4 (b) shows a second way of measuring the pointing vector: align FSO transceiver located at C_1 to a pre-determined target at C_2 (with previously determined position coordinates). From the pointing vector (u) in Equation (1) and position coordinates of C_2, the pointing vector centered at C_2 is obtained as shown in Figure 2-4 (a) (or C_1 in Figure 2-4 (b)), which is the current location of the FSO transceiver.

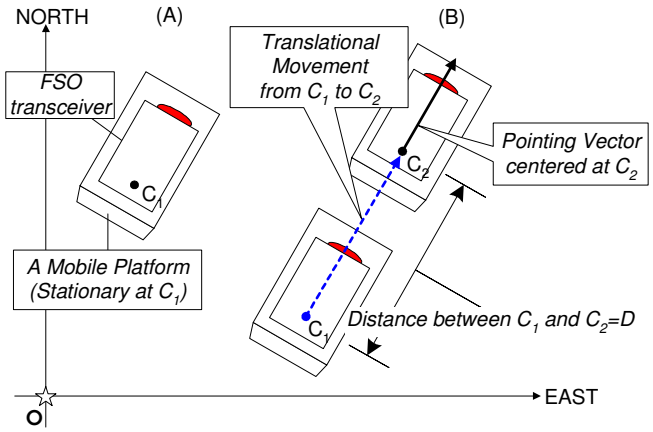

(a) Translational movement of GPS antenna

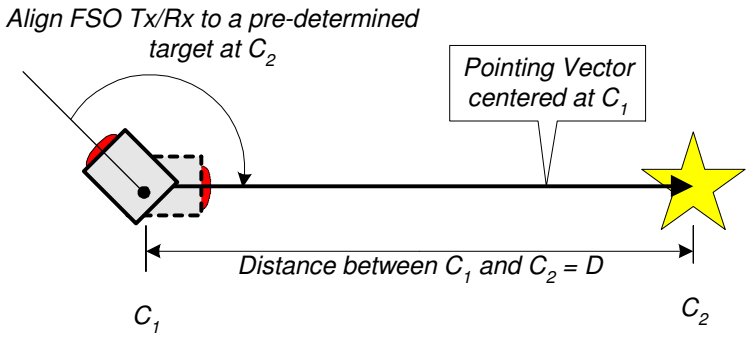

(b) Aligning FSO transceiver to a pre-determined target with known position coordinates

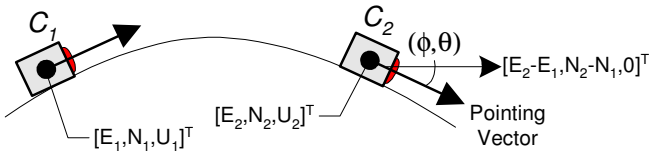

(c) Pointing Vector measurement on a curved surface with the method (a)

Figure 2-4. Pointing vector measurement

The RTK GPS position coordinates at C_1 and C_2 contain measurement errors at the centimeter level. If we denote ε_1 and ε_2 as the three-dimensional measurement errors in C_1 and C_2, respectively, then the unit vector u is expressed as:

$$u = \frac{\left[E_2 - E_1, N_2 - N_1, U_2 - U_1\right]^T + \left(\varepsilon_2 - \varepsilon_1\right)}{D_\varepsilon}, \tag{2}$$

where $D_\varepsilon = \left\| \left[E_2 - E_1, N_2 - N_1, U_2 - U_1\right]^T + (\varepsilon_2 - \varepsilon_1) \right\|$ and $D_\varepsilon \le D + \left\|\varepsilon_2 - \varepsilon_1\right\|$ by the Triangle Inequality (Meyer, 2000). Figure 2-5 shows u and D_ε. If we assume that $\left\|\varepsilon_1\right\|$ and $\left\|\varepsilon_2\right\|$ are less than or equal to 3 cm, then $\left\|\varepsilon_2 - \varepsilon_2\right\| \le \left\|\varepsilon_2\right\| + \left\|\varepsilon_1\right\| \le 6$ cm. Therefore, if D is much larger than both $\left\|\varepsilon_1\right\|$ and $\left\|\varepsilon_2\right\|$ (e.g., $D = 6$ m), then the following relations are hold:

$$\frac{\left(\varepsilon_2 - \varepsilon_1\right)}{D_\varepsilon} \le \frac{\left\|\varepsilon_2 - \varepsilon_1\right\|}{D_\varepsilon} \le \frac{\left\|\varepsilon_2\right\| + \left\|\varepsilon_1\right\|}{D_\varepsilon} \simeq \frac{\left\|\varepsilon_2\right\| + \left\|\varepsilon_1\right\|}{D} \simeq 0 \tag{3}$$

$$u \simeq \frac{\left[E_2 - E_1, N_2 - N_1, U_2 - U_1\right]^T}{D} \tag{4}$$

Hence, as D increases, the pointing vector becomes closer to the true one without measurement errors.

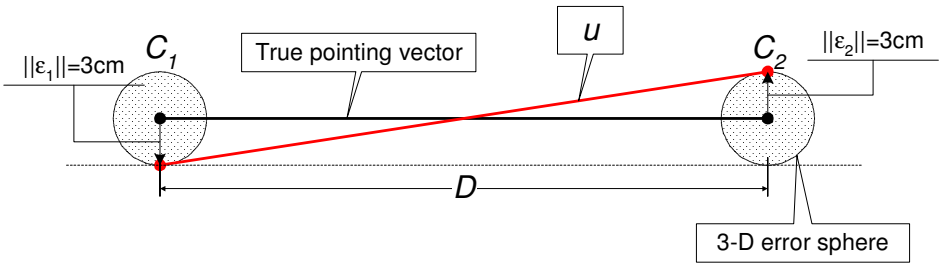

Figure 2-5. 3-D measurement errors in C_1 and C_2

The east and north components of the pointing vector determine yaw (ψ). With roll (ϕ) and pitch (θ) from local angular sensors and yaw from RTK GPS, we have complete attitude angle information of the FSO transceiver, which is necessary to convert the pointing vector in the navigation frame (ENU coordinates) to the one in the body frame by the following equations:

$$P_B = C_{ENU}^{B} P_{ENU} = C(\phi)C(\theta)C(\psi)P_{ENU}, \quad (5)$$

where

(ϕ, θ, ψ) : Attitude angles

$C(\phi), C(\theta), C(\psi)$: Rotation matrices

$C_{ENU}^{B} = C(\phi)C(\theta)C(\psi)$: Transformation matrix from the ENU coordinates to the body frame.

P_{ENU} : Position in the ENU coordinates

P_B : Position in a body frame.

With the baseline vector $\overrightarrow{AB}$ or $\overrightarrow{BA}$ in Figure 2-2 transformed to the body frame by Equation (5), the control inputs to the gimbal (i.e., heading and elevation angles) is computed from the pointing vector and the baseline vector transformed to the body frame (see Appendix A for details).

The advantages of this pointing method are summarized as:

1) Conceptually simple and easy to implement.

2) A complete attitude angle can be measured by RTK GPS alone, if the surface is flat or as long as we can keep the surface level using a stabilizer.

3) RTK GPS consists of a GPS unit and a wireless RF data transceiver; its precise position data will be sufficient to track mobile nodes. Its high accuracy will improve the performance of position and velocity estimation of a mobile node.

4) The precise heading information from RTK GPS can be combined with the roll and pitch outputs from INS mounted on an aircraft (Lee et al., 2001; Lee et al., 1998); thus enabling us to use the pointing technique in a dynamic environment.

5) Because the same pointing sensors are used at C_1 and C_2 in Figure 2-5 to measure the pointing vector, it makes a pointing system compact as much as the total dimension of the pointing sensors (i.e., GPS antenna and local angular sensors).

Since RTK GPS requires the observation of at least five GPS satellites to yield such high accurate position coordinates, our basic assumption in this pointing method is that there is no significant GPS signal blockage at the site where the pointing system is being operated, thus being observed at least five GPS satellites and $1 \leq PDOP \leq 6$. The GPS modernization plan (Enge, 2003) and the European global positioning satellite system, Galileo (www.esa.int/esaNA), will increase the least number of observable satellites up to eight, which subsequently satisfies the minimum number of observable satellites (i.e., five satellites).

2.2 Approximating the Distribution of Pointing Error

In the previous section, a unique method of pointing vector measurement for mobile and static platforms was presented. The measure utilizes the GPS coordinates (E, N, U) and attitude angles (ϕ, θ, ψ) of an FSO transceiver mounted on a two-axis gimbal; this information is subsequently used to compute the control inputs to the two-axis gimbal. Since the coordinates and attitude angles are from the RTK GPS and local angular sensors, they contain measurement errors. These sensor measurement errors propagate into the pointing vector measurement in (2) and the coordinate transformation in (5); thus, they finally affect the computation of control angles (heading and elevation) by which each axis of the gimbal is rotated to align the pointing vector ($\overrightarrow{AB}$) to the baseline vector ($\overrightarrow{AC}$) as shown in Figure A-4 (b) (see Appendix A for details).

In this section, it is shown by computer simulation with MATLAB how the sensor measurement errors affect the pointing accuracy. The simulation provides the variance (or standard deviation) of heading and elevation (i.e., σ_h and σ_e), which represent the pointing error distribution according to the sensor measurement errors (i.e., σ_E, σ_N, σ_U, σ_ϕ, σ_θ).

2.2.1 Error Propagation

Breipohl (1970) and Arras (1998) approximated the distribution of the output Y when the distribution of the input X is known and $Y = f(X)$ where $f(\bullet)$ is some

known nonlinear function (Figure 2-6). By assuming X and Y are normally distributed (i.e., $X \sim N(\mu_X, \sigma_X)$ and $Y \sim N(\mu_Y, \sigma_Y)$), $Y = f(X)$ is approximated by a first-order Taylor series expansion at $X = \mu_X$ as follows:

$$Y = f(X) \simeq f(\mu_X) + \left.\frac{\partial f}{\partial X}\right|_{X=\mu_X} (X - \mu_X) \tag{6}$$

Thus, the distribution of Y is approximated as follows:

$$\mu_Y = E[Y]$$

$$\simeq E\left[f(\mu_X) + \left.\frac{\partial f}{\partial X}\right|_{X=\mu_X} (X - \mu_X) \right] = f(\mu_X) + \left(\left.\frac{\partial f}{\partial X}\right|_{X=\mu_X} \right) E[X - \mu_X]$$

$$= f(\mu_X) + \left(\left.\frac{\partial f}{\partial X}\right|_{X=\mu_X} \right) E[X] - \left(\left.\frac{\partial f}{\partial X}\right|_{X=\mu_X} \right) \mu_X = f(\mu_X)$$

$$\therefore \ \mu_Y \simeq f(\mu_X) \tag{7}$$

$$\sigma_Y^2 = E\left[(Y - \mu_Y)^2 \right] = E\left[\left(f(X) - f(\mu_X) \right)^2 \right]$$

$$\simeq E\left[\left(f(\mu_X) + \left(\left.\frac{\partial f}{\partial X}\right|_{X=\mu_X} \right) (X - \mu_X) - f(\mu_X) \right)^2 \right]$$

$$= \left(\left.\frac{\partial f}{\partial X}\right|_{X=\mu_X} \right)^2 E\left[(X - \mu_X)^2 \right]$$

$$\therefore \ \sigma_Y^2 \simeq \left(\left.\frac{\partial f}{\partial X}\right|_{X=\mu_X} \right)^2 \sigma_X^2 \tag{8}$$

Figures 2-6 (a) and (b), respectively, show a diagram of the single input single output system $Y = f(X)$ and the error propagation corresponding to the 68 % probability interval $[\mu_X - \sigma_X, \mu_X + \sigma_X]$ through the system $f(\bullet)$. In general, since μ_X and σ_X

are unknown, the sample mean and standard deviation from actual measurements (e.g., sensor outputs) are used (Arras, 1998). The first-order Taylor series approximation is effective when:

- " $f(X)$ is not too far from linear within the region that is within one standard deviation of the mean (Breipohl, 1970)" because the approximation error becomes smaller as the linear approximation (6) in the range of $\mu_X - \sigma_X \le X \le \mu_X + \sigma_X$ resembles more closely the nonlinear function $f(X)$, and
- The slope $\left| \left(\left. \frac{\partial f}{\partial X} \right|_{X=\mu_X} \right) \right|$ at $X = \mu_X$ is not large (Figure 2-6 (c)) because $\sigma_Y = \left(\left. \frac{\partial f}{\partial X} \right|_{X=\mu_X} \right) \sigma_X$, which means that the bigger the slope at $X = \mu_X$, the wider the distribution of the output Y as shown in Figure 2-6 (c).

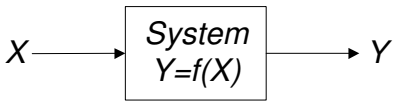

(a) One input random variable, and one output random variable

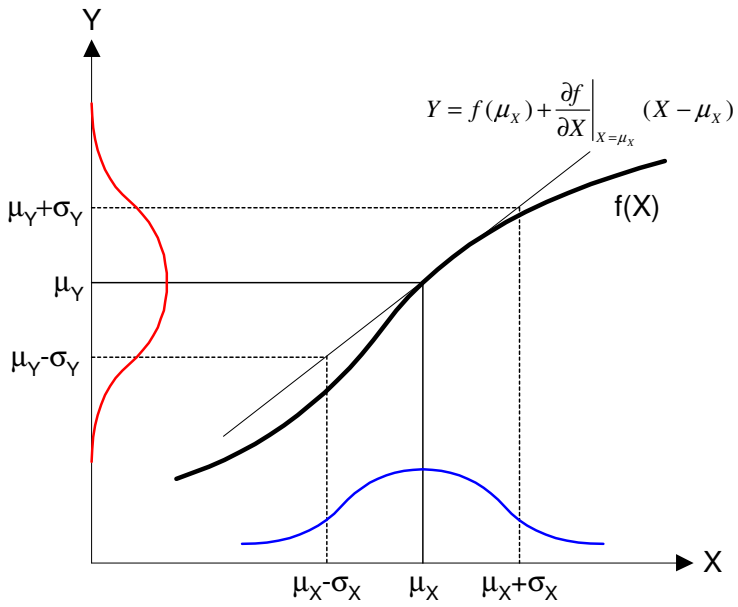

(b) One-dimensional case of a nonlinear error propagation problem (X-axis: Input signal distribution; Y-axis: Output signal distribution)

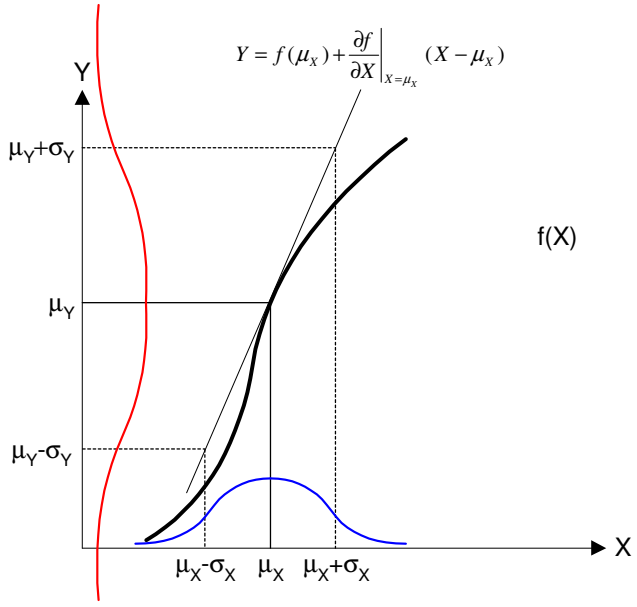

(c) Poor approximation when $\left|\left(\left.\frac{\partial f}{\partial X}\right|_{X=\mu_X}\right)\right| \gg 1$

Figure 2-6. A single-input and single-output system (Arras, 1998)

For a multi-input and single-output system in Figure 2-7,

$Y = f(X_1, X_2, ..., X_n)$ is approximated by a first-order Taylor series about the point $(\mu_1, \mu_2, ..., \mu_n)$ as follows:

$$Y \simeq f(\mu_1, \mu_2, ..., \mu_n) + \sum_{i=1}^{n} \left[\frac{\partial}{\partial X_i} f(\mu_1, \mu_2, ..., \mu_n) \right] [X_i - \mu_i]$$

$$\mu_Y = E[Y]$$

$$\simeq f(\mu_1, \mu_2, ..., \mu_n) + E\left[\sum_{i=1}^{n} \left[\frac{\partial}{\partial X_i} f(\mu_1, \mu_2, ..., \mu_n) \right] [X_i - \mu_i] \right]$$

$$= f(\mu_1, \mu_2, ..., \mu_n) + \sum_{i=1}^{n} \left[\frac{\partial}{\partial X_i} f(\mu_1, \mu_2, ..., \mu_n) \right] E[X_i - \mu_i]$$

$$= f(\mu_1, \mu_2, ..., \mu_n)$$

$$\therefore \ \mu_Y = f(\mu_1, \mu_2, ..., \mu_n) \tag{9}$$

$$E\left[(Y - \mu_Y)^2 \right] = E\left[\left(f(X_1, X_2, ..., X_n) - f(\mu_1, \mu_2, ..., \mu_n) \right)^2 \right]$$

$$\simeq E\left[\left(\sum_{i=1}^{n} \left(\left. \frac{\partial f}{\partial X_i} \right|_{X=\mu_i} \right) (X - \mu_X) \right)^2 \right]$$

$$= \sum_{i=1}^{n} \sum_{j=1}^{n} \left(\left. \frac{\partial f}{\partial X_i} \right|_{X=\mu_i} \right) \left(\left. \frac{\partial f}{\partial X_j} \right|_{X=\mu_j} \right) E\left[(X_i - \mu_i)(X_j - \mu_j) \right]$$

$$\therefore \ \sigma_Y^2 \simeq \sum_{i=1}^{n} \left(\left. \frac{\partial f}{\partial X_i} \right|_{X=\mu_i} \right)^2 \sigma_{X_i}^2 + \sum_{i=1}^{n} \sum_{\substack{j=1 \\ i \neq j}}^{n} \left(\left. \frac{\partial f}{\partial X_i} \right|_{X=\mu_i} \right) \left(\left. \frac{\partial f}{\partial X_j} \right|_{X=\mu_j} \right) \left(E[X_i X_j] - \mu_i \mu_j \right)$$

$$= \left[\left.\frac{\partial f}{\partial X_1}\right|_{X=\mu_1} \cdots \left.\frac{\partial f}{\partial X_n}\right|_{X=\mu_n} \right] \begin{bmatrix} \sigma_{X_1}^2 & \sigma_{X_1}\sigma_{X_2} & \cdots & \sigma_{X_1}\sigma_{X_n} \\ \sigma_{X_2}\sigma_{X_1} & \sigma_{X_2}^2 & \cdots & \sigma_{X_2}\sigma_{X_n} \\ \vdots & \vdots & \cdots & \vdots \\ \sigma_{X_n}\sigma_{X_1} & \sigma_{X_n}\sigma_{X_2} & \cdots & \sigma_{X_n}^2 \end{bmatrix} \begin{bmatrix} \left.\frac{\partial f}{\partial X_1}\right|_{X=\mu_1} \\ \vdots \\ \left.\frac{\partial f}{\partial X_n}\right|_{X=\mu_n} \end{bmatrix}$$

If the X_i's are independent,

$$\sigma_Y^2 \simeq \sum_{i=1}^{n} \left(\left.\frac{\partial f}{\partial X_i}\right|_{X=\mu_i} \right)^2 \sigma_{X_i}^2$$

$$= \left[\left.\frac{\partial f}{\partial X_1}\right|_{X=\mu_1} \cdots \left.\frac{\partial f}{\partial X_n}\right|_{X=\mu_n} \right] \begin{bmatrix} \sigma_{X_1}^2 & 0 & \cdots & 0 \\ 0 & \sigma_{X_2}^2 & \cdots & 0 \\ \vdots & \vdots & \cdots & \vdots \\ 0 & 0 & \cdots & \sigma_{X_n}^2 \end{bmatrix} \begin{bmatrix} \left.\frac{\partial f}{\partial X_1}\right|_{X=\mu_1} \\ \vdots \\ \left.\frac{\partial f}{\partial X_n}\right|_{X=\mu_n} \end{bmatrix} \qquad (10)$$

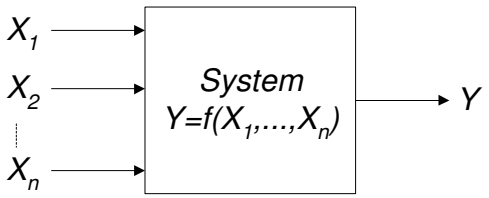

Figure 2-7. A multi-input and single-output system

2.2.2 Derivation of the Variance of Pointing Error

Figure 2-8 shows how the GPS and local angular sensor measurement errors propagate in determining the control angles for the two-axis gimbal, i.e., heading (h) and elevation (e). Each function block in Figure 2-8 and the details about deriving the variance of pointing error are described in Appendix B.

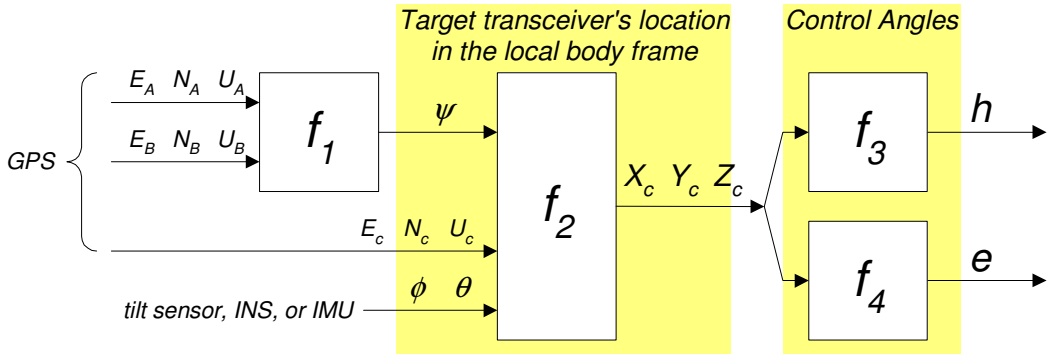

Figure 2-8. Diagram of error propagation in determining the control angles (h and e)

The derivation is based on the following assumptions:

- The distribution of the outputs of GPS and local angular sensors (i.e., $[E_A, N_A, U_A]$, $[E_B, N_B, U_B]$, $[E_C, N_C, U_C]$, ϕ, θ) are normal (e.g., Figures 2-9 and 2-10).
- The outputs of the GPS are uncorrelated:
  - $\sigma_{E_i}\sigma_{N_i} = \sigma_{N_i}\sigma_{E_i} = 0$, $\sigma_{E_i}\sigma_{U_i} = \sigma_{U_i}\sigma_{E_i} = 0$, and $\sigma_{N_i}\sigma_{U_i} = \sigma_{U_i}\sigma_{N_i} = 0$ for $i \in \{A, B, C\}$, where σ_E, σ_N, and σ_U are the variance of the coordinates in the east-axis, north-axis, and up-axis, respectively.
  - $\sigma_{E_i}\sigma_{E_j} = \sigma_{E_j}\sigma_{E_i} = 0$, $\sigma_{N_i}\sigma_{N_j} = \sigma_{N_j}\sigma_{N_i} = 0$, and $\sigma_{U_i}\sigma_{U_j} = \sigma_{U_j}\sigma_{U_i} = 0$ for $i \in \{A, B, C\}$, $j \in \{A, B, C\}$, and $i \neq j$, where σ_E, σ_N, and σ_U are the variance of the coordinates in the east-axis, north-axis, and up-axis, respectively.

- The outputs of the local angular sensors are uncorrelated: $\sigma_\phi \sigma_\theta = \sigma_\theta \sigma_\phi = 0$, where σ_ϕ and σ_θ are the variance of the roll and pitch measurements, respectively.
- GPS and local angular sensors outputs are uncorrelated: $\sigma_i \sigma_j = \sigma_j \sigma_i = 0$ for $i \in \{E_A, N_A, U_A\}$ and $j \in \{A, B, C\}$.
- The actual mean and variance of GPS and local angular sensors outputs are close to the sample mean and variance of the current measurements.
- Any other probable errors (mechanical misalignment of the two-axis gimbal, etc) are all zero.
- The distributions of heading (h) and elevation (e) are normal, and their means are true values leading to the pointing target without error. The magnitude of pointing error is defined as $\sqrt{\sigma_h^2 + \sigma_e^2}$ in which the approximately 68 % pointing errors reside in the range of $\left[\mu_h - \sqrt{\sigma_h^2 + \sigma_e^2}, \mu_h + \sqrt{\sigma_h^2 + \sigma_e^2} \right]$ and $\left[\mu_e - \sqrt{\sigma_h^2 + \sigma_e^2}, \mu_e + \sqrt{\sigma_h^2 + \sigma_e^2} \right]$ (see Appendix C for more details).

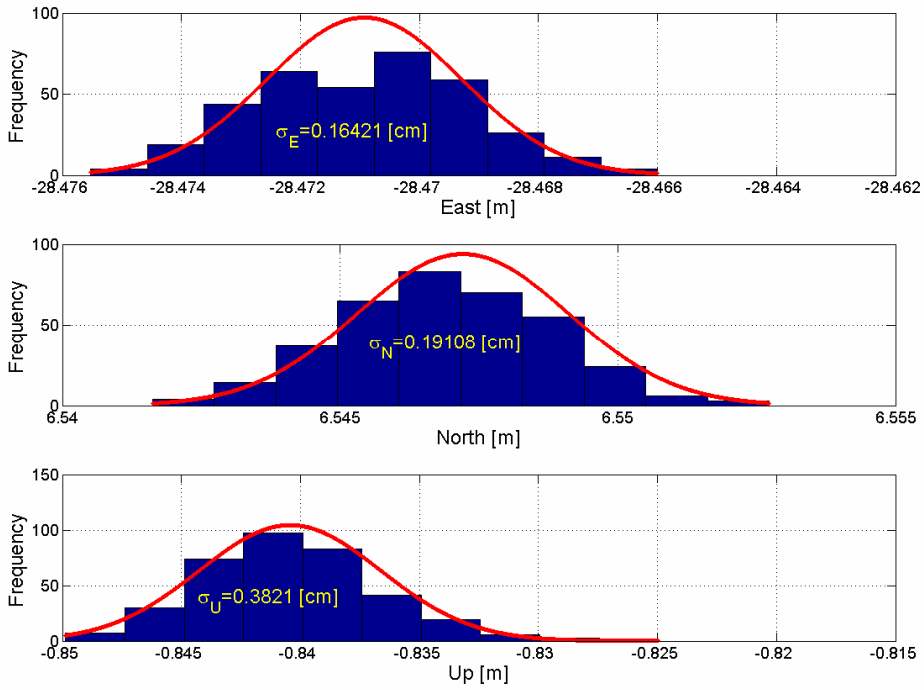

Figure 2-9. Distribution of RTK GPS measurements for 6 minutes (1 per second)

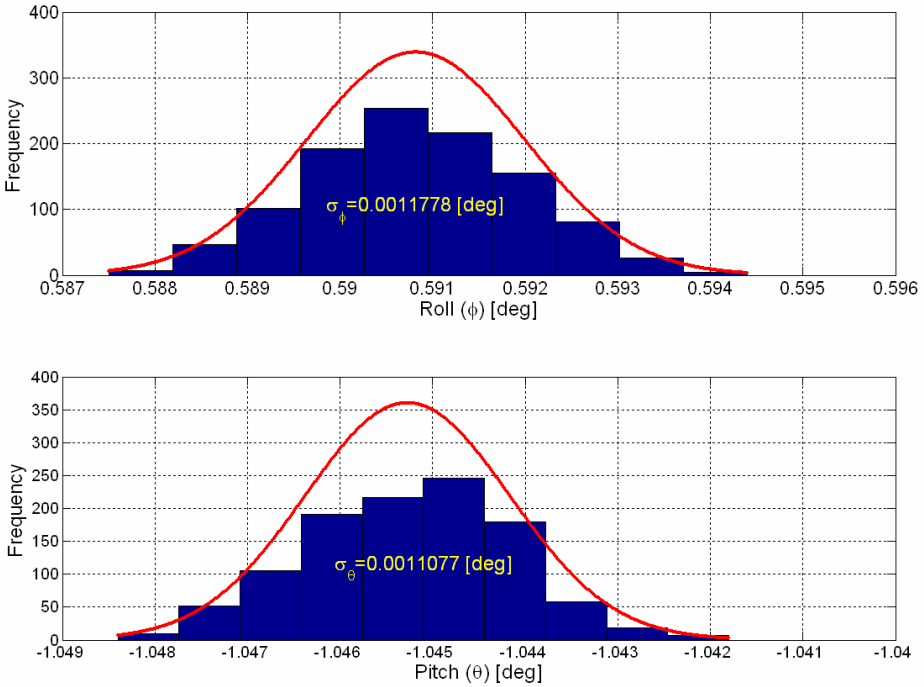

Figure 2-10. Distribution of tilt sensor measurements for 30 minutes (1 per second)

2.2.3 Simulation Results

As derived in Appendix B, the variance of ψ, h and e depends on the measurement errors of GPS and local angular sensors (i.e., σ_E, σ_N, σ_U, σ_ϕ, σ_θ), which are obtained from product specification or actual measurement. The tables in Appendix C show the changes in σ_ψ, σ_h and σ_e according to various measurement errors. Column A represents the length of pointing vector $\overrightarrow{AB}$; Column B shows the length of the baseline vector $\overrightarrow{AC}$ (i.e., link distance) in Figure A-4 (a). Column C represents the measurement errors of GPS and local angular sensors. Column D shows σ_ψ to the GPS measurement error; Columns E and F display σ_h and σ_e, respectively, of both GPS and local angular sensors measurement errors. The columns of each table in Appendix C are generated as follows (see Figure 2-11):

- For simplicity, assume that $\sigma_E = \sigma_N$ and $\sigma_U = 2\sigma_E = 2\sigma_N$ (by observation; e.g., Figure 2-9) and the same relation holds at the locations A, B and C; this assumption reduces the number of possible cases for the GPS measurement error.

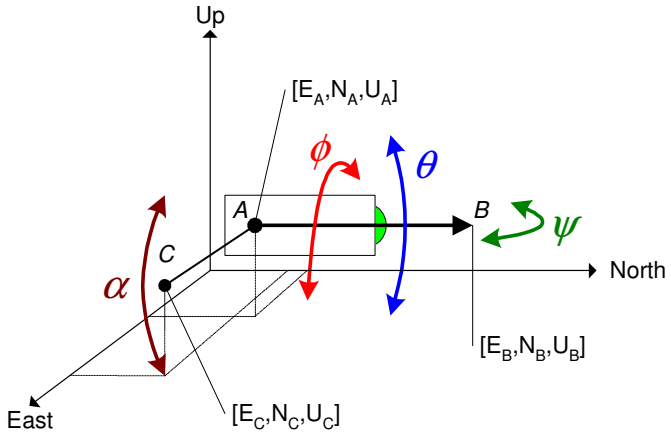

Figure 2-11. Parameters for simulation

- Assume $\sigma_\phi = \sigma_\theta$. This assumption is from the observation (e.g., Figure 2-10).
- For GPS measurement error, seven cases are considered as $\sigma_E (= \sigma_N) \in \{0.5 \text{ cm}, 1 \text{ cm}, 2 \text{ cm}, 0.5 \text{ m}, 1 \text{ m}, 5 \text{ m}, 10 \text{ m}\}$ (Table 2-2); for local angular sensors measurement error, five cases are considered, $\sigma_\phi (= \sigma_\theta) \in \{0.005^o, 0.01^o, 0.04^o, 1.0^o, 2.0^o\}$ (Table 2-3).

Table 2-2. GPS performance and sample models

GPS performance	RTK GPS	Code DGPS	Stand-alone GPS
Horizontal Accuracy	0.5cm, 1cm, 2cm	0.5m, 1m	5m, 10m
Model (price)	NovAtel RT2W > $12,000	FLEXPAK-V1-L1 $2,000	Garmin GPS 18 $200

Table 2-3. Local angular sensors performance and sample models

Local Angular Sensors' performance	High accuracy	Mid accuracy	Low accuracy
Angular accuracy	0.005°, 0.01°, 0.04°	0.3°~1°	1°, 2°
Model (price)	MD900-TS (tilt sensors) $1,254	H746G (INS) $85,000	AHRS400CD (AHRS) n/a

- For the length of $\overrightarrow{AB}$ (i.e, the length of pointing vector), seven cases were considered: i.e., $\left|\overrightarrow{AB}\right| \in \{7.5 \text{ m}, 15 \text{ m}, 40 \text{ m}, 150 \text{ m}, 1\text{km}, 1000 \text{ km}, 1.5\text{E+08 km}\}$, where the first three values (7.5 m, 15 m, 40m) are used in the pointing experiment introduced later section, 1 km and 100 km are approximate distance of building-to-building and ground-to-satellite (LEO), respectively, and 1.5E+08 km is the approximate distance between the earth and the sun (Table 2-4).

Table 2-4. Example of pointing vector with the associated $\left|\overrightarrow{AB}\right|$

	Short range	Mid range	Long range
Length of pointing vector	7.5m, 15m, 40m	150m, 1km	1000km, 1.5E+08km
Example of pointing vector	Two landmarks on the same roof	roof-to-roof	Ground-to-Satellite (1000km) Ground-to-Sun (1.5E+08km)

- For the length of $\overrightarrow{AC}$ (i.e., link distance), five cases were considered: i.e., $\left|\overrightarrow{AC}\right| \in \{39\text{ m}, 264\text{ m}, 1\text{km}, 10\text{km}, 100\text{km}\}$, where the first two values (39 m and 264 m) are used in the mid-range pointing experiments introduced later section, and the others are randomly chosen for a long $\left|\overrightarrow{AC}\right|$ (Table 2-5). In the simulation, first, level $\overrightarrow{AB}$ and $\overrightarrow{AC}$ on the same plane (i.e., setting $U_C = U_B$), and then the position of C was changed by rotating $\overrightarrow{AC}$ upward or downward by the angle α for $-25^\circ \le \alpha \le +25^\circ$ (step size increase: $\Delta\alpha = 5^\circ$). Thus, for each $\left|\overrightarrow{AC}\right| \in \{39\text{ m}, 264\text{ m}, 1\text{km}, 10\text{km}, 100\text{km}\}$, the position of C was changed as many as 11 times.

Table 2-5. Example of pointing with the associated $\left|\overrightarrow{AC}\right|$

	Short range	Mid range	Long range
Link distance	39m	264m	1km, 10km, 100km
Example of pointing		roof-to-roof	Air-to-Ground (1km, 10km) Ground-to-Satellite (100km)

- Roll (ϕ), pitch (θ) and yaw (ψ) were considered in a range of $-25^\circ \le \phi \le +25^\circ$, $-25^\circ \le \theta \le +25^\circ$, and $-90^\circ \le \psi \le +90^\circ$, respectively, with step size of $\Delta\phi = 5^\circ$, $\Delta\theta = 5^\circ$, and $\Delta\psi = 5^\circ$; thus, 11 cases of ϕ and θ and 37 cases of ψ were tried.

- For each set of input parameters (i.e., $\left|\overrightarrow{AB}\right|$, $\left|\overrightarrow{AC}\right|$, σ_E, σ_N, σ_U, σ_ϕ, σ_θ), a total of 49,247 (=11 ×11 ×11 ×37) sets of $(\sigma_\psi, \sigma_h, \sigma_e)$ were generated. Their mean and standard deviation of σ_ψ, σ_h and σ_e are shown in Columns D, E and F of the tables in Appendix C, respectively.

Figure 2-12 plots σ_ψ to $\left|\overrightarrow{AB}\right|$; both axes are on *log 10* scale. Each symbol represents σ_ψ in milliradian; the symbols with the same GPS measurement error are plotted on the same line. The figure implies the followings:

- σ_ψ depends on the GPS measurement error (σ_E, σ_N, σ_U).
- As the GPS measurement error increases (i.e., the performance of GPS is lowered), σ_ψ becomes larger (i.e., the accuracy of yaw measurement becomes worse).
- As $\left|\overrightarrow{AB}\right|$ increases, σ_ψ decreases; thus, the longer $\left|\overrightarrow{AB}\right|$, the smaller the pointing vector error in (2). Figure 2-13 illustrates that the deviation angle from the true pointing vector, ε_1 (i.e., pointing vector error), for short $\left|\overrightarrow{AB}\right|$, which occurs due to the GPS measurement error, is bigger than ε_2 for a longer $\left|\overrightarrow{AB}\right|$; thus, the longer $\left|\overrightarrow{AB}\right|$, the smaller the pointing vector error in (2). Since ψ is computed by the north and east components of the pointing vector, the more accurate ψ is obtained by the pointing vector with the smaller error.

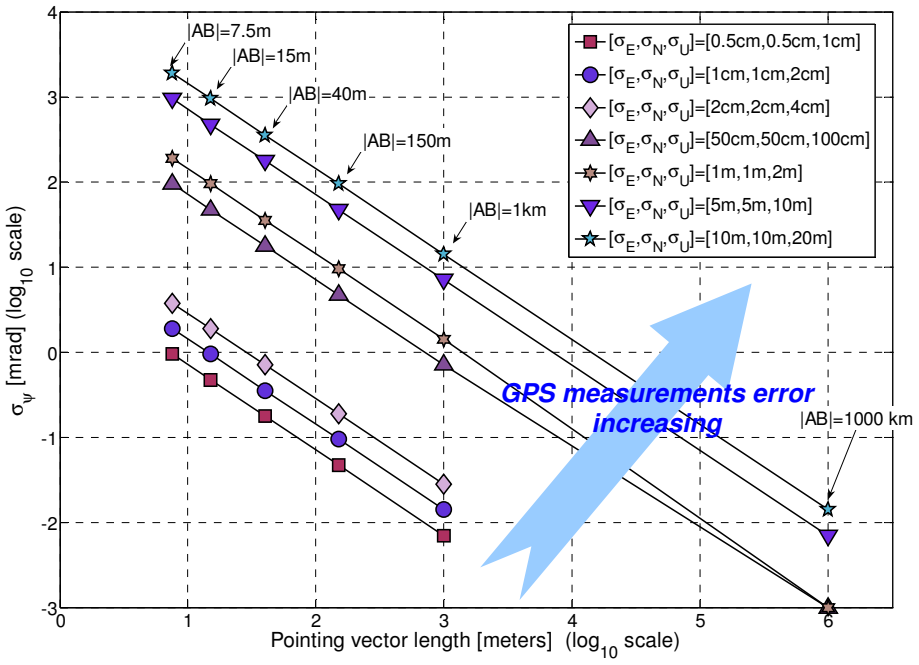

Figure 2-12. σ_{ψ} for various lengths of $\overrightarrow{AB}$ and GPS measurement error

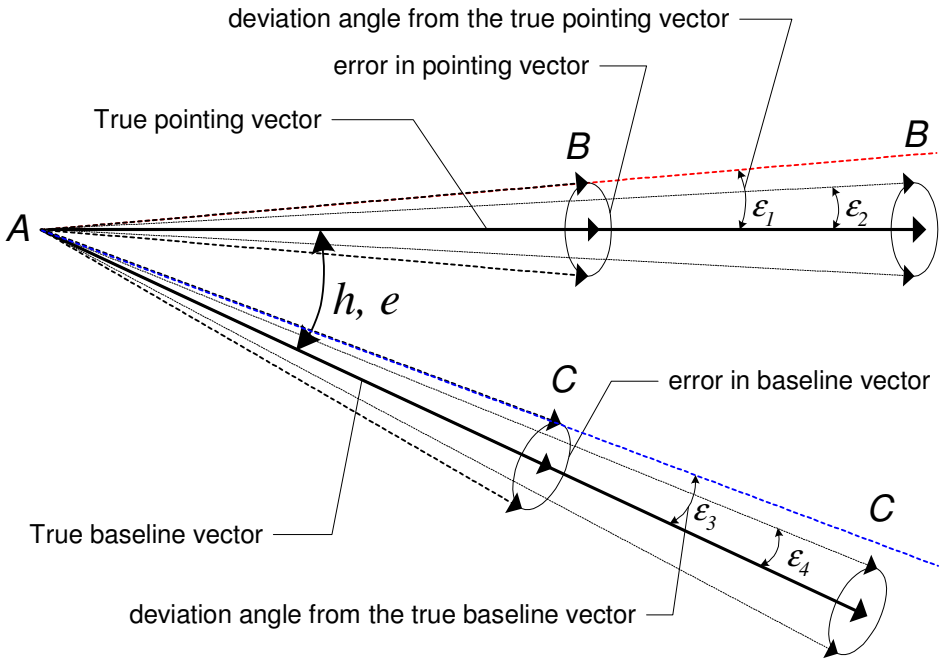

Figure 2-13. Effect of the lengths of $\overrightarrow{AB}$ and $\overrightarrow{AC}$ on σ_h and σ_e

Figures 2-14 (a), (b) and (c) display σ_h and σ_e (both in milliradian) to $\left|\overrightarrow{AB}\right|$ when RTK GPS, Code DGPS, or Stand-alone GPS is employed; the x-axis is on a *log 10* scale. The symbols with the same value of $\left|\overrightarrow{AC}\right|$ are plotted on the same curve. The figures show that:

- The higher the GPS positioning accuracy, the lower σ_h and σ_e. For instance, σ_h and σ_e are less than 2 milliradian when the GPS measurement error is close to the one of RTK GPS ($\sigma_E (= \sigma_N) = 1$ cm and $\sigma_U = 2$ cm) as shown in Figure 2-14 (a). However, Figure 2-14 (b) shows that σ_h and σ_e are much increased when RTK GPS is replaced with Code DGPS ($\sigma_E (= \sigma_N) = 1$ m and $\sigma_U = 2$ m); when Code DGPS is replaced with Stand-alone GPS (i.e., $\sigma_E (= \sigma_N) = 10$ m and $\sigma_U = 20$ m), σ_h and σ_e are increased as much as ten times as shown in Figure 2-14 (c).
- For the same length of $\left|\overrightarrow{AB}\right|$, the longer $\left|\overrightarrow{AC}\right|$, the lower σ_h and σ_e. As illustrated in Figure 2-13, the heading (h) and elevation (e) is angles between $\overrightarrow{AB}$ and $\overrightarrow{AC}$; aligning $\overrightarrow{AB}$ on $\overrightarrow{AC}$ requires rotating it by the angles h and e. The longer $\left|\overrightarrow{AC}\right|$, the smaller the deviation angle from the true baseline vector (i.e., $\varepsilon_3 > \varepsilon_4$) and thus the more accurate $\overrightarrow{AC}$.
- σ_h and σ_e become smaller as the values σ_ϕ and σ_θ decrease, as shown in Figure 2-14 (a).

- If the pre-determined target at B is a stellar target (e.g., star or satellite) with known position coordinates whose distance to the Earth's surface is over hundreds of kilometers (e.g., Low Earth Orbit: 200~2,000 km, Geosynchronous Orbit: 35,786 km above Earth's surface) and $\left|\overrightarrow{AC}\right| \geq 1$ km, even Code DGPS and Stand-alone GPS can provide around 0.091 milliradian and 0.326 milliradian pointing accuracy at best (i.e., $\sqrt{\sigma_h^2 + \sigma_e^2} = 0.091$ or 0.326 milliradian), respectively, with $\sigma_\phi (= \sigma_\theta) = 0.005^o$ (Table 2-6).

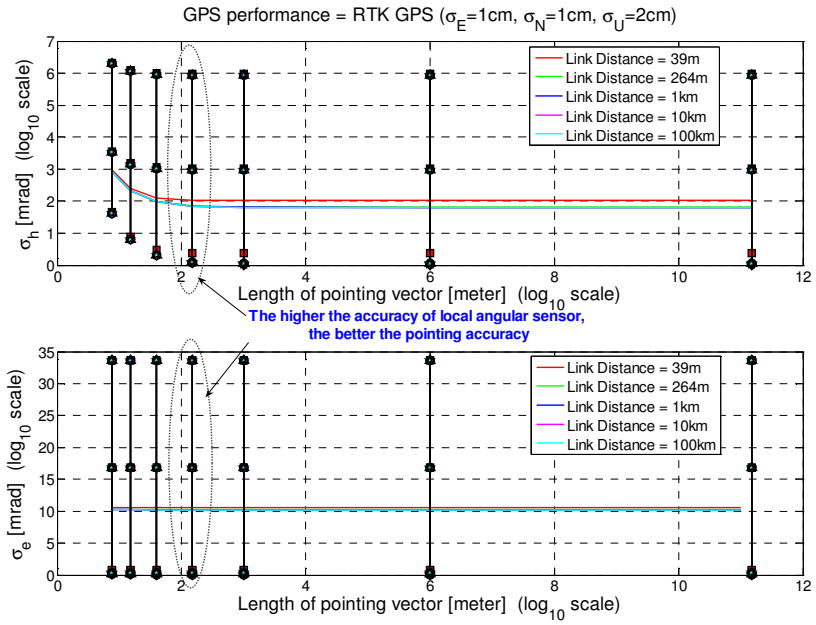

(a) σ_h and σ_e: when RTK GPS is employed

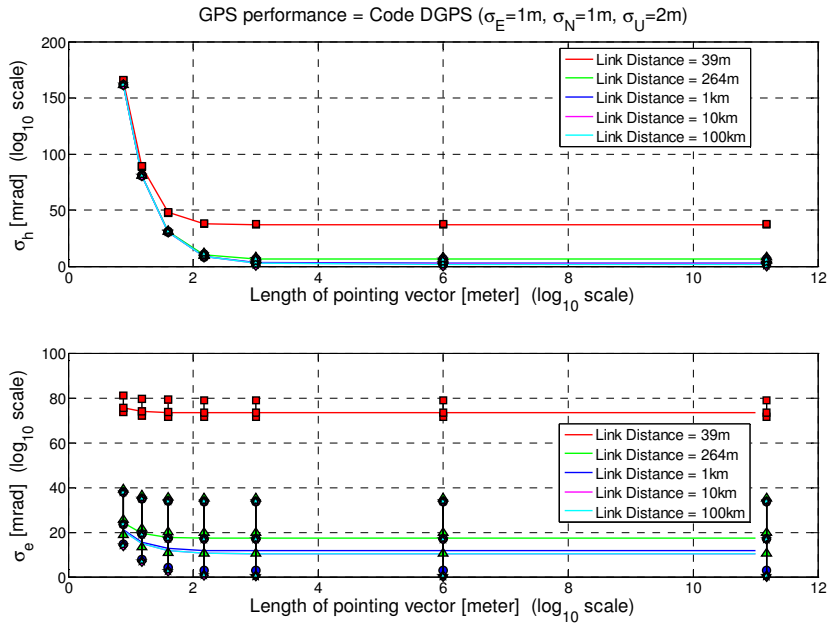

(b) σ_h and σ_e : when Code DGPS is employed

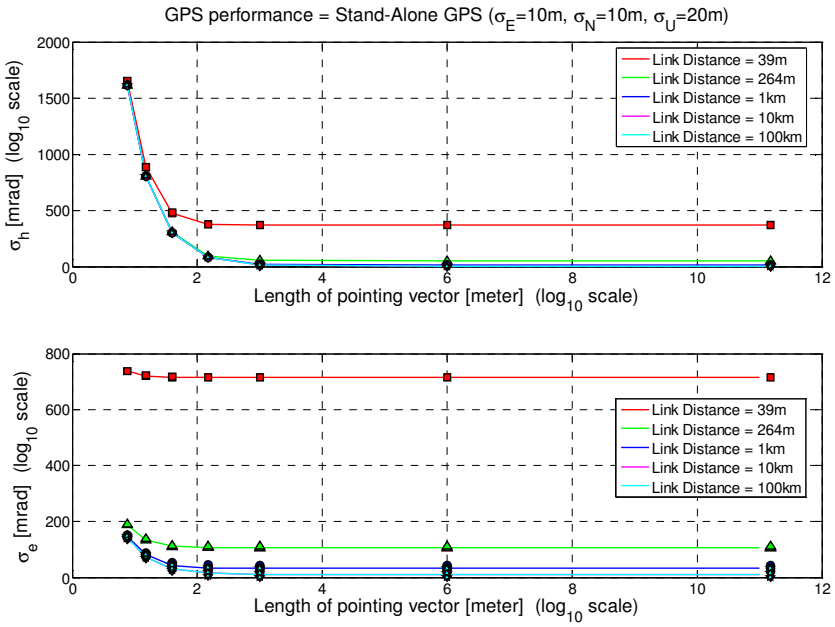

(c) σ_h and σ_e : when stand-alone GPS is employed

Figure 2-14. σ_h and σ_e for various lengths of $\overrightarrow{AB}$ and $\overrightarrow{AC}$ and GPS and local angular sensor measurement errors

Table 2-6. Pointing accuracy variation to the GPS and local angular sensors performance with $\left|\overrightarrow{AB}\right| > 100$ km and $\left|\overrightarrow{AC}\right| \geq 1$ km (Tables C-6 and C-7)

Local Angular Sensors Performance	GPS Performance	
	Code DGPS (σ_E=σ_N=1 m)	Stand-alone GPS (σ_E=σ_N=10 m)
$0.005^\circ \leq \sigma\_\phi, \sigma\_\theta \leq 0.02^\circ$	0.091~3.159 mrad	0.326~31.399 mrad
$1^\circ \leq \sigma\_\phi, \sigma\_\theta \leq 2^\circ$	17.099~34.367 mrad	17.104~46.535 mrad

(A) Sub-milliradian Pointing Accuracy with Highly Accurate Pointing Sensors

Tables in Appendix C show that when RTK GPS with $\sigma_E (= \sigma_N) \leq 0.5$ cm and $\sigma_U \leq 1\ cm$ and local angular sensors with $0.005^o \leq \sigma_\phi (= \sigma_\theta) \leq 0.02^o$ are used, one milliradian pointing accuracy (i.e., $\sqrt{\sigma_h^2 + \sigma_e^2} = 0.001$ radian) can be obtained for $\left|\overrightarrow{AB}\right| \geq 7.5$ m and $\left|\overrightarrow{AC}\right| \geq 39$ m; when RTK GPS with $\sigma_E (= \sigma_N) \leq 1$ cm and $\sigma_U \leq 2$ cm and local angular sensors with $0.005^o \leq \sigma_\phi (= \sigma_\theta) \leq 0.02^o$ are used, one milliradian pointing accuracy can be obtained for $\left|\overrightarrow{AB}\right| \geq 15$ m and $\left|\overrightarrow{AC}\right| \geq 264$ m; when RTK GPS with $\sigma_E (= \sigma_N) \leq 1$ cm and $\sigma_U \leq 2$ cm and local angular sensors with $\sigma_\phi (= \sigma_\theta) \leq 0.005^o$ are used, tens of microradian pointing accuracy can be obtained for $\left|\overrightarrow{AB}\right| \geq 1$ km and $\left|\overrightarrow{AC}\right| \geq 1$ km.

(B) Special Case with $\sigma_\phi = \sigma_\theta = 0$ and $\sigma_\psi \neq 0$

This case corresponds to when there is no error in the roll (ϕ) and pitch (θ) measurements of mobile or static platform. It means that either the accuracy of local

angular sensors is very high or the platform is placed at a location whose roll and pitch angle are precisely determined in advance. In this case, GPS measurement error dominates the pointing error by assuming there are no other error sources except for GPS. Figure 2-15 shows the pointing error (i.e., $\sqrt{\sigma_h^2 + \sigma_e^2}$) on a log 10 scale for $1 \text{ km} \le \left|\overrightarrow{AB}\right| \le 10^4 \text{ km}$ and $1 \text{ km} \le \left|\overrightarrow{AC}\right| \le 10^4 \text{ km}$; for the GPS performance, Stand-alone GPS (i.e., $\sigma_E (= \sigma_N) = 10 \text{ m}$ and $\sigma_U = 20 \text{ m}$) was considered.

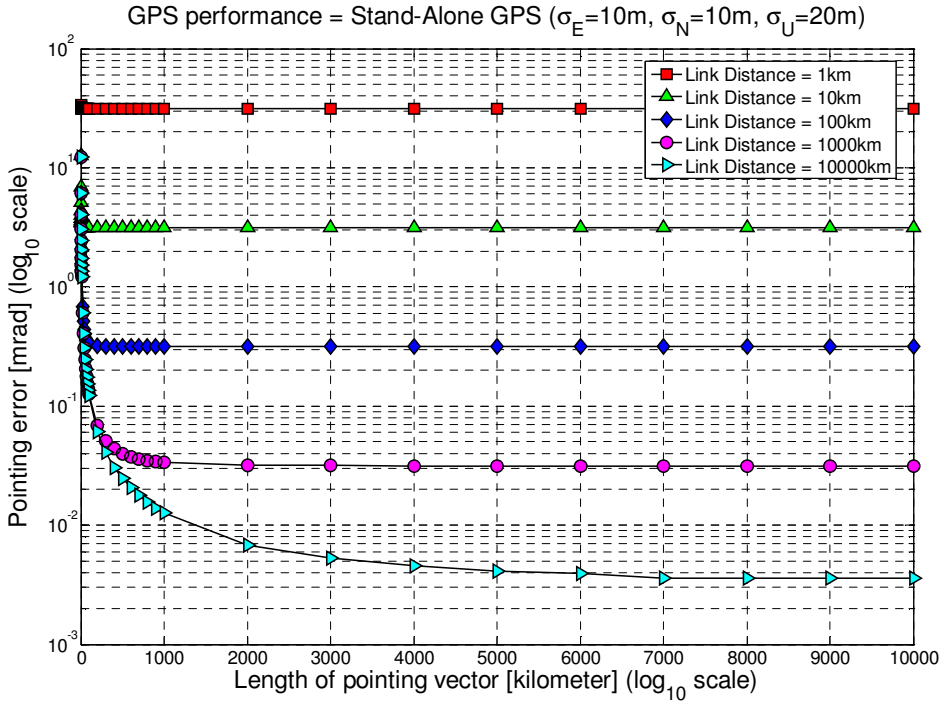

Link distance	1 km	10 km	100 km	1000 km	10000 km
Minimum pointing error	31.398 mrad	3.140 mrad	0.314 mrad	0.031 mrad	0.004 mrad

Figure 2-15. Pointing error ($\sqrt{\sigma_h^2 + \sigma_e^2}$) for $1 \text{ km} \le \left|\overrightarrow{AB}\right| \le 10^4 \text{ km}$ and $1 \text{ km} \le \left|\overrightarrow{AC}\right| \le 10^4 \text{ km}$ when $\sigma_\phi = \sigma_\theta = 0$ (GPS performance: Stand-alone GPS)

Figure 2-16 shows $\sqrt{\sigma_h^2+\sigma_e^2}$ values on a log 10 scale for $1\text{ km} \le \left|\overrightarrow{AB}\right| \le 10^4$ km and $1\text{ km} \le \left|\overrightarrow{AC}\right| \le 10^3$ km; for the GPS performance, Code GPS (i.e., $\sigma_E (= \sigma_N) = 1$ m and $\sigma_U = 2$ m) was considered.

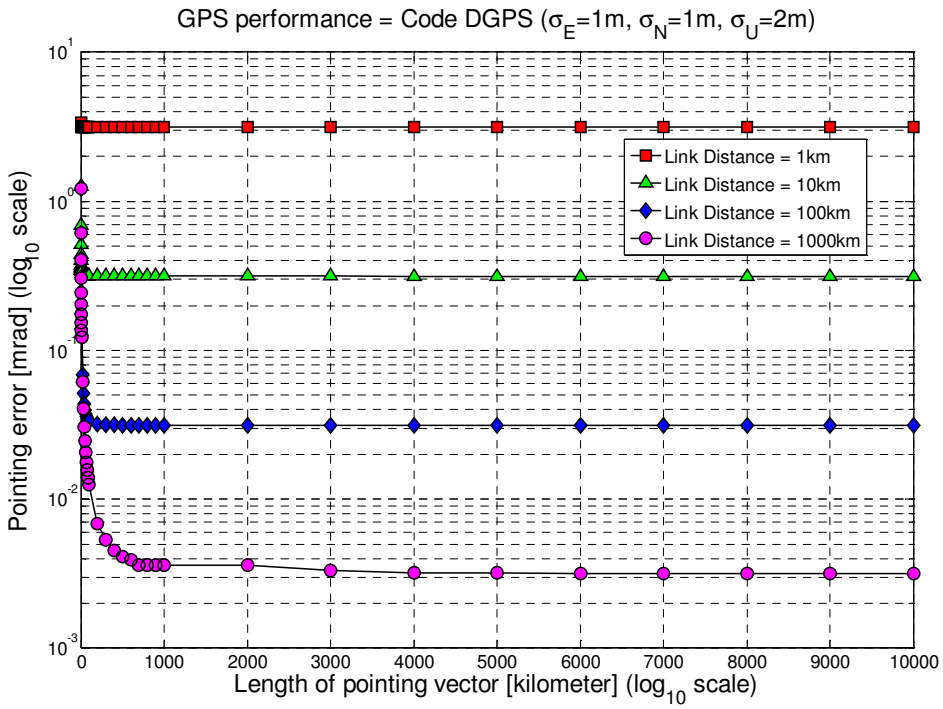

Link distance	1 km	10 km	100 km	1000 km
Minimum pointing error	3.140 mrad	0.314 mrad	0.031 mrad	0.003 mrad

Figure 2-16. Pointing error ($\sqrt{\sigma_h^2+\sigma_e^2}$) for $1\text{ km} \le \left|\overrightarrow{AB}\right| \le 10^4$ km and $1\text{ km} \le \left|\overrightarrow{AC}\right| \le 10^3$ km when $\sigma_\phi = \sigma_\theta = 0$ (GPS performance: Code DGPS)

Figure 2-17 shows $\sqrt{\sigma_h^2+\sigma_e^2}$ values on a log 10 scale for $1\text{ km} \le \left|\overrightarrow{AB}\right| \le 10^4$ km and $1\text{ km} \le \left|\overrightarrow{AC}\right| \le 10^2$ km; for the GPS performance, RTK GPS (i.e., $\sigma_E (= \sigma_N) = 1$ cm and $\sigma_U = 2$ cm) was considered.

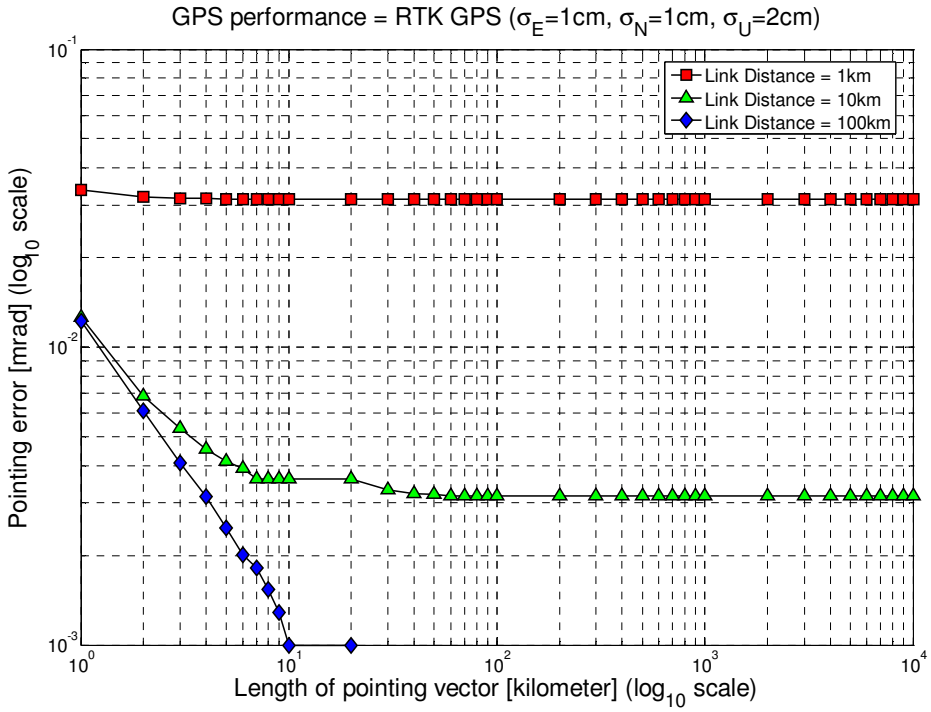

Link distance	1 km	10 km	100 km
Minimum pointing error	0.031 mrad	0.003 mrad	0.000 mrad

Figure 2-17. Pointing error (σ_ψ) for $1\text{ km} \le \left|\overrightarrow{AB}\right| \le 10^4$ km and $1\text{ km} \le \left|\overrightarrow{AC}\right| \le 10^2$ km when $\sigma_\phi = \sigma_\theta = 0$ (GPS performance: RTK GPS)

(C) Cost Consideration: Low-Cost Pointing System

The measurement errors of GPS and local angular sensors are closely related to the accuracy specification and hardware cost of the position and angular sensor devices. For example, the positioning accuracy of a GARMIN GPS receiver (Model: GPS 18 – 5 Hz) is less than 15 m and its price is around $200 (www8.garmin.com). The price of the NovAtel RTK GPS receiver is more than $12,000; the positioning accuracy is much higher than the GARMIN GPS receiver (2 cm versus 15 m). For a higher pointing accuracy of milliradian to microradian, the NovAtel RTK GPS

receiver is preferred to the cheap and less accurate GARMIN GPS receiver. However, if the beam divergence angle (θ_{beam} in Figure 1-2) of FSO transceiver is wide enough to cover 30 milliradian pointing error, then the GARMIN GPS receiver is preferable when $\left|\overrightarrow{AB}\right| \geq 1\,\text{km}$ and $\left|\overrightarrow{AC}\right| \geq 10\,\text{km}$. The formula and tables for σ_h and σ_e over the GPS and local angular sensors measurements in Appendices B and C would be useful to select GPS receiver and local angular sensors with reasonable cost.

(D) Application to the Point-to-Point Radio Antenna Alignment

The pointing method in Section 2.1 can be applied to the initial alignment of directional point-to-point radio transceivers such as AirMux200 which uses a relatively narrow RF beam (9°=157.08 millradian) to transmit and receive data at 48 Mbps. "To achieve the best benefit and link budget from the AirMux installation," the directional antennas between two transceivers must be aligned to face each other (see Site Survey and Alignment Guide at http://www.rad.com). If the link distance (i.e., $\left|\overrightarrow{AC}\right|$) is over 1 km, then the Stand-alone GPS (i.e., $\sigma_E (= \sigma_N) = 10\,\text{m}$) can provide about 80 milliradian pointing accuracy with $\left|\overrightarrow{AB}\right| = 150\,\text{m}$; the pointing accuracy would be more improved with $\left|\overrightarrow{AB}\right| > 150\,\text{m}$ (see the tables in Appendix C).

2.3 Experimental Results

In the previous sections, we have presented a precise pointing method with RTK GPS and local angular sensors in which the pointing accuracy was improved as the length of pointing vector and the distance between local optical transceiver and remote target transceiver increases (Section 2.1). In Section 2.2, it was described how the pointing sensors measurement errors propagates into the pointing system and how they affect the pointing accuracy.

In this section, we present experimental results obtained by the implementation of the pointing method in Section 2.1 with a pre-determined target as shown in Figure 2-4 (b). First, we describe a mid-range pointing experiment using an outdoor testbed on the University of Maryland campus in College Park. The experiment employed only RTK GPS with a static platform (i.e., two-axis gimbal) on a flat surface by which the roll and pitch was kept to zero. The purpose of the experiment was observing pointing accuracy improvement as the length of pointing vector increases (the distance to the pointing target is fixed to 264 m). Next, a reliability test was conducted to show how quickly (in seconds) and successfully (in %) the sub-milliradian accuracy would be obtained with an automatic pointing system (Figure 2-27); the length of pointing vector was around 15 m and the distance to the pointing target was around 39 m. For both experiments, a He-Ne laser ($\lambda = 633$ nm) was used to mimic the FSO transceiver because of the low load bearing capacity of our small two-axis gimbal. The following sections provide more details on the two pointing experiments.

2.3.1 Components of Pointing System

The pointing system used in the experiments consists of RTK GPS, bi-axial tilt sensors, personal computer, and two-axis gimbal as shown in Figure 2-18. The two pointing sensors and two-axis gimbal have RS-232 serial interface. National Instruments USB-232/4 (4-Port USB to RS-232 Converter) and serial port input/ouput functions in MATLAB (version 7.0) were used to control the serial interfaces for *i)* collecting measurement data from the RTK GPS and bi-axial tilt sensors and *ii)* controlling two axes of the gimbal with stepping motors and motor controllers (Model: VEXTA AS66AAP2-H50 and AS46AAP2-H50). The angle resolution of each stepping motor is 0.0072° (= 0.12566 milliradian) which is equivalent to 50,000 steps per circle (360°); Figure 2-19 shows the two-axis gimbal in our outdoor testbed. The time to compute the control angles (heading and elevation) was taken less than 0.02 sec by MATLAB (version 7.0).

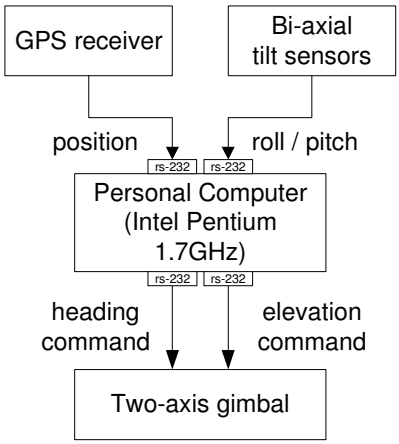

Figure 2-18. Diagram of a pointing system

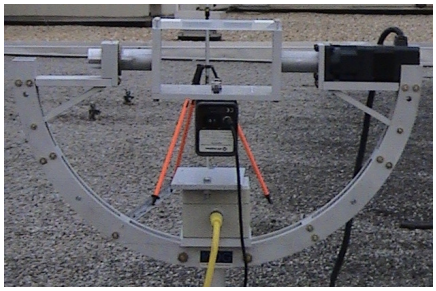

Figure 2-19. A two-axis gimbal with stepping motors (0.0072°/step)

(A) Pointing Sensors: RTK GPS and Bi-axial Tilt Sensors

Figure 2-20 shows two high accurate sensors, RTK GPS and bi-axial tilt sensors, which are used to implement the pointing method in Section 2.1:

- Real-Time Kinematic GPS (Model: NovAtel RT2W):

  It provides 2 cm (=0.79 inch) horizontal positioning accuracy on the fly (in a real-time differential GPS mode) as shown in Figure 2-22; it was used to measure yaw (ψ) of the pointing vector as well as a precise position of the two nodes.

- Biaxial tilt sensor (Model: Applied Geomechanics MD900-TS):

  Its repeatability and angle resolution are 0.01° and 0.004°, respectively, at ±25 degree range in two-axis; it was used to measure roll (ϕ) and pitch (θ) of the platform (e.g., gimbal or optical transceiver).

(a) NovAtel RT2W (185×154×71 *mm*) (b) MD900-TS (120×80×60 *mm*)

Figure 2-20. RTK GPS and biaxial tilt sensor

The RTK GPS is designed for both static and mobile platforms. In a dynamic environment with a mobile platform such as a vehicle, the bi-axial tilt sensor can be replaced with an inertial navigation sensor to measure the roll and pitch of the mobile platform.

(B) RTK GPS System

A RTK GPS system consists of two sets of RTK GPS receivers and antennas (one set for Base Station, and the other for Rover Station) and wireless (or wired) data transceivers as shown in Figure 2-21. The Base Station broadcasts the GPS signal error corrections (RTK messages) measured on its known location. The Rover Station corrects its positioning error with the RTK messages.

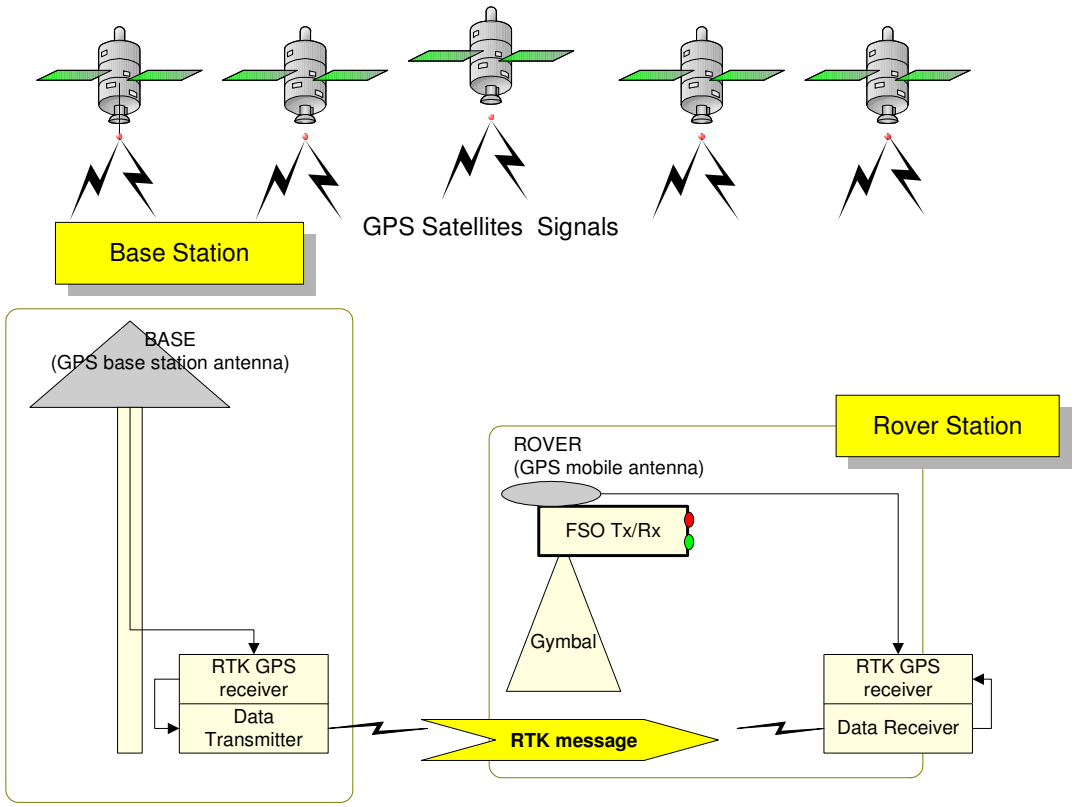

Figure 2-21. RTK GPS system

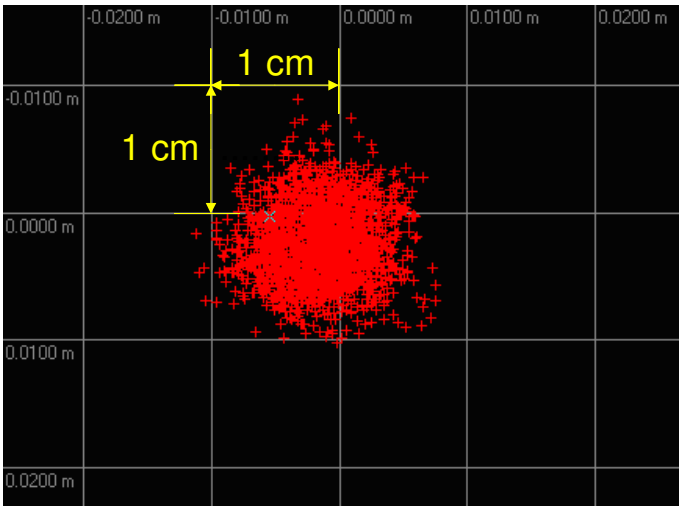

Figure 2-22. Horizontal Accuracy of RTK GPS receiver
(NovAtel RT2W; data collection time: 3 minutes)

(C) Inertial Navigation System

An INS consists of three-axis accelerometers and three-axis gyroscopes. It is widely used in air navigation, and provides the position (P), velocity (V), and acceleration (A) by sensing the accelerations and angular velocities of a vehicle by accelerometers and gyroscopes, respectively. In principle, a vehicle's position is obtained by double integration of the acceleration; vehicle's attitude angles (i.e., roll, pitch, and yaw) are obtained by integration of the angular velocities. The resulting position and attitude angles correspond to their total changes from the initial position. Figure 2-23 shows the attitude angles of an aircraft.

However, this integration accumulates position errors due to the measurement noise and non-linearity of accelerometers and gyroscopes; thus the position error increases with time (Nebot 1999). This shortcoming of INS can be overcome by

using GPS position information in the integration because GPS provides stable accuracy of position for long periods of time (Lee et al., 2001). Figure 2-24 shows an example of a GPS/INS integration system.

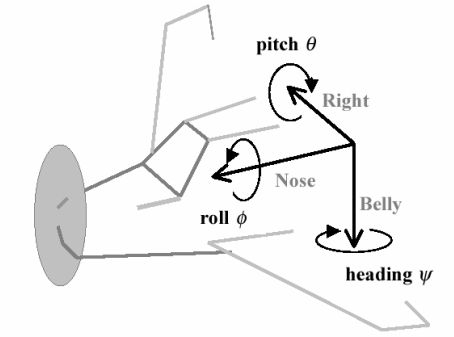

Figure 2-23. Attitude angles of aircraft (www.javad.com)

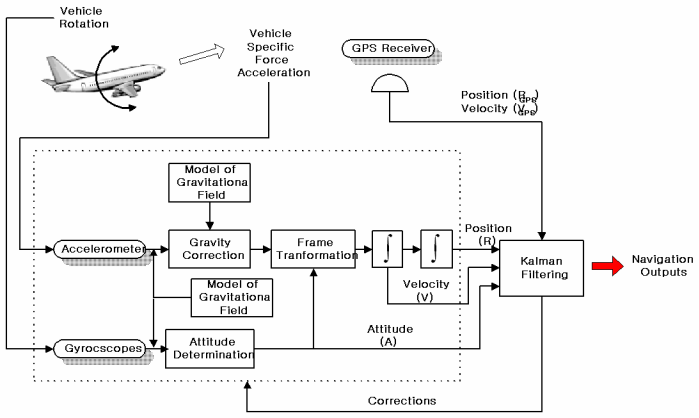

Figure 2-24. Example of GPS/INS integration system (Lee et al., 2001)

2.3.2 A Mid-Range Pointing Experiment

We have carried out a mid-range pointing experiment between two distant buildings (roof-to-roof) on the University of Maryland campus in College Park; its purpose was to test how the length of D affects pointing accuracy of the proposed

method.

By keeping roll and pitch close to zero (i.e., $\phi = 0$, $\theta = 0$), Equation (5) is simplified to $P_B = C(\psi)P_{ENU}$, which means that RTK GPS positioning error is a major error source influencing the pointing accuracy. As D increases, the measurement error in the pointing vector becomes smaller, which renders measurement error in yaw (ψ) smaller; consequently the pointing vector transformed to the body frame becomes more accurate. Hence, we can control the heading and elevation angles of the two-axis gimbal more precisely.

In this experiment, the pointing vector was measured by the pointing method depicted in Figure 2-4 (b). Figure 2-25 shows the diagram of the experiment. The position coordinates at B was pre-determined by RTK GPS (Model: NovAtel RT2W). A pointing target mimicking an FSO transceiver placed at a remote site C (equivalent to the location B in Figure 2-4 (a)). The distance between the two points A and C was 264 m.

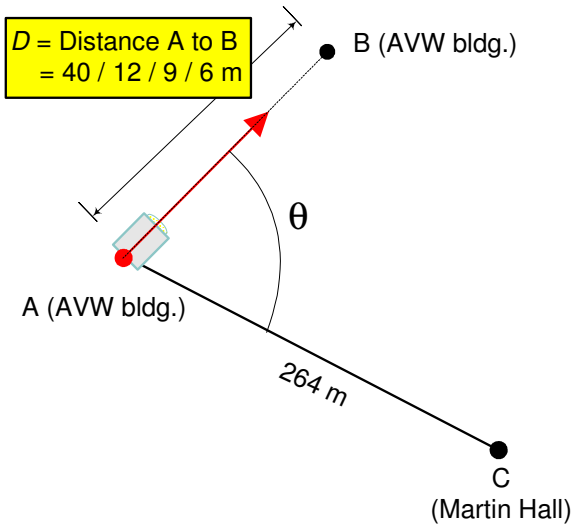

Figure 2-25. Diagram of the mid-range pointing experiment

Table 2-7 presents the pointing accuracy obtained from the experiment. Figure 2-26 shows our definition of the pointing error in Table 2-7. The pointing error is defined as the distance from the pointing target C. Because the distance between A and C is 264 m, a distance of 0.264 m corresponds to a 1 milliradian pointing error.

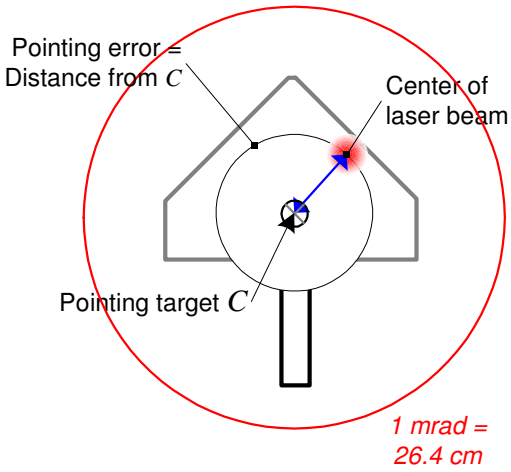

Figure 2-26. The pointing target used in the experiment.

In Table 2-7, the first column represents the distance between A and B. The position coordinates of A were $[50.621, 259.58, 1.4734]^T$ with $\sigma_E = 0.26$ cm, $\sigma_N = 0.36$ cm, and $\sigma_U = 0.88$ cm. For each distance, we conducted the pointing experiment at four different sites for B with one site for A; thus, the total number of pointing trials was sixteen. The second column shows the pointing error range corresponding to the different locations of B. The third column summarizes the standard deviation values of the ENU coordinates of B; they show that the horizontal and vertical positioning errors of RTK GPS coordinates are within ±1 cm and ±2 cm with 95 % confidence limits, respectively. The last column displays the Position Dilution of Precision (PDOP) for the RTK GPS position coordinates, in which PDOP was within the normal range between 1 and 6. As we mentioned in the previous section, the pointing error decreases with increasing D. We observed that fourteen of the sixteen pointing trials satisfied the 1 milliradian pointing accuracy; two cases (one with D=6 m and the other with D=9 m) were outside the 1 milliradian radius.

Table 2-7. The mid-range pointing experiment results

D (m)	Pointing Error		$(\sigma_E, \sigma_N, \sigma_U)$ in P_{ENU} at B (unit: cm)	PDOP
	min	max		
40	0.06 m (0.23 mrad)	0.17 m (0.64 mrad)	min: (0.18, 0.19, 0.48) max: (0.29, 0.41, 0.73)	1.3~1.9
12	0.10 m (0.38 mrad)	0.20 m (0.76 mrad)	min: (0.15, 0.23, 0.40) max: (0.25, 0.31, 0.75)	1.4~1.9
9	0.05 m (0.19 mrad)	0.27 m (1.02 mrad)	min: (0.14, 0.19, 0.56) max: (0.33, 0.56, 0.86)	1.3~3.1
6	0.12 m (0.45 mrad)	0.50 m (1.89 mrad)	min: (0.11, 0.17, 0.42) max: (0.41, 0.32, 0.91)	1.4~3.0

2.3.3 A Reliability Test with an Automatic Pointing System

In the previous section, the sub-milliradian pointing accuracy was achieved with $D = 12$ and 40 meters by using RTK GPS. This section provides a reliability test result presenting how quickly (in seconds) and successfully (percentage success) the pointing method can obtain such accuracy. The test was conducted as follows:

- An automatic pointing system was built as Figure 2-27. The system employed RTK GPS (model: NovAtel RT2W), bi-axial tilt sensors (model: Applied Geomechanics MD900-TS) and a two-axis gimbal (step size per axis: 0.0072°/step).
- The pointing vector $\overrightarrow{AB}$ ($\left|\overrightarrow{AB}\right| = 15\ m$) was measured by the same pointing method as the mid-range pointing experiment. A helium-neon laser ($\lambda = 633\ nm$) was used to imitate an FSO transceiver; the laser pointer was located at A. The position coordinate at B was pre-determined by the RTK GPS. A pointing target imitating an FSO transceiver was placed at a remote site C ($\left|\overrightarrow{AC}\right| = 39\ m$). Figure 2-28 (a) shows the diagram of the experiment.
- A personal computer collected the RTK GPS measurement for 0.5 second (update rate: 1 per 0.1 second) and the bi-axial tilt sensors measurement for 0.5 second (update rate: 1 per 0.25 second). Then, the five measurements of RTK GPS are averaged to generate the ENU coordinates of B; the mean value of two measurements of bi-axial tilt sensors is set as roll (ϕ) and pitch (θ) of FSO transceiver mounted on the two-axis gimbal. Finally, the personal computer calculated the heading (h) and elevation

(e) to the target C, and controlled the two-axis gimbal by the control angles (Figure 2-28).

- Three pointing experiments were conducted at three different heights (i.e., U_B) of B with one site of A; the pitch angle (θ) corresponding to the height change was around 1°, 1.5°, or 2° as shown in Figure 2-28 (b). Each experiment consisted of 50 automatic pointing trials. Each trial contained 0.5 second RTK GPS measurement and 0.5 second bi-axial tilt sensors measurement; after the data collection, the two-axis gimbal was rotated by the heading and elevation commands from the personal computer. Then, the position of each axis of gimbal was reset to the original position. The actual pointing error (i.e., how much distance or angle was deviated from the center of target at C) for the 50 trials of each experiment is displayed in Figures 2-29~2-31.

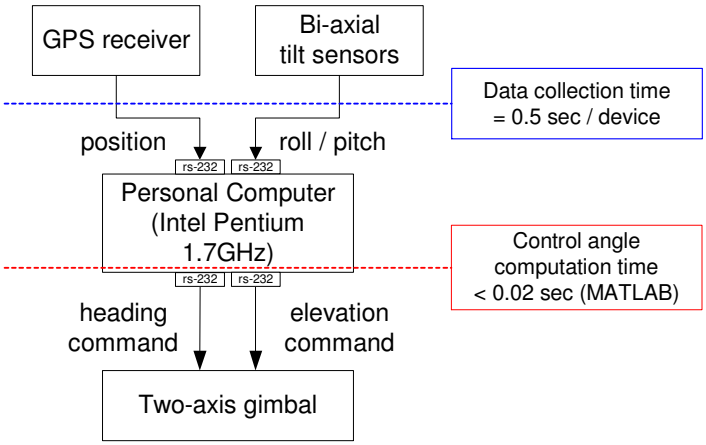

Figure 2-27. Diagram of an automatic pointing system

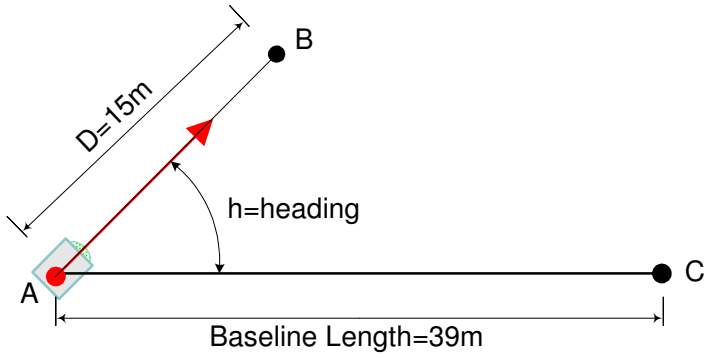

(a) Top-down view

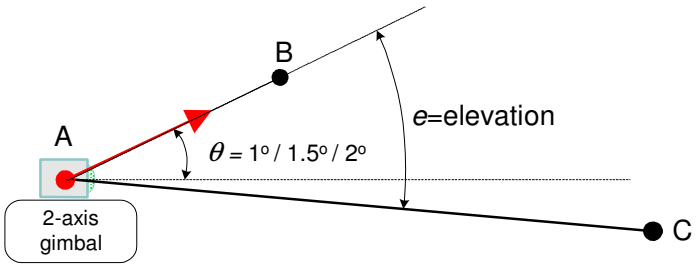

(b) Lateral view

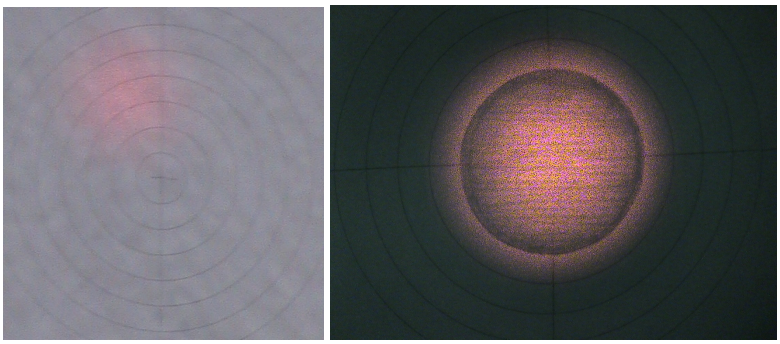

(c) Pointing target at C (a laser beam on bull's eye)

Figure 2-28. Diagram of the reliability test with an automatic pointing system

Figures 2-29~2-31 show the heading and elevation commands and the pointing errors for each experiment; the heading and elevation commands were generated by $h \times \frac{50000\ steps}{360^{\circ}}$ and $e \times \frac{50000\ steps}{360^{\circ}}$. The heading error ($\varepsilon_h$) and

elevation error (ε_e) were measured by horizontal and vertical distances from the center of target at C as shown in Figure 2-28 (c); the distance (meters) was converted to the associated angle (milliradians); $\sqrt{\varepsilon_h^2 + \varepsilon_e^2}$ is the actual pointing error in milliradians. Table 2-8 summarizes the experimental results. Column A represents the experiment number 1 to 3; each number corresponds to a change in the height (U) of location B. Column C contains the measurements errors of RTK GPS and bi-axial tilt sensors which are listed in Table C-2 (Appendix C). The reference pointing error in Column D was computed by $\sqrt{\sigma_h^2 + \sigma_e^2}$ in which σ_h and σ_e are the associated values to the measurement errors in Column C. Column B shows the actual measurement errors from the five sample measurements of the RTK GPS and the two sample measurements of the bi-axial tilt sensors; since the sample size was small, the actual measurement error of RTK GPS may not represent the real distribution of the errors (i.e., σ_E, σ_N, σ_U). The success rate in Column E is the number of successful trials over 50 trials whose actual pointing error $\sqrt{\varepsilon_h^2 + \varepsilon_e^2}$ is less than or equal to the value in Column D.

The success rate in Experiments 1 and 2 was greater than or equal to 96 %. The success rate of Experiment 3 was 30 % when the reference pointing error was set to $\sqrt{\sigma_h^2 + \sigma_e^2} = 0.5784$ milliradian (i.e., when $\sigma_E = \sigma_N = \frac{\sigma_U}{2} = 0.5$ cm and $\sigma_\phi = \sigma_\theta = 0.005°$); 0.5 cm was from the sample measurements of the RTK GPS. However, the success rate was increased to 100 % when the reference pointing error

was set to $\sqrt{\sigma_h^2 + \sigma_e^2} = 1.1472$ milliradian with $\sigma_E = \sigma_N = \frac{\sigma_U}{2} = 1$ cm and $\sigma_\phi = \sigma_\theta = 0.005°$. Note that both $\sigma_E = \sigma_N = \frac{\sigma_U}{2} = 0.5$ cm and $\sigma_E = \sigma_N = \frac{\sigma_U}{2} = 1$ cm are less than the NovAtel RT2W accuracy specification which is $\sigma_E = \sigma_N = \frac{\sigma_U}{2} = 2$ cm. Figure 2-32 shows three histograms of pointing errors for the above reliability test.

Figure 2-27 implies that the speed of the automatic pointing system is dependent on *i)* the output rate of pointing sensors (i.e., GPS, tilt sensors, INS), *ii)* the position data latency of the remote pointing system, and *iii)* the angular speed of two-axis gimbal; the computation time for generating control angles (heading and elevation) was less than 20 msec with MATLAB (version 7.0).

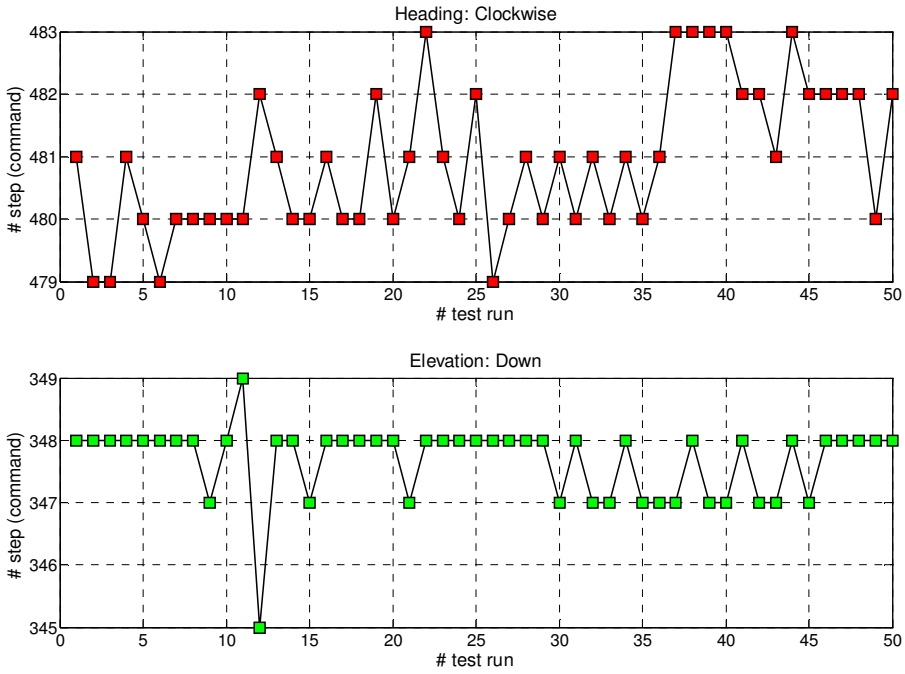

(a) Heading and elevation command

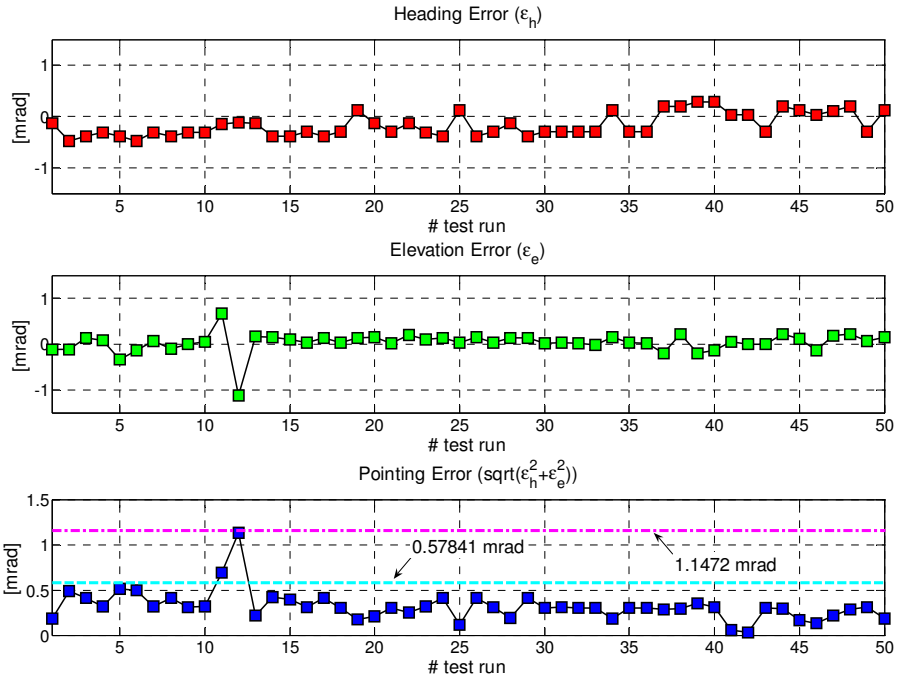

(b) Pointing error

Figure 2-29. Experiment #1: θ=1°

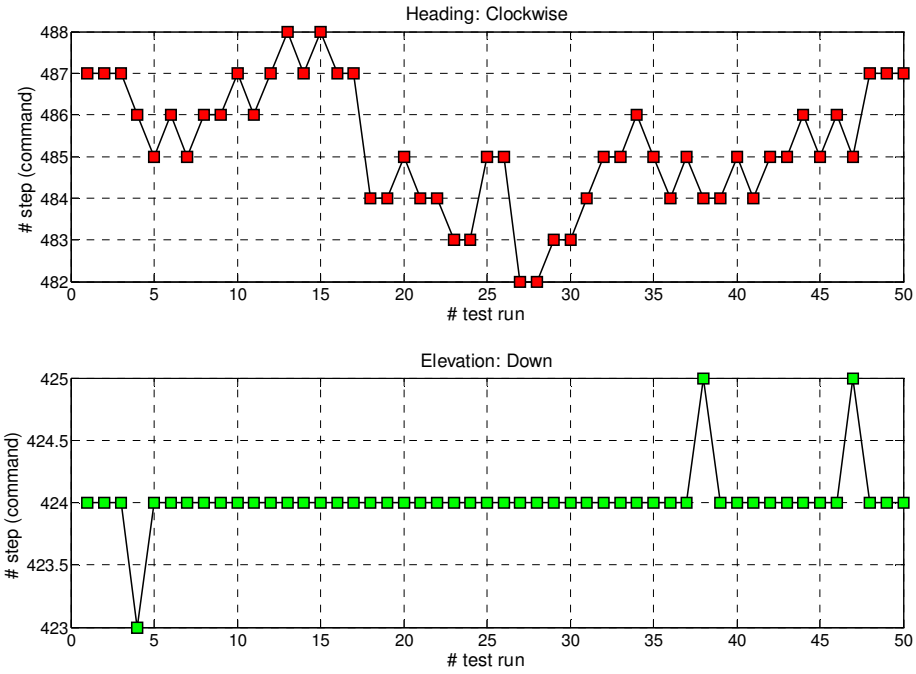

(a) Heading and elevation command

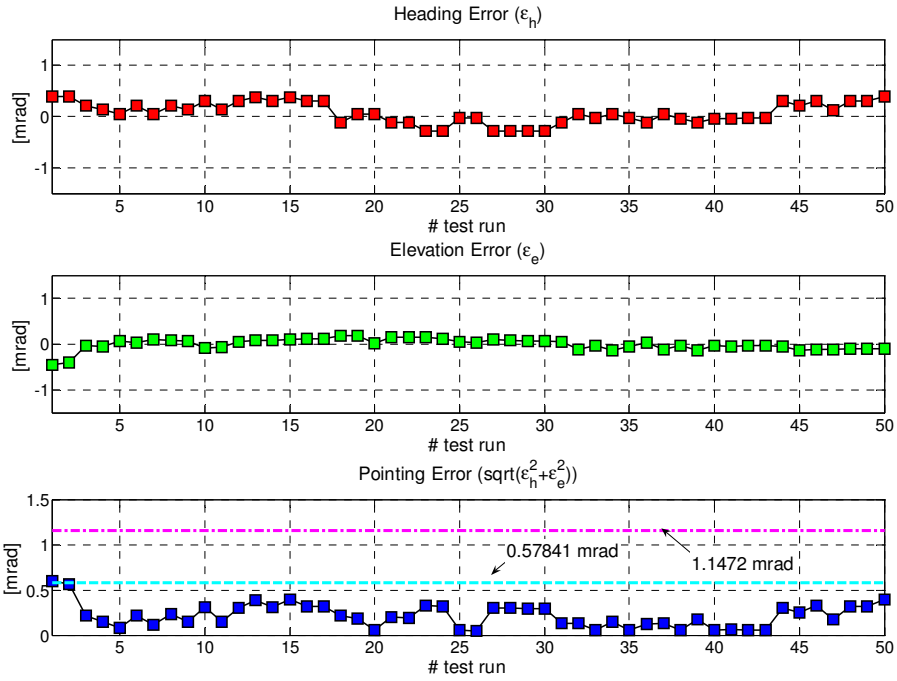

(b) Pointing error

Figure 2-30. Experiment #2: θ=1.5°

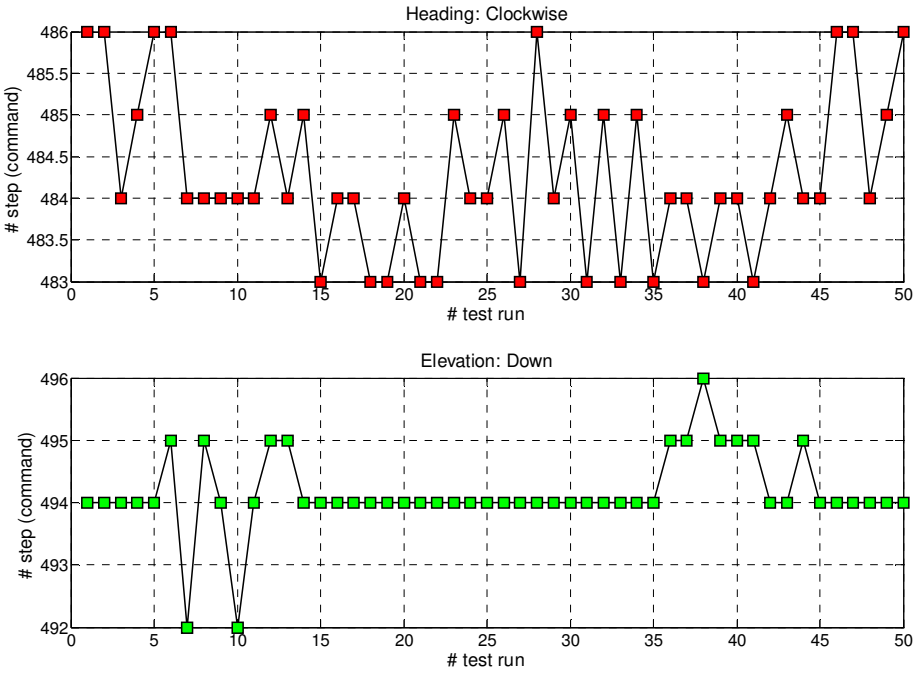

(a) Heading and elevation command

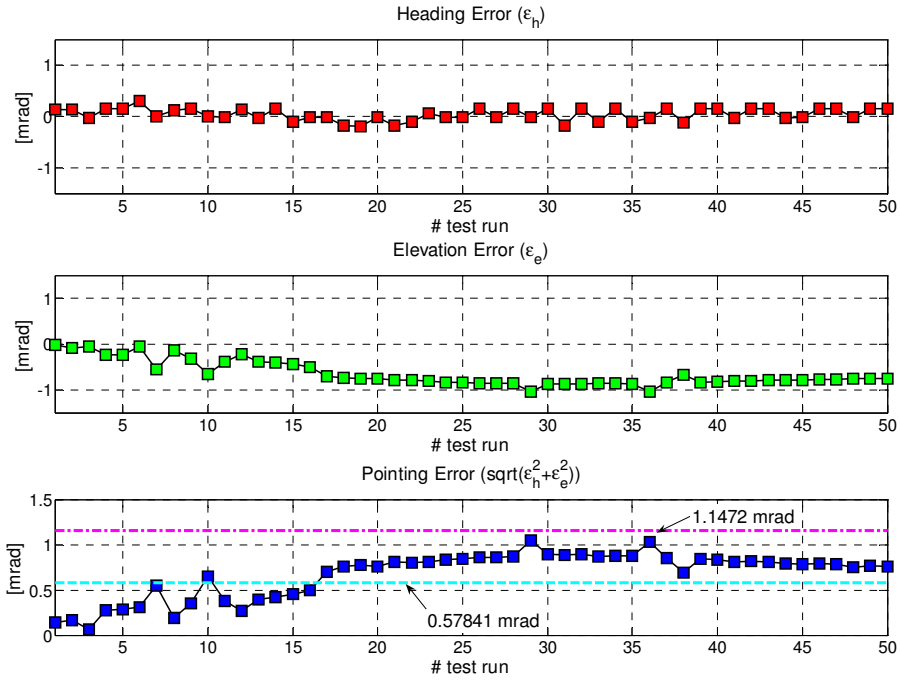

(b) Pointing error

Figure 2-31. Experiment #3: θ=2°

Table 2-8. Pointing error

A	B							C						D	E
Experiment	Actual Measurement Errors							Measurement Errors in Table C-2						Reference pointing_error in Table C-2 (mrad)	Success Rate
		RTK			Local Angular Sensor			RTK			Local Angular Sensor				
		sigma_E (cm)	sigma_N (cm)	sigma_U (cm)		sigma_phi (mrad)	sigma_theta (mrad)	sigma_E (cm)	sigma_N (cm)	sigma_U (cm)	sigma_phi (mrad)	sigma_theta (mrad)			
#1 (theta = -1 deg) (U=1.52 m)	min	0.0194	0.0323	0.0744	min	0.0000	0.0000	0.5	0.5	1	0.0873	0.0873		0.5784	96.00%
	max	0.1739	0.2374	0.3647	max	0.0395	0.1210	1	1	2	0.0873	0.0873		1.1472	100.00%
					mean	0.0049	0.0175	2	2	4	0.0873	0.0873		2.2896	100.00%
#2 (theta = -1.5 deg) (U=1.67 m)	min	0.0101	0.0313	0.0370	min	0.0000	0.0000	0.5	0.5	1	0.0873	0.0873		0.5784	98.00%
	max	0.2228	0.5149	0.5167	max	0.0099	0.0234	1	1	2	0.0873	0.0873		1.1472	100.00%
					mean	0.0032	0.0050	2	2	4	0.0873	0.0873		2.2896	100.00%
#3 (theta = -2 deg) (U=1.80 m)	min	0.0257	0.0300	0.0206	min	0.0000	0.0000	0.5	0.5	1	0.0873	0.0873		0.5784	30.00%
	max	0.2114	0.1945	0.4339	max	0.0605	0.2962	1	1	2	0.0873	0.0873		1.1472	100.00%
					mean	0.0075	0.0189	2	2	4	0.0873	0.0873		2.2896	100.00%

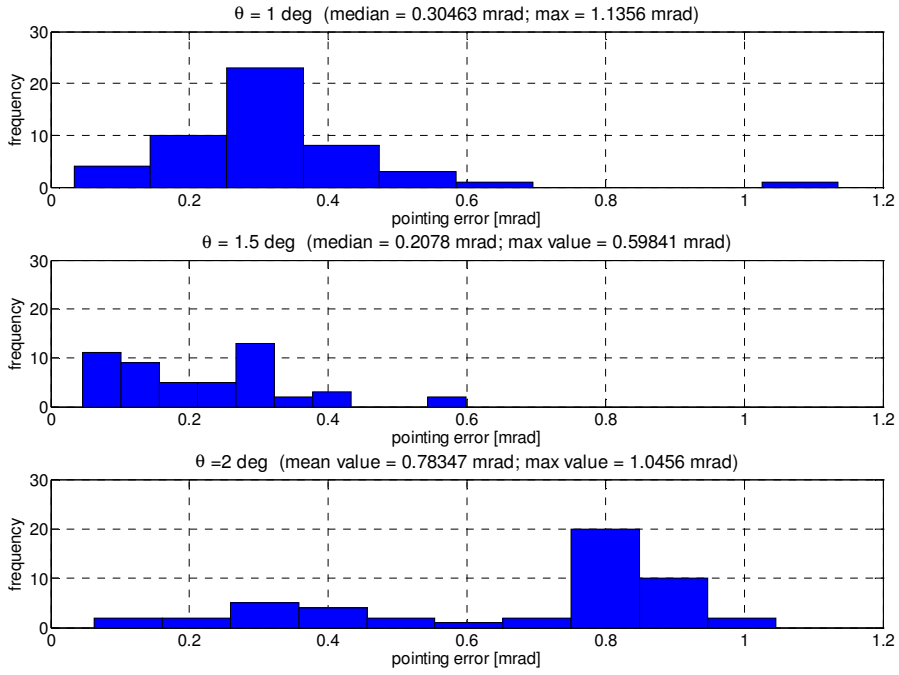

Figure 2-32. A histogram of pointing errors in the reliability test (I)

2.3.4 Consideration of Error Sources affecting Pointing Accuracy

In this section, we consider major error sources for the pointing method in Figure 2-4. The pointing method utilizes GPS satellite signals, local angular sensors (e.g., tilt sensors or INS) and a gimbal. Thus, there may exist undesirable pointing

errors due to GPS signal loss and inaccuracy in the gimbal's angular position. In addition, a mechanical mis-alignment between optical transceivers and the gimbal's rotation axes causes an offset error in heading and elevation control angles.

Our suggestions for reducing the above possible error sources follow: The local angular sensors, such as tilt sensors and INS, react only to the gravitational field and platform's motion; their malfunction may be connected to sensor failure without any other exterior influence (e.g., a GPS receiver does not work properly when it experiences signal blockage by a high-rise building even though this does not mean complete failure of the GPS receiver). Thus, the local angular sensor errors are not considered here.

(A) GPS signal blockage

The pointing method in Section 2.1 assumes no significant GPS signal blockage or signal loss. Such GPS signal loss can happen very often in urban environments; for example, when a car with GPS passes by high-rise buildings or an airplane with GPS experiences lateral inward tilting in turning a curve (i.e., when banking). In an urban environment, it may be necessary for a mobile platform to be equipped with an integration system of GPS and INS. The position and local angle measurements from the INS will be utilized until the GPS receiver locks on GPS satellites signals at some point; then, the pointing accuracy will be determined by the angular accuracy of INS. Many researches have been conducting on the GPS/INS integration (Berman et al., 1998; Bevly et al., 2000; Farrell et al., 2000; Gebre-

Egziabher et al., 1998; Hayward et al., 1999; Hong et al., 2001; Meister et al., 2007; Redmill et al., 2001; West et al., 2000). For an airplane undergoing a steep bank while flying, the GPS receiver will recover its function in a minute (e.g., 50 seconds for NovAtel RT2W). Thus, the GPS signal loss is not a problem for vehicles that operate in an open space. Also, a static platform such as a gimbal located on the roof of building does not have such GPS signal blockage problem because its location is carefully chosen in advance with a site survey. For a static platform, any malfunction of GPS receiver and any deterioration in GPS satellite signals can be easily detected by continuous monitoring; for example, by making the GPS receiver report its identification number (set by user) in regular time and by comparing the measured position coordinates from GPS receiver with the true one obtained by precise surveying. For a mobile platform, the position coordinates from GPS can be compared to the one from INS (or electronic map); thus, if the difference of the two position coordinates is larger than a pre-determined threshold, then it indicates that either one does not work properly. Because an INS responds to acceleration and GPS does to the satellite signals, they would make a good combination for pointing sensors in dynamic environments. For static and mobile platforms, Receiver Autonomous Integrity Monitoring (RAIM) helps to detect any fault in the GPS measurement (Lee, 1992; Michalson, 1995).

(B) Gimbal and Mis-Alignment Errors

The gimbal is a mechanical frame combined with motors and motor controllers. Non-linearity from backlash or a dead zone may be found in the motors,

which leads to error in the angular position of the motor. These errors can be significantly reduced by the use of angular encoder. The RTK GPS and bi-axial tilt sensors can be useful to detect such angular position error. For example, Figure 2-33 shows a sequential movement of the heading (horizontal) axis of a two-axis gimbal. At each 90° movement, the RTK GPS measures the location. If the sequential 90° angular motion is correct, then the inner product of two vectors $\overrightarrow{AC}$ and $\overrightarrow{BD}$ will produce an angle between the two vectors which is close to 90°. If not, it indicates that there exists an angular position error in the heading axis of the gimbal. This example is effective only if the heading error is larger than $\frac{r}{R}$ radian, where r is the magnitude of the RTK GPS measurement error. The angular position error in elevation (vertical) axis of the gimbal can be checked with bi-axial tilt sensors (e.g., MD900-TS). Since the angular accuracy of the bi-axial tilt sensor is high (i.e., 0.01°), the angle readout from the gimbal is examined with the actual angle measurement from the bi-axial tilt sensors. This example is effective only if the elevation error is larger than 0.01°.

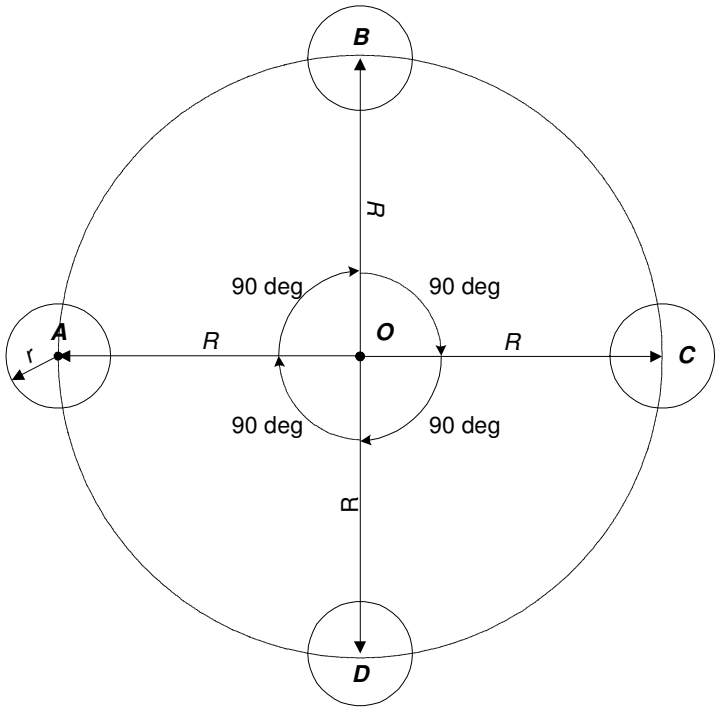

Figure 2-33. A sequential RTK GPS antenna rotation by 90°

For the pointing method in Figure 2-4 (b), each motor of the two-axis gimbal returns to its initial angular position after pointing is done (Figure 2-35). As illustrated in Figure 2-34, when the two motors do not perfectly reset to their initial position or there exists any mis-alignment error between optical transceiver and the gimbal, the laser beam emanating from C_1 does not reach the pre-determined target at C_2 but hits the photodetector installed around C_2 to sense the laser beam. The electrical signal from the photodetector may determine the deviation angle from the initial angular position; thus, enabling correction of the gimbal or mis-alignment error. This method is applicable to a mobile platform when it returns to its hangar or base for zeroing its pointing system. Figure 2-35 shows an actual example of such alignment with a GPS antenna pole; because centimeter or inch scales are engraved

on a thin pole (1.5 cm width), the mis-alignment error can be easily checked by the laser beam's position on the pole.

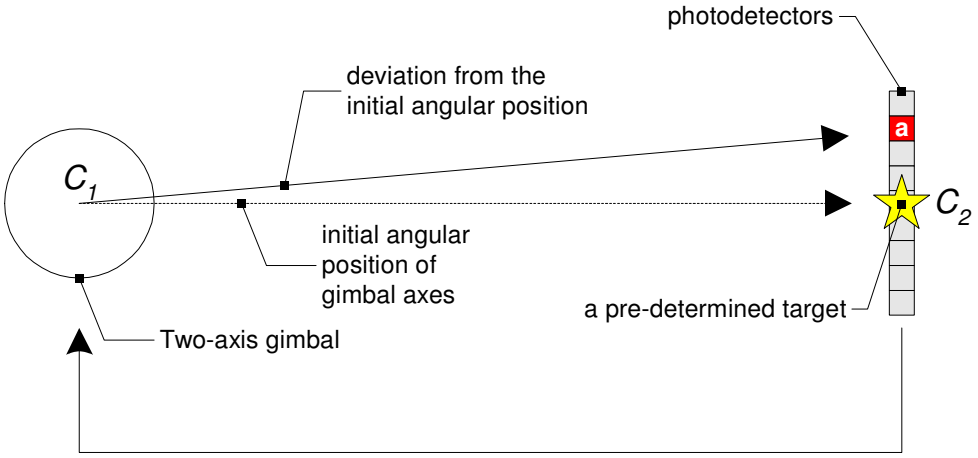

Figure 2-34. Gimbal and mis-alignment errors

Figure 2-35. Example of checking gimbal or mis-alignment error with GPS antenna pole

2.4 Self-Organized Pointing Methodology for Mobile Platforms

In this section, we provide a method of autonomous pointing vector measurement and self-organized pointing procedure for mobile nodes in a dynamic environment.

2.4.1 Autonomous Pointing Vector Measurement by Waypoint Navigation

For a high-speed vehicle such as airplane, it may be difficult to measure the pointing vector in Figure 2-4 (a) because it requires long translational movements with a straight path for accurate pointing accuracy. Waypoint navigation might be helpful for this situation. For example, an airplane is located at A in Figure 2-36. It sets two waypoints B and C to measure pointing vector. Then, $\overline{BC}$ is a pre-defined path in the air. Even though there is no mark in the air, a pilot can measure $\overline{BC}$ with the aid of GPS coordinates; he or she can continuously compare the difference between a current or future position and the pre-defined path $\overline{BC}$ until the pointing vector is measured. If the pointing vector is not measured at C or the straight path is not made, then the waypoint C is extended to D. This process can be automatically carried out with a waypoint navigation system (Meister et al., 2007; Pflimlin et al. 2006).

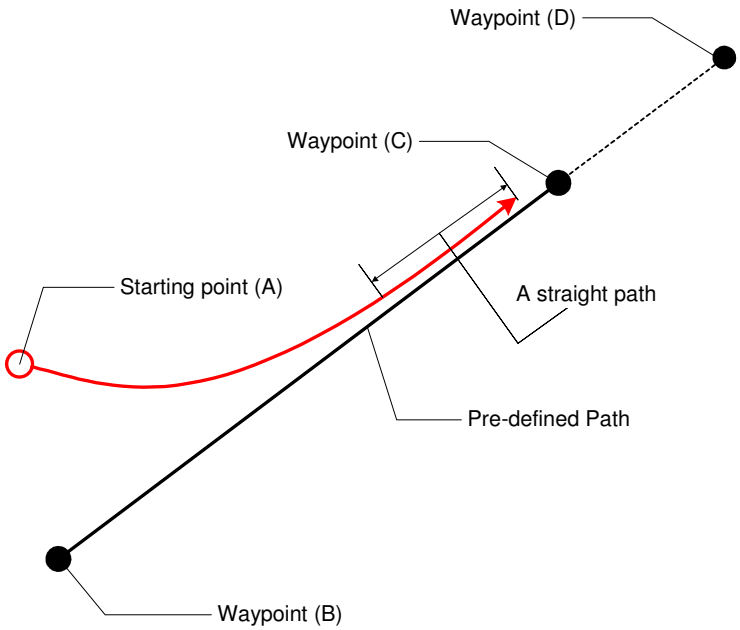

Figure 2-36. Example of waypoint navigation

Is it possible to generate the straight path with RTK GPS? The following experimental results show the possibility. NovAtel GPS antenna was placed on a top plate of two-axis gimbal and then it was rotated by 360°. Figure 2-37 (a) shows the first trial in clockwise direction; the RTK GPS (NovAtel RT2W) drew a circle with 28.5 cm radius. Figures 2-37 (b), (c), and (d) display the next sequential circular motions in counter-clockwise, clockwise, and counter-clockwise. The circles consisting of red dots show the trajectories of each circular motion; the dimension of one grid in each figure is 0.1 meter (10 centimeters). The trajectories of four circular motions were overlapped, which means the RTK GPS position measurements are reliable in an open space. If the circle generated by the gimbal's horizontal axis is supposed to represent a planned path (i.e., a circle), then the RTK GPS measurements show how the measurement can be close to the path.

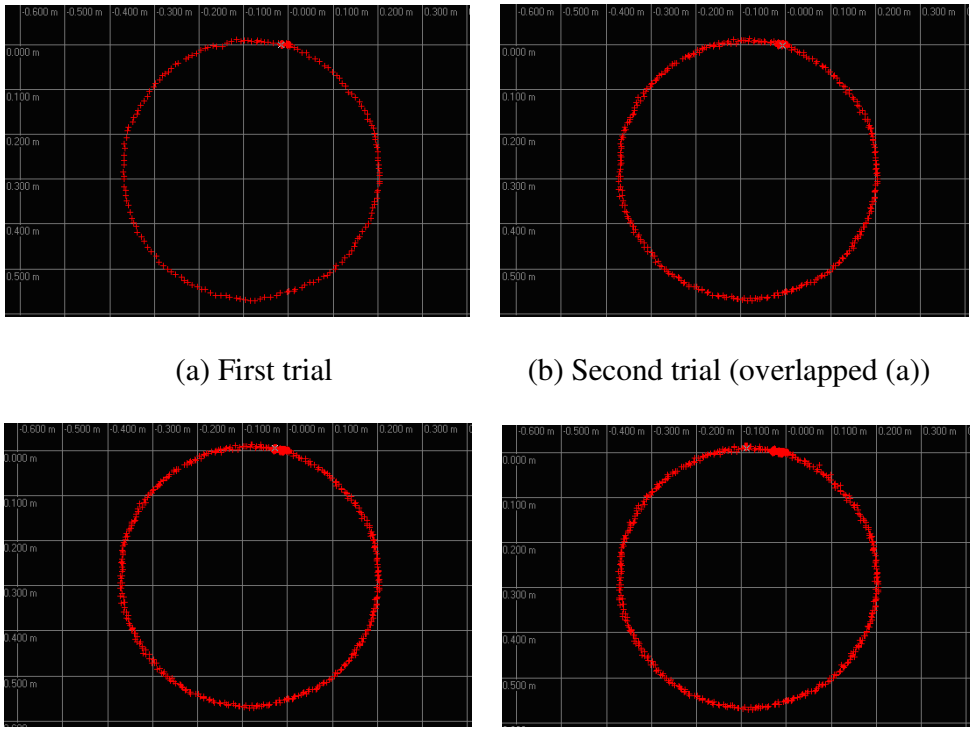

(a) First trial (b) Second trial (overlapped (a))

(c) Third trial (overlapped (b)) (d) Fourth trial (overlapped (c))

Figure 2-37. The trajectories of a circular motion using RTK GPS (NovAtel RT2W)

2.4.2 Self-Organized Pointing Procedure with Path Planning

The latency problem will occur when a mobile platform such as a vehicle is involved in FSO networking. If the mobile platform keeps moving, then the difference between GPS measurement times and the current vehicle's time which are T_1 and T_2, respectively, as shown in Figure 2-38. It means that the GPS positioning information (P_1) is useless because the vehicle has already passed the point.

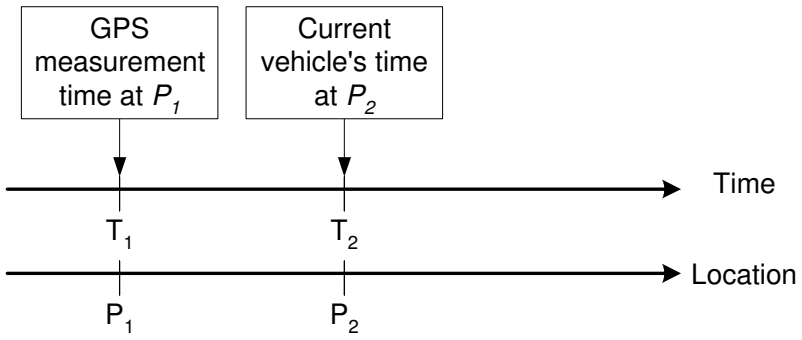

Figure 2-38. Data Latency

This latency problem can be minimized by *i)* using a high data rate GPS receiver (e.g., Javad LGG100-GG: 100 Hz position update with Code DGPS) or *ii)* defining a flight path with several waypoints. The second option (called path planning) would work as follows:

- First, set several waypoints on a straight path and plan when the vehicle should pass those points. For example, (T_1, P_1), (T_2, P_2), and (T_3, P_3) in Figure 2-39 are those waypoints and time marks.
- Then, a vehicle starts moving with a constant speed of $|v_1|$ at some point between P_1 and P_2. It can adjust its initial speed $|v_0|$ to the desired one $|v_1|$. At P_2, it keeps the same speed as $|v_1|$ and thus passes P_3 as planned.
- Finally, the future position P_i for T_i for $i \geq 4$ will be known in advance. The GPS measurement at T_i for $1 \leq i \leq 3$ will be used to compute the difference between the planned path and actual position. The position difference is fed back to adjust the vehicle's velocity.

This path planning may be reasonable because, for example, an airplane follows a pre-defined airway determined by air traffic control and an artificial satellite keeps its pre-determined trajectory around the Earth in space. Moreover, path planning would make pointing between two mobile platforms or between a mobile platform and a static one much easier than without path planning. Figure 2-40 displays how to establish the pointing between two mobile platforms by path planning.

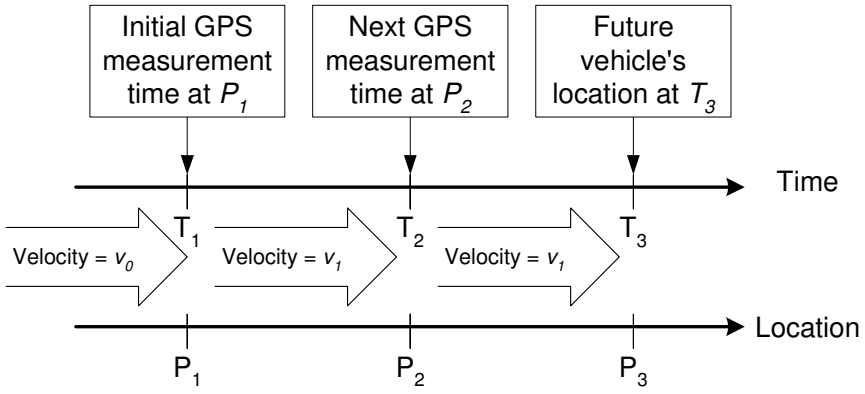

Figure 2-39. Path planning

In path planning, each airplane knows when and where the other passes. Then, for example, the two airplanes A and B start aligning their optical transceiver to the baseline vector between them at T_1 and T_2. Since the locations of two airplanes are known, the baseline vector at each time is also determined in advance. The pointing vectors of two airplanes are measured by the waypoint navigation mentioned above. During the initial alignment, the two airplanes may have enough time to adjust their pointing errors (i.e., learning and correcting the errors). Thus, after actual pointing established at T_3, they can maintain pointing. The pointing duration between two

mobile platforms may be temporary because of their speed and maneuvers on the way to their destination. The two airplanes' times can be synchronized to GPS time with nanosecond precision.

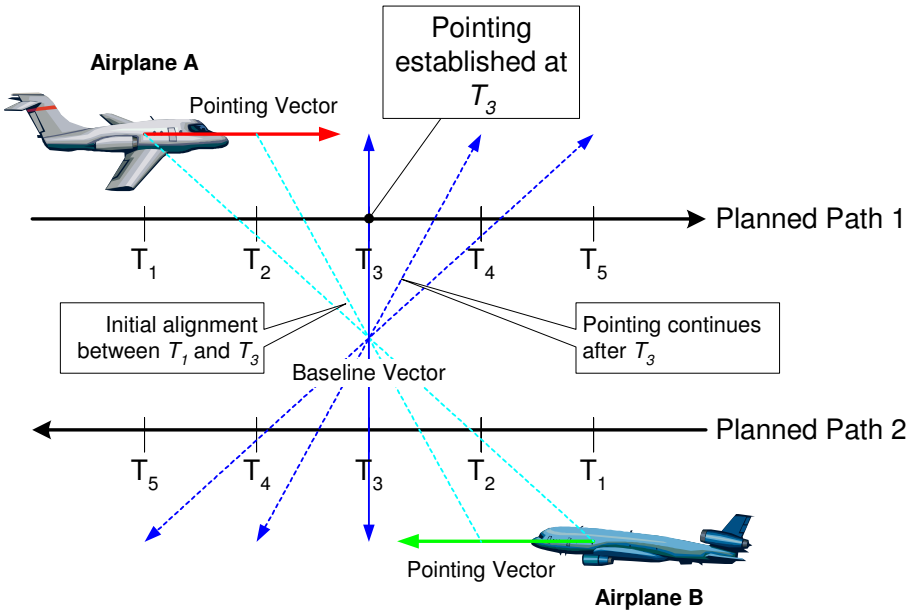

Figure 2-40. Pointing with path planning

2.5 GPS Signal Availability and Extended DGPS and RTK Service

The pointing method in Section 2.1 depends on the GPS satellite signals to measure the pointing vector and/or the baseline vector. Moreover, the RTK GPS requires observing at least five common GPS satellites both at the Base Station and Rover Station in Figure 2-21. Both the GPS modernization plan and the European GPS satellites, Galileo, would provide more reliable GPS satellite signals and increase the number of observable satellites to users. The Wide-Area Augmentation System (WAAS) and Nationwide Differential GPS (NDGPS) are examples of utilizing the highly accurate positioning service over a wide area; thus, enabling precise pointing for mobile platforms and reducing the installation cost of the Base Station for DGPS or RTK operation.

2.5.1 GPS Signal Availability

RTK GPS receivers (at base station and rover) should keep track of at least the same 5 GPS satellites above a mask angle (≥ 10° in elevation; preset inside the receiver) on both L1 (1,575 MHz) and L2 (1,227.60 MHz) frequencies to guarantee its RTK performance. In the GPS modernization plan, a new L5 (1,176.45 MHz) signal will be available for GPS users (Enge, 2003). The new signal will provide signal redundancy to the users so that they can choose any combination of the signals (e.g., L1/L2, L2/L5, or L1/L5) for their RTK operation.

The European global positioning satellite system (GNSS), Galileo, will also

increase signal availability in the future. Galileo will be composed of a constellation of 30 satellites (www.esa.int/esaNA/ESAAZZ6708D_galileo_0.html); the current GPS constellation consists of 30 satellites (tycho.usno.navy.mil/gpscurr.html). Since both GPS and Galileo are designed to so that at least four satellites are in sight of by anyone anywhere in the world, GPS users will be able to keep track of at least eight GNSS satellites, which subsequently satisfies the RTK GPS requirement on the minimum number of observable satellites (i.e., five satellites).

2.5.2 Wide-Area Differential GPS

The Federal Aviation Administration (FAA), a division of the United States Department of Transportation (DOT), is developing the Wide Area Augmentation System (WAAS). The WAAS is a differential GPS system covering the whole continent of the United States using satellite (Intelsat Galaxy XV). A network of WAAS ground reference stations monitors GPS satellite signals; a master station generates a GPS positioning error correction message and uploads to the geostationary WAAS satellite (Figure 2-41). Then, the WAAS satellite broadcast a correction message using its navigation transponder by which the GPS positioning accuracy is improved from 20 meters to approximately 1.5~2 meters. Table 2-9 shows the positioning accuracy improvement observed from 51 sites in the United States.

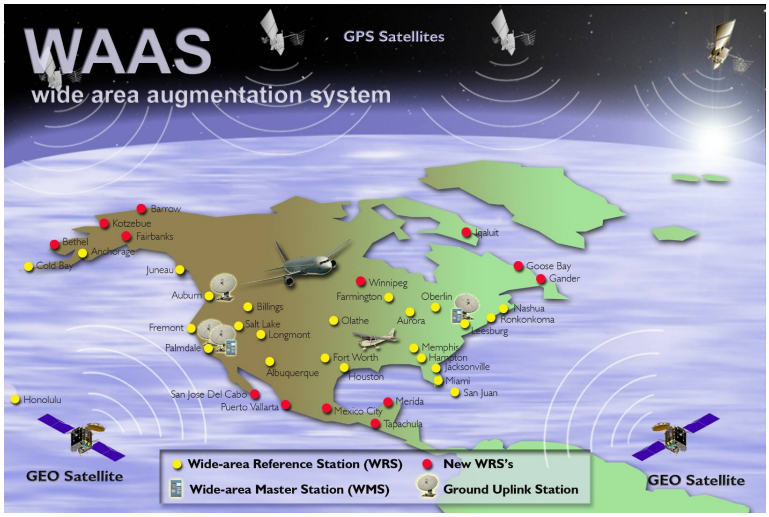

Figure 2-41. WAAS Architecture (www.faa.gov)

Table 2-9. Positioning accuracy of the WAAS
(CONUS: Continental United States)

Parameter	CONUS Site/Maximum	CONUS Site/Minimum
95% Horizontal Accuracy	Seattle 0.844 meters	Memphis 0.514 meters
95% Vertical Accuracy	Miami 1.231 meters	Seattle 0.754 meters

2.5.3 Extended RTK Service

For RTK operation, a RTK GPS base station (or reference station) regularly broadcasts its differential corrections compensating various GPS error sources to the rover (i.e., RTK GPS receiver on a fixed or mobile platform). RTK GPS positioning accuracy is dependent on the distance between base station and rover. For example, the NovAtel RT2W provides 2 cm horizontal accuracy to the rover within 10 km from the base station; however, the accuracy is degraded to 8 cm when the distance is over 10 km due to GPS error sources such as the ionospheric (dominant error over 10 km) and tropospheric delays. To provide accurate RTK GPS accuracy at a range of

over 10 km, we might need more RTK GPS base stations to form a network RTK (www.network-rtk.info). Or the Nationwide Differential GPS (NDGPS) could provide an alternative.

NDGPS is an expanded service of the Maritime Differential GPS designed to cover the entire surface area of the United States and provide 10 m positioning accuracy to surface users (www.navcen.uscg.gov). To date, there are 37 operational National DGPS sites (Figure 2-42). The service is operated in the RTCM SC-104 broadcast standard (RTCM: The Radio Technical Commission for Maritime Services) via radiobeacon frequencies (300 KHz); the standard reserves its Type-18 and Type-19 messages for RTK operation. If the 37 operational NDGPS sites (i.e., DGPS base station) broadcast the message types, then terrestrial and coastal areas will be covered by the RTK service.

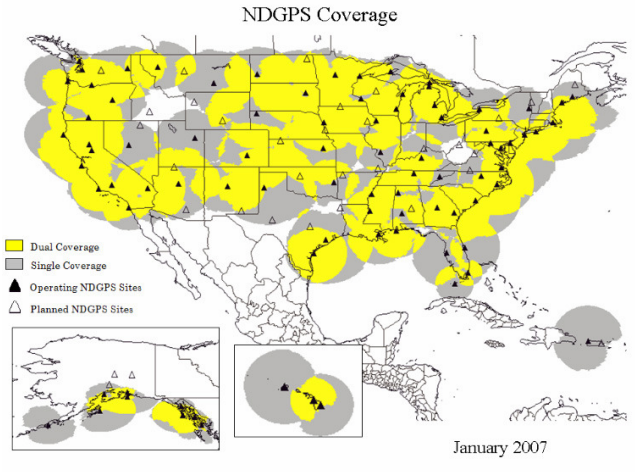

Figure 2-42. NDGPS coverage (source: USCG Navigation Center)

2.6 Summary

Section 2 describes our unique methodology for self-organized pointing and the associated autonomous and precise pointing technique applicable to link initiation in FSO networking. Since the link initiation should occur in less than 1 second with microradian to milliradian accuracy, the use of accurate position and angular sensor devices is therefore natural for the precise pointing. RTK GPS was used to provide accurate pointing information as to where nodes are (the position coordinates) as well as where an FSO transceiver directs its laser beam at local site (the pointing vector) with centimeter accuracy. The information was essential to precisely align laser beams between two FSO transceivers.

Because we employed the highly accurate GPS as a primary pointing sensor, our pointing method is distinct from existing pointing methods using optical devices (Ho et al., 2006; Ho et al., 2004; Epple, 2006; Wilkerson et al., 2006) or INS combined with GPS (Epple, 2006; Wilkerson et al., 2006; Yee et al., 1998). Since the RTK GPS provides centimeter level positioning accuracy on-the-fly, its high accuracy will improve the performance of position and velocity estimation of a mobile node for tracking.

The pointing method in Section 2.1 employed tilt sensors for static platform and INS for mobile platform to measure the attitude angles of both platforms. Because those local angular sensors and GPS are conventional navigation sensors, the precise yaw information from RTK GPS can be combined with the roll and pitch

outputs from the INS mounted on an aircraft (Lee et al., 1998; 2001); thus enabling us to use the pointing technique in a dynamic environment.

The pointing sensors' outputs contain measurement errors that affect accuracy of the pointing information, i.e., roll, pitch, yaw, pointing vector and baseline vector. In Section 2.2, how the pointing sensors' measurement errors affect the pointing accuracy was observed by computer simulation. The observation was based on the error propagation law (Arras, 1998; Breipohl, 1970). The simulation provided the variance (or standard deviation) of pointing accuracy, which represents the pointing error distribution according to the sensor measurement errors; it was assumed that the sensors' measurement errors and the pointing error were normally distributed. Tables C-1 through C-7 summarize the simulation results. The formula in Appendix B estimates pointing accuracy (i.e., σ_h and σ_e) for the given GPS and local angular sensor accuracy performance. Because the pointing sensors' accuracy performance relates to their cost, the formula would be useful in estimating the cost for a desired pointing accuracy.

A mid-range pointing experiment on the outdoor testbed on the University of Maryland campus in College Park showed that the pointing accuracy was improved as the length of pointing vector increases, as claimed in Section 2.1. The pointing system used in the experiment consisted of RTK GPS, two-axis gimbal, and helium-neon laser ($\lambda = 633\ nm$). The length of the pointing vector was 6, 9, 12, and 40 meters. Figure 2-43 shows the pointing errors observed during the experiment. The

experiment demonstrated sub-milliradian pointing accuracy with 12-meter and 40-meter pointing vector. The length of the pointing vector represented the distance between the pointing system and a pre-determined target with known position.

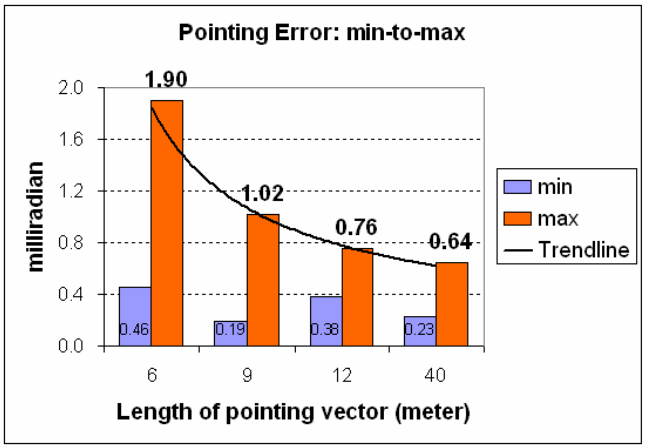

Figure 2-43. Pointing error observations in the mid-range pointing experiment

Next, a reliability test was conducted to show how quickly (in seconds) and successfully (in %) the sub-milliradian accuracy could be obtained with an automatic pointing system; Figure 2-27 shows a diagram of the automatic pointing system. The test with 150 pointing trials using an automatic pointing system demonstrated a 98 % success rate of sub-milliradian pointing accuracy and 73 % success rate of 0.5 milliradian pointing accuracy: the maximum pointing error was 1.1356 milliradian (distance to the pointing target: 40 m); Figure 2-44 shows a histogram of pointing errors for the 150 pointing trials. Figure 2-27 implies that the speed of the automatic pointing system is dependent on *i)* the output rate of pointing sensors (i.e., GPS, tilt sensors, INS), *ii)* the position data latency of the remote pointing system, and *iii)* the angular speed of two-axis gimbal; the computation time for generating control angles (heading and elevation) was less than 20 msec with MATLAB (version 7.0).

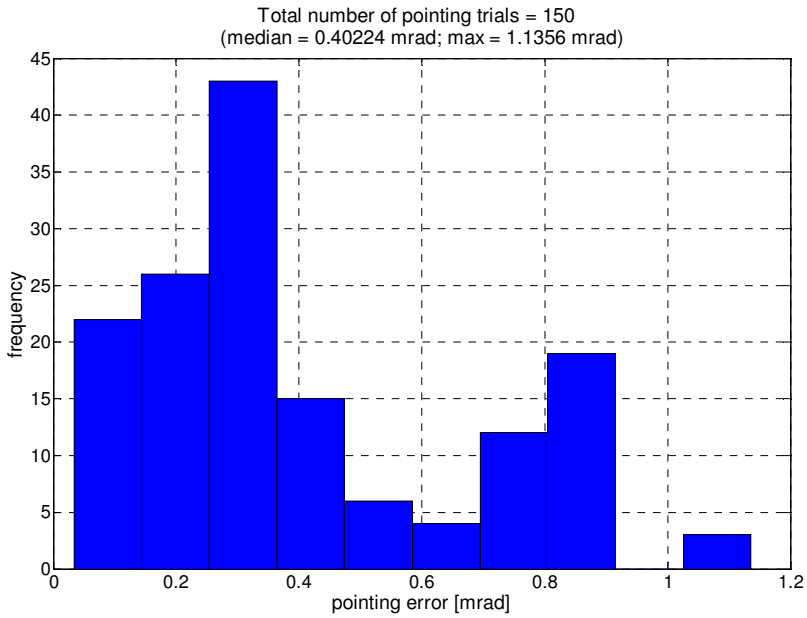

Figure 2-44. A histogram of pointing errors in the reliability test (II)

It is important to note that the mid-range and short range pointing trials were chosen for their difficulty to demonstrate sub-milliradian pointing accuracy. For example, Figure 2-45 (b) shows pointing errors computed by the simulation method (Section 2.2) for various lengths of pointing vector and baseline vector; for simplicity, only GPS measurement error is considered as a pointing error source (Figure 2-45 (a)). The graph in Figure 2-45 (b) implies that the shorter the lengths of the two vectors, the more difficult to obtain the sub-milliradian pointing accuracy; on the contrary, the longer the two vectors, the much smaller the pointing error (i.e., the higher the pointing accuracy). Figure 2-45 (c) displays GPS positioning accuracy for different GPS systems.

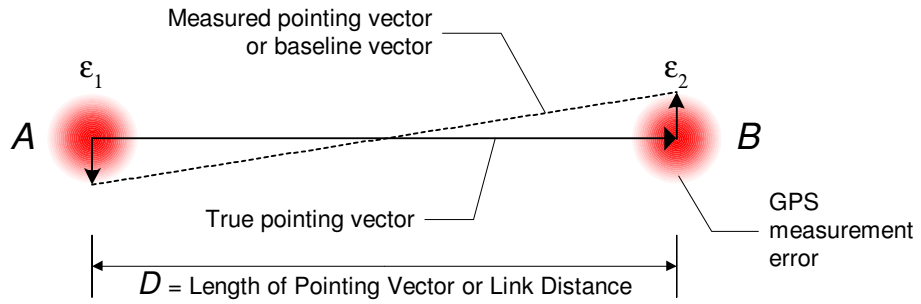

(a) GPS measurement errors in pointing and baseline vectors

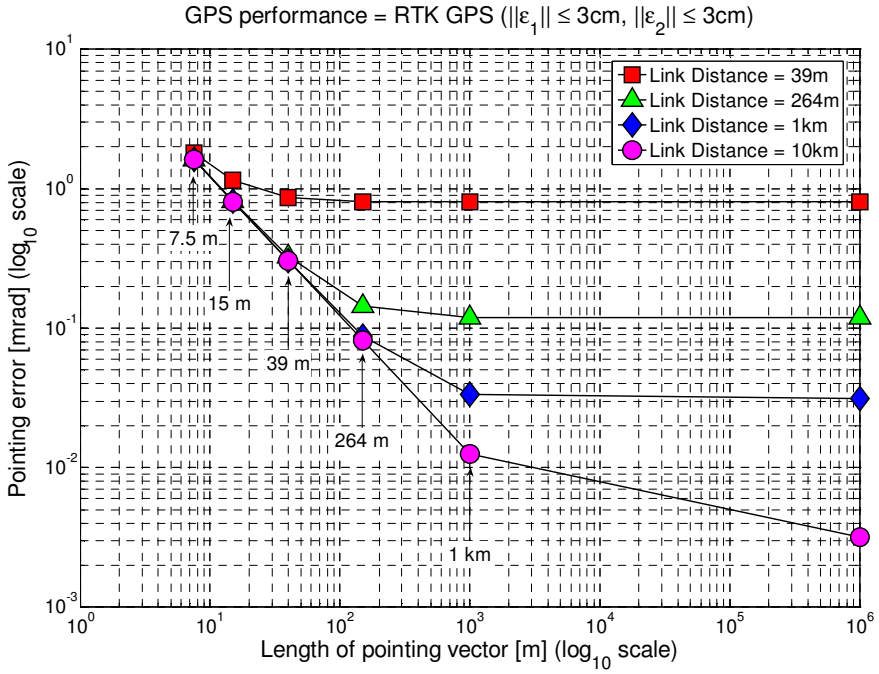

Link distance	39 m	264 m	1 km	10 km
Pointing error range	0.8~1.8 mrad	0.12~1.62 mrad	0.03~1.62 mrad	0.003~1.62 mrad

(b) A graph of pointing error vs. lengths of pointing and baseline vectors

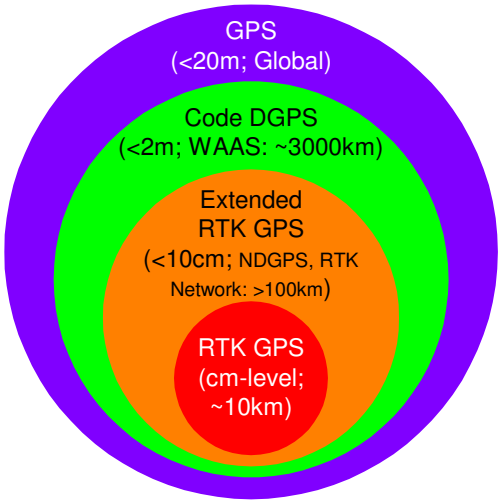

(c) GPS accuracy vs. range (WAAS: Wide Area Augmentation System; NDGPS: Nationwide Differential GPS)

Figure 2-45. Pointing accuracy improvement with increase in lengths of pointing and baseline vectors

If either the accuracy of local angular sensors is very high or the platform is placed at a location whose roll and pitch angle are precisely determined in advance, then we can keep the local sensor measurement errors close to zero (i.e., $\sigma_\phi = \sigma_\theta = 0$). Thus, pointing accuracy depends on the GPS performance. For example, it may be possible to obtain 30 microradian pointing accuracy with link distance of 1~2 km using the RTK GPS; 3 microradian pointing accuracy is obtainable with link distance of 10 km using the RTK GPS (horizontal positioning accuracy: 2 cm). Even the stand-alone GPS (horizontal positioning accuracy: 10 m) can provide milliradian accuracy with the link distance of 10~20 km. Section 2.2.3 shows this possibility.

Chapter 3: Topology Optimization

A FSO network must be capable of autonomous physical and logical reconfiguration responding to changes in its link or traffic states due to the node mobility and atmospheric obscuration (e.g., dense fog, dust, or snow). In the previous chapter, a pointing technique for the physical reconfiguration was introduced. The purpose of this chapter is twofold. First, we will provide logical reconfiguration algorithms with the perspective of minimizing congestion due to varying traffic demands to solve the *Network Layer Topology Control Problem*. Second, similar algorithms will be applied to simultaneously optimize the two objectives of physical network cost (due to node mobility and atmospheric obscuration) and congestion, i.e., solving *Multiobjective Optimization Problem*.

At the physical layer, performance is measured in terms of a bit-error-rate (BER), which is a function of the received power at the FSO transceiver. A FSO link is considered to be feasible if its BER is less than 10^{-9} (i.e., -45dBm=31.6×10^{-9} W). Link distance and obscuration are the main factors which cause attenuation of the optical signal, which results in increased (i.e., worse) BER; the longer the link distance and the heavier the obscuration, the higher the link attenuation. Thus, the higher the link attenuation, the more power needs to be transmitted in order to maintain a given BER. The link attenuation (dBm) or transmission power (W) between any origin and destination pairs of node is defined as the link cost. The objective at the physical layer is to compute a topology with minimum overall cost. In a bi-connected FSO network, this problem is reduced to finding an optimal ring

network topology with minimum cost and is known to be NP complete (Llorca et al. 2004a)

An FSO transceiver uses a narrow, directional laser beam as its media. Thus, in a bi-connected FSO network (a ring network) with n nodes, the traffic demand between origin and destination nodes is routed in either of the two directions, clockwise or counter-clockwise as shown in Figure 3-1.

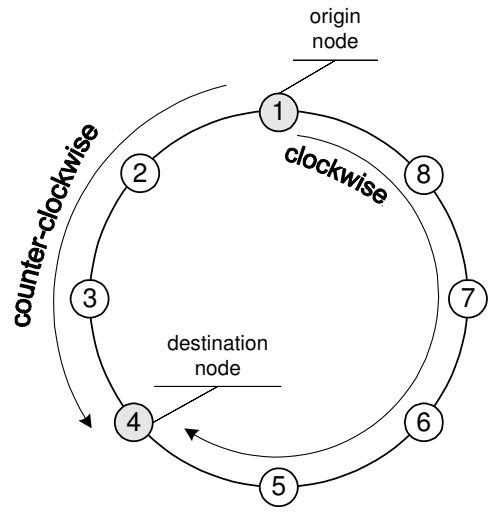

Figure 3-1. Two routing directions in a ring network with eight nodes ($n=8$)

Since there are $n(n-1)$ possible origin-destination (OD) pairs in a bi-connected FSO network with n nodes, so each topology has $2^{n(n-1)}$ possible routing directions; routing is the process of selecting the sequence of paths in a network along which to move data from origin-node to destination-node. Moreover, for a n-node ring network, there are $(n-1)!/2$ possible topologies because node 1 (center) is fixed. The NLTCP can be defined as the pseudo-code in Figure 3-2.

```
For i=1 to (n−1)!/2,
    Given the i-th topology,
    For j=1 to n(n−1),
        Decide a routing direction (clockwise or counter-clockwise) for the
        j-th OD pair which yields the least congestion;
    End-For
    Record the i-th topology (say TP(i)) and its congestion (say
    congestion(i));
End-For

Take a minimum value of congestion(k) among (n−1)!/2 congestion
values); then the k-th topology TP(k) is the solution to NLTCP with n
nodes.
```

Figure 3-2. Pseudo-code for NLTCP

As the above pseudo-code shows, solving NLTCP requires an exhaustive search of the $2^{n(n-1)} \times (n-1)!/2$ possible routings. For example, there exists 2.4329×10^{18} topologies for a ring network with $n=20$ and it would take 2.4329×10^{12} seconds or 2.8159×10^{7} days to complete the entire for-loops in the pseudo-code if each i-th for-loop took one microsecond. This complexity of NLTCP makes it hard to solve the problem in a reasonable time. However, the reconfiguration process must create a new topology responding to the degradation in near-real time. Thus, a heuristic approach might provide a solution to this dilemma. Finding a fast heuristic which provides a near-optimal solution is one of the objectives of this research.

In this research, a ring network topology is considered. A ring network topology can form a backbone network with a sub-network at each node (Figure 3-3 (a)). Figure 3-3 (b) illustrates that a mesh network topology is formed by adding two

new links (i.e., links $(1,3)$ and $(2,4)$) to the ring network topology in Figure 3-3 (a) with supplementary FSO transceiver at each node (i.e., three transceivers at each node). The exterior ring network topology still forms a basic backbone network. The additional link would be used to split demand when the demand is large or send data with priority directly to the destination node. Figure 3-3 (c) shows a mesh network which decomposes into two ring network topologies. The coverage area of the ring network is constrained by the range of the directional laser beam of the FSO transceiver ("A" in Figure 3-3 (d)). Hence, nodes need to spread out for extending the coverage area ("B" and "C" in Figure 3-3 (d)). In this case, a tree topology might be a proper choice to represent the configuration of nodes (dotted line). Llorca et al. (2006) used a tree topology to configure an initial connected topology in a FSO network; their objective was to minimize network cost. However, a ring topology can also map the configuration with achieving the multiobjective purpose of minimizing both cost and congestion ("C" in Figure 3-3 (d)).

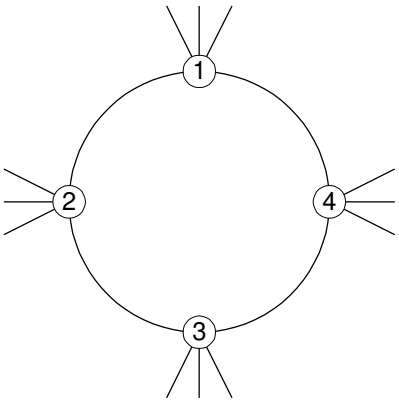

(a) A backbone network in a local area

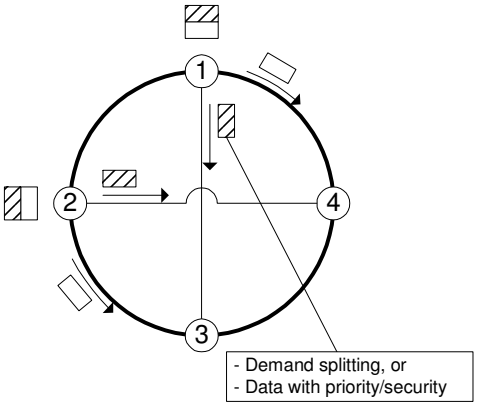

(b) A mesh network in a local area

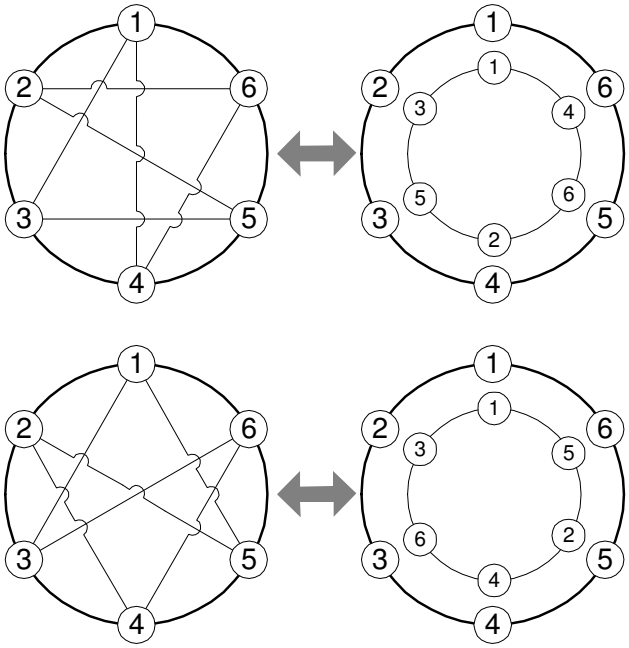

(c) Mesh networks and their equivalent ring network topologies

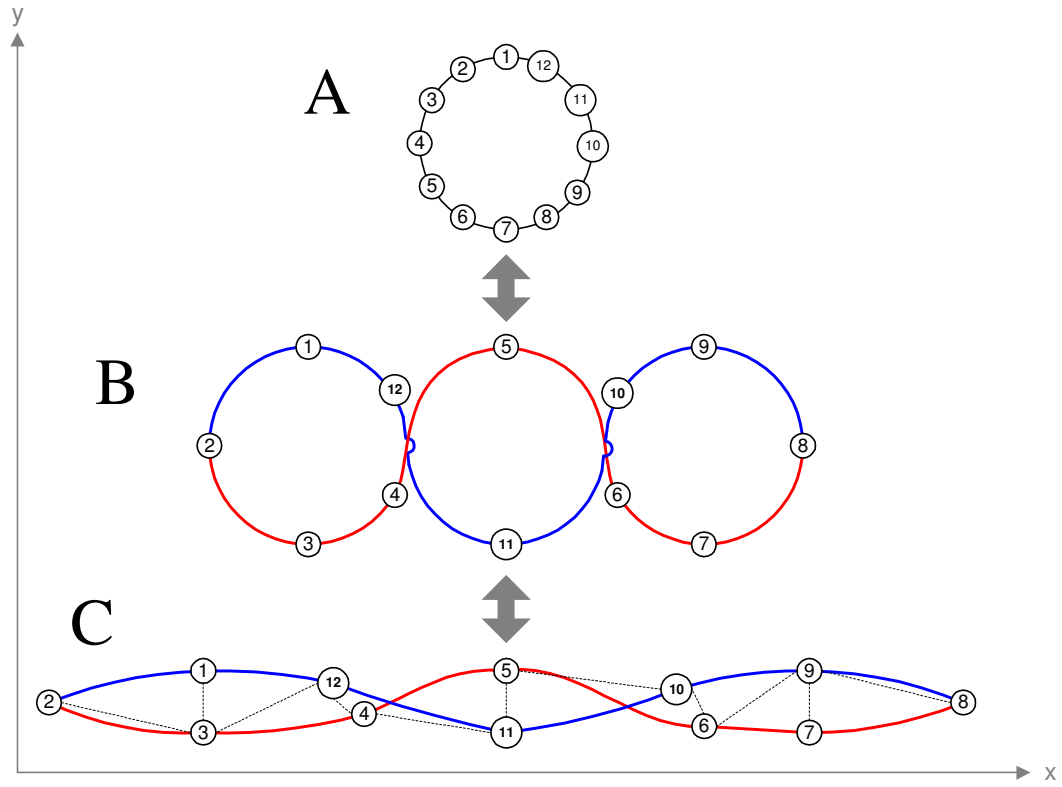

(d) Elongation

Figure 3-3. Ring network topologies

The assumptions are that *i)* all possible links are feasible, *ii)* the links are uncapacitated (thus NLTCP and MOP are examples of an uncapacitated network design problem) by which all links are assumed to have sufficient capacity so that sum of flow in any link is under its link capacity, *iii)* the shortest hop route is chosen when a longer path exists between origin and destination nodes, and *iv)* the number of nodes and the cost and traffic matrices are known (or continuously updated). The shortest hop route in assumption *iii)* is unidirectional and considers multi-hop path by which to send data from origin-node to destination-node through two or more links.

The rest of this chapter is organized as follows. First, literature reviews are presented to review optimization problems in fiber optic networks. These types of networks are important since synchronous optical and wavelength division multiplexing networks deal with routing and logical topology control problems to efficiently utilize a high capacity of optical fiber, which is similar to the congestion minimization problem in FSO networks. Then heuristic algorithms for dynamic reconfiguration of ring network topologies in FSO networks responding to changes in the physical layer cost and network layer congestion are provided. Through various numerical tests, the performance (optimality gap) of heuristic algorithms is measured for a bi-connected FSO network with $n \leq 15$. Next, a measure of estimating the optimality gap is introduced; the measure is quite useful for the ring network with $n > 15$. Finally, a sample application of the heuristic algorithms is presented.

3.1 Background: Multiobjective Programming Methods

This section introduces terminology for multiobjective programming and techniques for generating Pareto optimal solutions. The general multiobjective optimization problem with n decision variables, m constraints and p objectives is

$$\begin{aligned}
&\text{minimize} \quad z_1(x_1, x_2, ..., x_n) \\
&\text{minimize} \quad z_2(x_1, x_2, ..., x_n) \\
&\qquad\qquad \vdots \\
&\text{minimize} \quad z_p(x_1, x_2, ..., x_n) \\
&\quad \text{subject to} \\
&\qquad g_i(x_1, x_2, ..., x_n) \le 0, \quad i = 1, ..., m \\
&\qquad x_j : \text{ continuous or discrete}, \quad j = 1, ..., n
\end{aligned} \quad , \qquad (11)$$

where $z_k(x_1, ..., x_n)$ is the k-th single objective function out of p objectives, and $g_i(x_1, x_2, ..., x_n)$ is the i-th constraint out of m constraints. The decision space consists of the decision variables $(x_1, ..., x_n)$ satisfying the constraints above, and the objective space is composed of the objective function values $(z_1, ..., z_p)$ for each feasible variables. If a decision maker provides his utility function $U(z_1, ..., z_p)$ which can map the p objective function values to a real number, then it is possible to solve the multiobjective optimization problem with the given utility function as (assuming it is linear):

$$\begin{aligned}
&\text{minimize} \quad U = c_1 z_1 + c_2 z_2 + ... + c_p z_p \\
&\quad \text{subject to} \\
&\qquad g_i(x_1, x_2, ..., x_n) \le 0, \quad i = 1, ..., m \\
&\qquad x_j : \text{ continuous or discrete}, \quad j = 1, ..., n
\end{aligned} \quad , \qquad (12)$$

where c_k is the cost coefficient for achieving the k-th single objective, and p objectives $c_k z_k$ for $k = 1, ..., p$ are in the same unit. However, if such utility function

does not exist, then the decision maker might want to find the Pareto optimal solutions x^* to (11). Pareto optimal solutions and dominance are defined as follows (Marler et al., 2004; Steuer, 2004):

> Definition. A point, $x^* \in X$, is *Pareto optimal* if and only if there does not exist another point, $x \in X$, such that $\mathbf{F}(x) \leq \mathbf{F}(x^*)$ and $F_i(x) < F_i(x^*)$ for at least one function, where $\mathbf{F}(x) = (F_1(x), F_2(x), ..., F_p(x))$.
>
> Definition. Let $\mathbf{z}^1, \mathbf{z}^2 \in R^p$ be vectors in an objective space. Then $\mathbf{z}^1 = (z_1^1, z_2^1, ..., z_p^1)$ *dominates* $\mathbf{z}^2 = (z_1^2, z_2^2, ..., z_p^2)$ if and only if $\mathbf{z}^1 \geq \mathbf{z}^2$ and $\mathbf{z}^1 \neq \mathbf{z}^2$ (i.e., $z_k^1 \geq z_k^2$ for all k and $z_k^1 > z_k^2$ for at least one k).

Consider the following example:

- $\mathbf{z}^1 = \mathbf{z}(x^1) = (10, 30)$ for $x^1 = (1,1)$
- $\mathbf{z}^2 = \mathbf{z}(x^2) = (10, 20)$ for $x^2 = (2,2)$
- $\mathbf{z}^3 = \mathbf{z}(x^3) = (20, 10)$ for $x^3 = (3,3)$

x^1 is not Pareto optimal because there exists x^2 such that $\mathbf{z}^1 = (10, 30) \geq \mathbf{z}^2 = (10, 20)$ and $z_2^1 = 30 > z_2^2 = 20$; thus, $\mathbf{z}^1$ is dominated by $\mathbf{z}^2$. x^2 and x^3 are Pareto optimal solutions, and $\mathbf{z}^2(x^2)$ and $\mathbf{z}^3(x^3)$ are non-dominated in objective space.

Figure 3-4 shows an example of a feasible region and Pareto optimal solutions in objective space for a two-objective optimization problem. In the figure, the Pareto optimal solutions are distributed on the southwestern-most boundary of feasible region (i.e., between points A and B) (called Southwest Rule) (Cohon,

2003). A graphical representation of the feasible region in objective space for the multiobjective optimization problem is useful to figure out the Pareto optimal solutions as shown in Figure 3-4. Conversely, the Pareto optimal solutions can also be generated by a number of approaches such as the weighting method and the constraint method (Cohon, 2003).

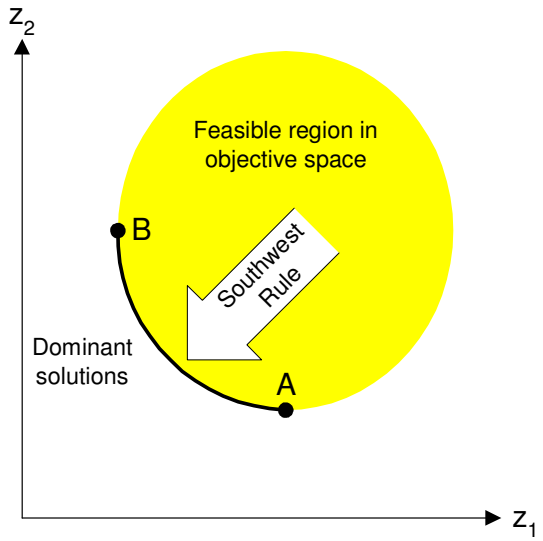

Figure 3-4. Pareto optimality: minimize both objectives (z_1, z_2)

A. The Weighting Method

For the weighting method, the single objective functions in (11) are combined with weights w_k as follows:

$$\text{minimize} \quad z(x_1, x_2, ..., x_n) = \sum_{k=1}^{p} w_k z_k(x_1, x_2, ..., x_n)$$

subject to

$$g_i(x_1, x_2, ..., x_n) \le 0, \quad i = 1, ..., m$$
$$x_j : \text{ continuous or discrete}, \quad j = 1, ..., n \qquad , \qquad (13)$$
$$\sum_{k=1}^{p} w_k = 1$$
$$w_k > 0, \quad k = 1, ..., p$$

where the units of each weighted objective $w_k z_k$ for all $k = 1, ..., p$ is same. The weight w_k represents relative importance (or preference) of each objective z_k to the decision maker. For each set of weights $(w_1, w_2, ..., w_p)$, an optimal solution to (13) is Pareto optimal for (11) as long as the weights are positive (Cohon, 2003; Theorem 3.1.2 in Miettinen, 1999) and the optimization problem is convex (Theorem 3.1.4 in Miettine, 1999). For example, Figure 3-5 (c) displays the feasible region in objective space for a two-objective optimization problem to minimize both cost and congestion in a bi-connected ring network topology with ten nodes given the traffic matrix and cost matrix from Figures 3-5 (a) and (b). The five circles in Figure 3-5 (c) represents Pareto optimal solutions in objective space for $w \in \{0.005, 0.01, ..., 0.99, 0.995\}$; the equally spaced 199 different weight sets $(w, 1-w)$ with $\Delta w = 0.005$ were used. This example shows that the weighting method approximates the Pareto optimal set; however, it might skip over some solutions (e.g., A and B in Figure 3-5 (c)). The problem of skipping some Pareto optimal solutions may happen in an integer programming problem because its Pareto optimal set is non-convex. Figure 3-5 (d) shows three solutions in objective space. A Pareto optimal solution C is under the line which is a linear combination of two Pareto optimal solutions A and B; thus, it

may not be discovered. This phenomenon is called a “duality gap”. Since the best weight sets which provide the entire Pareto optimal set are unknown, the weighting method would be useful to proceed by first with large step sizes (Δw) for the weights to find a rough approximation of the dominant solutions. Then, the process should repeat with a smaller step size for a range of weight sets of particular interest (Cohon, 2003)

0	33	35	24	25	37	40	30	3	33
32	0	2	36	42	5	44	12	51	47
41	14	0	49	43	2	3	3	19	29
30	11	42	0	21	38	49	46	12	31
21	32	25	50	0	18	32	18	3	3
41	33	8	49	8	0	14	4	45	24
34	32	40	21	5	3	0	3	16	3
12	28	31	15	5	21	39	0	10	14
20	18	15	30	39	44	29	13	0	51
5	43	10	48	2	20	5	24	42	0

(a) Traffic matrix

0	47	20	40	9	32	17	32	19	21
47	0	13	16	38	21	30	31	28	33
20	13	0	48	18	29	29	21	12	36
40	16	48	0	32	19	25	27	26	23
9	38	18	32	0	32	48	30	13	35
32	21	29	19	32	0	13	27	18	18
17	30	29	25	48	13	0	32	19	33
32	31	21	27	30	27	32	0	34	44
19	28	12	26	13	18	19	34	0	23
21	33	36	23	35	18	33	44	23	0

(b) Cost Matrix

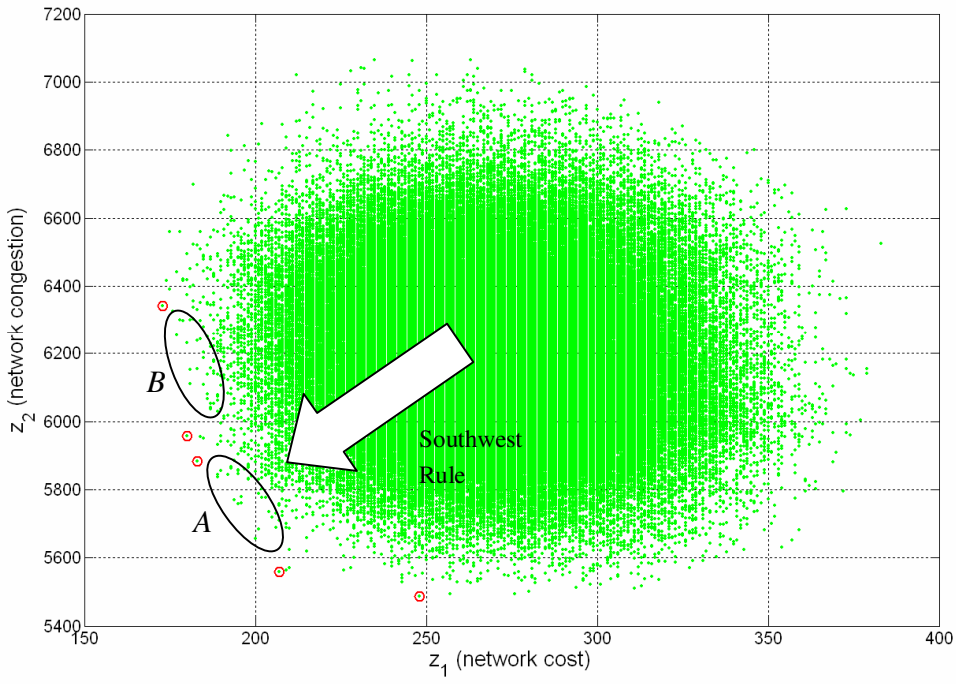

(c) Feasible and Pareto optimal solutions in objective space with $w = 0.005$

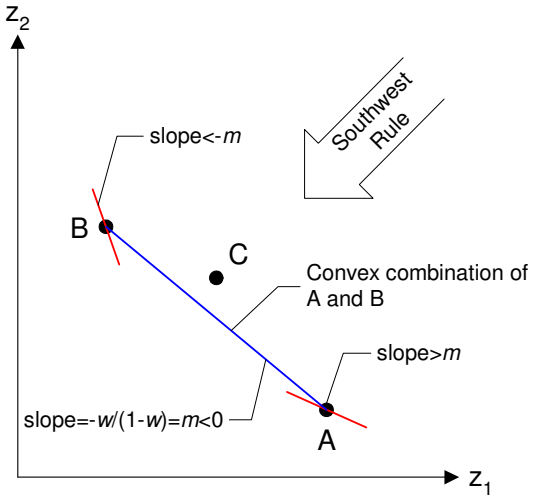

(d) Example of skipping a Pareto-optimal solution

Figure 3-5. Application example of the weighting method

B. The Constraint Method

Instead of articulating weights, the one can solve a single-objective problem using just z_h by constraining the other objectives z_k by some values L_k for $k = 1,...,h-1,h+1,...,p$. In this way, the Pareto optimal solutions in objective space are generated by solving a series of single-objective problems. This method is called the constraint method, and the single-objective subproblem is expressed as:

$$\begin{aligned} &\text{minimize} \quad z_h(x_1, x_2, ..., x_n) \\ &\quad \text{subject to} \\ &\qquad g_i(x_1, x_2, ..., x_n) \le 0, \quad i = 1,...,m \\ &\qquad x_j : \text{ continuous or discrete}, \quad j = 1,...,n \\ &\qquad z_k \le L_k, \quad k = 1,...,h-1,h+1,...,p \end{aligned} \tag{14}$$

The bounds L_k must be chosen so that the resulting single-objective problem (14) should be feasible. For a linear program, the optimal solution x^* to (14) must satisfy

$z_k(x^*) = L_k$ for $k = 1,...,h-1,h+1,...,p$. If the binding condition does not hold for some $k \in \{1,...,h-1,h+1,...,p\}$, then the resulting $(z_1,...,z_p)$ may not be Pareto optimal (Cohon, 2003). For a mixed-integer linear program (MILP) whose decision variables are discrete, the binding condition may not hold because the non-convexity of the feasible region in decision space and objective space (Theorems 3.2.6 and 3.2.8 in Miettinen, 1999). For example, if $L_k = 180.5$ and z_k is always integer in objective space, then $z_k \leq 180.5$ which means the constraint does not bind; if the solution for z_k is 180, then there is a gap of $L_k - z_k = 0.5$. In this case, a continuous slack variable can be used to compute the gap $L_k - z_k$, and then L_k is adjusted to 180 so that the gap is zero (i.e., z_k is bound to L_k) (Gabriel et al., 2006). For this purpose, the single objective problem (14) can be changed as follows:

$$
\begin{aligned}
&\text{minimize} \quad z_h(x_1, x_2, ..., x_n) \\
&\quad \text{subject to} \\
&\qquad g_i(x_1, x_2, ..., x_n) \leq 0, \quad i = 1,...,m \\
&\qquad x_j : \text{ continuous or discrete}, \quad j = 1,...,n \\
&\qquad z_k + s_k \leq L_k, \quad k = 1,...,h-1,h+1,...,p \\
&\qquad s_k \geq 0, \quad k = 1,...,h-1,h+1,...,p
\end{aligned}
\tag{15}
$$

The application of the constraint method starts with a payoff table which consists of the optimal solution x_j^* to each single objective in (11) and the p objective function values to the optimal solution (i.e., $z_k(x_j^*)$ for $j = 1,...,n$ and for $k = 1,...,p$. Thus, the payoff table is a $n \times p$ matrix whose cells are filled with $z_k(x_j^*)$. For the example from Figure 3-6, the payoff table is as follows:

	$z_1(x_1^*)$	$z_2(x_2^*)$
x_1^*	173	6342
x_2^*	248	5487

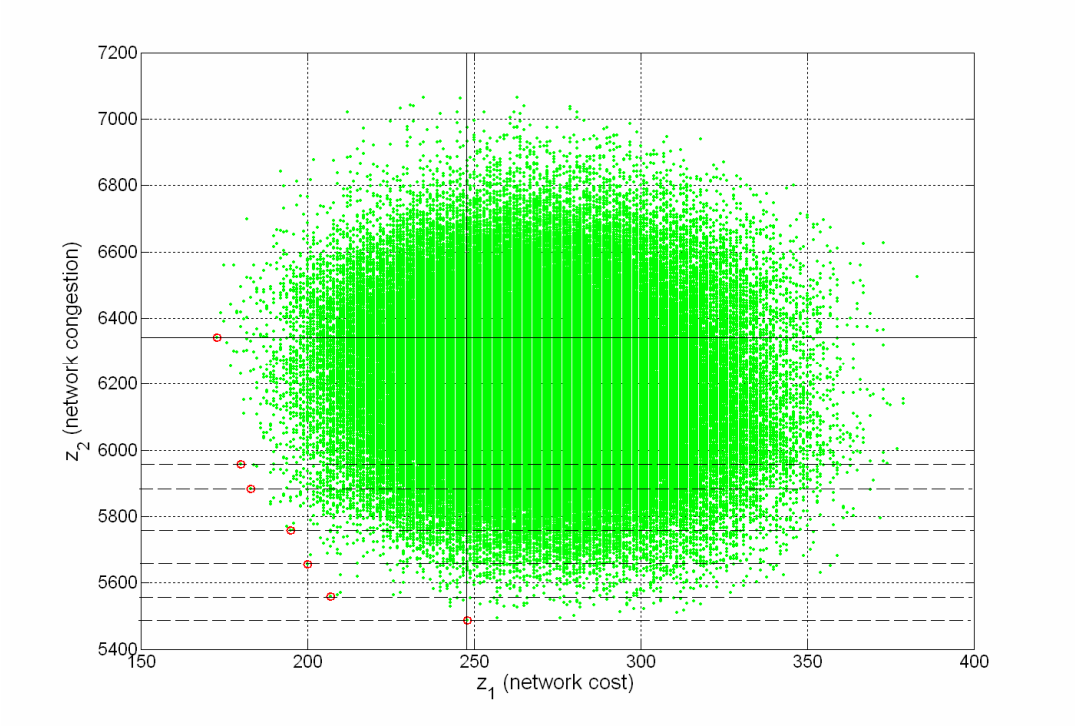

Figure 3-6. Application example of the constraint method (each dotted line corresponds to the constraint $z_2 \le L_2$)

The points $A = [173, 6342]$ and $B = [248, 5487]$ represent the solutions in the payoff table. Then, using the points in the payoff table, L_k is chosen as:

$$L_k = n_k + \frac{t}{r-1}(M_k - n_k) \text{ for } k = 1, ..., p, \qquad (16)$$

where M_k and n_k are the maximum and minimum value for the k-th column in the payoff table, r is the number of step size between M_k and n_k, and

$t = 0, 1, 2, ..., (r-1)$. For example, for the 1st column in the payoff table above, $M_1 = 248$, $n_1 = 173$, $M_2 = 6342$, and $n_2 = 5487$. With $r = 10$, L_1 and L_2 are set as follows:

$$L_1 = 173 + \frac{t}{10-1}(248-173) \text{ for } t = 0,...,9, \text{ and}$$

$$L_2 = 5487 + \frac{t}{10-1}(6342-5487) \text{ for } t = 0,...,9.$$

The single objective problem (15) is solved with r^{p-1} combinations of L_k for $k = 1,...,h-1,h+1,...,p$. Thus, the total number of the single-objective problems to solve is $p \times r^{p-1}$. Since the r^{p-1} combinations of L_k for $k = 1,...,h-1,h+1,...,p$ create a new feasible region in decision space and objective space, it is helpful to find new Pareto optimal points.

For higher dimensional problems with $p \geq 3$, the constraint method can generate infeasible solutions. For example, Figure 3-7 shows a feasible region in three dimensional objective space with $p = 3$. When z_3 is minimized with $z_1 \leq L_1$ and $z_2 \leq L_2$, the five combinations of (L_1, L_2) which are five points, A, B, C, D, and E in Figure 3-7. Because the five points are out of the feasible region, they lead to infeasible problems.

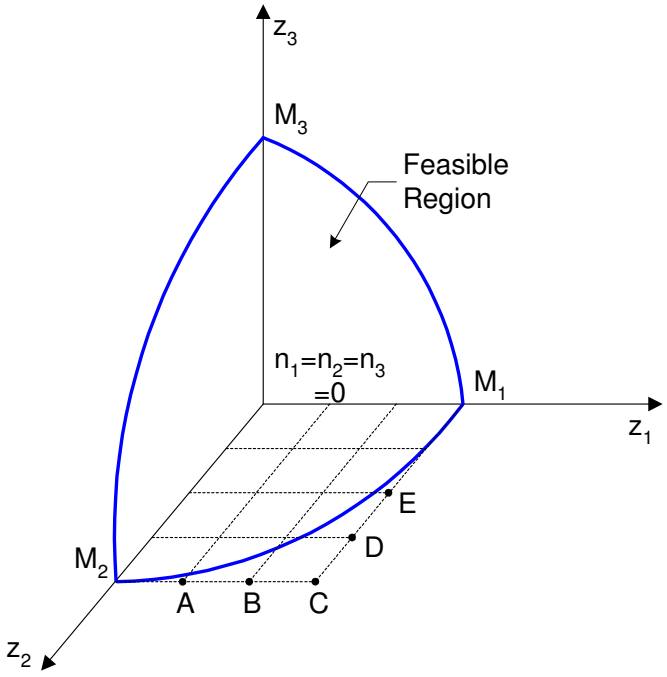

Figure 3-7. Applying the constraint method to a three-objective problem: some of the constrained problems are infeasible (Cohon, 2003)

C. Selection of the Generating Technique for the MOP: The Weighting Method

For the two-objective optimization problem minimizing both network cost and congestion simultaneously, the weighting method was chosen to approximate Pareto optimal solutions. The heuristic method for the MOP is based on a two-swapping method for a neighborhood search. The weighting method is a good fit for the heuristic method, in which the weighted objective function value is computed for each swap. However, the constraint method requires implementing the binding constraints $z_k \leq L_k$ in (14) and (15). Since the number of binding constraints is r^{p-1} and each binding constraint is implemented by IF-THEN statements, the heuristic contains r^{p-1} IF-THEN condition statements. This means that the constraint method would make the structure of heuristic code much bulkier than the weighting method.

In addition, the IF-THEN condition statements can block some good feasible solutions which may lead to improved objective function value in the next neighborhood search. For this reason, only the weighting method was used.

3.2 Fiber Optic Network

3.2.1 Synchronous Optical Network

A Synchronous Optical NETwork (SONET) is equipped with high-speed add-drop multiplexing capability up to 9.953 Gbps (Optical Carrier-192). Its Self-Healing Ring architecture (SHR) provides a self-healing capability which automatically restores disrupted services due to damage on an optical fiber link. The self-healing capability is carried by a second protection ring parallel to the working ring as 1:1 Unidirectional SHR (Figure 3-8 (a)), or by a single ring where its half capacity is reserved for protection as Bidirectional SHR /2 (BSHR/2) (Figure 3-8 (b)).

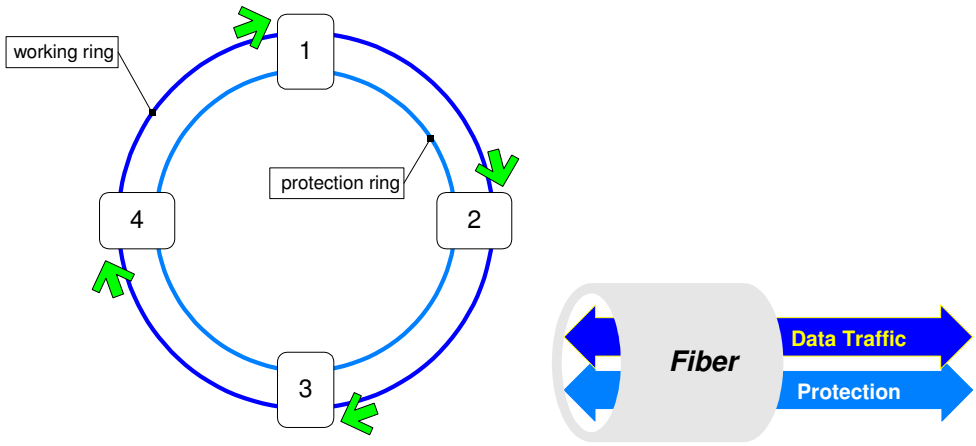

(a) 1:1 USHR (b) BSHR/2

Figure 3-8. SHR architecture in SONET

In BSHR/2, SONET consists of a single fiber ring; working traffic utilizes a half of the capacity and the rest is reserved for protection. Hence a load balancing is required so that any traffic on the fiber should not be over half of the capacity of the ring. An associated optimization problem is called the Ring Loading Problem (RLP).

RLP is defined on an undirected ring network $R = (N, A)$ with a node set $N = \{1, 2, ..., n\}$ and an arc set A. The goal of RLP is to minimize the maximum traffic load on a link by considering how to route the traffic demand between origin-destination pairs. This is accomplished by routing in *i)* either of two directions (clockwise or counter-clockwise), or *ii)* routing a fraction (a, where $0 < a < 1$) of the traffic demand in clockwise and the rest fraction $(1 - a)$ of traffic demand in counter-clockwise (Goldschmidt et al., 2003; van Hoesel, 2005; Karunanithi et al., 1994; Lee et al., 1997; Myung et al., 1997; Schrijver et al., 1998; Myung et al., 2004; Wang, 2005). The problem in which each demand is entirely routed in clockwise or counter-clockwise is called as the RLPWO and it has been shown to be NP-complete (Cosares et al., 1992). RLP is a routing problem which finds optimal routing on a fixed physical topology.

3.2.2 Wavelength Division Multiplexing Network

A Wavelength Division Multiplexing (WDM) network transmits multi-channel (or multiple wavelengths) signals on a single optical fiber to utilize a high capacity of optical fiber. Given that the physical topology of WDM is fixed, each wavelength is assigned between two nodes to make a lightpath. For instance, a

wavelength λ_2 is assigned between node i and node k as shown in Figure 3-9 (b); it forms a lightpath consisting of physical links (i, j) and (j, k) and a wavelength λ_2 assigned on the two links. There are two constraints to form a lightpath:

- A lightpath is spanned by the same wavelength;
- Lightpaths passing the same physical link must have different wavelengths to avoid conflict (interference).

Figure 3-9 (c) shows an example of wavelength assignment by those two constraints and its corresponding logical topology consisting of four wavelengths and seven lightpaths. Any origin-destination (or source-destination) nodes pair in traffic demand that are not directly connected by a lightpath routes its data packets through two or more lightpaths (multi-hopping). For instance, traffic demand between origin node 4 and destination node 5 can be routed through multiple lightpaths: (4,2) →(2,1) →(1,5), (4,3) →(3,1) →(1,5) or (4,2) →(2,6) →(6,5). New logical topology is obtained by rearranging the lightpaths (i.e., using different wavelength assignment) as shown in Figure 3-9 (d).

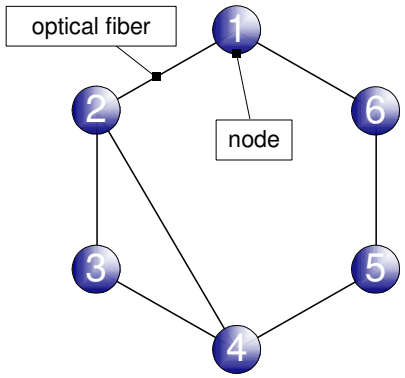

(a) Physical Topology

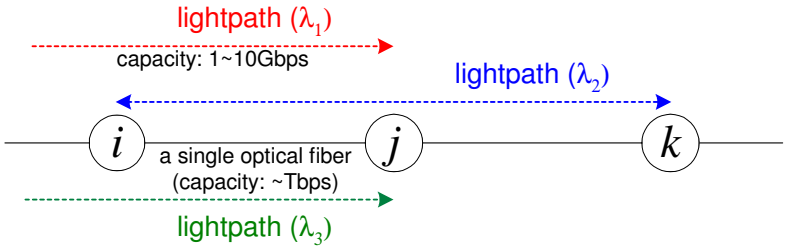

(b) Multiple-channel transmission on physical links (optical fibers)

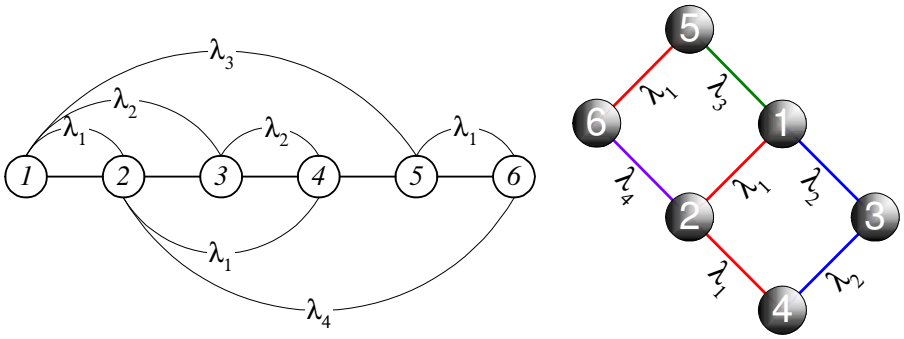

(c) Wavelength assignment and its corresponding logical topology

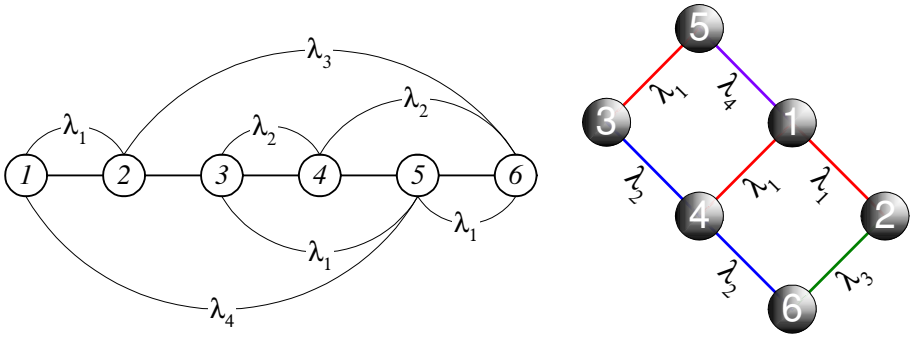

(d) New topology creation by rearranging the lightpaths

Figure 3-9. WDM network

In a WDM network, the logical topology is dynamically reconfigured corresponding to traffic pattern change, network element failures and network element additions. The logical topology reconfiguration is carried out to minimize the network congestion (Ramaswami et al., 1996), or minimize the average packet

delay due to queueing delays at the intermediate nodes with link propagation delays (Mukherjee et al., 1996). An associated mixed-integer linear optimization problem can be solved which consists of two subproblems, a logical topology design problem and a routing problem; but as shown previously it is NP-complete (Banerjee et al., 2004; Chlamtac et al., 1993; Narula-Tam et al., 2000).

The search space for the best logical topology relative to the objective of minimizing the network congestion or the average packet delays grows at least as fast as $n!$, where n is the number of nodes in the network. For example, Figure 3-10 (a) shows a logical ring network topology formed by disconnecting the lightpath between node 1 and node 4 in Figure 3-9 (a) with six nodes (*1-2-3-4-5-6*) and four wavelengths $\lambda_1 \sim \lambda_4$. A new topology is obtained by changing the order of six nodes in the logical ring network topology (e.g., *1-2-3-4-6-5* or *1-2-4-3-5-6*, etc.); thus there are $5!$ possible topologies. If a second transceiver is added to each node and it can switch one of four wavelengths $\lambda_5 \sim \lambda_8$ (Figure 3-10 (b)), then the total number of logical ring network topologies is increased to $(5!)\times(5!) = (5!)^2$. A ring network with n nodes and p transceivers per node consists of $\left((n-1)!\right)^p$ possible logical topologies (Narula-Tam et al., 2000).

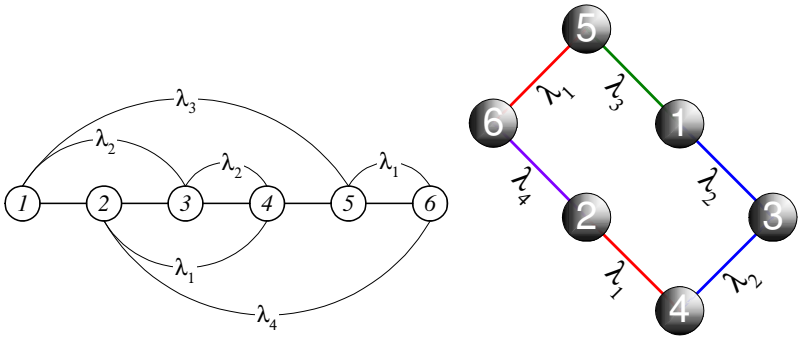

(a) Ring network topology with one optical transceiver per node

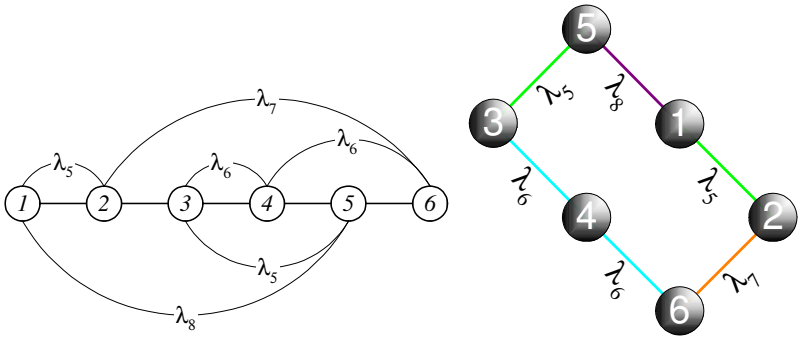

(b) Ring network topology with two optical transceivers per node

Figure 3-10. WDM network with ring network topology

Because it is impractical to determine the optimal topology with optimal routing by solving a mixed-integer linear program, heuristic approaches were introduced: a local search by applying 2-branch exchange or 3-branch exchange (Labourdette et al., 1991; Narula-Tam et al., 2000) or a combination of simulated annealing and flow deviation (Mukherjee et al., 1996). Narula-Tam et al. (2000), Mukherjee et al. (1996), Ramaswami et al. (1996), and Zhang et al. (1995) used shortest hop routing in their heuristic algorithms to simplify the routing subproblem.

3.3 Free-Space Optical Network: Dynamic Reconfiguration of Ring Network Topologies

RLP in SONET BSHR/2 is a routing problem in which the physical topology is fixed. In a WDM network, the physical topology is also fixed, but, however, the logical topology is reconfigured to minimize the network congestion or the average packet delay between any origin-destination nodes pair in traffic demand.

An FSO network consists of fixed or mobile nodes and both the physical and logical topologies should be reconfigured because it is a wireless optical communication network. Thus the physical distance between nodes and the atmospheric condition surrounding each node is varying. If the physical distance is so large or the atmospheric obscuration (e.g., dense fog, dust, or snow) is so high that their directional links experience optical signal attenuation, then it brings about link failure or large increase in transmission power to compensate the attenuation. The physical distance and atmospheric obscuration can be construed as network costs (Llorca et al., 2004a). With such an approach in an optimization problem which seeks the minimum cost topology given the network cost of all possible physical links in the network can be solved. Such a problem is called the Physical Layer Topology Control Problem (PLTCP) (Llorca et al., 2004b).

In contrast, logical topology is reconfigured responding to changes in traffic pattern. The reconfiguration is carried out to minimize the network congestion defined as either the sum of loads on all active links in the network or the maximum

load on an active link in the network. An associated optimization problem to solve is called the NLTCP (Shim et al., 2005). In a bi-connected FSO network (a ring network), the NLTCP finds a best ring network topology (i.e., physical links between nodes) whose congestion is minimal by assuming that all possible optical links between any two nodes in the network are feasible (no optical signal attenuation). Since there are $n(n-1)$ possible origin-destination pairs in a bi-connected FSO network with n nodes, each topology has $2^{n(n-1)}$ possible routings. Moreover, for a n-node ring network, there are $\frac{(n-1)!}{2}$ possible topologies. Hence NLTCP requires an exhaustive search of the $2^{n(n-1)} \times \frac{(n-1)!}{2}$ possible routings, which implies that the complexity of NLTCP is $O\left(2^{n^2} \times n!\right)$. This complexity of NLTCP makes it hard to solve the problem in a reasonable time. However the reconfiguration process must create a new ring network topology responding to the traffic demand change in near-real time. Thus, a heuristic approach might be a solution to this dilemma. Finding a fast heuristic which provides a near-optimal solution to NLTCP is one of the objectives of this research.

For the dynamic reconfiguration of an FSO network, a multiobjective optimization approach is necessary to find a best topology whose network cost and congestion is as low as possible.

In Sections 3.3.1 and 3.3.2, we introduce the mathematical formulations for NLTCP and MOP in a bi-connected FSO network (ring network).

3.3.1 Network Layer Topology Control Problem

Figure 3-11 shows an example of a ring network topology in a bi-connected FSO network with five nodes. Each node is equipped with two FSO transceivers, and each arc represents a bi-directional data link. An important objective in managing such a network involves minimizing the network congestion. Figure 3-12 illustrates the notion of traffic congestion on a link: the traffic congestion on each link, (A,B) or (B,C), is the sum of traffic flows passing through the link. The traffic demand between any OD pair is defined as the bits per second (bps); a traffic matrix R represents traffic demand of all OD pairs. However, each entry in the traffic matrix R may express the average rate of traffic flow (in the unit of packets per second) for the OD pair (Mukherjee et al., 1996) or the arrival rate of packets (in the unit of packets per second) at node o whose destination is node d (Ramaswami et al., 1996).

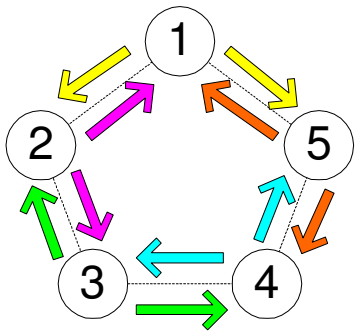

Figure 3-11. A ring network topology (n =5)

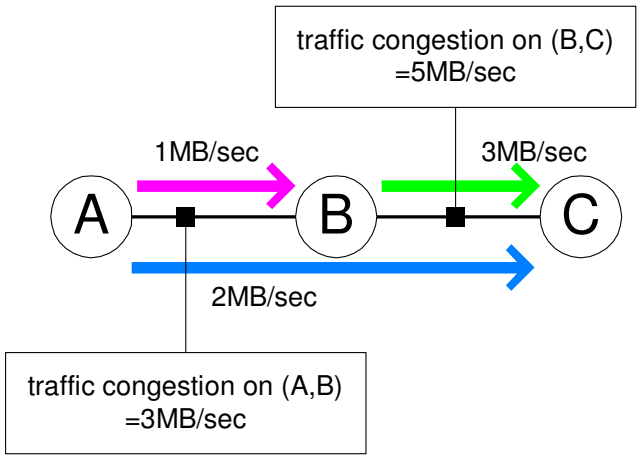

Figure 3-12. Example of cumulative traffic congestion on a link

Notation and model formulation

For a given ring network topology, the following notation is used:

N : Set of all nodes in the system

i, j : Nodes in N

(i, j) : Arc connecting nodes i and j

Ω : Set of all OD pairs, $\Omega = \{(o,d) \in N \times N, o \neq d\}$

ω : OD pair, $\omega = (o,d)$

$o(\omega)$: Origin node of OD pair, $o(\omega) \in N$

$d(\omega)$: Destination node of OD pair, $d(\omega) \in N$, $o(\omega) \neq d(\omega), \forall \omega$

r_ω : Traffic demand between OD pair $\omega = (o,d)$ (in bit-per-second)

R : Traffic matrix, $R(o,d) = r_\omega$ for each $\omega = (o,d)$

A topology matrix Y is defined as follows:

$$y_{ij} = \begin{cases} 1 & \text{if arc (i, j) exists in the topology} \\ 0 & \text{otherwise} \end{cases}$$

with $y_{ij} = y_{ji}$. Also, the flow indicator for OD-pair ω using arc (i, j) is given as:

$$f_{\omega ij} = \begin{cases} 1 & \text{if the traffic of OD pair } \omega \text{ uses arc (i,j)} \\ 0 & \text{otherwise} \end{cases}$$

with $f_{\omega ij} \neq f_{\omega ji}$ constraining the flow at arc (i, j) for OD-pair ω in just one direction at a time. Note that the variables y_{ij} are binary variables associated with the existence of physical data link (e.g., narrow and directional laser beam) from node i to j, and variables $f_{\omega ij}$ are associated with the utilization of the link (i, j) to route the traffic of the particular OD pair. Then the mathematical formulation for NLTCP is expressed as follows:

$$\left[\min_{y,f} \quad z_1 = \sum_{\omega=(o,d)} \sum_{(i,j)} r_\omega f_{\omega ij} \right] \text{ or } \left[\min_{y,f} \quad z_2 = \left(\max_{(i,j)} \sum_{\omega=(o,d)} r_\omega f_{\omega ij} \right) \right] \tag{17}$$

s.t. $$\sum_{i=1}^{n} y_{ij} = 2 \qquad \forall j \tag{18}$$

$$\sum_{j=1}^{n} y_{ij} = 2 \qquad \forall i \tag{19}$$

$$f_{\omega ii} = 0 \qquad \forall \omega, i \tag{20}$$

$$f_{\omega ij} \leq y_{ij} \qquad \forall \omega, i, j \tag{21}$$

$$f_{\omega ij} + f_{\omega ji} \leq 1, \quad \forall \omega, i, j \tag{22}$$

$$\sum_{i=1}^{n} f_{\omega, o(\omega), i} = 1, \ \forall \omega \tag{23}$$

$$\sum_{i=1}^{n} f_{\omega, i, o(\omega)} = 0, \ \forall \omega \tag{24}$$

$$\sum_{i=1}^{n} f_{\omega,i,d(\omega)} = 1\,,\ \forall \omega \tag{25}$$

$$\sum_{i=1}^{n} f_{\omega,d(\omega),i} = 0\,,\ \forall \omega \tag{26}$$

$$\sum_{i=1}^{n} f_{\omega ij} = \sum_{i=1}^{n} f_{\omega ji}\ ,\ \forall \omega \text{ and } i, j \neq o(\omega), d(\omega) \tag{27}$$

$$y_{ij} \in \{0,1\},\ \forall (i, j) \in N \times N \tag{28}$$

$$f_{\omega ij} \in \{0,1\},\ \forall \omega, i, j$$

The objective function (17) has either form of minimizing the total traffic congestion on the network (i.e., $\min\limits_{y,f} \sum\limits_{\omega=(o,d)} \sum\limits_{(i,j)} r_\omega f_{\omega ij}$) or minimizing the maximum traffic congestion in a link on the network (i.e., $\min\limits_{y,f} \left(\max\limits_{(i,j)} \sum\limits_{\omega=(o,d)} r_\omega f_{\omega ij} \right)$). The purpose of the former objective is to minimize the total transmission delay for packets traversing the network. The purpose of the latter objective is to minimize the largest link congestion (or load) which may result in more evenly balanced load across links. Constraints (18) and (19) ensure that each node is of degree two (i.e., FSO transceivers at each node). Constraint (20) stipulates that there is no traffic flow between a node and itself. When a link (i, j) does not exist ($y_{ij} = 0$), no OD pair will use this link for communication ($f_{\omega ij} = 0\,,\forall \omega$) as enforced by constraint (21). Constraint (22) specifies that for any OD pair, the link (i, j) is unidirectional at any given time so as to avoid traffic loops. Additionally, the origin node can use only one link to send out the traffic as shown in constraint (23), and this node does not receive

traffic from any other nodes as shown in constraint (24). For the destination node, it can receive traffic from only one link (constraint (25)) and also does not send out any traffic to other nodes (constraint (26)). For any OD pair, the degree for entering arcs for each node, which is not an origin node nor a destination node, is equal to the degree for exiting arcs, as stipulated in constraint (27). Thus, we see that NLTCP is a binary linear program. Since the NLTCP is an uncapacitated network design problem, it does not impose any link capacity constraints such as "the sum of flow in a link ≤ link capacity". The link constraints prevent any overflow in a link so that the capacities of links are not exceeded and that the link bandwidths are economically distributed to the traffic demand by binding the link capacity constraints (i.e., reducing an unused capacity) under a set of routing and flow constraints (Pióro et al., 2004). The uncapacitated problem may be considered in a network planning to determine how much resource capacity is needed. Once the capacity in a network is known and the traffic demand is given, the capacitated problem decides how to allocate the traffic flow among the links in a network that optimizes a given network performance goal (e.g., minimum congestion routing) (Pióro et al., 2004).

Lastly, note that subtours will be avoided due to the presence of constraints (7) and (9). For example, suppose that a ring network topology with eight nodes has two subtours as shown in Figure 3-13. Then the subtours cannot satisfy constraints (7) and (9) (i.e., $\sum_{i=1}^{n} f_{\omega,o(\omega),i} = 1,\ \forall \omega$ and $\sum_{i=1}^{n} f_{\omega,i,d(\omega)} = 1, \forall \omega$, respectively) because $\sum_{i=1}^{n} f_{\omega,o(\omega),i} \neq 1$ with $\begin{cases} \omega = (3,6),\ o(\omega) = 3 \\ \omega = (6,3),\ o(\omega) = 6 \end{cases}$, and $\sum_{i=1}^{n} f_{\omega,i,d(\omega)} \neq 1$ with

$\begin{cases} \omega = (3,6), d(\omega) = 6 \\ \omega = (6,3), d(\omega) = 3 \end{cases}$. Since the constraints (7) and (9) should be satisfied for all OD pairs $\Omega = \{\omega = (o,d) \in N \times N, o \neq d\}$. Thus, NLTCP model does not allow subtours.

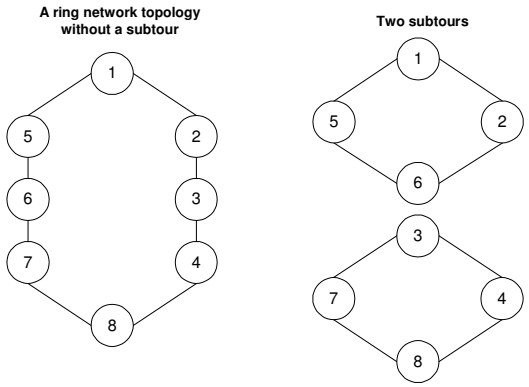

Figure 3-13. $n = 8$ ring network topology and its subtours

Shim et al. (2005) mentioned that NLTCP is a computationally hard problem as the number of nodes n increases because it is a binary linear program; they applied branch-and-bound technique to solve the problem with a commercial solver (e.g., XPRESS-MP). They introduced two new *Shortest Path Constraints* and *Partition Constraints* to efficiently solve the problem. The Shortest Path Constraints and Partition Constraints increase the lower bound of the LP (linear program) relaxation, thereby reducing the number of branches in the branch-and-bound tree in the MIP (mixed-integer program) search. They showed that the two constraints speed up the solution time in the solver for networks with ten or less nodes. In what follows, we describe these two sets of constraints.

Shortest Path Constraints

The Shortest Path Constraints enforce the traffic demand of each OD pair route by the smaller number of arcs (hops) between the OD pair. For example, there are two paths between $\omega = (1,2)$, *(1,2)* or $(1,4) \rightarrow (4,3) \rightarrow (3,2)$ in a four-node ring network topology as shown in Figure 3-14. The former path *(1,2)* has one arc between node 1 and node 2; the latter one $(1,4) \rightarrow (4,3) \rightarrow (3,2)$ has three arcs. Thus, the former path is shorter. The Shortest Path Constraints in a bi-connected ring network with n nodes is mathematically stated as follows:

$$\sum_{i=1}^{n}\sum_{j=1}^{n} f_{\omega ij} \le \left\lfloor \frac{n}{2} \right\rfloor \text{ for } \forall \omega \in \Omega,$$

in which $\sum_{i=1}^{n}\sum_{j=1}^{n} f_{\omega ij}$ is the number of arcs between the OD pair, $\omega = (o,d)$. For the example in Figure 3-14, the longer path $(1,4) \rightarrow (4,3) \rightarrow (3,2)$ for $\omega = (1,2)$ cannot satisfy this constraint because:

$$\sum_{i=1}^{4}\sum_{j=1}^{4} f_{\omega=(1,2)ij} = f_{\omega=(1,2)ij=(1,4)} + f_{\omega=(1,2)ij=(4,3)} + f_{\omega=(1,2)ij=(3,2)} = 3 > \left\lfloor \frac{4}{2} \right\rfloor = 2.$$

But, $\sum_{i=1}^{4}\sum_{j=1}^{4} f_{\omega=(1,2)ij} = f_{\omega=(1,2)ij=(1,2)} = 1 \le \left\lfloor \frac{4}{2} \right\rfloor = 2$. It is important to note that the right-hand side $\left\lfloor \frac{4}{2} \right\rfloor$ is related to going around the ring at most half way.

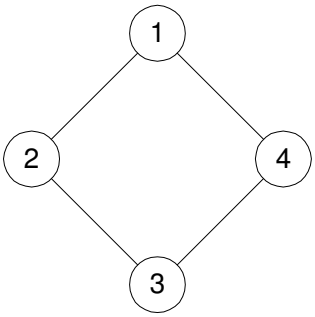

Figure 3-14. Example of a $n = 4$ ring network topology

Motivated by the Shortest Path Constraints, we can generate a distance matrix $DIST$, measuring the shorter number of arcs between each OD pair (e.g., the length of the shortest path). For the example in Figure 3-14, the distance matrix is:

$DIST =$

o \ d	1	2	3	4
1	0	1	2	1
2	1	0	1	2
3	2	1	0	1
4	1	2	1	0

Figure 3-15. A distance matrix for a topology in Figure 3-14

As can be seen, each element in the distance matrix is the number of arcs in the shortest path for each OD pair. For example, the shortest path between $\omega = (1,2)$ is *(1,2)*; thus, $DIST(1,2) = 1$. Shim et al. (2005) showed that the objective function for the total traffic congestion can be expressed as:

$$\sum_{\omega=(o,d)} \sum_{(i,j)} r_\omega f_{\omega ij} = \sum_{\omega=(o,d)} r_\omega \left(\sum_{(i,j)} f_{\omega ij} \right) = \sum_{o=1}^{n} \sum_{d=1}^{n} r_{\omega=(o,d)} DIST(o,d) \qquad (29)$$

The objective function is a simple summation of element-by-element products of two separate terms, r_ω and $DIST(o,d)$. Equation (29) allows us to find optimal solutions by enumerating all possible ring network topologies. Also, because the objective function value is computed by (29) for each topology, (29) is used in a heuristic algorithm described later, to calculate the objective function value (Shim et al., 2005).

One of the main advantages of the Shortest Path Constraints is that they simplify the routing decision in NLTCP. There are $2^{n(n-1)}$ possible routing directions (i.e., clockwise or counter-clockwise) for $n(n-1)$ possible OD pairs in a ring network with n nodes. However, the shortest path constraint $\sum_{i=1}^{n}\sum_{j=1}^{n} f_{\omega ij} \le \left\lfloor \frac{n}{2} \right\rfloor$ for $\forall \omega \in \Omega$ reduces the $2^{n(n-1)}$ possible routing directions by $n(n-1)$ because the shorter path between each OD pair is enforced. Hence the Shortest Path Constraints reduce the computational complexity of NLTCP from $O\left(2^{n(n-1)} \times \frac{(n-1)!}{2} \right) \simeq O\left(2^{n^2} \times n!\right)$ to $O\left(n(n-1) \times \frac{(n-1)!}{2} \right) \simeq O\left(n^2 \times n!\right)$, which is a significant computational gain. Note that the optimal objective function value of NLTCP with the Shortest Path Constraints is the same as the one without the constraints because of the relation in (29). However, the NLTCP with the Shortest Path Constraints provides a solution faster than the one without the constraints (Shim et al., 2005).

Partition Constraints

Partition Constraints (for n even only) are based on patterns in the $n \times n$ topology matrix Y and distance matrix $DIST$. Constraints (30)~(33) are examples of such patterns; Figure 3-16 illustrates the meaning of those constraints.

$$n(B) = \sum_{i=1}^{7} \sum_{j=i+1}^{8} y_{ij} = n(H) = \sum_{i=9}^{15} \sum_{j=i+1}^{16} y_{ij} = 7 , \tag{30}$$

$$0 \le n(B) = \sum_{i=1}^{\frac{n}{2}-1} \sum_{j=i+1}^{\frac{n}{2}} y_{ij} \le \frac{n}{2} - 1 = 7 , \tag{31}$$

$$0 \le n(H) = \sum_{i=\frac{n}{2}+1}^{n-1} \sum_{j=i+1}^{n} y_{ij} \le \frac{n}{2} - 1 = 7 , \tag{32}$$

$$d(B) = \sum_{i=1}^{7} \sum_{j=i+1}^{8} DIST(i, j) = d(H) = \sum_{i=9}^{15} \sum_{j=i+1}^{16} DIST(i, j) = 84 . \tag{33}$$

Here $n(P)$ and $d(P)$ represent, respectively, the number of elements equal to 1 in partition P of the matrix Y and the sum of elements in partition P of $DIST$. Figure 3-16 (b) shows that the number of elements equal to 1 in the two partitions B and H (defined in Figure 3-16 (a)) is equal, and the number is less than or equal to $n/2$ (i.e., constraints (30), (31) and (32)). For the $DIST$ matrix, the sum of elements in partition B is equal to the one in partition H as shown in Figure 3-16 (c).

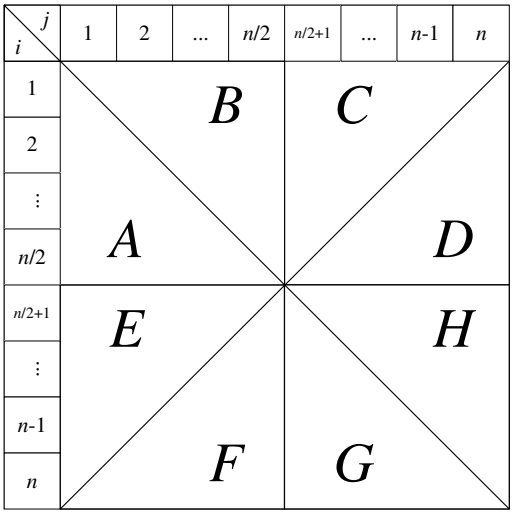

(a) Partitions on Y and $DIST$

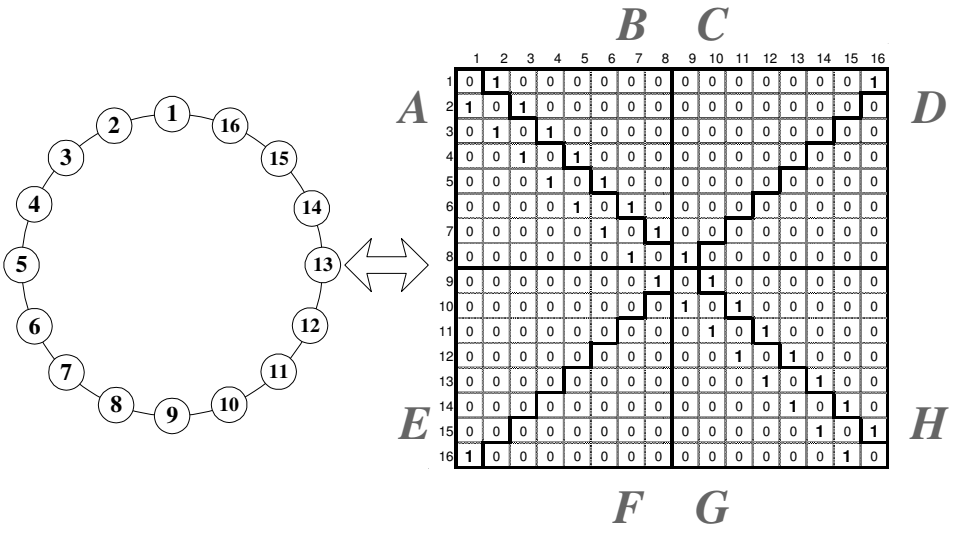

(b) Partitions on a topology matrix Y for $n = 16$

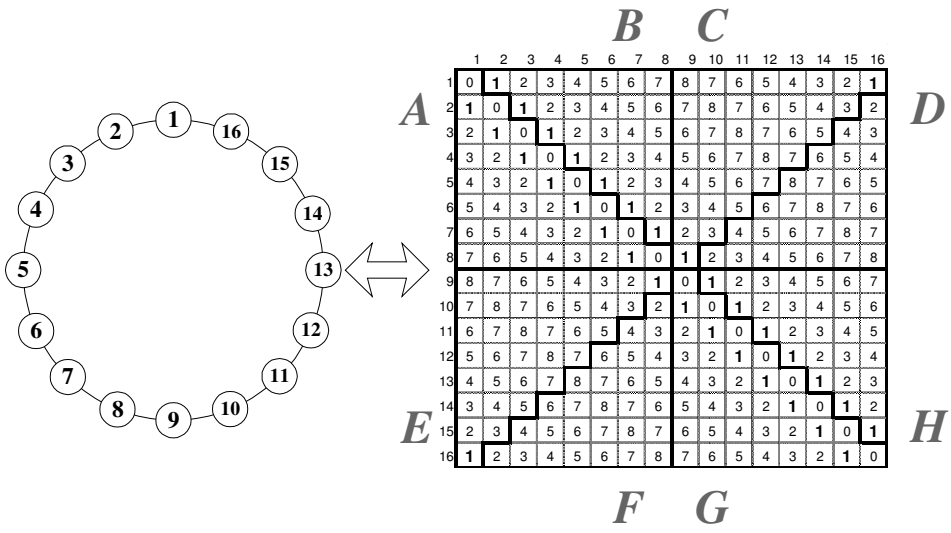

(c) Partitions on a distance matrix $DIST$ for $n = 16$

Figure 3-16. Examples of Partition Constraints for $n = 16$ (Gabriel et al., 2006)

Triangle Inequality Constraints

Shim et al. (2005) used $DIST(o,d)$ variable to define the number of arcs of the shortest path for OD pair, $\omega = (o,d)$: $DIST(o,d) = \sum_{i=1}^{n}\sum_{j=1}^{n} f_{\omega ij}$. Here, we propose two new constraints denoted as *Triangle Inequality Constraints*, whose purpose, like for the Shortest Path and Partition Constraints, is to increase the lower bound in a continuous relaxation of NLTCP.

First, we define some terms used in the proof. Let $v(o,d)$ be the number of arcs in the shorter direction between node o and node d around the topology. Figure 3-17 (a) shows the shorter and longer paths in a bi-connected ring network

topology. Note that the "left" and "right" sides of the circles are relative to the nodes o and d in question as well as where the center line is drawn. Let $N = \{1, 2, ..., n\}$ be a set of nodes in the topology. Let S be an ordered set of nodes which are on the shorter path between node o and node d, in which nodes o and d are included. Let $\hat{S}$ be an ordered set of nodes which are on the longer path between node o and node d, in which nodes o and d are included. Thus, the intersection of S and $\hat{S}$ is $\{o, d\}$. Figure 3-17 (c) shows an example of the ordered sets, S and $\hat{S}$. It is assumed that node o and node d are end-to-end nodes in the shorter and longer path, and an intermediate node k must not be an end node (i.e., $k \neq o, d$).

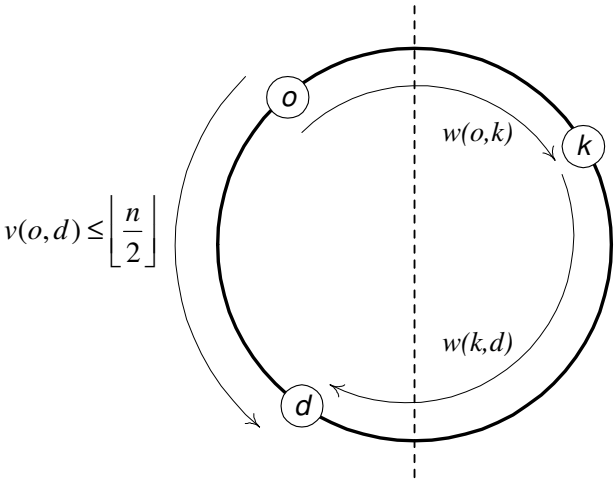

(a) When OD pair (o, d) is on the "left" side of the circle of a ring topology

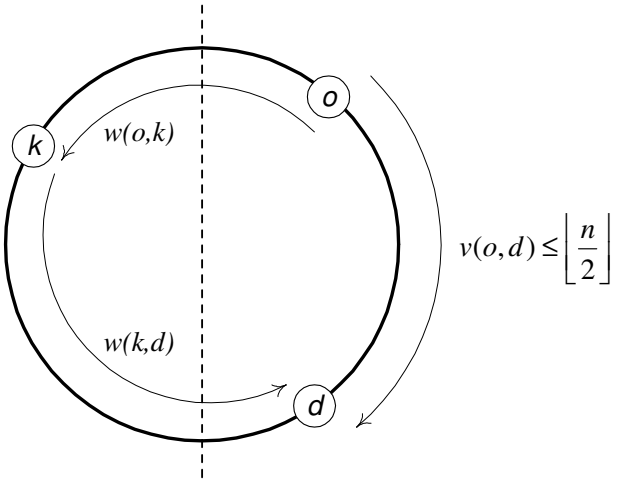

(b) When OD pair (o,d) is on the "right" side of the circle of a ring topology

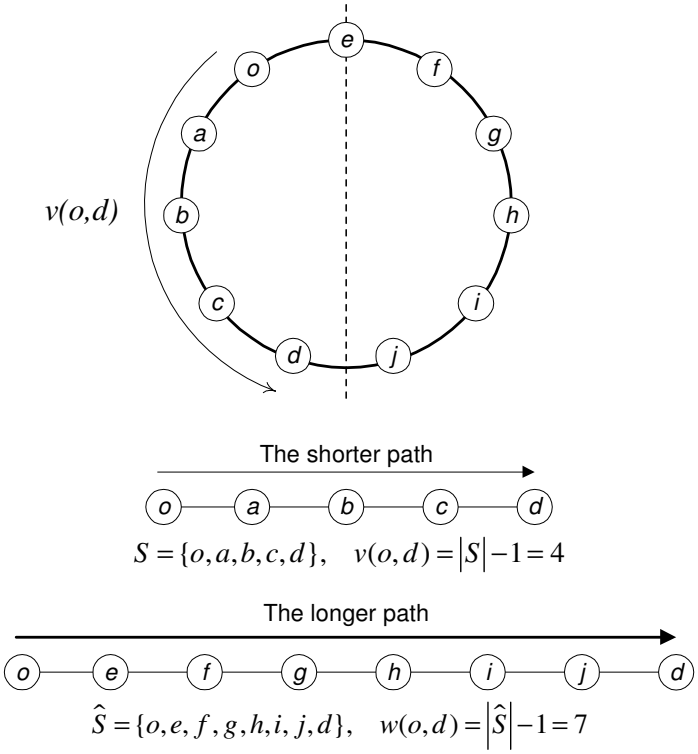

(c) An illustration of ordered set, S and $\hat{S}$

Figure 3-17. Shorter and longer paths in a bi-connected ring network topology

If node o and node d are on the left side of the circle of the ring topology as shown in Figure 3-17 (a), then the number of arcs between node o and node k and between node k and node d in the clockwise direction are $w(o,k)$ and $w(k,d)$, respectively. If node o and node d are on the right side of the circle of the ring topology as shown in Figure 3-17 (b), the number of arcs between node o and node k and between node k and node d in the counter-clockwise direction are $w(o,k)$ and $w(k,d)$, respectively.

Triangle Inequality Constraints:

Theorem: The following two sets of constraints are valid for any feasible topology.

i) $DIST(o,k)+DIST(k,d) \geq DIST(o,d)$ for $\forall\ o,k,d \in N$, $k \neq o,d$ and $o \neq d$.

ii) $DIST(o,k)+DIST(k,d) \leq n - DIST(o,d)$ for $\forall\ o,k,d \in N$, $k \neq o,d$ and $o \neq d$.

Proof

Case A) If a node k belongs to the shorter path between the OD pair (o,d) whose length is $DIST(o,d)$, then $v(o,k) \leq DIST(o,d) \leq \left\lfloor \frac{n}{2} \right\rfloor$ and $v(k,d) \leq DIST(o,d) \leq \left\lfloor \frac{n}{2} \right\rfloor$. This means that $v(o,k)$ and $v(k,d)$ are the shorter paths between the OD pairs (o,k) and (k,d), respectively, since the longer path has a length which is greater than $\left\lfloor \frac{n}{2} \right\rfloor$. Hence, $v(o,k) = DIST(o,k)$, $v(k,d) = DIST(k,d)$ and $v(o,k)+v(k,d) = DIST(o,d)$.

Therefore, $\lfloor \frac{n}{2} \rfloor \geq DIST(o,d) = DIST(o,k) + DIST(k,d)$ in particular

$DIST(o,k) + DIST(k,d) = DIST(o,d)$ so *i)* is shown and

$DIST(o,k) + DIST(k,d) \leq \lfloor \frac{n}{2} \rfloor \leq n - \lfloor \frac{n}{2} \rfloor \leq n - DIST(o,d)$ so *ii)* is shown.

Case B) We now consider node k belonging to the longer path from node o to node d. Since the total number of arcs in a bi-connected ring network topology with n nodes is n, we have $n = DIST(o,d) + w(o,k) + w(k,d)$. Now we consider four subcases to show that *i)* and *ii)* hold.

Case B-1) $w(o,k) \leq \left\lfloor \frac{n}{2} \right\rfloor$ and $w(k,d) \leq \left\lfloor \frac{n}{2} \right\rfloor$.

Then, $w(o,k) = DIST(o,k)$ and $w(k,d) = DIST(k,d)$

$\Rightarrow DIST(o,d) = n - w(o,k) - w(k,d) = n - DIST(o,k) - DIST(k,d)$

$\Rightarrow DIST(o,d) \leq n - DIST(o,d) = DIST(o,k) + DIST(k,d)$

$\Rightarrow DIST(o,k) + DIST(k,d) \geq DIST(o,d)$.

Therefore, *i)* is shown, and $DIST(o,k) + DIST(k,d) = n - DIST(o,d)$ so *ii)* is shown.

Case B-2) $w(o,k) \leq \left\lfloor \frac{n}{2} \right\rfloor$ and $w(k,d) > \left\lfloor \frac{n}{2} \right\rfloor$.

$w(o,k) = DIST(o,k)$ and $w(k,d) = n - DIST(k,d)$

$$\begin{aligned} \Rightarrow DIST(o,d) &= n - w(o,k) - w(k,d) \\ &= n - DIST(o,k) - w(k,d) \\ &= \big(n - w(k,d)\big) - DIST(o,k) \\ &= DIST(k,d) - DIST(o,k) \\ &\leq DIST(o,k) + DIST(k,d) \end{aligned}$$

So *i)* is shown. But we also see that

$$\begin{aligned} n - DIST(o,d) &= w(o,k) + w(k,d) \\ &= DIST(o,k) + w(k,d) \\ &= DIST(o,k) + (n - DIST(k,d)) \\ &= n + DIST(o,k) - DIST(k,d) \\ &= \left(n - DIST(k,d)\right) + DIST(o,k) \\ &\geq \left(n - \left\lfloor \frac{n}{2} \right\rfloor\right) + DIST(o,k) \\ &\geq \left\lfloor \frac{n}{2} \right\rfloor + DIST(o,k) \\ &\geq DIST(k,d) + DIST(o,k) \end{aligned}$$

So *ii)* is shown.

Case B-3) $w(o,k) > \left\lfloor \frac{n}{2} \right\rfloor$ and $w(k,d) \leq \left\lfloor \frac{n}{2} \right\rfloor$.

$w(k,d) = DIST(k,d)$ and $w(o,k) = n - DIST(o,k)$

$$\begin{aligned} \Rightarrow DIST(o,d) &= n - w(o,k) - w(k,d) \\ &= n - w(o,k) - DIST(k,d) \\ &= \left(n - w(o,k)\right) - DIST(k,d) \\ &= DIST(o,k) - DIST(k,d) \\ &\leq DIST(o,k) + DIST(k,d) \end{aligned}$$

So *i)* is shown. But also, we see that

$$\begin{aligned} n - DIST(o,d) &= n - DIST(o,k) + DIST(k,d) \\ &\geq \left(n - \left\lfloor \frac{n}{2} \right\rfloor\right) + DIST(k,d) \\ &\geq \left\lfloor \frac{n}{2} \right\rfloor + DIST(k,d) \\ &\geq DIST(o,k) + DIST(k,d) \end{aligned}$$

So *ii)* is shown.

Case B-4) $w(o,k) > \left\lfloor \frac{n}{2} \right\rfloor$ and $w(k,d) > \left\lfloor \frac{n}{2} \right\rfloor$.

We will show that this case cannot actually happen. First, since $n = DIST(o,d) + w(o,k) + w(k,d) > DIST(o,d) + \left\lfloor \frac{n}{2} \right\rfloor + \left\lfloor \frac{n}{2} \right\rfloor$, we see that $n = DIST(o,d) + w(o,k) + w(k,d) \geq DIST(o,d) + 2\left(\left\lfloor \frac{n}{2} \right\rfloor + 1 \right) > n$, which is a contradiction. So this case cannot happen. □

The Triangle Inequality Constraints with the Shortest Path Constraints can increase the lower bound of the LP relaxation more than the Shortest Path Constraints. Figure 3-18 displays a computational example for NLTCP with $n = 10$; it shows the upper and lower bounds of the objective value (y-axis) and the solution time in seconds (x-axis). It compares the lower bound of the objective value when NLTCP is solved *i)* with the Triangle Inequality Constraints, Shortest Path Constraints, and Partition Constraints and *ii)* with the Shortest Path Constraints and Partition Constraints. As depicted in the figure, the Triangle Inequality Constraints improve the lower bound of the objective value, thus reducing the solution time (90 seconds with the two constraints versus 2240 seconds with only the Shortest Path Constraints).

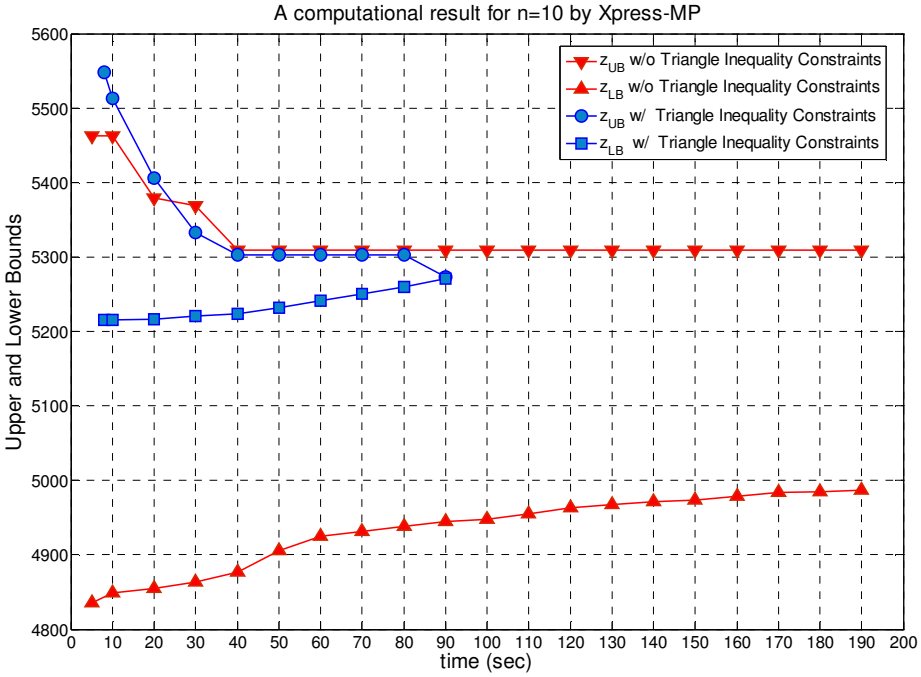

Figure 3-18. The effectiveness of the Triangle Inequality Constraints ($n = 10$)

3.3.2 Multiobjective Optimization Problem

The objective of the multiobjective optimization problem is to find a Pareto optimal solution which jointly minimizes network cost and congestion and Figure 3-19 shows an example of Pareto optimality. Figure 3-19 (a) shows two ring network topologies with four nodes. Topology 1 is better than Topology 2 with respect to minimizing cost, whereas Topology 2 is better than Topology 1 for minimizing congestion. Thus, the best topology depends on the objective function being considered.

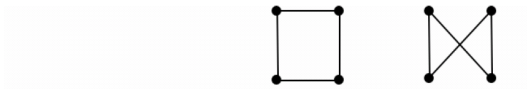

	Topology 1	Topology 2
Physical layer: Aggregate Network Cost (BER)	10	12
Network layer: Traffic congestion (BPS)	15	5

(a) Example of physical/network layer topology mismatch (Zhuang et al., 2004)

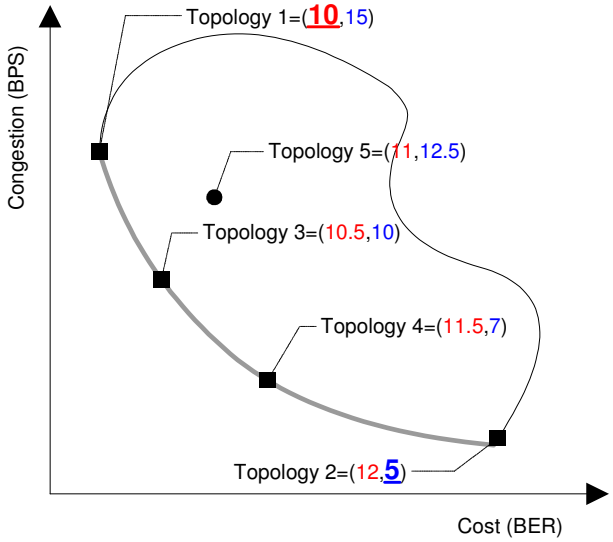

(b) Pareto optimality: minimizing both cost and congestion

Figure 3-19. Example of a Pareto optimal solution

A conceptual Pareto optimal set is illustrated in Figure 3-19 (b). In this figure, the kidney-shaped set is the entire feasible region (i.e., a set of all possible topologies) in objective space with cost on the x-axis and congestion on the y-axis. The objective values of topology 1 and 2 from Figure 3-19 (a) are plotted at the leftmost and rightmost parts of the Pareto frontier, respectively. If we move from topology 3 to topology 4, then congestion is improved at the expense of cost; cost is improved by sacrificing congestion in the opposite direction. Thus, either topology 3 and 4 are Pareto optimal points. The choice of which topology on the Pareto frontier to select is then dependent on the decision maker's preference. One way to state this preference is by a weight appearing in the objective function (e.g., the weighting method). All points on the bold curve between topology 1 and topology 2 consists of a Pareto optimal set (i.e., any two points on the curve are neither superior to nor inferior to each other). By contrast, feasible topologies such as topology 5 that are not on the frontier are dominated by Pareto optimal points because their cost and/or congestion values can be improved without worsening the other objective.

The formulation for MOP is as follows:

$$\min_{y,f} \quad w\sum_{(i,j)} \tfrac{1}{2} c_{ij} y_{ij} + (1-w) \sum_{\omega=(o,d)} \sum_{(i,j)} \sum_{k=1}^{K} p^k r_\omega^k f_{\omega ij}^k \tag{34}$$

$$\text{s.t.} \quad \sum_{i=1}^{n} y_{ij} = 2 \qquad \forall j \tag{35}$$

$$\sum_{j=1}^{n} y_{ij} = 2 \qquad \forall i \tag{36}$$

$$f_{\omega ij}^k \le y_{ij} \qquad \forall \omega, i, j, k \tag{37}$$

$$f^k_{\omega ii} = 0 \qquad \forall i,k \qquad (38)$$

$$f^k_{\omega ij} + f^k_{\omega ji} \le 1 \qquad \forall \omega, i, j, k \qquad (39)$$

$$\sum_{i=1}^{n} f^k_{\omega,o(\omega),i} = 1, \qquad \forall \omega, k \qquad (40)$$

$$\sum_{i=1}^{n} f^k_{\omega,i,o(\omega)} = 0, \qquad \forall \omega, k \qquad (41)$$

$$\sum_{i=1}^{n} f^k_{\omega,i,d(\omega)} = 1, \qquad \forall \omega, k \qquad (42)$$

$$\sum_{i=1}^{n} f^k_{\omega,d(\omega),i} = 0, \qquad \forall \omega, k \qquad (43)$$

$$\sum_{i=1}^{n} f^k_{\omega ij} = \sum_{i=1}^{n} f^k_{\omega ji}, \qquad \forall \omega, k \text{ and } i, j \ne o(\omega), d(\omega) \qquad (44)$$

$$y_{ij} \in \{0,1\} \qquad \forall (i,j) \in N \times N \qquad (45)$$

$$f^k_{\omega ij} \in \{0,1\} \qquad \forall \omega, i, j, k \qquad (46)$$

In MOP, we consider that the traffic demands are uncertain. The uncertainty in the traffic demand is represented by a set of K scenarios $\{1,\ldots,K\}$ with a random load r^k_ω for scenario k and OD pair ω. We call this formulation "Stochastic Problem (SP)," and the probability of scenario k is p^k. In addition to (35)-(46), the Shortest Path Constraints and Partition Constraints that are used to improve the solution time in NLTCP are also included. The weighting method (Cohon, 1978) is applied to combine both cost and congestion objectives using a positive weight w. The shortest hop condition assumes that the "weight" of each arc is the same, i.e., just

the number of arcs is important. When this is not the case so that the cost c_{ij} of arc (i, j) is more relevant (or maybe the physical distance of the link), a shortest hop approach can be extended by letting c_{ij} instead of "1" be the arc weight. This will change the Shortest Path Constraints, however, which may have a deleterious effect on computational times.

Gabriel et al. (2006) showed that the above stochastic version of NLTCP (S-NLTCP) can be replaced by a deterministic problem shown below, for which the solution sets are essentially the same. In the deterministic equivalent, the scenario superscripts do not appear on the flow variables ($f^k_{\omega ij} \rightarrow f_{\omega ij}$), and the expected load (r_ω) replaces the scenario-specific one (r^k_ω). Thus, there are less binary flow variables than the stochastic version so that solution times are generally better. In addition, the reformulation allows us to more easily generate a Pareto optimal set of topologies comparing the two objectives cost versus congestion.

(Deterministic Equivalent)

$$\min_{y,f} \quad w\sum_{(i,j)} \tfrac{1}{2} c_{ij} y_{ij} + (1-w) \sum_{\omega=(o,d)} \sum_{(i,j)} r_\omega f_{\omega ij}, \text{ where } r_\omega = \sum_{k=1}^{K} p^k r^k_\omega \qquad (47)$$

$$\text{s.t.} \quad \sum_{i=1}^{n} y_{ij} = 2 \qquad \forall j \qquad (48)$$

$$\sum_{j=1}^{n} y_{ij} = 2 \qquad \forall i \qquad (49)$$

$$f_{\omega ij} \le y_{ij} \qquad \forall \omega, i, j \qquad (50)$$

$$f_{\omega ii} = 0 \qquad \forall i \tag{51}$$

$$f_{\omega ij} + f_{\omega ji} \le 1 \qquad \forall \omega, i, j \tag{52}$$

$$\sum_{i=1}^{n} f_{\omega, o(\omega), i} = 1, \qquad \forall \omega \tag{53}$$

$$\sum_{i=1}^{n} f_{\omega, i, o(\omega)} = 0, \qquad \forall \omega \tag{54}$$

$$\sum_{i=1}^{n} f_{\omega, i, d(\omega)} = 1, \qquad \forall \omega \tag{55}$$

$$\sum_{i=1}^{n} f_{\omega, d(\omega), i} = 0, \qquad \forall \omega \tag{56}$$

$$\sum_{i=1}^{n} f_{\omega ij} = \sum_{i=1}^{n} f_{\omega ji}, \qquad \forall \omega \text{ and } i, j \ne o(\omega), d(\omega) \tag{57}$$

$$y_{ij} \in \{0,1\} \qquad \forall (i, j) \in N \times N \tag{58}$$

$$f_{\omega ij} \in \{0,1\} \qquad \forall \omega, i, j \tag{59}$$

3.4 Heuristic Algorithms for Dynamic Reconfiguration of Ring Network Topologies

The logical topology reconfiguration problem of WDM network for a ring network topology (Narula-Tam et al., 2000) discussed in Section 3.2.2 is similar to NLTCP in that it also requires an exhaustive search of all possible ring network topologies to find a best ring network topology with optimal routing scheme. However, sometimes it is not possible to ever compute optimal solutions as was the case in Narula-Tam et al. (2000), where only a ten-node ring networks was tried, or in the case of Labourdette et al. (1991), Mukherjee et al. (1996), Ramaswami et al. (1996), and Zhang et al. (1995). For example, Narula-Tam et al. (2000) approximated the optimality gap of their heuristic solutions with lower and upper bounds on the objective function value; the optimality gaps for 100 test problems with ten-node ring network were within 14 % on average. Labourdette et al. (1991) used a lower bound on the objective function value to estimate the optimality gap of their heuristic solution; the optimality gaps for eight test problems with an eight-node network were in the range of 0~35.2 %. Shim et al. (2005) also discussed the lack of a performance measure for optimal solutions in the Uncapacitated Network Design Problem (UNDP) such as the optimization problem in WDM network; since NLTCP does not impose any capacity constraint in a link to limit the sum of traffic flows through it, NLTCP is a UNDP. Finding a heuristic and presenting performance accuracy of the heuristic is one of objectives of this research, which considerably contributes to the solution of UNDP.

In Sections 3.4.1 and 3.4.2, fast heuristics for NLTCP and MOP and their performance (optimality gap) are presented. To generate the optimal solutions for both optimization problems, we used XPRESS-MP (www.dashoptimization.com) or MATLAB; both software packages were run on a DELL 3.6 GHz personal computer with 3 GB of RAM.

3.4.1 Heuristics for NLTCP

The heuristic algorithm for NLTCP is based on a two-node swapping method and an iterative improvement to find a better solution. As long as an improved solution exists, it is adopted and the iterative procedure is repeated from the new solution. Its overall procedure is as follows:

(a) Generate a random feasible solution (a ring network topology) and compute its corresponding objective function value. Step 1 in Figure 3-20 shows this procedure. A feasible topology is randomly chosen and its initial objective function value ($TTC_{init} = 845$) is computed by (29).

(b) Then swap two nodes from this random solution. Compute and record the improvement in the objective function value (TTC) computed by (29) for the topology with the swapped nodes (i.e., the objective function value is improved when $TTC_{diff} = TTC - TTC_{init} \le 0$). Do this for every two node swapping possibility. The number of two node swapping applied in this step is $(n-1)(n-2)$ which is explained later. Step 2 in Figure 3-20 displays this procedure.

(c) Order, in a list, the improvements in the objective function based on this swapping method from largest (the most improved) to smallest (the least improved). If the length of the list is greater than or equal to four, then the top two and bottom two topologies can be always selected from the list. Thus picking out the top two and bottom two topologies from the list can be more practical than selecting the topologies which show improvement in the objective function in a regular manner (i.e., selecting the *i*-th, *j*-th, *k*-th, and *l*-th topology from the list), although this is somewhat arbitrary. These four ring network topologies that have been selected become new feasible solutions. Step 3 in Figure 3-20 shows the list of topologies whose objective function value is improved. The top two topologies (*1-2-5-4-3* and *1-2-4-3-5*) and bottom two topologies (*1-3-2-4-5* and *1-4-3-2-5*) are selected as new feasible solutions.

(d) Apply the same procedure from (b) and (c), to each new feasible solution in parallel except choosing the most improved topology and consider it as a new solution; this continues until a best topology is found. Step 4 in Figure 3-20 illustrates this procedure. For the rightmost feasible topology, (b) and (c) are repeated until there is no improvement in the objective function value.

The total number of two-opt swap used in the overall procedure (a)~(d) is a multiple of $(n-1)(n-2)$ because the number depends on how many times step (b) is repeated until the overall procedure ends. The two-opt swap in step (b) can be replaced with three-opt or more nodes swapping which increases the total number of

swaps in this step. For example, the total number of swaps for the three-opt swap is $(n-1)(n-2)(n-3)$; it searches more feasible solutions and thus provide a better heuristic solution than the two-opt swap in step (b). The core of the NLTCP HEURISTIC is step (c) in which the search direction for a local or global minimum is diversified as the number of the feasible topologies picked out from the list. Each feasible topology provides a different search direction, and it is called a *RULE*. The search direction is more diversified by increasing the number of RULEs to more than four or by replacing $TTC_{diff} \leq 0$ with $TTC_{diff} \leq \alpha$ (where $\alpha > 0$) in the step (b), which is the main factor of the heuristic improvement algorithm described later.

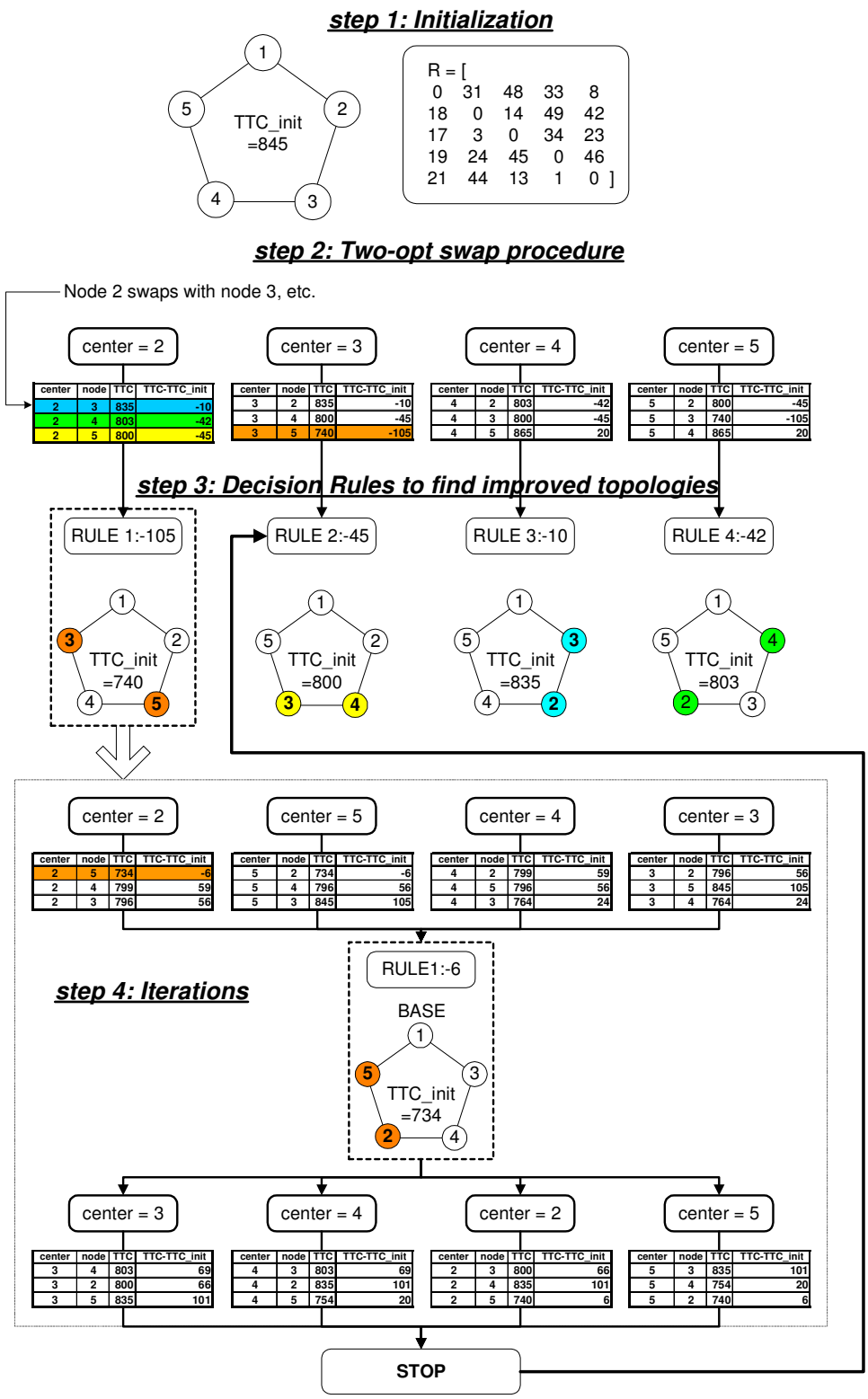

Figure 3-20. Example of NLTCP HEURISTIC procedure

A more formal version of the procedure stated above is as follows:

NLTCP Heuristic

Step 1: Initialization

(a) Generate a vector of nodes $node_{init} = \{1, i_2, \ldots, i_n\}$ where $\{i_2, \ldots, i_n\}$ is a permutation of $\{2, \ldots, n\}$.

(b) Using $node_{init}$, compute the corresponding topology matrix Y and set $Y_{init} = Y$.

(c) Compute the distance matrix $DIST$ from Y_{init} and set $DIST_{init} = DIST$.

(d) Compute the total traffic congestion TTC and set $TTC_{init} = TTC$.

Step 2: Two-Opt Swap Procedure

(a) Set $node_{base} = node_{init}$, and $count = 1$.

FOR k=2 to n DO (k is an index number of $node_{base}$.)

(b) Set $center = node_{base}(k)$, where $center$ is the k th node number in $node_{base}$.

For $i = 2, \ldots, n, i \neq k$ and $node_{base}(i) \geq center$ DO

i) Exchange the position of the k th node ($center$) and the i th node in $node_{base}$

ii) Using $node_{base}$ with i and k swapped, compute the corresponding topology matrix Y and set $Y_{base} = Y$.

iii) Compute the distance matrix $DIST$ from Y_{base} and set $DIST_{base} = DIST$

iv) Compute TTC and $TTC_{diff} = TTC - TTC_{init}$

v) Save TTC, TTC_{diff}, and the swapped $node_{base}$ in a data structure as follows:

$DATA(count) = \{[TTC, TTC_{diff}, node_{base}]\}$ and set

$count = count + 1$.

vi) Reset $node_{base}$ to $node_{init}$.

END DO

Reset $node_{base}$ to $node_{init}$.

END DO

Step 3: Decision rules to find improved topologies

(a) Find vectors of $[TTC, TTC_{diff}, node_{base}] \in DATA$ which satisfy $TTC_{diff} \leq 0$ (if there is a pair of vectors whose (TTC, TTC_{diff}) values are the same, then choose only one); set the number of topologies with an improved total traffic congestion as m.

(b) Among the m topologies selected in STEP 3a, pick out four of them corresponding to:

- The largest negative value of TTC_{diff} (RULE 1)
- The second largest negative value of TTC_{diff} (RULE 2)
- The least negative (or zero) value of TTC_{diff} (RULE 3)
- The second least negative value of TTC_{diff} (RULE 4)

(c) Save each topology from RULES 1-4.

Step 4: Iterations

(a) Take each of the four topologies selected in Step 3 and apply the swapping procedure Step 2 to obtain a new topology with the most improvement.

(b) Record relevant information as before

(c) Repeat until no further improvement in TTC values. Or Step 4c is enforced to finish in a finite number of iteration to avoid an excessive search time for the improvement in TTC values.

Step 5: Final Step

Choose $[TTC, node_{base}]$ which has the smallest TTC among the TTC values collected from the result in STEP 4 to each RULE.

End of procedure.

The above (standard) algorithm is improved by a heuristic improvement algorithm, employing more than four rules (i.e., $m \geq 5$) or replacing $TTC_{diff} \leq 0$ with $TTC_{diff} \leq \alpha$, where α is a positive value, in Step 3a (Shim et al., 2005).

NLTCP HEURISTIC is based on a two-opt swap. From the initial solution (e.g., Step 1 in Figure 3-20), it selects m feasible solutions. Steps 2 and 3 in Figure 3-20 show the procedure of selecting four feasible topologies (m=4). In the next iteration, a new neighborhood is found in a greedy way from each feasible solution in Step 3. This diversified neighborhood search gives us a better chance to find a global optimal

solution than a greedy heuristic because we can still expect that the rest of the $m-1$ feasible solutions can help us find global optima.

NLTCP HEURISTIC is a polynomial time algorithm. According to the definition of National Institute of Standards and Technology (www.nist.gov/dads), the execution time of the polynomial time bound algorithm is a polynomial function of the problem size n, more formally $O(n^k)$ where k is a constant (www.nist.gov/dads). Figure 3-21 shows that the execution time of NLTCP HEURISTIC is a polynomial function of the network size with $7 \le n \le 15$. For each n, one hundred input traffic matrices were randomly generated. Each element (r_ω) in the input traffic matrix was an integer value between 1 and 50 except the diagonals which were all zero. The total number of iterations of the two-opt swap in Step 2 was counted to approximate the execution time of NLTCP HEURISTIC code implemented in MATLAB (version 7.0) because the heuristic keeps searching for a best ring network topology by swapping two nodes and computing the corresponding objective function value of the newly generated ring network topology. In Step 2, the number of iterations of the two-opt swap is $(n-1)(n-2)$ because the outer and inner FOR-loops iterate $(n-1)$ and $(n-2)$ times, respectively. In Step 4, the two-opt swap continues with four (or at most m) topologies from Step 3b. In Step 4, for each topology selected in Step 3b, the two-opt swap procedure in Step 2 repeats until there is no improvement in TTC values. If the iteration in Step 4c is assumed to end in a finite number of iterations, the total number of iterations of the two-opt swap in the NLTCP HEURISTIC is measured by:

$$(n-1)(n-2)+\nu_1(n-1)(n-2)+...+\nu_m(n-1)(n-2), \qquad (60)$$

where ν_i denotes the number of the iterations in Step 4c for topology i among the m topologies selected in Step 3b. (60) shows that the NLTCP HEURISTIC is a polynomial algorithm.

Each "×" symbol in Figure 3-21 represents the total number of iterations of the two-opt swap in Step 2 for each input traffic matrix; one hundred "×" symbols were plotted for each n. The "□" symbol represents the mean of one hundred of the "×" symbols for each n. In Figure 3-21, the curve connecting the "□" symbols is a polynomial function of n which is expressed as $p(n) = 101.99n^2 - 1366.1n + 5061.9$; Table 3-1 summarizes the coefficient values calculated by least squares (Wolf et al., 1997) for a quadratic ($c_2 n^2 + c_1 n^1 + c_0$), qubic ($c_3 n^3 + c_2 n^2 + c_1 n^1 + c_0$), and biquadratic ($c_4 n^4 + c_3 n^3 + c_2 n^2 + c_1 n^1 + c_0$) function. The curves with "△" and "◊" symbols are upper and lower bounds of $p(n)$, respectively. Since the "×" symbols for each n are bounded by the quadratic function, the complexity of NLTCP HEURISTIC is $O(n^2)$.

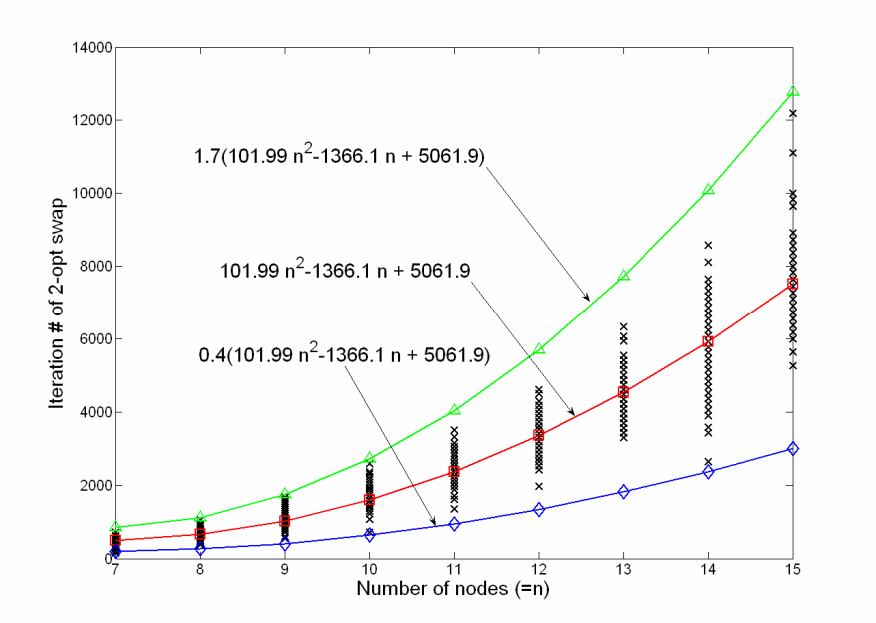

Figure 3-21. NLTCP Heuristic: polynomial time bound algorithm

Table 3-1. The coefficients for polynomial curve fitting

	c4	c3	c2	c1	c0	Ra^2
coefficient value			101.99	-1366.1	5061.9	93.4762%
t statistic			28.898589	-17.50184	12.241492	
confidence interval			99.90%	99.90%	99.90%	
coefficient value		5.9699	-95.016	730.53	-2109.1	93.5654%
t statistic		3.664313	-1.76354	1.265196	-1.054762	
confidence interval		99.97%	92.18%	79.39%	70.82%	
coefficient value	0.83774	-30.891	499.42	-3426.8	8516.7	93.5660%
t statistic	1.044649	-0.874526	0.873762	-0.85216	0.821573	
confidence interval	70.35%	61.79%	61.75%	60.56%	58.85%	

Ra^2: adjusted coefficient of multiple detrmination

Generated by StatTool statistical software (version 1.1.0) (www.palisade.com)

Figure 3-22 displays that the NLTCP HEURISTIC finds its best solution with a relatively small number of feasible solutions (or neighbors visited) relative to the size of the whole decision space (i.e., $(n-1)!/2$) as the number of nodes in a ring network topology increases. The ratio displayed in the vertical axis is given by

$\frac{p(n)}{(n-1)!/2} \times 100\%$ for $10 \le n \le 15$, where $p(n) = 101.99n^2 - 1366.1n + 5061.9$. The graph shows that the NLTCP HEURISTIC is a fast heuristic and efficiently works for a ring network topology with large n.

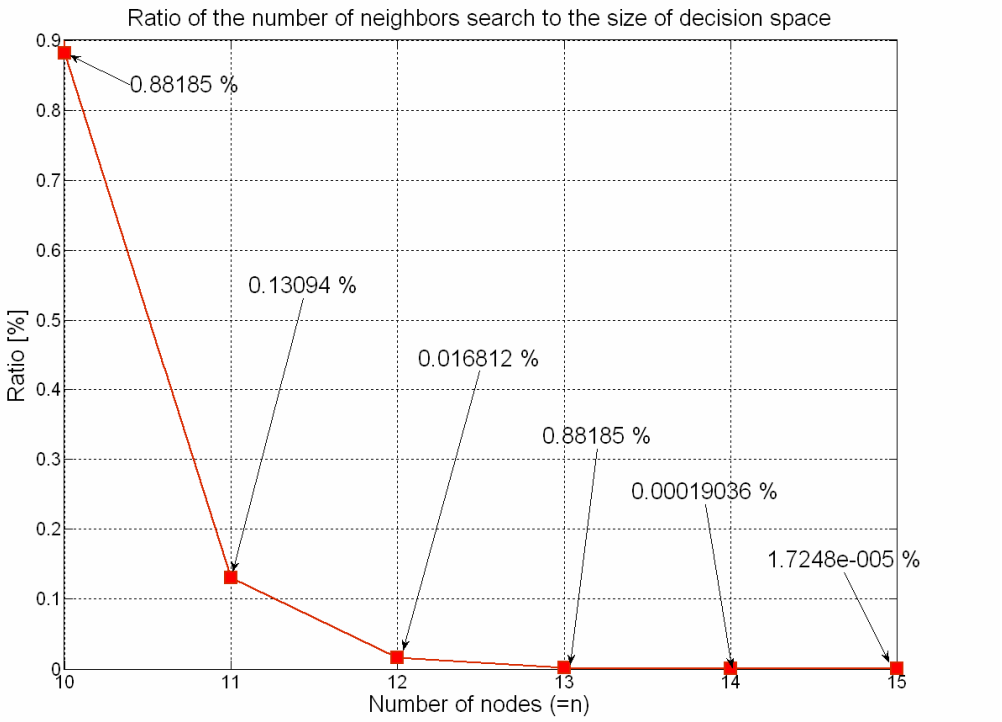

Figure 3-22. Ratio of the number of neighbors search to the size of decision space

Numerical Results

The performance of the NLTCP HEURISTIC was tested for networks of size eight to fifteen nodes. For each node, ten $n \times n$ traffic matrices were randomly generated and best solutions from the heuristic code implemented in MATLAB were compared with the optimal solutions from XPRESS-MP or with an enumeration code in MATLAB. Figure 3-23 (a) summarizes the test results of the optimality gap of the

best integer solution from the heuristic code for $n = 8, 9, 10, 12, 14$, and 15 ring network topologies. The results are encouraging in that: 56 cases out of a total of 60 trials showed an optimality gap within 1.5 % and 58 cases out of the 60 trials were within a 2.0 % optimality gap. In addition, most of the search times to find the best integer solution were less than 60 seconds (Figure 3-23 (b)), with the exception for two cases for the 15 ring network topology, where the search times were more than 60 seconds (the most was 73 seconds). The solution time would be much improved by coding the heuristic procedure with machine languages such as C/C++. Figure 3-24 shows that the heuristic improvement algorithm brings about smaller optimality gaps than the standard heuristic algorithm (or at worst the same values); see Shim et al. (2005) for more details.

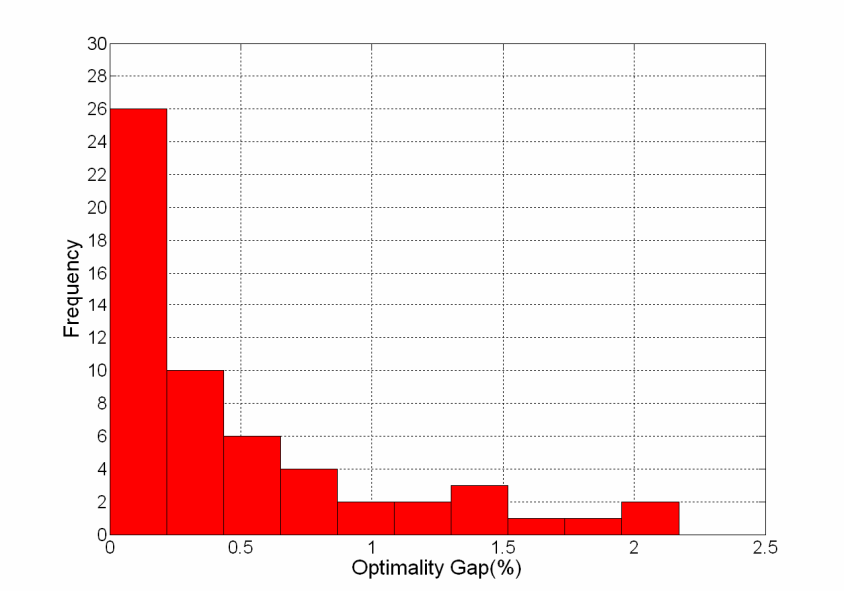

(a) Optimality gap

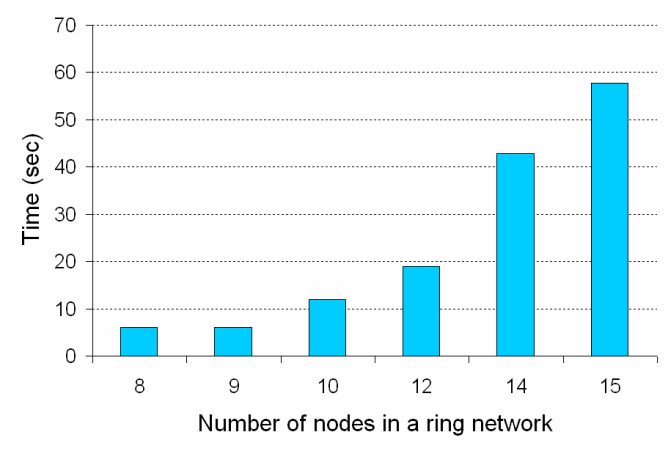

(b) Solution times

Figure 3-23. Performance of the heuristic algorithm for NLTCP

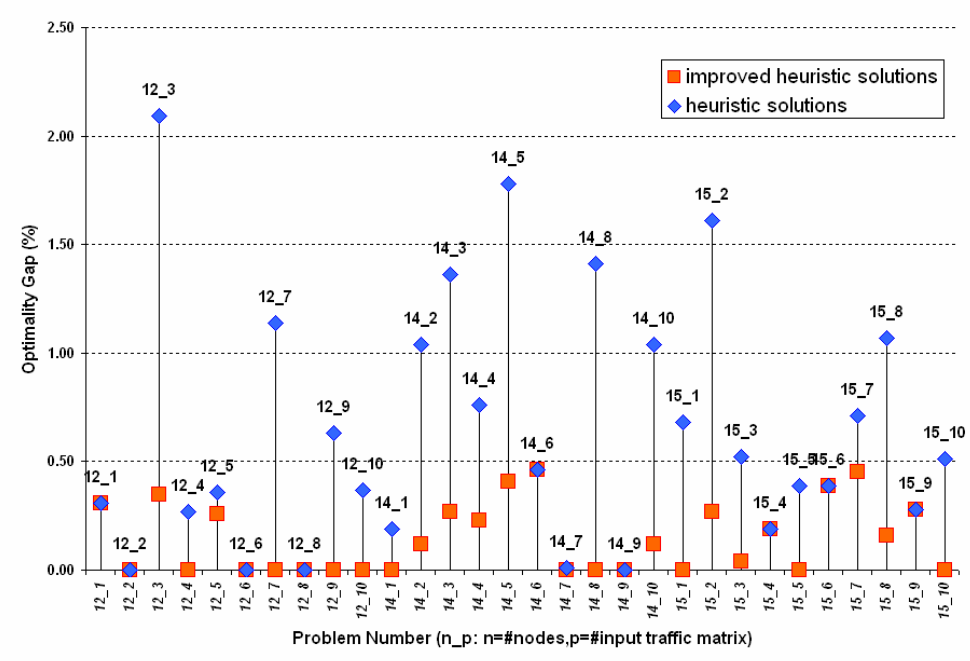

Figure 3-24. Optimality gap (%) of heuristic algorithm and heuristic improvement algorithm

3.4.2 Heuristics for MOP

The heuristic algorithm for MOP is almost same as the heuristic algorithm for NLTCP in Section 3.4.1. The difference between two heuristic algorithms is the input and objective function formats. Inputs to the heuristic algorithm are both cost (c_{ij}) and the expected load (r_ω^k) with its probability (p^k) for a set of K scenarios; the objective function is a weighted sum of cost and congestion, that is,

$$w\sum_{(i,j)} \tfrac{1}{2} c_{ij} y_{ij} + (1-w) \sum_{\omega=(o,d)} \sum_{(i,j)} r_\omega f_{\omega ij} \text{ , where } r_\omega = \sum_{k=1}^{K} p^k r_\omega^k \qquad (61)$$

MOP Heuristic

MOP HEURISTIC is based on 2-opt swap and the standard four RULEs in NLTCP HEURISTIC to select new feasible solutions for the next iteration. MOP HEURISTIC consists of the same steps as the ones in NLTCP HEURISTIC. The only difference is the format of the objective function; the mathematical symbol TTC must be replaced with $MOBJ$ in the whole steps of NLTCP HEURISTIC. The objective function value (denoted as $MOBJ$) is computed by (61) and replaces TTC in each step of NLTCP HEURISTIC. The MOP HEURISTIC algorithm is improved by employing more than four RULEs (i.e., $m \geq 5$) or $MOBJ_{diff} \leq \alpha$, where $MOBJ_{diff} = MOBJ - MOBJ_{init}$ and α is a positive value. If $w = 1$ in (61), then the congestion objective vanishes from the multiobjective function. Thus, the MOP HEURISTIC with $w = 1$ finds a minimum cost topology in the Traveling Salesman Problem. The cost matrix can be symmetric or asymmetric.

To test the performance of MOP HEURISTIC, three types of atmospheric obscuration scenarios and three types of traffic patterns were considered as follows (resulting in a stochastic multiobjective optimization problem to solve):

Obscuration Scenarios

The obscuration scenario is characterized by a cost matrix whose entries indicate the attenuation of all potential links in the network. We only considered the effects of cloud attenuation, which is the main and most common obscurant affecting laser propagation. In Figure 3-25, three types of low, medium and high obscuration scenarios are generated with 2 %, 5 % and 8 % cloud cover, respectively. The cloud cover is defined as the cloud density in the three dimensional space of 16km×16km×8km (Llorca et al., 2005).

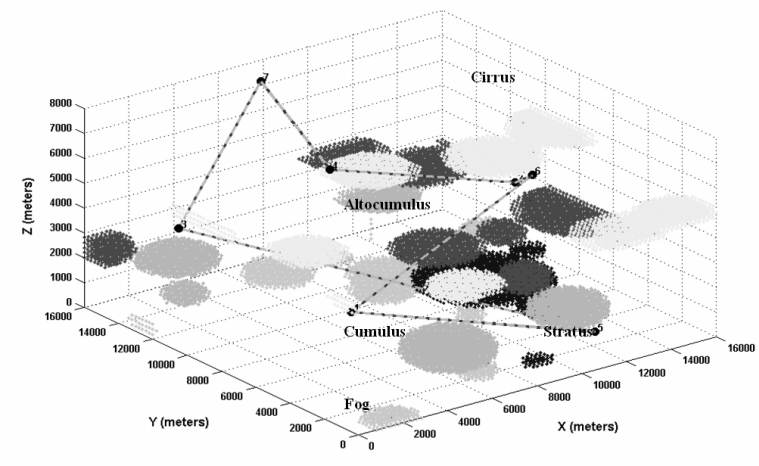

Figure 3-25. Example of a 3-dimensional scenario with cloud layers at different heights and 7 nodes communicating using FSO technology (Llorca et al., 2005).

0	42	51	50	50	131	49	41	41	48
42	0	53	50	51	51	49	41	42	50
51	53	0	51	201	721	52	53	52	50
50	50	51	0	37	48	41	52	48	38
50	51	201	37	0	45	45	52	182	40
131	51	721	48	45	0	424	51	98	313
49	49	52	41	45	424	0	144	45	39
41	41	53	52	52	51	144	0	45	51
41	42	52	48	182	98	45	45	0	46
48	50	50	38	40	313	39	51	46	0

(a) Low cost

0	47	43	51	50	51	50	54	47	51
47	0	48	51	45	47	234	54	51	46
43	48	0	51	382	51	510	54	47	53
51	51	51	0	845	878	48	44	48	51
50	45	382	845	0	34	36	51	51	44
51	47	51	878	34	0	39	50	52	46
50	234	510	48	36	39	0	575	52	41
54	54	54	44	51	50	575	0	51	846
47	51	47	48	51	52	52	51	0	53
51	46	53	51	44	46	41	846	53	0

(b) Medium cost

0	320	45	314	810	45	538	43	299	47
320	0	48	42	46	42	45	43	189	145
45	48	0	43	200	226	53	44	590	35
314	42	43	0	50	31	49	40	302	45
810	46	200	50	0	50	41	51	167	53
45	42	226	31	50	0	49	38	44	270
538	45	53	49	41	49	0	50	408	53
43	43	44	40	51	38	50	0	48	47
299	189	590	302	167	44	408	48	0	836
47	145	35	45	53	270	53	47	836	0

(c) High cost

Figure 3-26. Example: three types of cost patterns for $n=10$

Three Types of Traffic Patterns

In addition, three types of traffic patterns were considered: uncorrelated traffic, weakly correlated traffic, and strongly correlated traffic. Each off-diagonal element in the three types of traffic matrices is an integer value in the range [1,50]; the diagonal elements are set to zero. For the uncorrelated traffic (Figure 3-27 (a)), there is no pattern *a priori* between the traffic matrix elements. For the weakly correlated traffic, there are clusters of higher demand indicated by the shaded regions in Figure 3-27 (b). Lastly, the strongly correlated traffic had roughly the same level of traffic demand between any OD pair (Figure 3-27 (c)).

0	35	9	30	17	26	16	32	24	37
17	0	25	14	38	8	15	12	47	19
39	43	0	43	21	39	18	47	12	27
16	24	32	0	23	22	40	3	37	7
47	32	26	45	0	44	34	30	40	42
35	22	40	48	40	0	18	16	28	47
44	1	14	32	18	47	0	40	21	29
47	14	37	39	37	47	11	0	28	12
34	9	35	9	8	6	36	7	0	21
7	17	50	10	11	19	14	17	14	0

(a) Uncorrelated

0	10	1	6	6	4	6	8	**46**	5
9	0	1	10	**41**	7	11	7	1	5
7	10	0	2	6	5	10	4	4	**43**
46	3	2	0	5	10	7	8	7	4
7	6	8	10	0	10	4	**50**	9	4
8	**45**	9	8	3	0	4	6	8	4
7	5	3	9	1	5	0	7	4	6
10	6	3	**43**	7	10	2	0	5	9
6	2	11	9	7	6	**44**	10	0	4
9	7	4	3	7	**48**	10	7	3	0

(b) Weakly correlated

0	35	27	31	26	29	30	30	33	32
26	0	35	26	34	30	27	30	28	26
27	30	0	30	27	30	28	32	25	29
30	25	33	0	32	31	31	30	33	29
34	34	28	29	0	32	35	29	28	29
32	32	26	27	28	0	28	30	27	31
34	27	25	33	33	29	0	33	33	26
29	31	28	29	25	30	34	0	30	32
34	30	26	30	26	28	30	29	0	32
30	30	28	31	32	34	28	35	32	0

(c) Strongly correlated

Figure 3-27. Example: three types of traffic patterns for $n=10$

Numerical Results

The performance of the MOP HEURISTIC implemented in MATLAB (version 7.0) was tested for networks with n=8 and n=10. The MIP solver XPRESS-MP or an exhaustive search based on MATLAB code was used to obtain an optimal topology against which the heuristic solution was compared. For the test, nine positive weights $w \in \{0.1, 0.2, 0.3, 0.4, 0.5, 0.6, 0.7, 0.8, 0.9\}$ were considered. In addition, the uncertainty in the traffic demand is represented by ten scenarios (K=10) with arbitrarily chosen probability set $p^1 = p^2 = ... = p^{10} = 0.1$. Thus, for each weight $w \in \{0.1, 0.2, 0.3, 0.4, 0.5, 0.6, 0.7, 0.8, 0.9\}$, nine combinations of cost and traffic matrices were tried (Figure 3-28). For either n=8 or n=10, there were 81 cases; 162 cases in all. The test was limited to n=8 and n=10 because both XPRESS-MP and MATLAB showed slow progress for networks with n>10 (e.g., more than 2 days by XPRESS-MP and 5 minutes by MATLAB per each test problem for n=12). Columns E, G, and H in Table 3-8 (for n=8) and Table 3-9 (for n=10) present the heuristic solutions, optimal solutions, and optimality gaps for the test.

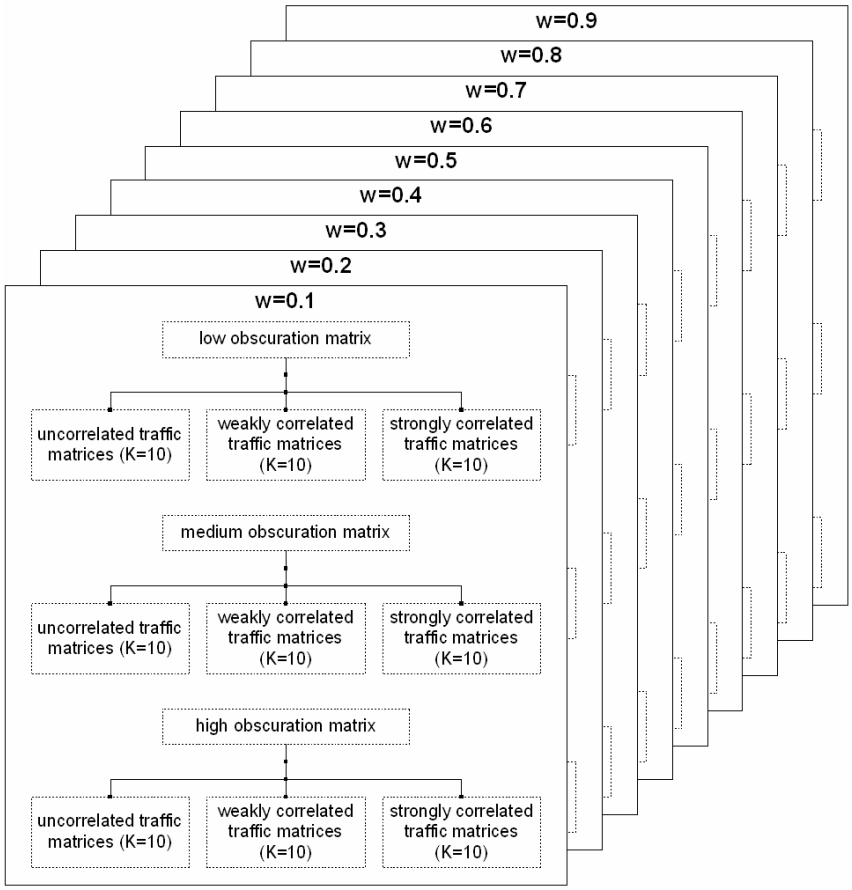

Figure 3-28. Nine combinations of cost and traffic matrices for each weight

Figure 3-29 presents the optimality gap between the best solutions from the XPRESS-MP (or MATLAB enumeration) and those obtained by the heuristic approaches outlined above. The results are encouraging in that the optimality gap in 89 of 162 cases (54.9 %) was less than 0.1 % and in 136 out of 162 cases (83.9 %) it was less than 0.5 %.

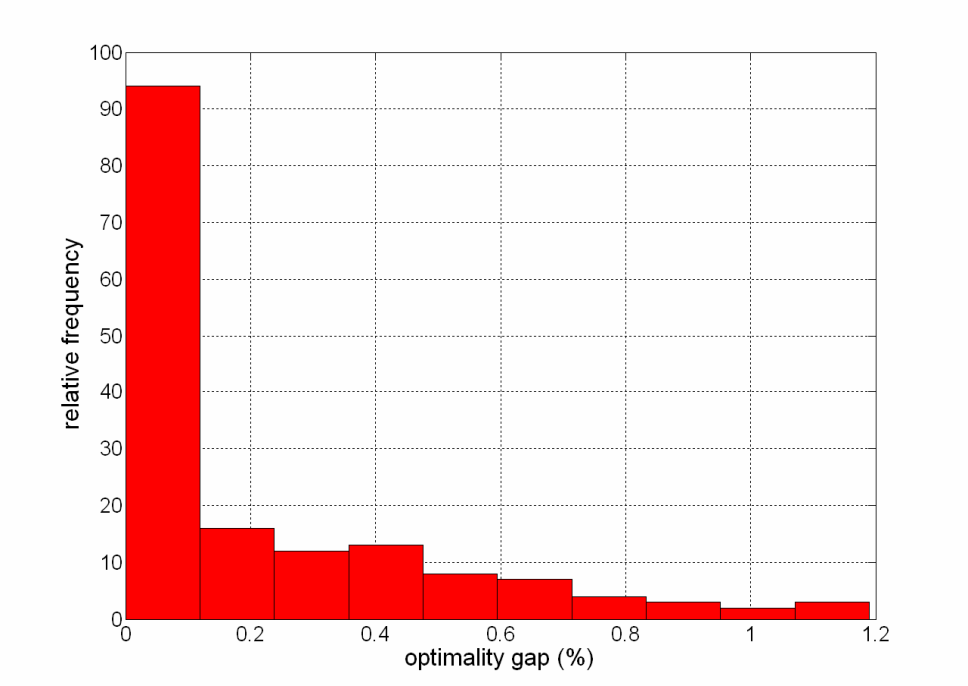

Figure 3-29. Histogram of optimality gap

The above results indicate that the MOP HEURISTIC can provide near-Pareto optimal curves which are close to the optimal curve for a ring network with $n \leq 10$. Three examples of the solutions (plotted in objective space) for $n = 10$ node network are shown in Figure 3-30 with Pareto curves in objective space for the optimal and heuristic solutions plotted; Tables 3-2 (a)~(c) display the objective function values for the solutions. The average optimality gap was within 4.4 % in cost and 0.5 % in congestion with low cost and uncorrelated traffic (Table 3-2(a)); the average optimality gap was within 1.8 % in cost and 0.6 % in congestion with medium cost and weakly correlated traffic (Table 3-2 (b)); the average optimality gap was within 0.5 % in cost and 0.1 % in congestion with high cost and strongly correlated traffic (Table 3-2 (c)).

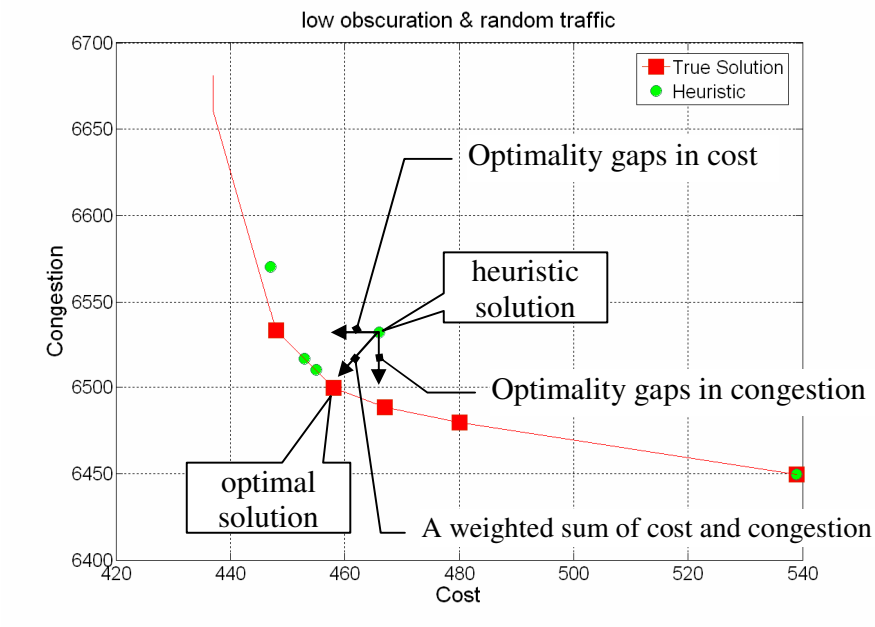

(a) With low obscuration and uncorrelated traffic (Table 3-2 (a))

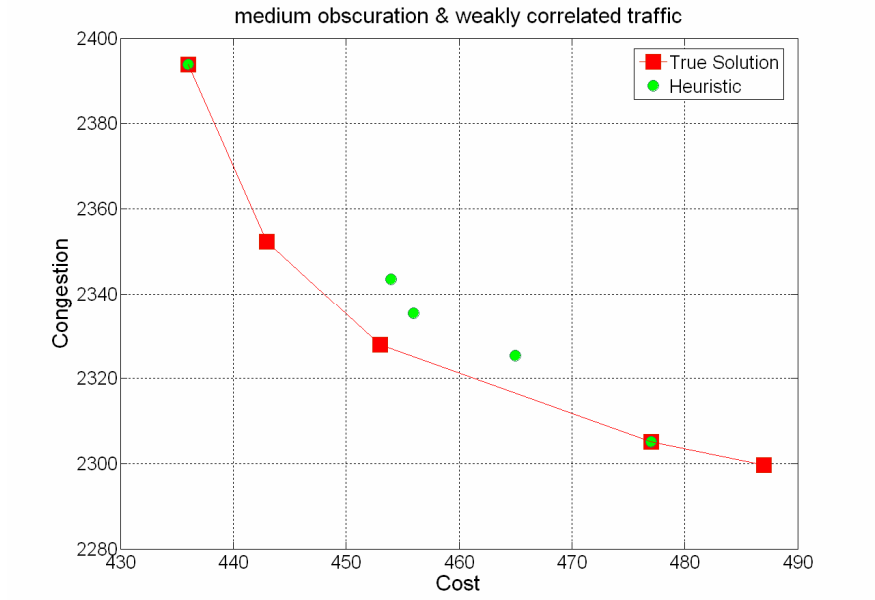

(b) With medium obscuration and weakly correlated traffic (Table 3-2 (b))

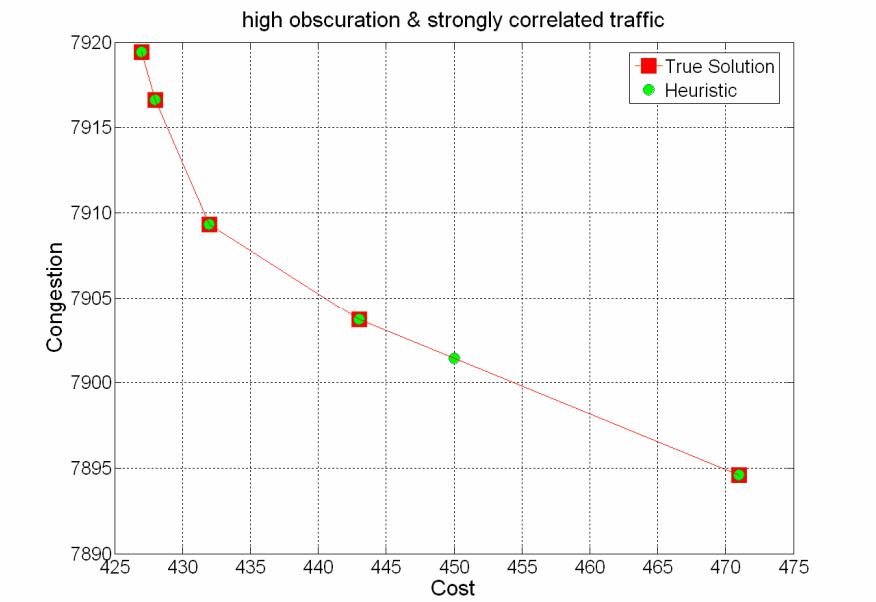

(c) With high obscuration and strongly correlated traffic (Table 3-2 (c))

Figure 3-30. Pareto optimal curves for $n=10$

Table 3-2. Optimal and heuristic solutions for $n=10$

(a) With low obscuration and uncorrelated traffic

A	B1	B2	B3	B4	C1	C2	C3	C4	D
	MATLAB (enumeration)				MATLAB (heuristic)				
weight (=w)	obj. val.	total_cost	total_congestion	solution time (sec)	obj. val.	total_cost	total_congestion	solution time (sec)	optimality gap (%)
0.1	5858.45	539	6449.50	11.1	5858.40	539	6449.50	6.5	0.00%
0.2	5267.40	539	6449.50	11.0	5299.00	455	6510.00	7.5	0.60%
0.3	4676.35	539	6449.50	11.2	4693.50	455	6510.00	6.8	0.37%
0.4	4079.88	480	6479.80	10.9	4105.50	466	6531.90	4.5	0.63%
0.5	3477.75	467	6488.50	11.1	3482.50	455	6510.00	5.8	0.14%
0.6	2874.72	458	6499.80	11.2	2877.00	455	6510.00	6.5	0.08%
0.7	2270.54	458	6499.80	10.6	2271.50	455	6510.00	5.8	0.04%
0.8	1664.96	448	6532.80	10.8	1665.70	453	6516.50	7.0	0.04%
0.9	1056.48	448	6532.80	10.7	1059.30	447	6570.40	5.0	0.27%

(b) With medium obscuration and weakly correlated traffic

A	B1	B2	B3	B4	C1	C2	C3	C4	D
	MATLAB (enumeration)				MATLAB (heuristic)				
weight (=w)	obj. val.	total_cost	total_congestion	solution time (sec)	obj. val.	total_cost	total_congestion	solution time (sec)	optimality gap (%)
0.1	2118.43	487	2299.70	11.1	2139.40	465	2325.40	6.9	0.99%
0.2	1937.16	487	2299.70	11.4	1939.50	477	2305.10	7.0	0.12%
0.3	1755.89	487	2299.70	12.3	1756.70	477	2305.10	7.4	0.05%
0.4	1573.86	477	2305.10	10.7	1573.90	477	2305.10	7.3	0.00%
0.5	1390.45	453	2327.90	11.1	1391.10	477	2305.10	7.7	0.05%
0.6	1202.96	453	2327.90	10.7	1207.70	456	2335.20	6.9	0.39%
0.7	1015.47	453	2327.90	10.9	1020.80	454	2343.40	7.3	0.52%
0.8	824.86	443	2352.30	10.5	827.58	436	2393.90	6.5	0.33%
0.9	631.79	436	2393.90	10.4	631.79	436	2393.90	7.0	0.00%

(c) With high obscuration and strongly correlated traffic

A	B1	B2	B3	B4	C1	C2	C3	C4	D
	MATLAB (enumeration)				MATLAB (heuristic)				
weight (=w)	obj. val.	total_cost	total_congestion	solution time (sec)	obj. val.	total_cost	total_congestion	solution time (sec)	optimality gap (%)
0.1	7152.24	471	7894.60	11.1	7152.20	471	7894.60	6.3	0.00%
0.2	6409.88	471	7894.60	11.4	6411.10	450	7901.40	6.1	0.02%
0.3	5665.49	443	7903.70	11.3	5665.50	443	7903.70	6.9	0.00%
0.4	4918.38	432	7909.30	11.3	4918.40	432	7909.30	6.5	0.00%
0.5	4170.65	432	7909.30	11.2	4170.60	432	7909.30	6.6	0.00%
0.6	3422.92	432	7909.30	11.3	3422.90	432	7909.30	6.6	0.00%
0.7	2674.58	428	7916.60	11.1	2674.60	428	7916.60	6.5	0.00%
0.8	1925.48	427	7919.40	11.3	1925.50	427	7919.40	8.2	0.00%
0.9	1176.24	427	7919.40	11.0	1176.20	427	7919.40	7.7	0.00%

Significant Advantages of the MOP Heuristic

Figure 3-31 shows a near-Pareto optimal curve for a twenty-node ring network generated by the MOP HEURISTIC code. For the example, thirty nine positive weights (w) were considered: $w \in \{0.025, 0.05, 0.075, 0.1, \ldots, 0.9, 0.925, 0.95, 0.975\}$. The circle symbols represent heuristic solutions and the dotted line connects the solutions on the frontier. The optimality gap for heuristic solutions was at most 0.35 % on average. This result came from measuring upper bound to the optimality gap for each heuristic solution and then averaging the upper bounds of the 39 heuristic solutions; the method for measuring upper bound to the optimality gap will be introduced in later section (Section 3.5). Hence the circle symbols on the dotted line are the near-Pareto optimal solutions; the dotted line approximates the Pareto

optimal set. Table 3-3 shows the expected computer time to get true Pareto optimal solutions by enumeration for $n = 14 \sim 20$. As the number of nodes in a ring network increases from n to $n+1$, the number of ring network topologies enumerated is increased from $(n-1)!$ to $n!$; thus the corresponding enumeration time is also multiplied by n. For example, it took fourteen hours and one week to enumerate all possible ring network topologies for $n=14$ and $n=15$, respectively, on a personal computer. The solution time is multiplied by fourteen, that is, 0.5 day to 7 days. According to the table, for a twenty-node ring network, the MATLAB enumeration code would take approximately 9,767,520 days to produce a Pareto optimal curve by generating all possible topologies. However, the MATLAB heuristic code took only 195 minutes (39 points × 5 minutes/point) to provide the curve in Figure 3-31. This example clearly presents the significant advantage of using the MOP HEURISTIC to solve MOP.

Table 3-3. Expected computer time taken by the enumeration (Machine: Intel Pentium 4 3.6 GHz personal computer and MATLAB version 7.0)

n	14	15	16	17	18	19	20
days	0.5	7	105	1,680	28,560	514,080	9,767,520

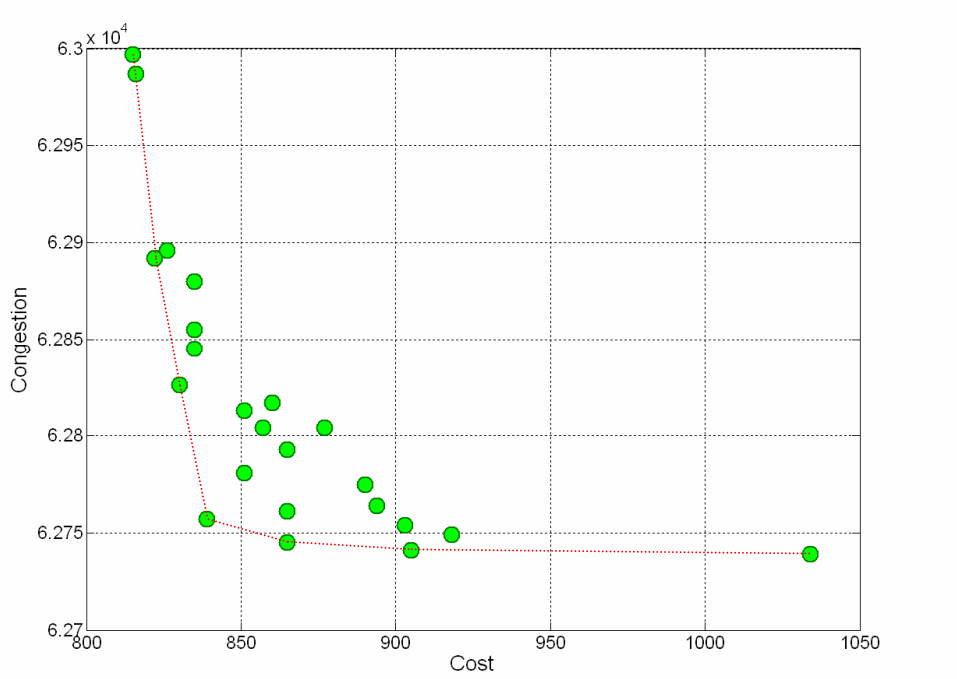

Figure 3-31. A near-Pareto optimal curve for $n = 20$ generated by heuristics (Red dotted curve: a near-Pareto optimal curve)

Physical Layer Consideration

The physical link cost is related to the transmission power of the optical transceiver for establishing or maintaining a feasible FSO link (e.g., $BER < 10^{-9}$ (link attenuation=-45 dBm)). The higher the link attenuation, the more transmission power is needed, hence the higher the cost. Thus, the number of infeasible links will be increased when network nodes cannot generate the required transmission power to handle high obscuration. In that case, directional RF communications technology would be an alternative because it operates with a higher level of transmission than an FSO transceiver. Further work is needed to model the combined FSO/directional RF communications.

3.4.3 Comparison to Simulated Annealing and Genetic Algorithms

Heuristic approaches are attractive for solving combinatorial optimization problems which are NP-hard or NP-complete. Since their set of feasible solutions contains discrete (binary or integer) elements and their size is huge, it is impractical to find optimal solutions by searching the whole space. For instance, the Traveling Salesman Problem (TSP) is such a combinatorial optimization problem. The TSP is defined as:

> "A salesman must visit each of n cities once before returning to his home. What ordering of the cities minimizes the total distance the salesman must travel before returning home?" (Winston, 2003)

Thus the set of feasible solutions consists of all permutation of the numbers one to n, where n is the number of cities. Since its complexity is $O(n!)$, a greedy heuristic such as neighborhood exchanges (e.g., 2-opt swap) or local search is used to obtain a best solution in efficient time. The greedy heuristic begins with an arbitrary chosen point x_0 (i.e., an initial solution) and iteratively proceeds to another point (solution) whose objective function value is at least good or better than the previous one. However, if the new solution is a local optimal solution, then the greedy heuristic is trapped in the local optimum (i.e., cycling around the local optimum) and fails to find a global optimum. Simulated Annealing, Genetic Algorithms, or Tabu Search can help overcoming this flaw of a greedy heuristic.

Tabu Search

Tabu Search is a memory-based local search which avoids the local minimum traps by using its short-term memory and long-term memory in the form of a tabu list. In the short-term memory, recent solutions (e.g., local optimal solutions in TSP) or their attributes (e.g., neighboring cities in the recent solutions in TSP) are recorded in a tabu list *i)* to prevent from being revisited to the local optimum and *ii)* to find or discard any solution with those attributes in the next iteration. Long-term memory allows the Tabu Search to: *i)* search neighbors of elite solutions (intensification strategy), *ii)* examine unvisited feasible solutions in short-term memory and thus prevent from cycling around local optimal solutions (diversification strategy), and *iii)* alternatively apply the intensification and diversification strategies to improve outcome of Tabu Search (strategic oscillations). Glover (1995; 2007) introduced the principal features of Tabu Search and its application area, and Glover (1996) summarized Tabu Search applications including telecommunication network design problems.

Simulated Annealing

Simulated Annealing consists of two WHILE-loops, an inner loop for iteration and an outer loop for "temperature cooling" by which it resembles a physical process of cooling down a heated material. At high temperature, particles of material randomly change their energy state. However, if the temperature is gradually lowered, then their energy states reach a minimum. The parameter T for the outer loop is analogous to temperature. The inner loop simply iterates its process while

$iteration \le I$, where I is the number iterations. When the inner loop ends, the outer loop reduces its temperature T by ΔT (*temperature cooling*). The whole process in Simulated Annealing ends at $T = T_f$, where T_f is a final temperature (cooling schedule). Figure 3-32 shows a pseudo-code for Simulated Annealing in a minimization problem.

Initialization
$x = x_0$; *** initial solution
$x_{best} = x$; *** current best solution
$z_{best} = z(x_{best})$; *** the objective function value to the x_{best}
While $T < T_f$, *** T is the current temperature
While $iteration < I$,
$x_{iteration} \in N(x)$; *** $N(x)$ is a set of neighbors of x
$x = x_{iteration}$
$z_{current} = z(x)$;
$\Delta z = z_{current} - z_{best}$;
If $\Delta z \le 0$, *then*
$x_{best} = x_{iteration}$;
$z_{best} = z(x_{best})$;
End
If $\Delta z > 0$, *then*
Draw a random number, rand;
If rand $< e^{-\Delta z / T}$, *then*
$x_{best} = x$;
End
If rand $\ge e^{-\Delta z / T}$, *then*
Discard $x_{iteration}$;
End
End
$iteration = iteration + 1$;
End % End-of-loop for $iteration$
$T = T - \Delta T$ % Cooling schedule
End % End-of-loop for T

Figure 3-32. Pseudo-code for Simulated Annealing

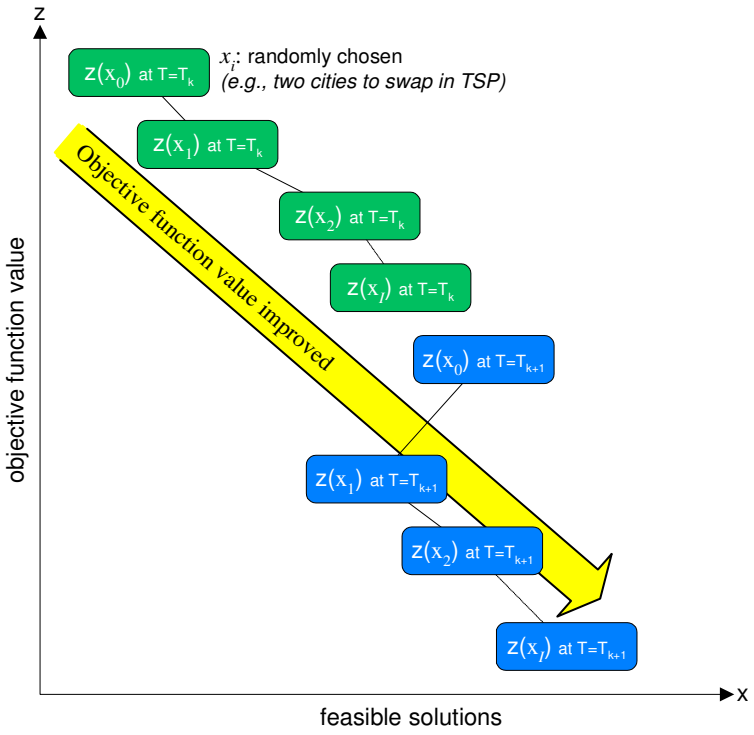

(a) A downhill move

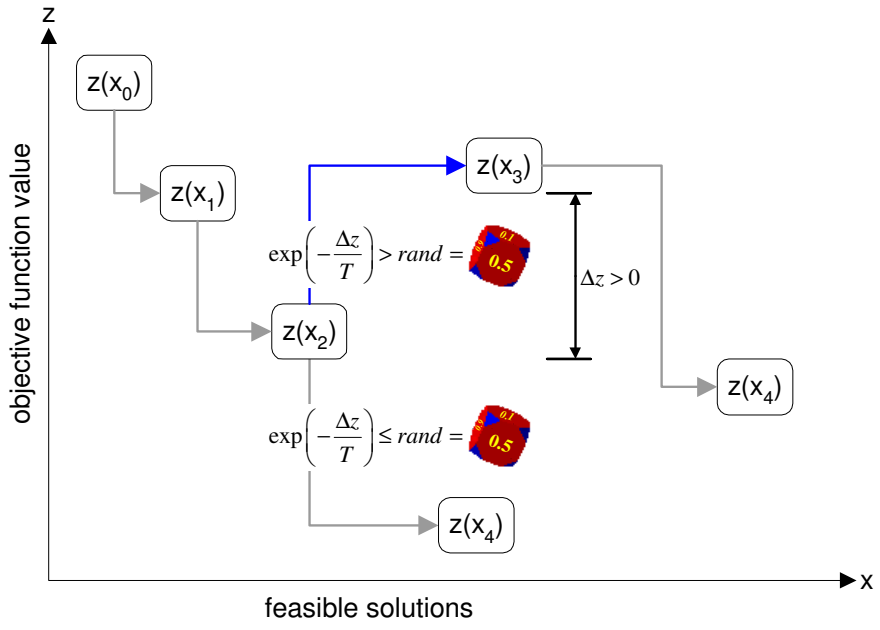

(b) Acceptance of a uphill move

Figure 3-33. Examples in Simulated Annealing process

In a minimization problem, Simulated Annealing is similar to the greedy heuristic which iteratively proceeds to another point in the direction of improving the objective function value. Figure 3-33 (a) shows such a downhill move. The distinction between the two heuristics is when they cross over a local minimum (e.g., $z(x_2)$ in Figure 3-33 (b)). At the third iteration, the objective function value $z(x_3)$ is greater than the one at $x = x_2$. Then the greedy heuristic stops at the third iteration (or keeps cycling around $x = x_2$) and reports $(x_2, z(x_2))$ as the best solution because it cannot move out from the local minimum. However, Simulated Annealing probabilistically decides to accept the uphill move from $x = x_2$ to $x = x_3$. First, it computes $\Delta z = z_{current} - z_{best} = z(x_3) - z(x_2)$ and $exp\left(-\frac{\Delta z}{T}\right)$, where T is the current temperature, and then draws a random real number (*rand*) between 0 and 1. Next, it compares two values, $exp\left(-\frac{\Delta z}{T}\right)$ and the random number. If $exp\left(-\frac{\Delta z}{T}\right) \le rand$, then the point $x = x_3$ is discarded and a new point $x = x_4$ is generated at the next iteration; else the uphill move is accepted and thus the move presents a chance to meet a better solution $x = x_4$ than the previous local optimum at $x = x_2$ (i.e., $z(x_4) < z(x_2)$). As the temperature T is lowered, the probability of accepting a worse solution is lowered. For example, $exp\left(-\frac{50}{1800}\right) = 0.94596$ at $T = 1800$ is less than $exp\left(-\frac{50}{2000}\right) = 0.97531$ at $T = 2000$ when $\Delta z = 50$. Thus, the probability of accepting a worse solution at $T = 1800$ is lower than the one at $T = 2000$. Simulated

annealing requires the user to define the performance parameters such as to initial point x_0, the number of iterations I, initial temperature T_0, final temperature T_f, and cooling rate $\Delta T = \alpha T_0$ where α is a factor in a range of $0 \le \alpha \le 1$. If we increase I or T_0, or decrease ΔT, then the number of total iterations for both WHILE-loops will be increased. It subsequently increases the number of local optima found (visited) by Simulated Annealing, thus more likely getting close to a global optimum. On the contrary, a greater number of iterations can require significantly more computing time, which makes the process of Simulated Annealing slow. Hence, "*Simulated Annealing parameters can be controlled to converge in a given time* (Winston 2003)." Bertsimas et al. (1993), Brooks et al. (1995), Connolly (1992), and Johnson et al. (1991; 1997) present examples of an implementation of a Simulated Annealing algorithm. Winston (2003) provides a step-by-step procedure in solving TSP problem by Simulated Annealing.

Genetic Algorithms

Simulated Annealing begins with an initial solution, whereas Genetic Algorithms starts with an initial population (i.e., multiple solutions). The initial population undergoes a series of genetic processes which are reproduction, crossover, and mutation. Potts (1994) presents a survey of studies concerning those genetic processes and control parameters in Genetic Algorithms. Reproduction is a process of pairing; two individuals (solutions) are chosen to be a parent for the next generation. For example, Figure 3-34 shows a binary tournament selection (Goldberg,1990; Jin, 2002). First, two individuals are randomly selected from the

current population and their "fitness" is measured. Then the fitness measures the quality of each individual x. One possible form of the fitness function is $f(x) = -z(x) + \gamma$ for a minimization problem, where $z(x)$ is the objective function value of x and γ is the maximum objective function value of the current population. Next the individual with a higher fitness is chosen to reproduce. Because the two individuals are randomly selected, some of the individuals may be repeatedly copied into the new population. At the final step of the binary tournament selection, two individuals are paired in order (i.e., i-th and $(i+1)$-th, where i is an odd number) as a parent for the next generation.

For $i = 1 : N$, *** N : *size of population*

1) Randomly pick two individuals x *and* y *from the current population;*

2) Measure their fitness $f(x)$ *and* $f(y)$*;*

3) Pick out one with the larger fitness;

4) Save the individual with the larger fitness value to the new population in order;

End

Figure 3-34. Binary tournament selection

At crossover, a parent exchanges their partial string (substring) to generate offspring. For example, Figure 3-35 illustrates a two-point crossover. The substring between the two points, c_1 and c_2, of parent A and B are exchanged to produce offspring if $P_{crossover} \geq rand$, where $P_{crossover}$ is the crossover rate ($0 \leq P_{crossover} \leq 1$) and $rand$ is a random number between 0 and 1; if $P_{crossover} < rand$, then crossover does not occur.

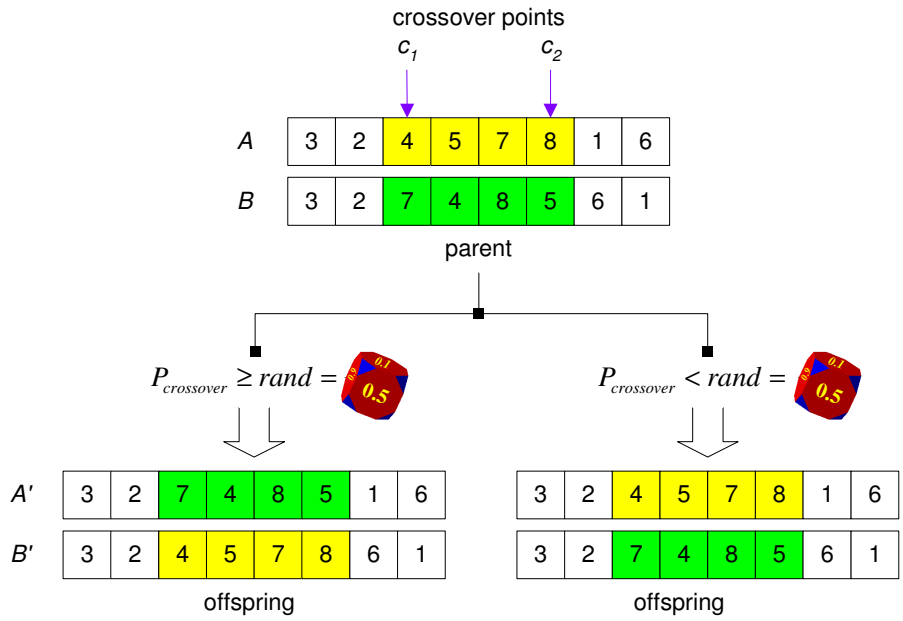

Figure 3-35. Two-point crossover with strings in the integer representation

The two offspring A' and B' in Figure 3-35 have the same substring '3-2' in their string as their parents do. If the substring descends to the offspring by several generations, then the number of individuals with the substring will be increased in the newly generated population. This can lead to lack of diversity in the new population and potentially converge to a local optimum. Mutation helps to increase the population diversity. For example, Figure 3-36 shows inversion mutation (Larrañaga, 1999; Jin 2002). The substring between the two points, m_1 and m_2, of offspring A' and B' is reversed in order if $P_{mutation} \geq rand$, where $P_{mutation}$ is the mutation rate ($0 \leq P_{mutation} \leq 1$) and $rand$ is a random real number between 0 and 1; if $P_{crossover} < rand$, then mutation does not occur. By the inversion mutation, the substring '3-2' is disjointed when $P_{mutation} \geq rand$. For example in Figure 3-36, the

order of the substring 2-7-4-8-5 is reversed to 5-8-4-7-2 in A' and 2-4-5-7-8 is changed to 8-7-5-4-2 in B'.

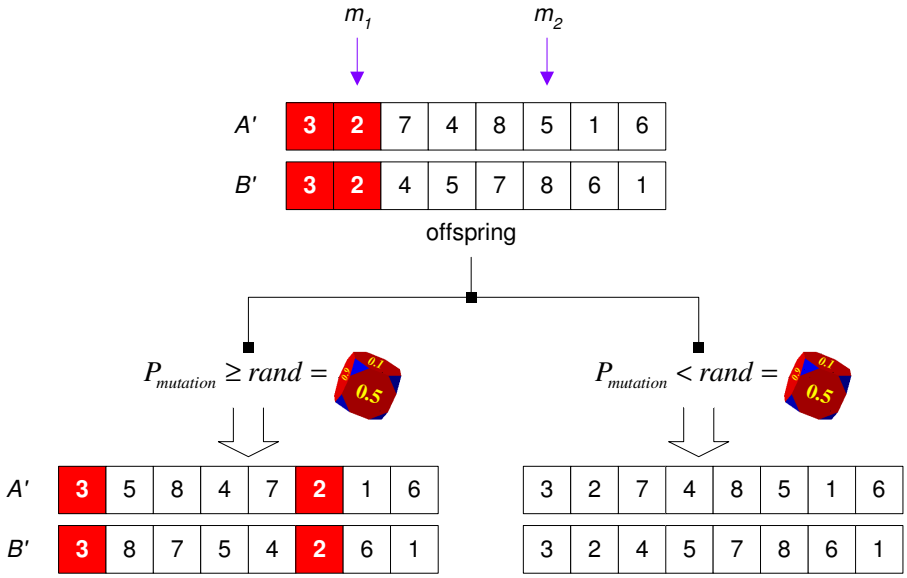

Figure 3-36. Example of mutation: inversion mutation

Genetic Algorithms repeats reproduction, crossover, and mutation until they do not improve the best solution for some number of generations. The parameters of Genetic Algorithms include the population size N, crossover rate $P_{crossover}$, mutation rate $P_{mutation}$, and the number of generations (iteration number). The proper choice for the parameters is under control of the user; the choice affects the performance and convergence speed of the algorithm. Examples of Genetic Algorithms for the TSP are presented in Freisleben et al. (1996), Gendreau et al. (1992), Larrañaga et al. (1999), Merz et al. (1997), and Michalewicz et al. (1999). Sinclair (1999) provides a summary on the application of Genetic Algorithms for the telecommunication

network design problem (i.e., node location, topology, routing, and wavelength allocation) in optical, radio, and computer networks

Numerical Examples

In this section, the applicability of Simulated Annealing (SA) and Genetic Algorithms (GA) to the NLTCP is examined through numerical tests. The numerical tests were carried out as follows:

- The tests were executed on a personal computer with 3.6 GHz Intel Pentium 4 processor and 3 GB RAM; the operating system was Windows XP.
- Both SA and GA are implemented in MATLAB (version 7.0).
- Ten 15×15 traffic matrices were randomly generated. Each element (r_ω) in the traffic matrix was an integer value between 1 and 50 except the diagonals which were all zero.
- For each traffic matrix, the MATLAB code for SA and GA ran ten times, and the optimality gap was measured by $\frac{z_{heuristic} - z^*}{z^*}$ for each run, where $z_{heuristic}$ is the objective function value of the best solution (ring network topology) found by the GA or SA, and z^* is the optimal solution obtained by enumerating all possible topology for $n = 15$ with MATLAB. In SA, a new solution was found from the neighbors of the current solution by swapping the position of two nodes in a ring network topology; the selection of two nodes was random. 100 iterations were used for GA.

- Table 3-4 displays the NLTCP HEURISTIC objective function vlaues and their optimality gaps to the optimal objective function values for the ten 15×15 input traffic matrix used in both SA and GA. The standard 4 RULE NLTCP HEURISTIC algorithm showed the optimality gaps between 0.61 % and 1.19 %. The heuristic improvement algorithm provided the better solutions whose optimality gaps are between 0 to 0.45 %.
- The optimality gaps from SA and GA were compared against the ones from the NLTCP HEURISTIC (Figures 3-37 and 3-38).

Table 3-4. NLTCP HEURISTIC solutions and their optimality gaps for ten input traffic matrices and a ring network topology with fifteen nodes

Optimal Solution	NLTCP Heuristic (standard four rules)			NLTCP Heuristic (improvement algorithm)	
	Objective function value (=z_heuristic)	Optimality Gap (=H_standard)	Search Time (sec)	Objective function value (=z_heuristic)	Optimality Gap (=H_improvement)
19084	19214	0.68	56	19084	0.00
18919	19223	1.61	53	18970	0.27
21166	21277	0.52	56	21175	0.04
19472	19510	0.19	59	19510	0.19
19113	19189	0.39	64	19113	0.00
20519	20598	0.39	46	20598	0.39
21345	21496	0.71	55	21441	0.45
18162	18357	1.07	58	18191	0.16
19395	19450	0.28	57	19450	0.28
20325	20428	0.51	73	20325	0.00

Figures 3-37 and 3-38 plot the optimality gaps from SA and GA for a ring network topology with fifteen nodes. $H_{standard}$ ("○" symbol) and $H_{improvement}$ represent the optimality gaps ("□" symbol) for NLTCP HEURISTIC solutions by applying the standard rule (i.e., by setting m =4 and $TTC_{diff} \leq 0$ in Step 3b) and improvement

algorithm (i.e., by setting $TTC_{diff} \leq \alpha$, where $\alpha > 0$, or m >4 in Step 3b), respectively.

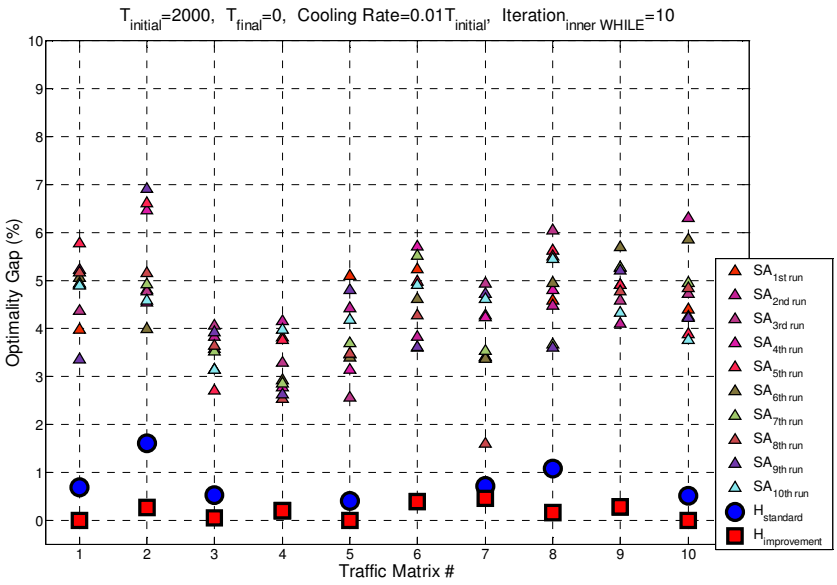

(a) Parameters: $T_0 = 2000$, $T_f = 0$, $\Delta T = 0.01T_0$, $I = 10$ (Mean optimality gap: 4.71 % for SA; Mean search time: 19 sec for SA)

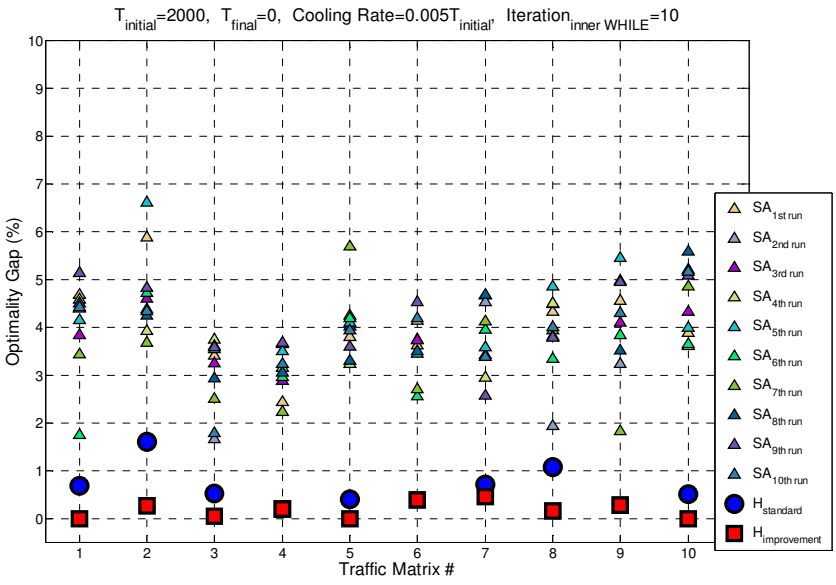

(b) Parameters: $T_0 = 2000$, $T_f = 0$, $\Delta T = 0.005T_0$, $I = 10$ (Mean optimality gap: 4.53 % in average for SA; Mean search time: 38 sec for SA)

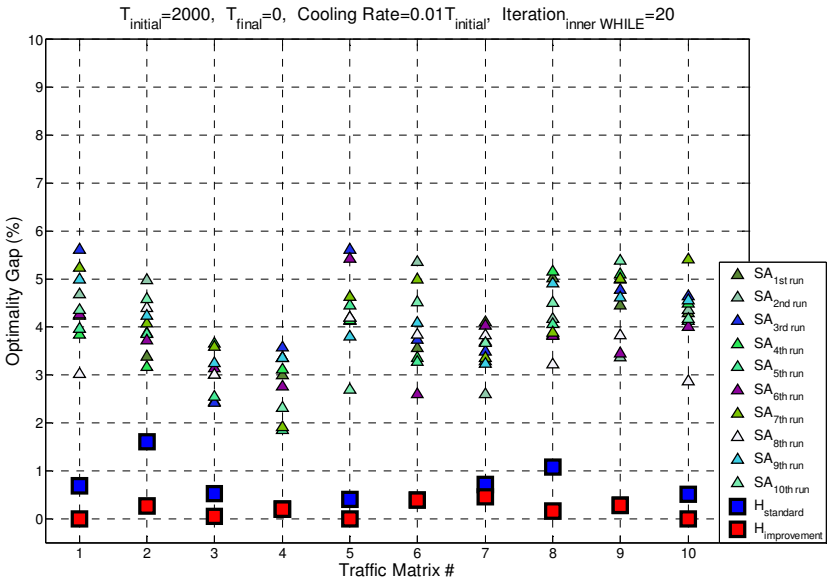

(c) Parameters: $T_0 = 2000$, $T_f = 0$, $\Delta T = 0.01T_0$, $I = 20$ (Mean optimality gap: 4.28 % for SA; Mean search time: 40 sec for SA)

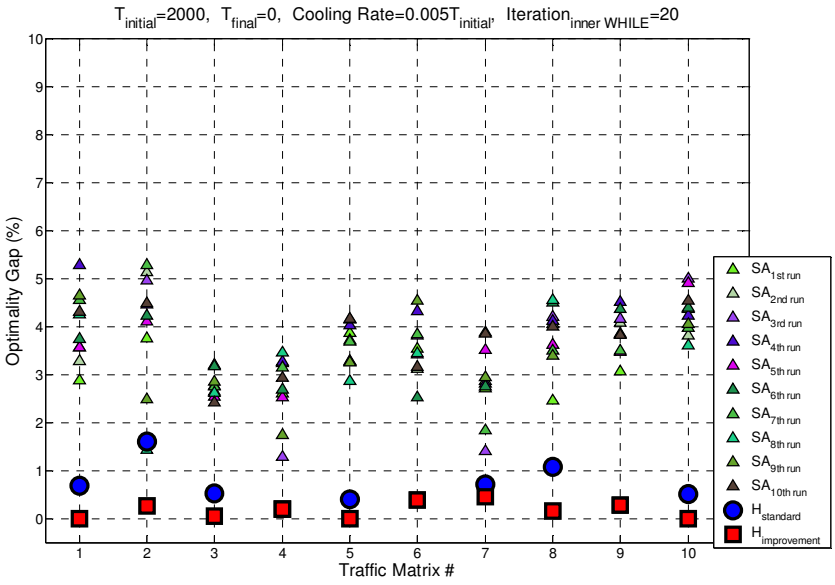

(d) Parameters: $T_0 = 2000$, $T_f = 0$, $\Delta T = 0.005T_0$, $I = 20$ (Mean optimality gap: 4.28 % for SA; Mean search time: 80 sec for SA)

Figure 3-37. The randomness of the solutions in SA

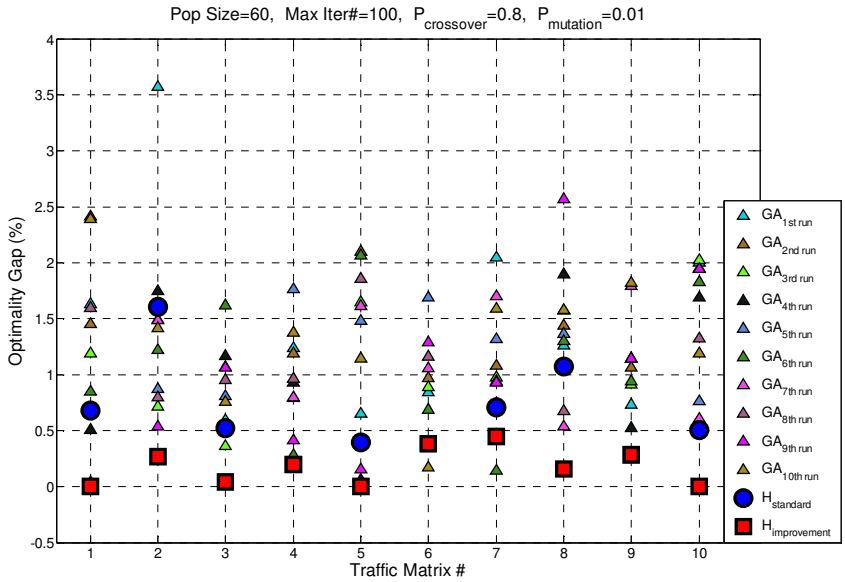

(a) Parameters: $N = 60$, $P_{crossover} = 0.8$, $P_{mutation} = 0.01$ (Mean optimality gap: 1.53 % for GA; Mean search time: 56 sec for GA)

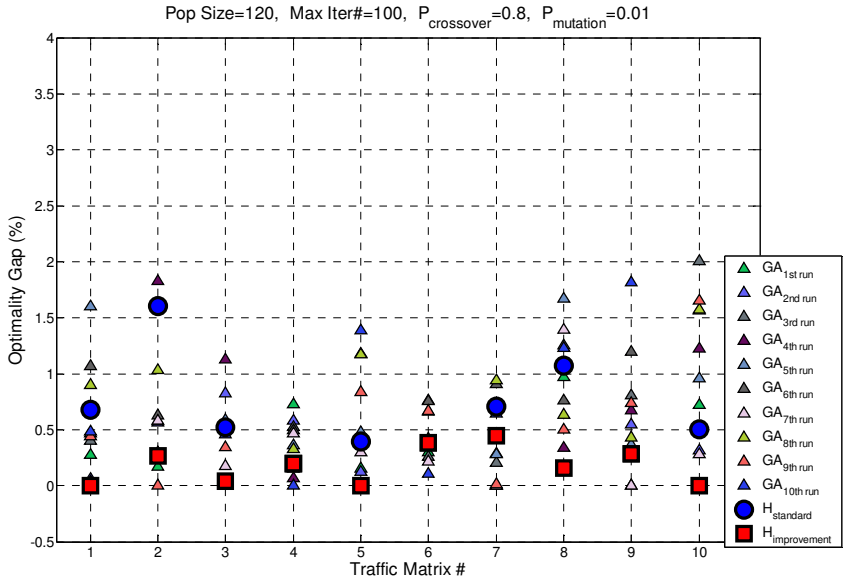

(b) Parameters: $N = 120$, $P_{crossover} = 0.8$, $P_{mutation} = 0.01$ (Mean optimality gap: 1.03 % for GA; Mean search time: 92 sec for GA)

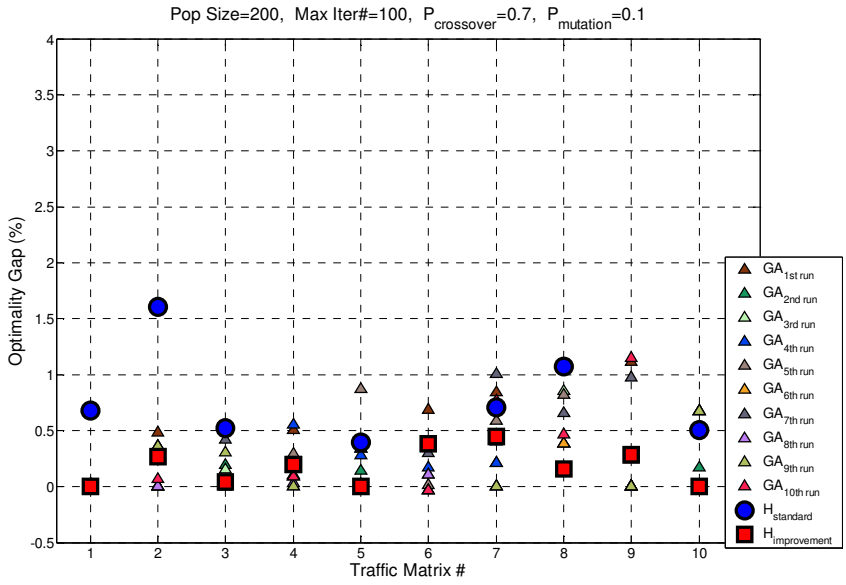

(c) Parameters: $N = 200$, $P_{crossover} = 0.7$, $P_{mutation} = 0.1$ (Mean optimality gap: 0.29 % for GA; Mean search time: 155 sec for GA)

Figure 3-38. The randomness of the solutions in GA

Figures 3-37 and 3-38 show that SA and GA for the NLTCP may yield different output to the same input (traffic matrix) and parameter sets while NLTCP HEURISTIC yields one set of output to the same input traffic matrix. This is because of *i)* the randomness in SA when it selects a new solution by swapping two nodes in a ring network topology and then deciding to accept an uphill move and *ii)* the randomness in GA when it makes a choice of an initial population and carries out its genetic processes (i.e., reproduction, crossover, and mutation). GA generates better solutions than the NLTCP HEURISTIC for the larger population size and specific parameter values. However, its mean search time is increased as the population size grows; the proper choice of parameter values is unknown in reality. Table 3-5 presents the comparisons between those three heuristic methods.

Table 3-5. Comparison of SA, GA, and NLTCP HEURISTIC

Heuristic	Number of Solutions	Neighborhood Search	Method of avoiding local optimum (in a mimization problem)	Identical outputs to the same input?
Simulated Annealing	one	random	acceptance of a uphill move	No
Genetic Algorithms	population	random	genetic processes	No
NLTCP Heuristic	multiple solutions (=no. of decision rules)	decision rules	decision rules	Yes

3.5 Evaluation of the Heuristic Algorithms

In Section 3.4, NLTCP HEURISTIC and MOP HEURISTIC and their performance were presented. In addition, the NLTCP HEURISTIC was compared to Simulated Annealing and Genetic Algorithms. While the NLTCP HEURISTIC exhibits deterministic characteristics, the other ones have randomness in their algorithm so different solutions can result. The empirical performance (optimality gap) of each of three methods was tested by various sizes of ring networks and traffic or cost input matrices with optimal solutions by a commercial solver (XPRESS-MP) or enumeration. However, the largest number of nodes was 15 due to the computational limitations in the solver and the enumeration process. This section introduces a measure of the upper bound on the optimality gap without knowing the optimal solution, which is useful in these settings with larger problems.

Labourdette et al. (1991) and Narula-Tam et al. (2000) measured the performance of heuristics in a congestion minimization problem with a lower bound on the maximum link congestion given as $LB = \frac{\tau}{pn}$. Here, the total traffic congestion (τ) on the network is divided by the number of transceivers (p) per node and the number of nodes in the network. Then this lower bound was used to get a reduction rate in the maximum link congestion (%) (not actually the optimality gap). The reduction rate was computed as $\frac{(z_H - LB)}{z_H}$ where z_H is an objective function value for heuristic solution. They applied the reduction rate to present the performance of their heuristics because an optimal solution had not been found.

3.5.1 LP Relaxation Approach

The NLTCP and MOP are MILPs with binary variables. If these variables are relaxed to be in $[0,1]$ as opposed to binary, then the feasible region of the MILP problem is contained in the feasible region of the LP relaxation. Thus, for a minimization problem such as NLTCP or MOP, the optimal objective function value (z^*_{MILP}) of the MIP problem is greater than or equal to the one of its LP relaxed problem: $0 < z_{LP} \le z^*_{MILP}$, where z_{LP} is positive by assuming the elements of cost or traffic input matrices except the diagonal ones are not all zero. Moreover the objective function value for heuristic solution (i.e., z_H) is such that: $z^*_{MILP} \le z_H$. Therefore, as shown in Figure 3-39, the following inequality holds:

$$0 < z_{LP} \le z^*_{MIP} \le z_H \tag{62}$$

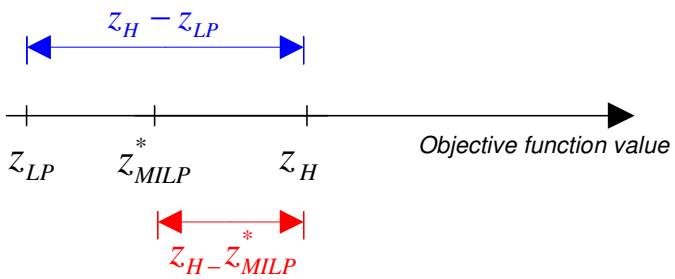

Figure 3-39. Diagram illustrating the inequality (62)

From the inequality (62), an upper bound for the optimality gap is:

$$0 < z_{LP} \le z^*_{MILP} \le z_H$$

$$\Rightarrow z_H - z_{LP} \ge z_H - z^*_{MILP} \ge 0$$

$$\Rightarrow \frac{z_H - z_{LP}}{z_{LP}} \ge \frac{z_H - z^*_{MILP}}{z_{LP}} \ge \frac{z_H - z^*_{MILP}}{z^*_{MILP}} = Optimality\ Gap$$

$$\Rightarrow UB = \frac{z_H - z_{LP}}{z_{LP}} \geq Optimality\ Gap\,, \tag{63}$$

where

z_H : Objective function value of heuristics,

z^*_{MILP} : Optimal objective function value,

z_{LP} : Objective function value of LP relaxation problem, and

UB : Upper bound of the optimality gap.

Equation (63) implies that we can approximate the optimality gap of the objective function value for heuristic solution (i.e., z_H) even without knowing the optimal objective function value (i.e., z^*_{MILP}). Both z_H and z_{LP} can be obtained by the heuristic code (MATLAB) or a commercial MIP solver (e.g., XPRESS-MP). In the next section, we present results that show that UB is quite useful to estimate the performance of the heuristic solution, and that the LP relaxation approach is computationally attractive.

3.5.2 Numerical Results

Network Layer Topology Control Problem

Table 3-6 summarizes the numerical results for applying the LP relaxation approach to NLTCP to obtain the upper bound on the optimality gap. The numerical tests were carried out as follows:

- The tests were executed on a personal computer with 3.6 GHz Intel Pentium 4 processor and 3 GB RAM; the operating system was Windows XP.
- For $n = 15, 20, 21, 22, 23, 24, 25, 26,$ and 27, ten $n \times n$ traffic matrices were randomly generated. Each element (r_ω) in the traffic matrix was an integer value between 1 and 50 except the diagonals which were all zero.
- z_H was obtained by the NLTCP HEURISTIC code (MATALB version 7.0) in Section 3.4.1; z_{LP} was provided by XPRESS-MP.

Figure 3-40 displays UB values for the ninety cases (Column E in Table 3-6). The average value of UB was 1.70 %, which indicates that the optimality gap may be less than or equal to 1.70 % on average. The numerical results in Table 3-6 show that the NLTCP HEURISTIC performed well for a large ring networks with $n \geq 15$. As shown in Figure 3-41 (a), the solution time of z_{LP} was much faster than the time for searching z^*_{MILP} by enumeration (Figure 3-41 (b)) (The enumeration was chosen for the ring network with $n > 10$ due to the slower progress in finding the optimal solution by XPRESS-MP). For instance, the solution time of the LP relaxation problem for $n = 15$ was twelve seconds on average, whereas the enumeration time for the corresponding MIP problem took approximately one week. Thus, the LP relaxation approach shows a significant computational advantage for evaluating the performance of heuristic solution in NLTCP.

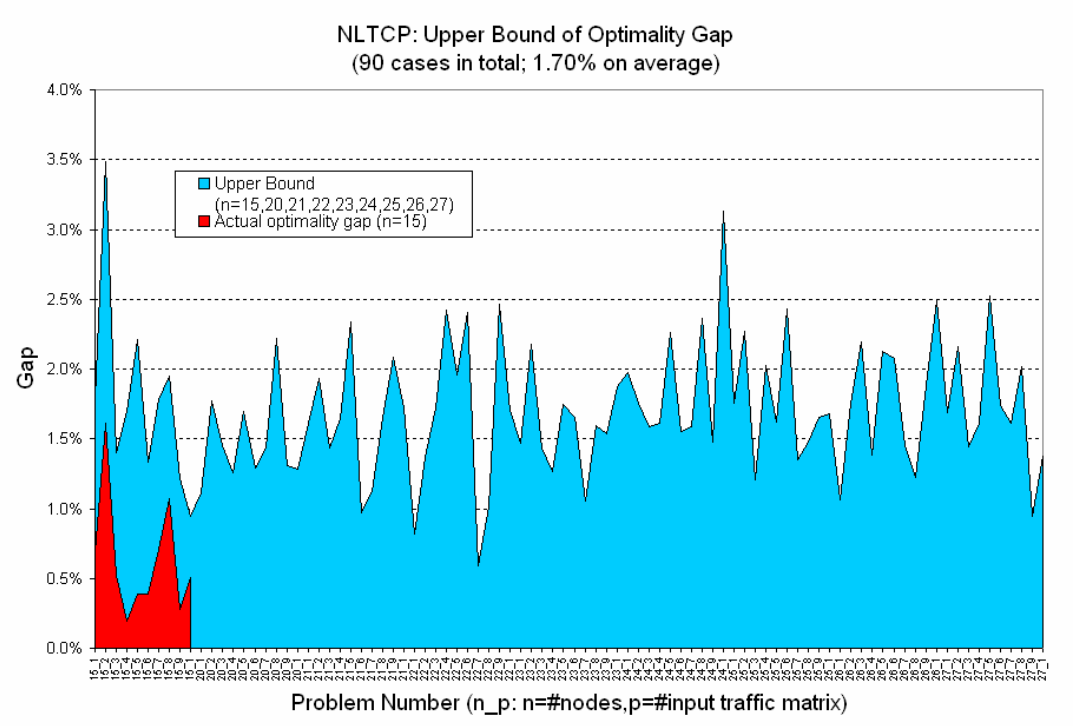

Figure 3-40. A graphical display for UB in Table 3-6

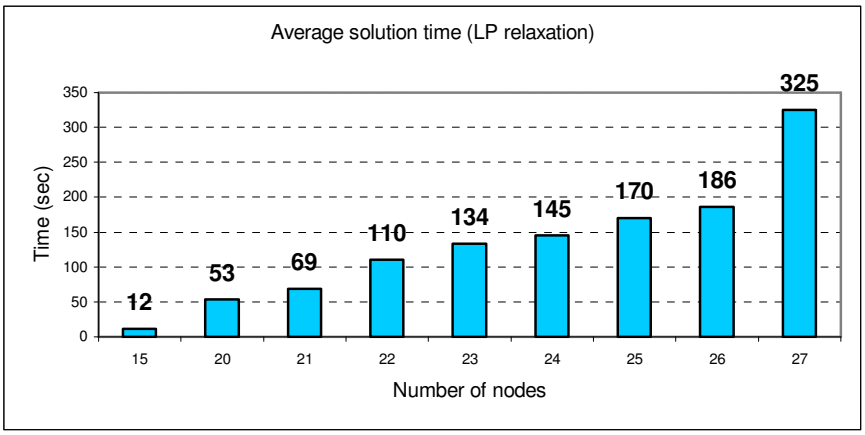

(a) Average solution time of the LP relaxation problem

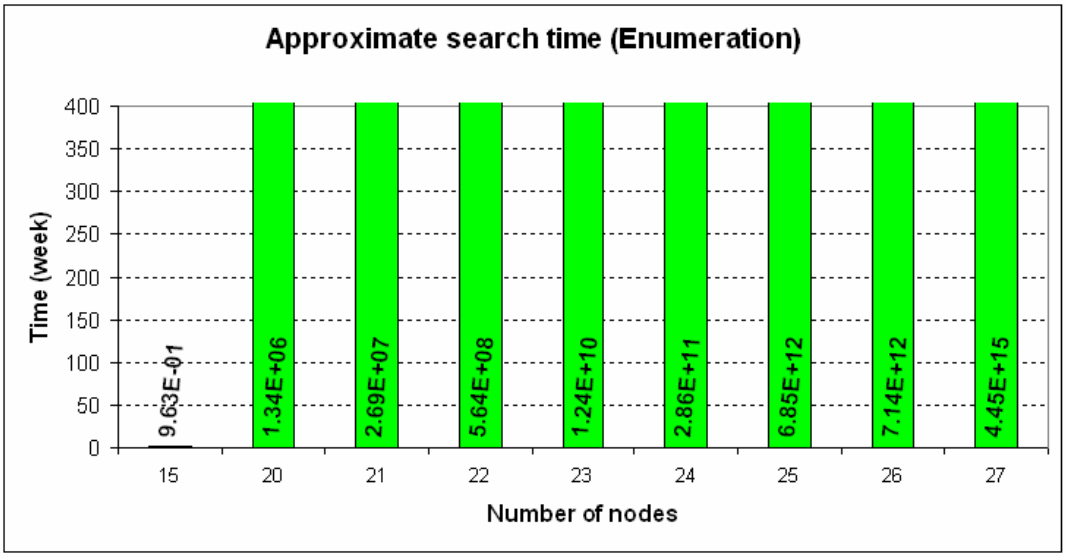

(b) Average search time of enumeration (a graphical display of Table 3-3)

Figure 3-41. Significant computational advantage of the LP relaxation approach over enumeration (Machine: Intel Pentium 4 3.6 GHz personal computer)

Table 3-6. Upper bound on optimality gap for n=15, 20, 21, 22, 23, 24, 25, 26, and 27 in NLTCP

A	B	C	D	E	F
n	# Input traffic matrix	z_LP	z_H (4 RULES)	UB	Optimality Gap
15	1	18877.2	19214	1.78%	0.68%
	2	18575.8	19223	3.48%	1.61%
	3	20983.8	21277	1.40%	0.52%
	4	19185.3	19510	1.69%	0.19%
	5	18773.9	19189	2.21%	0.39%
	6	20326.8	20598	1.33%	0.39%
	7	21119.1	21496	1.78%	0.71%
	8	18006.1	18357	1.95%	1.07%
	9	19216.7	19450	1.21%	0.28%
	10	20237	20428	0.94%	0.51%
20	1	45896.4	46407	1.11%	
	2	45062.2	45860	1.77%	
	3	47944	48640	1.45%	
	4	45070.7	45636	1.25%	
	5	48246.4	49063	1.69%	
	6	48859	49488	1.29%	
	7	47061.4	47737	1.44%	
	8	44539.1	45526	2.22%	
	9	47055.8	47672	1.31%	
	10	48480.5	49103	1.28%	
21	1	55816.4	56715	1.61%	
	2	53877.7	54919	1.93%	
	3	53752.6	54526	1.44%	
	4	54171.1	55064	1.65%	
	5	55401.1	56694	2.33%	
	6	55565	56105	0.97%	
	7	53793.6	54397	1.12%	
	8	53099.3	53977	1.65%	
	9	54401.2	55537	2.09%	
	10	55589.4	56547	1.72%	
22	1	63093.1	63607	0.81%	
	2	61617.5	62462	1.37%	
	3	62000.4	63067	1.72%	
	4	61048.4	62525	2.42%	
	5	61218.1	62418	1.96%	
	6	65597.1	67173	2.40%	
	7	65267	65654	0.59%	
	8	63666.7	64312	1.01%	
	9	62542.6	64083	2.46%	
	10	59321.6	60335	1.71%	
23	1	71639.9	72693	1.47%	
	2	73293.2	74889	2.18%	
	3	73876.9	74934	1.43%	
	4	72409.9	73329	1.27%	
	5	68517.7	69713	1.74%	
	6	65696.2	66783	1.65%	
	7	70504.5	71250	1.06%	
	8	73548.1	74722	1.60%	
	9	69762.9	70837	1.54%	
	10	70600.1	71921	1.87%	
24	1	78994.7	80556	1.98%	
	2	84045.8	85523	1.76%	
	3	82100.5	83400	1.58%	
	4	85201.2	86571	1.61%	
	5	78696.9	80476	2.26%	
	6	80513.7	81761	1.55%	
	7	78479	79726	1.59%	
	8	80310	82205	2.36%	
	9	81142.7	82338	1.47%	
	10	82394.3	84975	3.13%	

Table 3-6 Continued

A	B	C	D	E	F
n	# Input traffic matrix	z_LP	z_H (4 RULES)	UB	Optimality Gap
25	1	95386.2	97064	1.76%	
	2	91537.2	93612	2.27%	
	3	86975.4	88025	1.21%	
	4	91117	92961	2.02%	
	5	94184.3	95714	1.62%	
	6	91902.3	94137	2.43%	
	7	89033.1	90236	1.35%	
	8	89186.4	90500	1.47%	
	9	94879	96446	1.65%	
	10	92078.9	93624	1.68%	
26	1	104407	105521	1.07%	
	2	102160	103953	1.76%	
	3	102230	104469	2.19%	
	4	107138	108623	1.39%	
	5	103036	105231	2.13%	
	6	101911	104027	2.08%	
	7	104771	106295	1.45%	
	8	105297	106585	1.22%	
	9	100682	102576	1.88%	
	10	104117	106710	2.49%	
27	1	119113	121127	1.69%	
	2	119690	122273	2.16%	
	3	115412	117080	1.45%	
	4	117705	119607	1.62%	
	5	115342	118249	2.52%	
	6	120903	123002	1.74%	
	7	112441	114255	1.61%	
	8	105478	107605	2.02%	
	9	115336	116425	0.94%	
	10	116416	118017	1.38%	

Multiobjective Optimization Problem

Table 3-7 summarizes the numerical results for applying the LP relaxation approach to MOP to obtain the upper bound on the optimality gap. The numerical tests were carried out as follows:

- The tests were executed on a personal computer with 3.6 GHz Intel Pentium 4 processor and 3 GB RAM; the operating system was Windows XP.
- For $n = 20$ and $w = 0.5$, two types of cost matrices (low, medium) and three types of traffic matrices (uncorrelated, weakly correlated, strongly correlated) were used. Thus there were six combinations of cost and traffic types. For

each cost type, 10 cost matrices were generated with 2 % cloud cover for low atmospheric obscuration and 5 % cloud cover for low atmospheric obscuration (Gabriel et al. 2006).

- z_H was obtained by the MOP HEURISTIC code (MATALB version 7.0) in Section 3.4.2; z_{LP} was provided by XPRESS-MP.

Figure 3-42 displays UB values for the sixty cases (Column F in Table 3-7). The average value of UB was 1.27 %, which indicates the optimality gap could be less than 1.27 % on average. The strongly correlated traffic pattern shows the smallest value of UB on average (0.25 %); the weakly correlated traffic pattern shows the largest value of UB (2.35 %). Since the congestion objective value was bigger than the cost objective at $w = 0.5$, the multiobjective function values of the LP relaxation and the heuristic were more affected by the congestion objective than the cost objective. The congestion objective value was dependent on the input traffic matrix; thus, the three different traffic patterns might occur the difference in the average UB values. Because the flow variables in the LP relaxation are continuous (i.e., $0 \le f_{\omega ij} \le 1$), the each traffic demand could be split in both clockwise and counter-clockwise to evenly distribute the traffic in the network. On the other hand, the heuristic routed the traffic demand either direction. If all traffic demands for OD pairs are in the same approximate values, the load on each link in the network may be similar for both the LP relaxation problem and the heuristic. Thus, the difference between the two multiobjective function values, z_{LP} and z_H, would be small in the case of the strongly correlated traffic pattern. However, for the weakly correlated

traffic pattern, the LP relaxed flow variable may evenly distribute the traffic demand in both directions so that the load on each link in the network is about the same level. The one way routing of the heuristic may not keep the load on each link the same. Thus, the difference between z_{LP} and z_H could be larger than the strongly correlated traffic pattern. Since the uncorrelated traffic pattern does not correspond to the former two traffic patterns, its UB values were also in the middle. These patterns in UB values might be more influenced by the congestion objective when the weight w was closer to 0. On the other hand, if the weight is closer to 1, then the patterns in UB values might be dependent on the cost pattern, i.e., low, medium, or high. The numerical tests show that the heuristic algorithm for MOP performs well for a large node of network with twenty nodes.

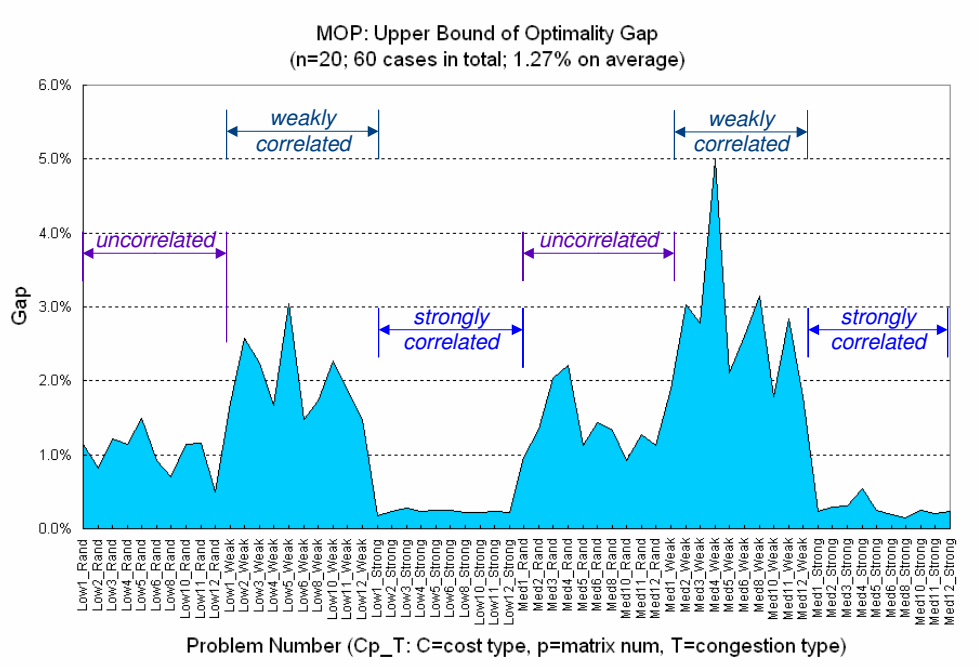

Figure 3-42. A graphical display for UB in Table 3-7 ($n = 20$)

Tables 3-8 and 3-9 summarize UB values to the objective function value for heuristic solutions (z_H) from the numerical results in Section 3.4.2 for ring networks with n=8 and n=10. Figures 3-43 and 3-44 display the UB values and the optimal solutions in Table 3-8 and 3-9.

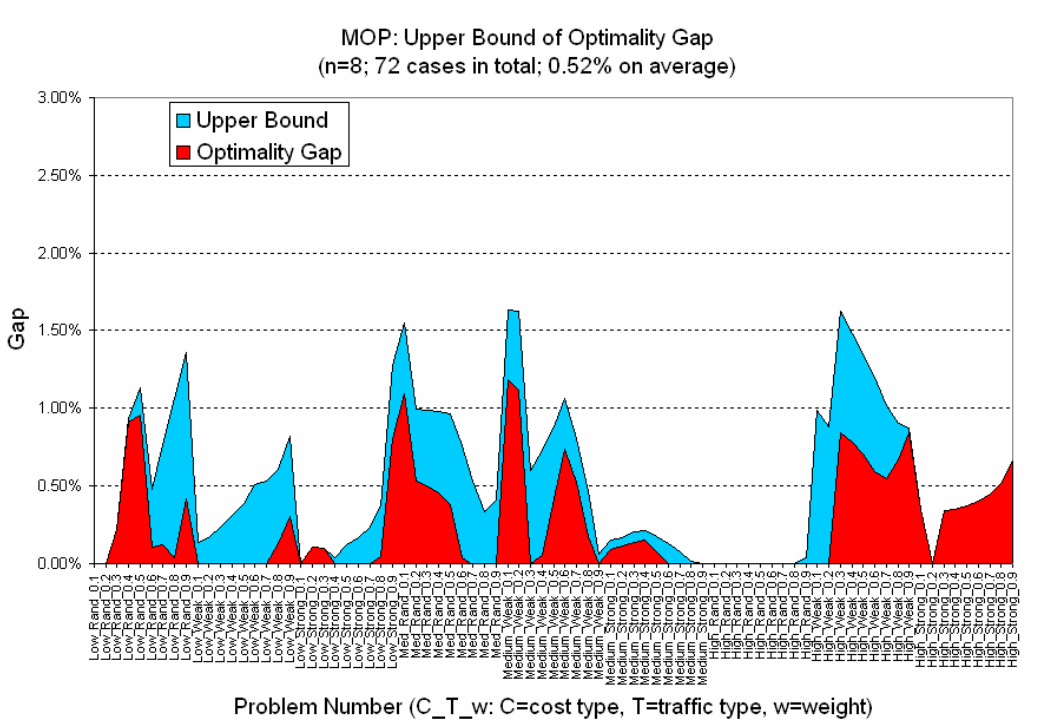

Figure 3-43. A graphical display for UB in Table 3-8 ($n = 8$)

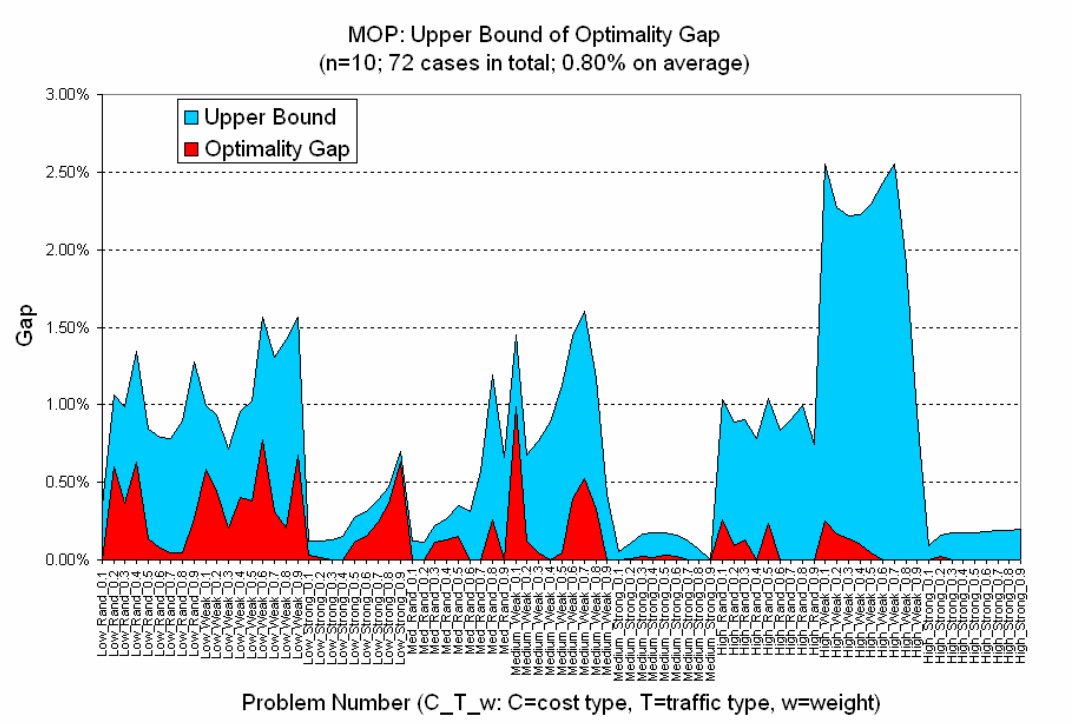

Figure 3-44. A graphical display for UB in Table 3-9 ($n = 10$)

Table 3-7. Upper bound of optimality gap ($n = 20$) in MOP

A	B	C	D	E	F
Cost	# cost matrix	Traffic	z_LP	z_H	UB
low	1	random	25578.4	25869	1.14%
	2		25599.7	25810	0.82%
	3		25614.3	25926	1.22%
	4		25596.4	25887	1.14%
	5		25621.4	26003	1.49%
	6		25608.1	25845	0.93%
	8		25616	25797	0.71%
	10		25594	25886	1.14%
	11		25591.2	25886	1.15%
	12		25603.4	25730	0.49%
low	1	weakly	7932.95	8068	1.70%
	2	correlated	7953.53	8158.8	2.58%
	3		7948.49	8126.7	2.24%
	4		7942.07	8074.3	1.66%
	5		7957.79	8200.1	3.04%
	6		7952.92	8070.3	1.48%
	8		7967.73	8105.5	1.73%
	10		7945.36	8125.9	2.27%
	11		7943.27	8092.6	1.88%
	12		7963.4	8081.5	1.48%
low	1	strongly	31753.1	31809	0.18%
	2	correlated	31770.5	31843	0.23%
	3		31764.2	31854	0.28%
	4		31757.6	31831	0.23%
	5		31772.8	31850	0.24%
	6		31768.9	31848	0.25%
	8		31785.5	31854	0.22%
	10		31758.4	31827	0.22%
	11		31758.9	31834	0.24%
	12		31782.1	31851	0.22%
medium	4	random	25605.2	25854	0.97%
	5		25637.1	25982	1.35%
	6		25621.1	26141	2.03%
	9		25668.6	26235	2.21%
	11		25601.2	25888	1.12%
	13		25614	25980	1.43%
	16		25629.9	25972	1.33%
	21		25607.2	25842	0.92%
	23		25622.5	25950	1.28%
	24		25610.3	25898	1.12%
medium	4	weakly	7947.44	8096.9	1.88%
	5	correlated	7974.86	8216.3	3.03%
	6		7953.01	8173.7	2.77%
	9		7988.36	8387.5	5.00%
	11		7935.16	8102.8	2.11%
	13		7954.69	8162	2.61%
	16		7972.8	8223.9	3.15%
	21		7951.02	8092.5	1.78%
	23		7972.46	8198.9	2.84%
	24		7956.7	8098.5	1.78%
medium	4	strongly	31765.4	31840	0.23%
	5	correlated	31790.6	31885	0.30%
	6		31767.7	31867	0.31%
	9		31798.2	31972	0.55%
	11		31749.2	31830	0.25%
	13		31772.2	31833	0.19%
	16		31789.5	31837	0.15%
	21		31769.4	31849	0.25%
	23		31786.8	31851	0.20%
	24		31773	31846	0.23%

Table 3-8. Upper bound of optimality gap ($n = 8$) in MOP

A	B	C	D	E	F	G	H
Cost	Traffic	Weight	z_LP	z_H	UB	Optimal Sol	Optimality Gap
low	random	0.1	2944.5	2944.50	0.00%	2944.5	0.00%
		0.2	2657.48	2657.50	0.00%	2657.48	0.00%
		0.3	2370.42	2375.60	0.22%	2370.42	0.22%
		0.4	2082.81	2102.30	0.94%	2083.36	0.91%
		0.5	1793.2	1813.50	1.13%	1796.3	0.96%
		0.6	1503.29	1510.50	0.48%	1508.88	0.11%
		0.7	1212.77	1222.10	0.77%	1220.66	0.12%
		0.8	920.917	930.68	1.06%	930.34	0.04%
		0.9	626.818	635.34	1.36%	632.72	0.41%
low	weakly correlated	0.1	1250.27	1252.00	0.14%	1252	0.00%
		0.2	1149.1	1151.00	0.17%	1151	0.00%
		0.3	1047.57	1050.00	0.23%	1050	0.00%
		0.4	946.019	949.00	0.32%	949	0.00%
		0.5	844.287	847.55	0.39%	847.55	0.00%
		0.6	742.253	746.04	0.51%	746.04	0.00%
		0.7	639.878	643.28	0.53%	643.26	0.00%
		0.8	537.258	540.52	0.61%	539.84	0.13%
		0.9	434.2	437.76	0.82%	436.42	0.31%
low	strongly correlated	0.1	3651.58	3651.60	0.00%	3651.58	0.00%
		0.2	3283.96	3287.50	0.11%	3283.96	0.11%
		0.3	2916.34	2919.30	0.10%	2916.34	0.10%
		0.4	2547.71	2548.70	0.04%	2548.72	0.00%
		0.5	2178.49	2181.10	0.12%	2181.1	0.00%
		0.6	1808.91	1812.00	0.17%	1812	0.00%
		0.7	1439.27	1442.70	0.24%	1442.75	0.00%
		0.8	1069.55	1073.50	0.37%	1073.02	0.04%
		0.9	699.726	708.67	1.28%	703.01	0.81%
medium	random	0.1	2960.86	3006.80	1.55%	2974.24	1.09%
		0.2	2674.44	2701.10	1.00%	2686.88	0.53%
		0.3	2387.96	2411.50	0.99%	2399.52	0.50%
		0.4	2101.29	2121.80	0.98%	2112.16	0.46%
		0.5	1814.18	1831.70	0.97%	1824.8	0.38%
		0.6	1526.41	1538.00	0.76%	1537.44	0.04%
		0.7	1237.65	1244.20	0.53%	1244.25	0.00%
		0.8	947.313	950.50	0.34%	950.5	0.00%
		0.9	654.055	656.75	0.41%	656.75	0.00%
medium	weakly correlated	0.1	1257.45	1278.00	1.63%	1263.03	1.19%
		0.2	1159.59	1178.40	1.62%	1165.36	1.12%
		0.3	1061.36	1067.70	0.60%	1067.69	0.00%
		0.4	963.018	970.02	0.73%	969.54	0.05%
		0.5	864.451	872.05	0.88%	868.45	0.41%
		0.6	764.902	773.04	1.06%	767.36	0.74%
		0.7	664.409	669.74	0.80%	666.27	0.52%
		0.8	563.541	566.16	0.46%	565.18	0.17%
		0.9	462.304	462.58	0.06%	462.58	0.00%
medium	strongly correlated	0.1	3657.82	3663.50	0.16%	3660.12	0.09%
		0.2	3293.51	3299.10	0.17%	3295.44	0.11%
		0.3	2928.61	2934.70	0.21%	2930.76	0.13%
		0.4	2563.27	2568.80	0.22%	2564.98	0.15%
		0.5	2196.96	2200.80	0.17%	2199.15	0.08%
		0.6	1830.05	1832.40	0.13%	1832.4	0.00%
		0.7	1462.94	1464.00	0.07%	1464.05	0.00%
		0.8	1095.52	1095.70	0.02%	1095.7	0.00%
		0.9	727.35	727.35	0.00%	727.35	0.00%
high	random	0.1	2956.44	2956.40	0.00%	2956.44	0.00%
		0.2	2668.28	2668.30	0.00%	2668.28	0.00%
		0.3	2380.12	2380.10	0.00%	2380.12	0.00%
		0.4	2091.96	2092.00	0.00%	2091.96	0.00%
		0.5	1803.8	1803.80	0.00%	1803.8	0.00%
		0.6	1515.64	1515.60	0.00%	1515.64	0.00%
		0.7	1227.48	1227.50	0.00%	1227.48	0.00%
		0.8	939.32	939.32	0.00%	939.32	0.00%
		0.9	650.892	651.16	0.04%	651.16	0.00%
high	weakly correlated	0.1	1259.71	1272.10	0.98%	1272.12	0.00%
		0.2	1161.16	1171.40	0.88%	1171.44	0.00%
		0.3	1062.5	1079.80	1.63%	1070.76	0.84%
		0.4	963.365	977.66	1.48%	970.08	0.78%
		0.5	863.89	875.55	1.35%	869.4	0.71%
		0.6	764.13	773.28	1.20%	768.72	0.59%
		0.7	663.974	670.71	1.01%	667.07	0.55%
		0.8	563.053	568.14	0.90%	564.38	0.67%
		0.9	461.544	465.57	0.87%	461.69	0.84%
high	strongly correlated	0.1	3654.3	3667.10	0.35%	3654.3	0.35%
		0.2	3288.6	3288.60	0.00%	3288.6	0.00%
		0.3	2922.9	2932.80	0.34%	2922.9	0.34%
		0.4	2556.8	2565.70	0.35%	2556.8	0.35%
		0.5	2190.5	2198.60	0.37%	2190.5	0.37%
		0.6	1824.2	1831.50	0.40%	1824.2	0.40%
		0.7	1457.9	1464.40	0.45%	1457.9	0.45%
		0.8	1091.6	1097.20	0.51%	1091.6	0.51%
		0.9	725.3	730.12	0.66%	725.3	0.66%

Table 3-9. Upper bound of optimality gap ($n = 10$) in MOP

A	B	C	D	E	F	G	H
Cost	Traffic	Weight	z_LP	z_H	UB	Optimal Sol	Optimality Gap
low	random	0.1	5837.86	5858.40	0.35%	5858.45	0.00%
		0.2	5243.13	5299.00	1.07%	5267.4	0.60%
		0.3	4647.64	4693.50	0.99%	4676.35	0.37%
		0.4	4051.07	4105.50	1.34%	4079.88	0.63%
		0.5	3453.38	3482.50	0.84%	3477.75	0.14%
		0.6	2854.47	2877.00	0.79%	2874.72	0.08%
		0.7	2253.88	2271.50	0.78%	2270.54	0.04%
		0.8	1650.87	1665.70	0.90%	1664.96	0.04%
		0.9	1045.99	1059.30	1.27%	1056.48	0.27%
low	weakly correlated	0.1	2110.96	2131.90	0.99%	2119.57	0.58%
		0.2	1928.61	1946.60	0.93%	1938.08	0.44%
		0.3	1745.06	1757.50	0.71%	1753.94	0.20%
		0.4	1560.84	1575.80	0.96%	1569.52	0.40%
		0.5	1376.3	1390.40	1.02%	1385.1	0.38%
		0.6	1191.37	1210.00	1.56%	1200.68	0.78%
		0.7	1006.26	1019.40	1.31%	1016.26	0.31%
		0.8	820.326	832.00	1.42%	830.32	0.20%
		0.9	631.237	641.13	1.57%	636.81	0.68%
low	strongly correlated	0.1	7145.29	7154.20	0.12%	7151.91	0.03%
		0.2	6401.94	6409.80	0.12%	6408.92	0.01%
		0.3	5657.98	5665.50	0.13%	5665.45	0.00%
		0.4	4913.22	4920.80	0.15%	4920.78	0.00%
		0.5	4168.11	4179.40	0.27%	4174.6	0.11%
		0.6	3422.82	3433.60	0.31%	3428.28	0.16%
		0.7	2677.04	2687.40	0.39%	2680.89	0.24%
		0.8	1930.91	1940.00	0.47%	1933	0.36%
		0.9	1184.22	1192.50	0.70%	1185	0.63%
medium	random	0.1	5839.91	5846.90	0.12%	5846.9	0.00%
		0.2	5244	5249.80	0.11%	5249.8	0.00%
		0.3	4647.67	4658.00	0.22%	4652.7	0.11%
		0.4	4050.11	4060.80	0.26%	4055.6	0.13%
		0.5	3451.69	3463.70	0.35%	3458.5	0.15%
		0.6	2852.44	2861.40	0.31%	2861.4	0.00%
		0.7	2251.41	2264.30	0.57%	2264.3	0.00%
		0.8	1649.19	1668.80	1.19%	1664.46	0.26%
		0.9	1045.47	1052.40	0.66%	1052.39	0.00%
medium	weakly correlated	0.1	2108.79	2139.40	1.45%	2118.43	0.99%
		0.2	1926.41	1939.50	0.68%	1937.16	0.12%
		0.3	1743.38	1756.70	0.76%	1755.89	0.05%
		0.4	1560.02	1573.90	0.89%	1573.86	0.00%
		0.5	1375.62	1391.10	1.13%	1390.45	0.05%
		0.6	1190.54	1207.70	1.44%	1202.96	0.39%
		0.7	1004.71	1020.80	1.60%	1015.47	0.52%
		0.8	818.037	827.58	1.17%	824.86	0.33%
		0.9	629.102	631.79	0.43%	631.79	0.00%
medium	strongly correlated	0.1	7144.44	7148.20	0.05%	7148.22	0.00%
		0.2	6401.18	6407.90	0.10%	6407.6	0.00%
		0.3	5657.62	5667.00	0.17%	5665.51	0.03%
		0.4	4913.4	4922.00	0.18%	4921.1	0.02%
		0.5	4168.46	4175.70	0.17%	4174.55	0.03%
		0.6	3423.13	3428.50	0.16%	3427.84	0.02%
		0.7	2677.49	2680.70	0.12%	2680.61	0.00%
		0.8	1931.11	1932.50	0.07%	1932.48	0.00%
		0.9	1184.24	1184.20	0.00%	1184.24	0.00%
high	random	0.1	5859.58	5920.20	1.03%	5905.13	0.26%
		0.2	5259.09	5305.70	0.89%	5300.92	0.09%
		0.3	4657.43	4699.60	0.91%	4693.68	0.13%
		0.4	4054.71	4086.40	0.78%	4086.44	0.00%
		0.5	3451.71	3487.50	1.04%	3479.2	0.24%
		0.6	2848.19	2872.00	0.84%	2871.96	0.00%
		0.7	2244.45	2264.70	0.90%	2264.72	0.00%
		0.8	1640.11	1656.40	0.99%	1656.38	0.00%
		0.9	1034.48	1042.20	0.75%	1042.19	0.00%
high	weakly correlated	0.1	2138.79	2193.40	2.55%	2187.86	0.25%
		0.2	1956.62	2001.00	2.27%	1997.68	0.17%
		0.3	1769.44	1808.70	2.22%	1806.22	0.14%
		0.4	1581.14	1616.30	2.22%	1614.76	0.10%
		0.5	1391.98	1423.90	2.29%	1423.3	0.04%
		0.6	1202.32	1231.50	2.43%	1231.52	0.00%
		0.7	1011.66	1037.50	2.55%	1037.52	0.00%
		0.8	819.644	835.24	1.90%	835.24	0.00%
		0.9	625.171	631.12	0.95%	631.12	0.00%
high	strongly correlated	0.1	7145.81	7152.20	0.09%	7152.24	0.00%
		0.2	6401.04	6411.10	0.16%	6409.88	0.02%
		0.3	5655.54	5665.50	0.18%	5665.49	0.00%
		0.4	4909.66	4918.40	0.18%	4918.38	0.00%
		0.5	4163.21	4170.60	0.18%	4170.65	0.00%
		0.6	3416.59	3422.90	0.18%	3422.92	0.00%
		0.7	2669.56	2674.60	0.19%	2674.58	0.00%
		0.8	1921.86	1925.50	0.19%	1925.48	0.00%
		0.9	1173.84	1176.20	0.20%	1176.24	0.00%

Application to Congestion Minimization Problem

The NLTCP HEURISTIC introduced in Section 3.4.1 can be applied to a congestion minimization problem whose objective is to find a bi-connected ring network topology which minimizes maximum congestion in a link (Desai et al., 2005). The formulation of the congestion minimization problem keeps the same constraints as NLTCP; however, its objective function has the form of $\min_{y,f} \left(\max_{(i,j)} \sum_{\omega=(o,d)} r_\omega f_{\omega ij} \right)$.

Figure 3-45 illustrates the definition of maximum congestion in a link for a given bi-connected ring network topology with an odd number of nodes. The maximum congestion in a link considers all possible shortest path routings using the link. The traffic flows for $r_{\omega=(1,3)}$, $r_{\omega=(2,3)}$, and $r_{\omega=(2,4)}$ can pass the link (2,3) as illustrated in Figure 3-45; hence the congestion value (denoted as LTC) for the link (2,3) is sum of the three traffic demands, $r_{\omega=(1,3)} + r_{\omega=(2,3)} + r_{\omega=(2,4)}$.

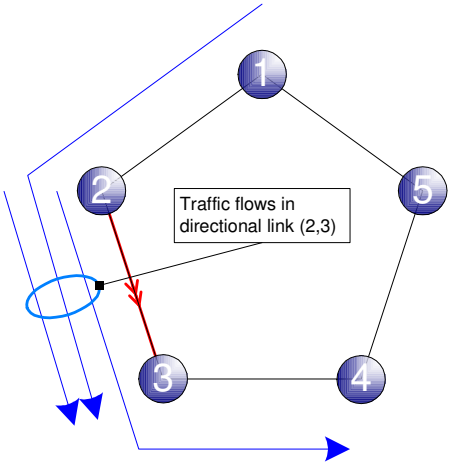

Figure 3-45. Definition of maximum congestion in a link for a bi-connected ring network topology

To find an optimal solution by enumeration, the maximum congestion in each link, LTC, is computed for each topology in $(n-1)!$ ring network topologies as illustrated in Figure 3-45. Hence the complexity of the problem is $O\left((n-1)!\right) \simeq O(n!)$ if the computation time of LTC is not considered; the problem is at least as hard to solve as the TSP, whose complexity is also $O(n!)$.

A variation of NLTCP HEURISTIC can be used to solve the congestion minimization problem in polynomial time. The heuristic algorithm for the congestion minimization problem is as follows:

Min-Max Load Heuristic

MIN-MAX LOAD HEURISTIC has the same procedures as NLTCP HEURISTIC by:

- Replacing the objective function value (TTC) with LTC in each step of NLTCP HEURISTIC; LTC is computed as in the definition in Figure 3-45 (or using MATLAB code in Appendix D).
- Removing steps for computing $DIST$ maxtrix in NLTCP HEURISTIC.

The heuristic improvement algorithm for NLTCP HEURISTIC is also applied to MIN-MAX LOAD HEURISTIC. The topology solutions from the two heuristic algorithms may be different because of the difference in their objectives (Figure 3-46).

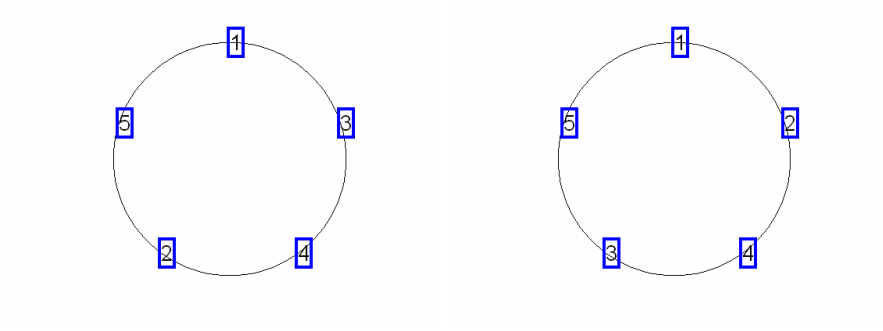

(a) NLTCP HEURISTIC (b) MIN-MAX LOAD HEURISTIC

Figure 3-46. Different topology solutions from NLTCP HEURISTIC and MIN-MAX LOAD HEURISTIC

Figure 3-47 shows an example of a heuristic solution for a bi-connected ring network topology with $n = 31$. The solution indicates that the directional link (20,2) has the maximum congestion which is the minimum among all possible ring network topologies (i.e., $(n-1)! = 30! = 2.6525 \times 10^{32}$ ring network topologies).

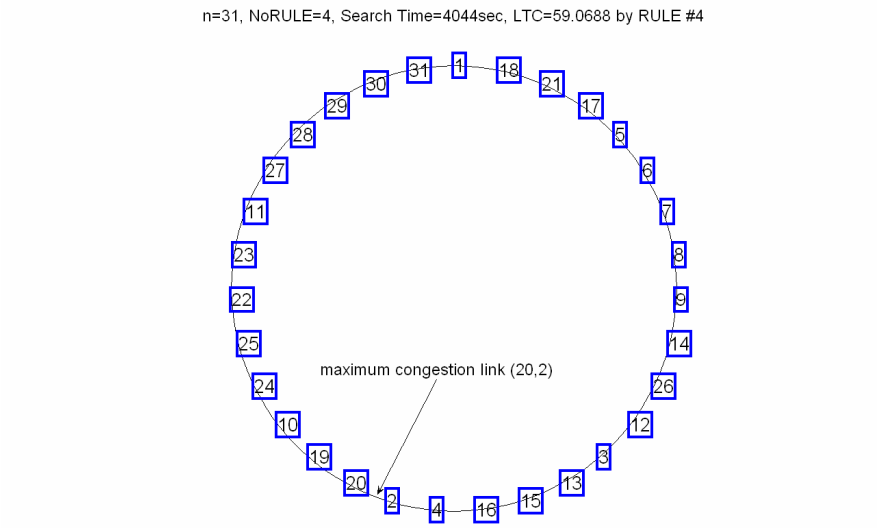

Figure 3-47. Example of heuristic solution for congestion minimization problem

Desai et al. (2005) used the same definition on the maximum congestion in a link (as illustrated in Figure 3-45) for a given bi-connected ring network topology with odd number of nodes. Figures 3-48 and 3-49 compare the heuristic solutions of MIN-MAX LOAD HEURISTIC and Desai et al.'s; Desai et al. used a combination of multihop and branch exchange method to solve the congestion minimization problem (Desai et al., 2005). In Figures 3-48 (a) and 3-49 (a), "$H_{standard}$" and "MULTIHOP+BE" represent the heuristic solution of MIN-MAX LOAD HEURISTIC and Desai et al.'s, respectively. For a ring network with a large number of nodes, the optimal solution cannot be known due to the complexity of the congestion minimization problem. In such case, $H_{standard}$ can be used to approximate the optimality gap. In Figures 3-48 (b) and 3-49 (b), the optimality gap of MULTIHOP+BE was approximated by $H_{standard}$ as follows:

$\frac{\left((Multihop+BE)-H_{standard}\right)}{H_{standard}}\times 100\%$ as shown in Figures 3-48 (a) and 3-49 (a).

Hence the MIN-MAX LOAD HEURISTIC can act as an evaluation tool for any other heuristics for the congestion minimization problem with a bi-connected ring network topology.

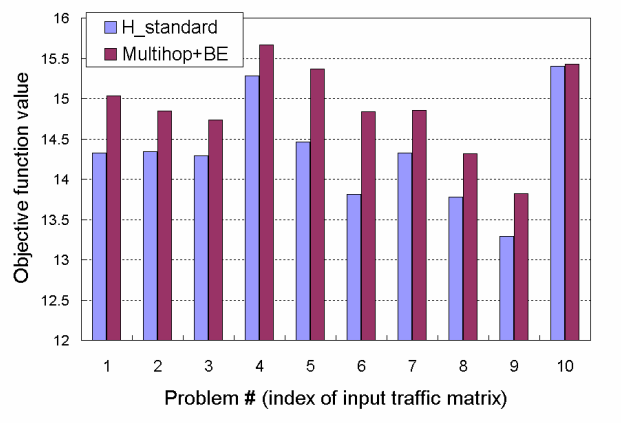

(a) Congestion values

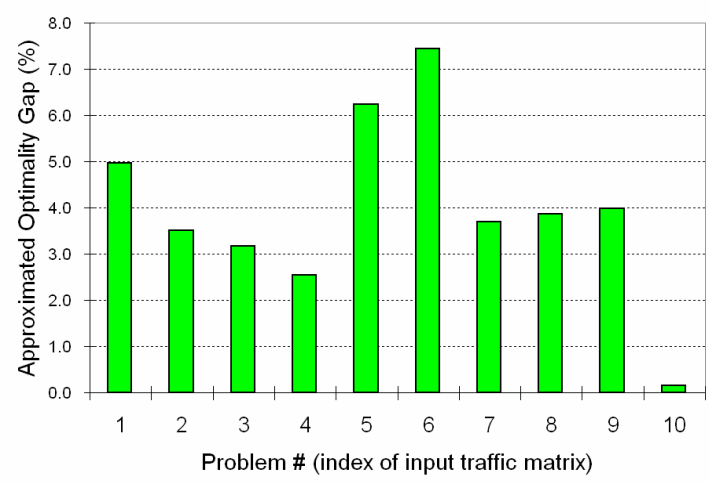

(b) Approximated optimality gap

Figure 3-48. Example of heuristic evaluation for $n = 15$[1]

[1] By "approximate", we mean the optimality gap can be measured by the MIN-MAX LOAD HEURISTIC solution if an optimal solution is unknown or it is hard to get the optimal solution for the specific problem.

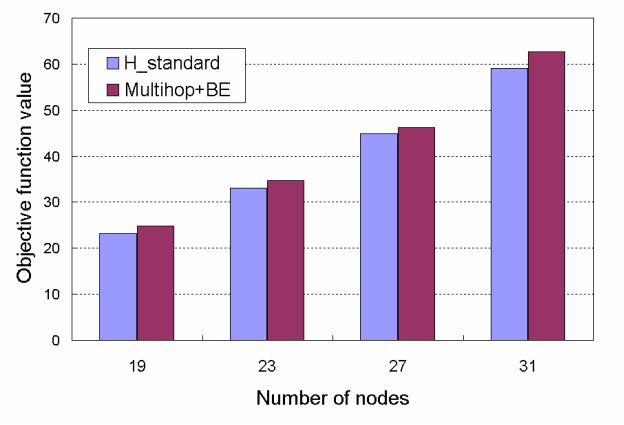

(a) Congestion values

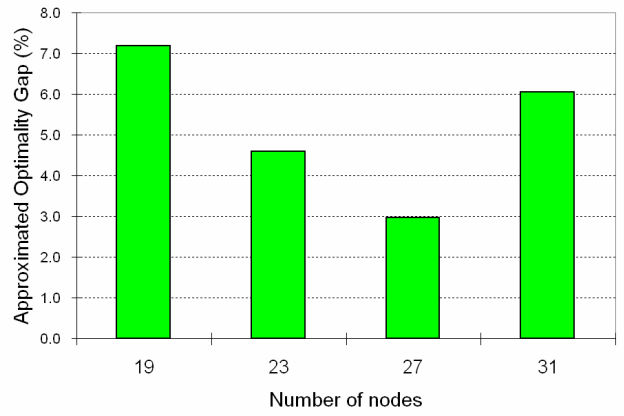

(b) Approximated optimality gap

Figure 3-49. Example of heuristic evaluation for $n = 19$, 23, 27, and 31

3.7 Summary

This chapter has presented efficient heuristic algorithms for dynamic reconfiguration of ring network topologies in FSO network, which are NLTCP HEURISTIC and MOP HEURISTIC.

The complexity of the NLTCP HEURISTIC is reduced to $O(n^2)$ as compared to $O(2^{n^2} \times n!)$ of the binary linear program version of NLTCP, which represents a significant reduction in computational time. In the numerical tests, the heuristic achieved a 0.5 % optimality gap in 50 % of the test problems and less than 2.5 % in 100 % of the test problems. The MOP HEURISTIC provided near-Pareto optimal solutions for the multiobjective optimization problem with various types of network cost and stochastic traffic load. The numerical results show that 100 % of the test problems were within 1.2 % optimality gap. The heuristic improvement algorithm for NLTCP HEURISTIC and MOP HEURISTIC improved the optimality gaps even more. In addition, the NLTCP HEURISTIC was compared to the metaheuristics, Simluated Annealing and Genetic Algorithms.

For evaluating the performance of NLTCP HEURISTIC and MOP HEURISTIC in a ring network with $n > 15$, a new measure of estimating the optimality gap (a theoretical bound for the optimality gap) was introduced. The new measure employed the objective function value of a relaxed LP version of NLTCP, in which the objective value was improved by Triangle Inequality Constraints from Section 3.3.1. This measure provides an upper bound on the optimality gap without actually

knowing the optimal objective function value, which is a significant computational advantage over using a commercial solver (XPRESS-MP) or enumeration. For NLTCP, numerical tests with $n = 15$ and $n = 20 \sim 27$ show that the optimality gaps were less than or equal to 1.70 % on average. For MOP, numerical tests with $n = 20$ show the optimality gaps were less than or equal to 1.27 % on average.

The topology solutions of NLTCP HEURISTIC and MOP HEURISTIC provide the shortest hop routing directions for each OD pair in traffic demand and the routing assures low cost and congestion on a bi-connected FSO network. The MIN-MAX LOAD HEURISTIC which is a variation of NLTCP HEURISTIC is used to measure the performance of the heuristic by Desai et al. (2005) and this example was used to show the effectiveness of the MIN-MAX LOAD HEURISTIC.

Table 3-10 summarizes the performance accuracy of those three heuristic methods, which were implemented in MATLAB (version 7.0). The empirical performance (optimality gap) of each of NLTCP HEURISTIC and MOP HEURISTIC was tested for various sizes of ring networks and traffic or cost input matrices with optimal solutions by a commercial solver XPRESS-MP (www.dashoptimization.com) or enumeration code. The table also shows that the upper bounds on the optimality gaps for the test problems with NLTCP HEURISTIC and MOP HEURISTIC are small, i.e., 1.70 % and 1.27 % on average, respectively. This means the optimality gaps for the heuristic solutions are equal to the upper bound values at most (i.e., optimality gap ≤

1.70 % for NLTCP HEURISTIC and optimality gap ≤ 1.27 % for MOP HEURISTIC), but were obtained relatively quickly.

Table 3-11 summarizes a comparison between the existing heuristic methods for dynamic reconfiguration of bi-connected ring topologies in fiber optic and FSO networks and the new ones in this thesis.

Table 3-10. The performance of heuristic methods in this thesis

	Network Size (number of nodes)	# of Test Problems	Optimality Gap with Global Optimum	Solution Time (n=number of nodes)	Related Section
NLTCP Heuristic (MATLAB version 7.0)	8,9,10,12,14,15	80	≤ 2.5%	6 sec (n=8) ~ 60 sec (n=15)	Section 3.4.1
	20~27	80	≤ 1.70% (mean)	5 min (n=20) ~ 40 min (n=27)	Section 3.5
Min-Max Load Heuristic (MATLAB version 7.0)	15,19,23,27,31	14	max 7.44% improved*	2 min (n=15) ~ 69 min (n=31)	Section 3.6
MOP Heuristic (MATLAB version 7.0)	8,10	162	≤ 1.2%	6 sec (n=8) ~ 12 sec(n=10)	Section 3.4.2
	20	60	≤ 1.27% (mean)	5 min	Section 3.5

*: The objective function value (A) to the best solution from Min-Max Load Heuristic was compared to the one (B) from "Multihop+BE" heuristic by Desai et al. (2005). The largest difference between A and B (i.e., (B-A)/A ×100%) was 7.44%.

Table 3-11. Comparison of existing heuristic methods with new ones in this thesis research

	A				*B*
	Existing Heuristic Methods				**Thesis Research**
Heuristics	Single-Hop (SH)	Multihop (MH)	Rollout (RO)	Branch Exchange (BE)	NLTCP Heuristic / MinMax Heuristic / MOP Heuristic
Topology	Ring				
Node degree	2				
Routing	Shortest hop				
Objectives	minimize the maximum link load				NLTCP Heuristic: minimize the total congestion Min-Max Load Heuristic: minimize the maximum link load
Polynomial algorithm	YES O(n^3)	YES O(n^3)	YES O(n^5)	YES O(n^5)	YES O(n^2)
Neighborhood search	Local search i) Link addition by the order of nondecreasing magnitude of traffic ii) Exchanging two existing links with two new links in a ring topology				Local search Decision rules are used to find improved topology solutions
Performance measure with optimality gap using global optimum	n/a				Yes
Multi-objective performance	n/a				Topology Control in both Physical Layer and Network Layer
Considering Stochastic load?	n/a				Yes
Real-time implementation	Desai et al. (2005) implemented a hybrid of MH+BE, RO-SH, and RO-MH with C++				Possible by converting to real-time code with machine languages (e.g., C++)

Chapter 4: Summary and Future Research

Free space optical communication provides special functionalities compared to fiber optic networks and omnidirectional RF wireless communications. FSO is optical wireless (no installation cost for fibers) and directional (no frequency interference). Moreover, its high-speed data transmission capability is an attractive solution to the first or last mile problem in bridging to current fiber optic network or is a preferable alternative to the low data rate directional point-to-point RF communications for an inter-building wireless local area network.

In order to be useful, FSO communication must deal with the following fundamental problems:

- How to quickly and precisely establish and maintain optical links between nodes in the network? (Question about Autonomous Physical Reconfiguration by Pointing, Acquisition, and Tracking)
- How to optimize network performance in terms of network cost and congestion? (Question about Autonomous Logical Reconfiguration by Topology Optimization)
- How to respond autonomously to possible network performance degradation due to link loss or sudden changes in traffic demands? (Question about Dynamic Reconfiguration by Topology Control)

This dissertation research has supplied solutions to the above problems with both a hardware approach for developing self-organized pointing and a software

approach for developing accurate heuristic algorithms for topology optimization in bi-connected FSO networks. The research results from the combined hardware and software approaches will be a step to realize dynamic reconfiguration in FSO networks.

4.1 Summary of Achievements

The purpose of the dissertation research was to *i)* develop a methodology for self-organized pointing and the associated autonomous and precise pointing technique for establishing optical links between optical transceivers in FSO networking and *ii)* develop accurate heuristic methods for topology optimization in bi-connected ring networks. The validity of the research results was confirmed by having our relevant papers accepted as follows:

Journal of the Operational Research Society

Shim Y, Gabriel SA, Desai A, Sahakij P and Milner S (2005). *A Fast Heuristic Method for Minimizing Traffic Congestion on Reconfigurable Ring Topologies*. Journal of the Operational Research Society (JORS). Advance online publication 7 February 2007; doi: 10.1057/palgrave.jors.2602360

Networks and Spatial Economics

Gabriel SA, Shim Y, Llorca J and Milner S (2006). *A Multiobjective Optimization Model for Dynamic Reconfiguration of Ring Topologies with Stochastic Load.*

Networks and Spatial Economics. Advance online publication 20 July 2007; doi: 10.1007/s11067-007-9025-8.

MILCOM 2007 Unclassified Proceedings

Shim Y, Milner SD and Davis CC (2007). *A Precise Pointing Technique for Free Space Optical Networking*. The MILCOM 2007 Unclassified Proceedings. Orlando, Florida. October 29–31. Accepted for publication.

SPIE Optics & Photonics

Shim Y, Milner SD and Davis CC (2007). *A Precise Pointing Technique for FSO Links and Networks using Kinematic GPS and Local Sensors*. The Free-Space Laser Communications VII conference. Proceedings of the SPIE. San Diego. CA. August 26-30. Published online 25 September 2007; doi: 10.1117/12.739113.

The 9th INFORMS Telecommunications Conference: Telecommunications Modeling, Policy, and Technology

Shim Y, Gabriel SA, Milner SD and Davis CC (2007). *Topology Control in a Free Space Optical Network*. The 9th INFORMS Telecommunications Conference: Telecommunications Modeling, Policy, and Technology. Robert H. Smith School of Business. University of Maryland. College Park. MD. 27-29 March 2008. Accepted for publication.

4.1.1 Unique, Autonomous, and Precise Method for Self-Organized Pointing

Existing pointing systems in FSO networking depend on optical devices or INS combined with GPS (Ho et al., 2006; Epple, 2006; Wilkerson et al., 2006; Yee et al., 1998). Their reported pointing accuracies are about 1 milliradian. This thesis research provides a precise pointing method whose pointing accuracy is improved to the sub-milliradian range. Our pointing method is applicable to both FSO networking and directional point-to-point RF communications. In addition, a pointing system implementing our method would be operable in a wide area because it employs global sensors, that is, GPS and local angular sensors (e.g., tilt sensors or INS). Moreover, since these are conventional air navigation sensors, they may enable us to use the pointing method in a dynamic environment and estimate position and velocity of a mobile node for tracking.

The main hardware-related contributions in pointing are summarized as follows:

- Development of a unique methodology for self-organized pointing which is an independent and interoperable pointing procedure to complete pointing between local and remote transceivers (Section 2.1.1)
- Development of a unique method of measuring pointing direction (pointing vector) of FSO transceiver and its directional, narrow laser beam (Section 2.1.2).
- Development of a unique, autonomous, and precise pointing method with RTK GPS and local angular sensors (e.g., tilt sensors, INS) (Section 2.1.2).

- Demonstration, by computer simulation, showing the accuracy of the pointing method increasing with length of pointing vector and link distance between nodes as well as the quality of sensor devices (Section 2.2).
- Implementation of the precise pointing method with an automatic pointing system using RTK GPS and bi-axial tilt sensors (Sections 2.3.1 and 2.3.3). Since RTK GPS consists of a GPS unit and a wireless RF data transceiver; its precise position data will be sufficient to track mobile nodes. Its high accuracy will improve the performance of position and velocity estimation of a mobile node.
- Achievement of "dead-reckoning" pointing accuracy in the sub-milliradian range in a mid-range (264 m) pointing experiment (Section 2.3.2).
- Development of self-organized pointing methodology for mobile platforms in a dynamic environment, which includes autonomous pointing vector measurement by waypoint navigation and self-organized pointing procedure with path planning (Section 2.4).

4.1.2 Accurate Heuristic Methods for Topology Optimization in bi-connected FSO networks

The weakness of existing heuristic methods for dynamic reconfiguration of bi-connected ring topologies in fiber optic and FSO networks is that *i)* their performance measure was not based on the optimality gap between an objective function value of the heuristic and global optimum, and *ii)* they have not included multiobjective

aspects for both the physical layer cost and the network layer congestion simultaneously. This thesis research overcomes the weakness of the existing heuristic methods (see a comparison between the existing heuristic methods and the current ones in Table 3-11). It provides a formal optimality gap measure tested on an extensive set of problems as well as a fast and accurate heuristic method for minimizing total congestion in a bi-connected ring network (NLTCP HEURISTIC). The NLTCP HEURISTIC is a polynomial time algorithm, and it has been evaluated and refined by a measure which provides an upper bound on the optimality gap accurately and quickly (e.g., Figures 3-40 and 3-41). The measure is especially efficient for the congestion minimization problem in a ring network with a large number of nodes (e.g., 15) for which it is very hard to find global optima. In addition, this research extends the single-objective heuristic method to the setting of a multiobjective stochastic optimization in which both cost in physical layer and congestion in network layer were simultaneously optimized. Pareto optimal points were generated using the weighting method (Cohon, 2003; Marler et al., 2004; Steuer, 2004).

The main optimization heuristic-related achievements are summarized as follows:

- Development of accurate polynomial time heuristic methods for NLTCP with deterministic traffic demand to achieve two objectives:
    - Minimize total congestion on a bi-connected ring network (NLTCP HEURISTIC).

- Minimize the maximum congestion on a link (MIN-MAX LOAD HEURISTIC).

- Development of accurate polynomial time heuristic methods for MOP with cost and stochastic load (MOP HEURISTIC).
- Implementation of meta-heuristic algorithms (Simulated Annealing and Genetic Algorithms) for solving NLTCP and comparison with the new heuristics in this thesis.
- Development of an evaluation method for estimating the performance of NLTCP HEURISTIC and MOP HEURISTIC. The method provides a theoretical bound for the optimality gap of both heuristics by which we know the upper bound on the optimality gap of a problem with a large number of nodes without finding its global optimum. Numerical evidence showing the computational attractiveness for NLTCP with n=20~27 and for MOP with n=20 was demonstrated.

There has been no known result in the literature, to our knowledge, which compares solutions obtained by heuristic procedures of UNDP against the true optimal solutions of that problem. Finding a heuristic and presenting performance accuracy of the heuristic was one of the objectives of this thesis research, which significantly contributes to solving UNDP.

4.2 Future Research

Future work would consist of realizing the GPS-based autonomous reconfiguration scenario in Section 1.3 in both static and dynamic environments. Figures 1-10 and 1-11 provide an overview of the work.

Immediate work for PAT may include:

- Realize an automatic pointing system for static nodes with FSO transceivers and high load capacity gimbals,
- Design and realize an automatic pointing system for mobile nodes with the pointing method in Section 2.1, and
- Find a solution to reduce time spent during physical reconfiguration (the faster the physical reconfiguration, the less the time delay for data packet transmission).

This work will consider: *i)* a proper choice of local angular sensors, *ii)* a trade-off between sensor quality and lengths of pointing vector and baseline for a desired pointing accuracy (Section 2.2.3), *iii)* error sources affecting pointing accuracy in dynamic environment (Section 2.3.4), and *iv)* real-time tracking for maintaining connectivity.

The current research for topology optimization could be extended with decision and control problems related to distributing mobile nodes to cover a service area (e.g., coordination and reassignment in Figure 1-10). In this case, new cost factors such as fuel, time, and relative distance between nodes (for avoiding collision)

may be considered. The heuristic methods for NLTCP and MOP must be revised with link capacity and cost constraints; for this purpose, the NLTCP and MOP could be reformulated to capacitated network design problems. Since the new constraints would break down the assumptions in Chapter 3 made for the current heuristic methods, new heuristic methods for the reformulated NLTCP and MOP would make its use much broader than the current ones because it may consider many unexpected cases such as infeasible links, or switching from FSO link to directional RF link due to high obscuration or node mobility.

Appendices

A. Coordinate Transformation of Pointing Vector and Baseline Vector

The attitude angles of FSO transceiver (i.e., roll, pitch, yaw) are defined as follows:

- Roll

  It is defined as a deviation angle from the local horizontal plane; it is a side-up or side-down angle as Figure A-1.

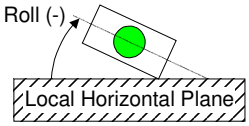

Figure A-1. Definition of roll (ϕ): a front view

- Pitch

  It is defined as a deviation angle from the local horizontal plane; it is a head-up or head-down angle as Figure A-2.

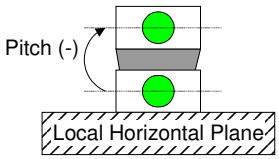

Figure A-2. Definition of pitch (θ): a front view

- Yaw

  It is defined as a deviation angle from the local origin as Figure A-3.

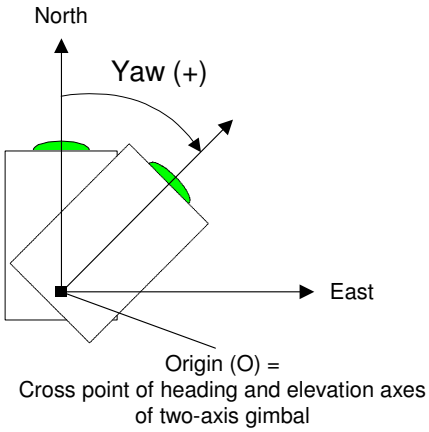

Figure A-3. Definition of yaw (ψ) in the ENU coordinates

Figure A-4 (a) shows a pointing vector ($\overrightarrow{AB}$) and baseline vector ($\overrightarrow{AC}$); the remote FSO transceiver is located at C ($\left|\overrightarrow{AC}\right|$ =link distance). The $\overrightarrow{AB}$ corresponds to the pointing vector centered at C_2 in Figure 2-4 (a) and the one centered at C_1 in Figure 2-4 (b). The coordinates of A , B , and C are, respectively,

$P_{ENU}^{A} = \left[E_A, N_A, U_A\right]$, $P_{ENU}^{B} = \left[E_B, N_B, U_B\right]$, and $P_{ENU}^{C} = \left[E_C, N_C, U_C\right]$.

Yaw angle is defined as follows:

$$\psi = f_1\left(E_A, N_A, U_A, E_B, N_B, U_B\right) = \frac{\pi}{2} \text{-} tan^{-1}\left(\frac{N_B - N_A}{E_B - E_A}\right), \tag{64}$$

where $-\frac{\pi}{2} < tan^{-1}(\bullet) < +\frac{\pi}{2}$.

The rotation matrix for the coordinate transformation from the ENU coordinates to the body frame is defined as:

$$R = \begin{bmatrix} \mathrm{c}\phi & 0 & \mathrm{s}\phi \\ 0 & 1 & 0 \\ -\mathrm{s}\phi & 0 & \mathrm{c}\phi \end{bmatrix} \text{ for roll,} \tag{65}$$

$$P = \begin{bmatrix} 1 & 0 & 0 \\ 0 & c\theta & s\theta \\ 0 & -s\theta & \mathrm{c}\theta \end{bmatrix} \text{ for pitch, and} \tag{66}$$

$$Y = \begin{bmatrix} c\psi & s\psi & 0 \\ -s\psi & c\psi & 0 \\ 0 & 0 & 1 \end{bmatrix} \text{ for yaw.} \tag{67}$$

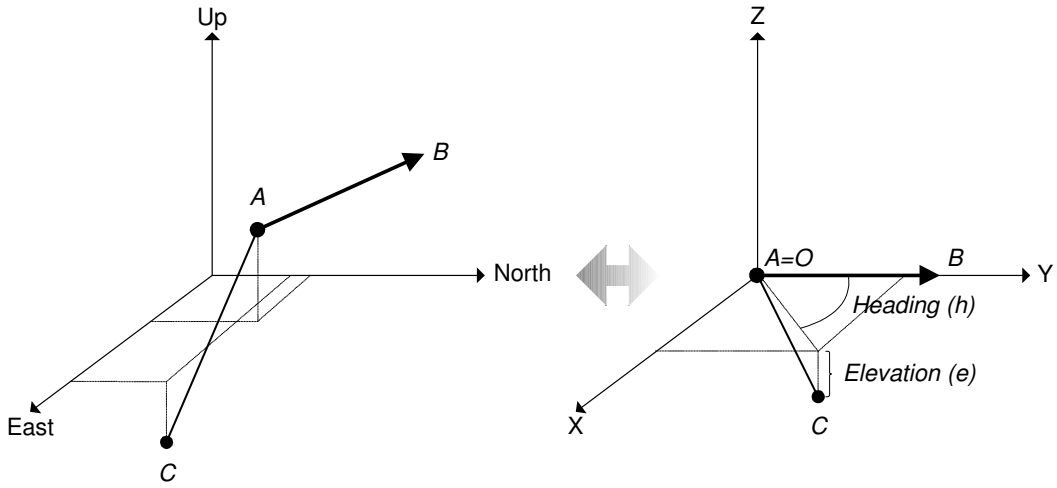

(a) ENU coordinates (b) Body Coordinate

Figure A-4. Coordinate Transformation from ENU to Body Coordinates (Local origin in (b) is the cross point of heading and elevation axes of two-axis gimbal)

The transformation matrix is defined as:

$$T = R^{-1}P^{-1}Y^{-1} = \begin{bmatrix} T_{11} & T_{12} & T_{13} \\ T_{21} & T_{22} & T_{23} \\ T_{31} & T_{32} & T_{33} \end{bmatrix}$$

$$= \begin{bmatrix} c\phi c\psi - s\phi s\theta s\psi & -c\phi s\psi - s\phi s\theta c\psi & -s\phi c\theta \\ c\theta s\psi & c\theta c\psi & -s\theta \\ s\phi c\psi + c\phi s\theta s\psi & -s\phi s\psi + c\phi s\theta c\psi & c\phi c\theta \end{bmatrix} \quad (68)$$

, where $s\alpha = sin(\alpha)$ and $c\alpha = cos(\alpha)$. The point C in the body frame is computed by

$$\begin{bmatrix} X_C \\ Y_C \\ Z_C \end{bmatrix} = f_2\left(E_A, N_A, U_A, E_C, N_C, U_C, \phi, \theta, \psi\right) = T \begin{bmatrix} E_C - E_A \\ N_C - N_A \\ U_C - U_A \end{bmatrix}. \quad (69)$$

The control angles (i.e., heading and elevation angles to align the pointing vector $\overrightarrow{AB}$ to $\overrightarrow{AC}$) are defined as:

$$h = f_3\left(X_C, Y_C, Z_C\right) = tan^{-1}\left(\frac{Y_C}{X_C}\right) - \frac{\pi}{2} \text{ for heading control and} \quad (70)$$

$$e = f_4\left(X_C, Y_C, Z_C\right) = -tan^{-1}\left(\frac{Z_C}{\sqrt{X_C^2 + Y_C^2}}\right) \text{ for elevation control,} \quad (71)$$

where $-\frac{\pi}{2} < tan^{-1}(\bullet) < +\frac{\pi}{2}$.

B. Derivation of the Variance of Pointing Error

By the error propagation law in Section 2.2.1, the variance values of yaw, heading, and elevation are approximated as follows:

(a) $\sigma_{\psi}^2 = \left[\frac{\partial f_1}{\partial E_A} \;\; \frac{\partial f_1}{\partial N_A} \;\; \frac{\partial f_1}{\partial U_A} \;\; \frac{\partial f_1}{\partial E_B} \;\; \frac{\partial f_1}{\partial N_B} \;\; \frac{\partial f_1}{\partial U_B} \right]$

$$diag\left(\left[\sigma_{E_A}^2 \;\; \sigma_{N_A}^2 \;\; \sigma_{U_A}^2 \;\; \sigma_{E_B}^2 \;\; \sigma_{N_B}^2 \;\; \sigma_{U_B}^2 \right] \right) \left[\frac{\partial f_1}{\partial E_A} \;\; \frac{\partial f_1}{\partial N_A} \;\; \frac{\partial f_1}{\partial U_A} \;\; \frac{\partial f_1}{\partial E_B} \;\; \frac{\partial f_1}{\partial N_B} \;\; \frac{\partial f_1}{\partial U_B} \right]^T$$

for yaw, where

$$\frac{\partial f_1}{\partial E_A} = -\frac{1}{1+\left(\frac{N_B - N_A}{E_B - E_A} \right)^2} \frac{\partial}{\partial E_A} \left(\frac{N_B - N_A}{E_B - E_A} \right) = \frac{-\left(N_B - N_A \right)}{\left(E_B - E_A \right)^2 + \left(N_B - N_A \right)^2},$$

$$\frac{\partial f_1}{\partial N_A} = -\frac{1}{1+\left(\frac{N_B - N_A}{E_B - E_A} \right)^2} \frac{\partial}{\partial N_A} \left(\frac{N_B - N_A}{E_B - E_A} \right) = \frac{E_B - E_A}{\left(E_B - E_A \right)^2 + \left(N_B - N_A \right)^2},$$

$$\frac{\partial f_1}{\partial E_B} = -\frac{1}{1+\left(\frac{N_B - N_A}{E_B - E_A} \right)^2} \frac{\partial}{\partial E_B} \left(\frac{N_B - N_A}{E_B - E_A} \right) = \frac{N_B - N_A}{\left(E_B - E_A \right)^2 + \left(N_B - N_A \right)^2},$$

$$\frac{\partial f_1}{\partial N_B} = -\frac{1}{1+\left(\frac{N_B - N_A}{E_B - E_A} \right)^2} \frac{\partial}{\partial N_B} \left(\frac{N_B - N_A}{E_B - E_A} \right) = \frac{-\left(E_B - E_A \right)}{\left(E_B - E_A \right)^2 + \left(N_B - N_A \right)^2},$$

$\frac{\partial f_1}{\partial U_A} = \frac{\partial f_1}{\partial U_B} = 0$, and

$\left(E_A - E_B \right)^2 + \left(N_A - N_B \right)^2 \neq 0$.

(b) $\sigma_h^2 = \begin{bmatrix} \frac{\partial f_3}{\partial X_C} & \frac{\partial f_3}{\partial Y_C} & \frac{\partial f_3}{\partial Y_C} \end{bmatrix} \begin{bmatrix} \sigma_{X_C}^2 & 0 & 0 \\ 0 & \sigma_{Y_C}^2 & 0 \\ 0 & 0 & \sigma_{Z_C}^2 \end{bmatrix} \begin{bmatrix} \frac{\partial f_3}{\partial X_C} & \frac{\partial f_3}{\partial Y_C} & \frac{\partial f_3}{\partial Y_C} \end{bmatrix}^T$ for heading,

where

$$\frac{\partial f_3}{\partial X_C} = \frac{1}{1+\left(Y_C/X_C\right)^2} \frac{\partial}{\partial X_C}\left(\frac{Y_C}{X_C}\right) = \frac{-Y_C}{X_C^2+Y_C^2},$$

$$\frac{\partial f_3}{\partial Y_C} = \frac{1}{1+\left(Y_C/X_C\right)^2} \frac{\partial}{\partial Y_C}\left(\frac{Y_C}{X_C}\right) = \frac{X_C}{X_C^2+Y_C^2},$$

$\frac{\partial f_3}{\partial Z_C} = 0$, and

$X_C^2 + Y_C^2 \neq 0$.

(c) $\sigma_e^2 = \begin{bmatrix} \frac{\partial f_4}{\partial X_C} & \frac{\partial f_4}{\partial Y_C} & \frac{\partial f_4}{\partial Y_C} \end{bmatrix} \begin{bmatrix} \sigma_{X_C}^2 & 0 & 0 \\ 0 & \sigma_{Y_C}^2 & 0 \\ 0 & 0 & \sigma_{Z_C}^2 \end{bmatrix} \begin{bmatrix} \frac{\partial f_4}{\partial X_C} & \frac{\partial f_4}{\partial Y_C} & \frac{\partial f_4}{\partial Y_C} \end{bmatrix}^T$ for

elevation, where

$$\frac{\partial f_4}{\partial X_C} = -\frac{1}{1+\left(Z_C \Big/ \sqrt{X_C^2+Y_C^2}\right)^2} \frac{\partial}{\partial X_C}\left(\frac{Z_C}{\sqrt{X_C^2+Y_C^2}}\right)$$

$$= \left(\frac{Z_C}{X_C^2+Y_C^2+Z_C^2}\right)\left(\frac{X_C}{\sqrt{X_C^2+Y_C^2}}\right) \quad ,$$

$$\frac{\partial f_4}{\partial Y_C} = -\frac{1}{1+\left(Z_C \Big/ \sqrt{X_C^2+Y_C^2}\right)^2} \frac{\partial}{\partial Y_C}\left(\frac{Z_C}{\sqrt{X_C^2+Y_C^2}}\right)$$

$$= \left(\frac{Z_C}{X_C^2+Y_C^2+Z_C^2}\right)\left(\frac{Y_C}{\sqrt{X_C^2+Y_C^2}}\right) \quad ,$$

$$\frac{\partial f_4}{\partial Z_C} = -\frac{1}{1+\left(Z_C \Big/ \sqrt{X_C^2+Y_C^2}\right)^2} \frac{\partial}{\partial Y_C}\left(\frac{1}{\sqrt{X_C^2+Y_C^2}}\right) = -\frac{\sqrt{X_C^2+Y_C^2}}{X_C^2+Y_C^2+Z_C^2}, \text{ and}$$

$$X_C^2+Y_C^2+Z_C^2 \neq 0.$$

The variance of pointing error (or pointing accuracy) is defined as $\sqrt{\sigma_h^2+\sigma_e^2}$. For the above (a), (b) and (c), the magnitude of all derivatives is less than or equal to 1, which means the first-order Taylor series approximation is effective.

By applying the error propagation law in Section 2.2.1, the $\sigma_{X_C}^2$, $\sigma_{Y_C}^2$, and $\sigma_{Z_C}^2$ are derived as follows:

(a) $\sigma_{X_C}^2 = \left[\frac{\partial X_C}{\partial \phi} \; \frac{\partial X_C}{\partial \theta} \; \frac{\partial X_C}{\partial \psi} \; \frac{\partial X_C}{\partial E_C} \; \frac{\partial X_C}{\partial N_C} \; \frac{\partial X_C}{\partial U_C} \; \frac{\partial X_C}{\partial E_A} \; \frac{\partial X_C}{\partial N_A} \; \frac{\partial X_C}{\partial U_A}\right]$

$$diag\left(\left[\sigma_\phi^2 \; \sigma_\theta^2 \; \sigma_\psi^2 \; \sigma_{E_C}^2 \; \sigma_{N_C}^2 \; \sigma_{U_C}^2 \; \sigma_{E_A}^2 \; \sigma_{N_A}^2 \; \sigma_{U_A}^2\right]\right)$$

$$\left[\frac{\partial X_C}{\partial \phi} \; \frac{\partial X_C}{\partial \theta} \; \frac{\partial X_C}{\partial \psi} \; \frac{\partial X_C}{\partial E_C} \; \frac{\partial X_C}{\partial N_C} \; \frac{\partial X_C}{\partial U_C} \; \frac{\partial X_C}{\partial E_A} \; \frac{\partial X_C}{\partial N_A} \; \frac{\partial X_C}{\partial U_A}\right]^T ,$$

where

$$\begin{bmatrix} \frac{\partial X_C}{\partial \phi} \\ \frac{\partial X_C}{\partial \theta} \\ \frac{\partial X_C}{\partial \psi} \end{bmatrix} = \begin{bmatrix} \frac{\partial T_{11}}{\partial \phi} & \frac{\partial T_{12}}{\partial \phi} & \frac{\partial T_{13}}{\partial \phi} \\ \frac{\partial T_{11}}{\partial \theta} & \frac{\partial T_{12}}{\partial \theta} & \frac{\partial T_{13}}{\partial \theta} \\ \frac{\partial T_{11}}{\partial \psi} & \frac{\partial T_{12}}{\partial \psi} & \frac{\partial T_{13}}{\partial \psi} \end{bmatrix} \begin{bmatrix} E_C - E_A \\ N_C - N_A \\ U_C - U_A \end{bmatrix}$$, and

$$= \begin{bmatrix} -T_{31} & -T_{32} & -T_{33} \\ -s\phi c\theta s\psi & -s\phi c\theta c\psi & s\phi s\theta \\ T_{12} & -T_{11} & 0 \end{bmatrix} \begin{bmatrix} E_C - E_A \\ N_C - N_A \\ U_C - U_A \end{bmatrix}$$

$$\begin{bmatrix} \frac{\partial X_C}{\partial E_C} & \frac{\partial X_C}{\partial N_C} & \frac{\partial X_C}{\partial U_C} & \frac{\partial X_C}{\partial E_A} & \frac{\partial X_C}{\partial N_A} & \frac{\partial X_C}{\partial U_A} \end{bmatrix} = \begin{bmatrix} T_{11} & T_{12} & T_{13} & -T_{11} & -T_{12} & -T_{13} \end{bmatrix}.$$

(b) $\sigma_{Y_C}^2 = \begin{bmatrix} \frac{\partial Y_C}{\partial \phi} & \frac{\partial Y_C}{\partial \theta} & \frac{\partial Y_C}{\partial \psi} & \frac{\partial Y_C}{\partial E_C} & \frac{\partial Y_C}{\partial N_C} & \frac{\partial Y_C}{\partial U_C} & \frac{\partial Y_C}{\partial E_A} & \frac{\partial Y_C}{\partial N_A} & \frac{\partial Y_C}{\partial U_A} \end{bmatrix}$

$$diag\left(\begin{bmatrix} \sigma_\phi^2 & \sigma_\theta^2 & \sigma_\psi^2 & \sigma_{E_C}^2 & \sigma_{N_C}^2 & \sigma_{U_C}^2 & \sigma_{E_A}^2 & \sigma_{N_A}^2 & \sigma_{U_A}^2 \end{bmatrix}\right)$$

$$\begin{bmatrix} \frac{\partial Y_C}{\partial \phi} & \frac{\partial Y_C}{\partial \theta} & \frac{\partial Y_C}{\partial \psi} & \frac{\partial Y_C}{\partial E_C} & \frac{\partial Y_C}{\partial N_C} & \frac{\partial Y_C}{\partial U_C} & \frac{\partial Y_C}{\partial E_A} & \frac{\partial Y_C}{\partial N_A} & \frac{\partial Y_C}{\partial U_A} \end{bmatrix}^T,$$

where

$$\begin{bmatrix} \frac{\partial Y_C}{\partial \phi} \\ \frac{\partial Y_C}{\partial \theta} \\ \frac{\partial Y_C}{\partial \psi} \end{bmatrix} = \begin{bmatrix} \frac{\partial T_{21}}{\partial \phi} & \frac{\partial T_{22}}{\partial \phi} & \frac{\partial T_{23}}{\partial \phi} \\ \frac{\partial T_{21}}{\partial \theta} & \frac{\partial T_{22}}{\partial \theta} & \frac{\partial T_{23}}{\partial \theta} \\ \frac{\partial T_{21}}{\partial \psi} & \frac{\partial T_{22}}{\partial \psi} & \frac{\partial T_{23}}{\partial \psi} \end{bmatrix} \begin{bmatrix} E_C - E_A \\ N_C - N_A \\ U_C - U_A \end{bmatrix}$$ and

$$= \begin{bmatrix} 0 & 0 & 0 \\ -s\theta s\psi & -s\theta c\psi & -c\theta \\ T_{22} & -T_{21} & 0 \end{bmatrix} \begin{bmatrix} E_C - E_A \\ N_C - N_A \\ U_C - U_A \end{bmatrix}$$

$$\begin{bmatrix} \frac{\partial Y_C}{\partial E_C} & \frac{\partial Y_C}{\partial N_C} & \frac{\partial Y_C}{\partial U_C} & \frac{\partial Y_C}{\partial E_A} & \frac{\partial Y_C}{\partial N_A} & \frac{\partial Y_C}{\partial U_A} \end{bmatrix} = \begin{bmatrix} T_{21} & T_{22} & T_{23} & -T_{21} & -T_{22} & -T_{23} \end{bmatrix}.$$

(c) $\sigma_{Z_C}^2 = \left[\begin{array}{cccccccccc} \frac{\partial Z_C}{\partial \phi} & \frac{\partial Z_C}{\partial \theta} & \frac{\partial Z_C}{\partial \psi} & \frac{\partial Z_C}{\partial E_C} & \frac{\partial Z_C}{\partial N_C} & \frac{\partial Z_C}{\partial U_C} & \frac{\partial Z_C}{\partial E_A} & \frac{\partial Z_C}{\partial N_A} & \frac{\partial Z_C}{\partial U_A} \end{array}\right]$

$$diag\left(\left[\begin{array}{cccccccccc} \sigma_\phi^2 & \sigma_\theta^2 & \sigma_\psi^2 & \sigma_{E_C}^2 & \sigma_{N_C}^2 & \sigma_{U_C}^2 & \sigma_{E_A}^2 & \sigma_{N_A}^2 & \sigma_{U_A}^2 \end{array}\right]\right)$$

$$\left[\begin{array}{cccccccccc} \frac{\partial Z_C}{\partial \phi} & \frac{\partial Z_C}{\partial \theta} & \frac{\partial Z_C}{\partial \psi} & \frac{\partial Z_C}{\partial E_C} & \frac{\partial Z_C}{\partial N_C} & \frac{\partial Z_C}{\partial U_C} & \frac{\partial Z_C}{\partial E_A} & \frac{\partial Z_C}{\partial N_A} & \frac{\partial Z_C}{\partial U_A} \end{array}\right]^T,$$

where

$$\left[\begin{array}{c} \frac{\partial Z_C}{\partial \phi} \\ \frac{\partial Z_C}{\partial \theta} \\ \frac{\partial Z_C}{\partial \psi} \end{array}\right] = \left[\begin{array}{ccc} \frac{\partial T_{31}}{\partial \phi} & \frac{\partial T_{32}}{\partial \phi} & \frac{\partial T_{33}}{\partial \phi} \\ \frac{\partial T_{31}}{\partial \theta} & \frac{\partial T_{32}}{\partial \theta} & \frac{\partial T_{33}}{\partial \theta} \\ \frac{\partial T_{31}}{\partial \psi} & \frac{\partial T_{32}}{\partial \psi} & \frac{\partial T_{33}}{\partial \psi} \end{array}\right] \left[\begin{array}{c} E_C - E_A \\ N_C - N_A \\ U_C - U_A \end{array}\right] \quad \text{and}$$

$$= \left[\begin{array}{ccc} T_{11} & T_{12} & T_{13} \\ c\phi c\theta s\psi & c\phi c\theta c\psi & -c\phi s\theta \\ T_{32} & -T_{31} & 0 \end{array}\right] \left[\begin{array}{c} E_C - E_A \\ N_C - N_A \\ U_C - U_A \end{array}\right]$$

$$\left[\begin{array}{cccccc} \frac{\partial Z_C}{\partial E_C} & \frac{\partial Z_C}{\partial N_C} & \frac{\partial Z_C}{\partial U_C} & \frac{\partial Z_C}{\partial E_A} & \frac{\partial Z_C}{\partial N_A} & \frac{\partial Z_C}{\partial U_A} \end{array}\right] = \left[\begin{array}{cccccc} T_{31} & T_{32} & T_{33} & -T_{31} & -T_{32} & -T_{33} \end{array}\right].$$

C. Simulation Results

The distributions of heading (h) and elevation (e) are assumed to be normal in Section 2.2.2. By assuming $\sigma_h \sigma_e = \sigma_e \sigma_h = 0$, their multivariate normal probability density in two dimensions is expressed as:

$$p(h,e) = \frac{1}{2\pi\sqrt{\sigma_h^2 \sigma_e^2}} \exp\left[-\frac{1}{2}(h-\mu_h, e-\mu_e)^T \begin{bmatrix} \sigma_h^2 & 0 \\ 0 & \sigma_e^2 \end{bmatrix}^{-1} (h-\mu_h, e-\mu_e) \right]$$

$$= \frac{1}{2\pi\sqrt{\sigma_h^2 \sigma_e^2}} \exp\left[-\frac{1}{2}\left(\frac{(h-\mu_h)^2}{\sigma_h^2} + \frac{(e-\mu_e)^2}{\sigma_e^2} \right) \right] \qquad \text{(C-1)}$$

The shaded region in Figure C-1 represents $p(h,e)$ for $\mu_h - \sigma_h \le h \le \mu_h + \sigma_h$, $\mu_e - \sigma_e \le e \le \mu_e + \sigma_e$, and $\frac{(h-\mu_h)^2}{\sigma_h^2} + \frac{(e-\mu_e)^2}{\sigma_e^2} \le 1$. The circle with bold line shows the magnitude of pointing error $\sqrt{\sigma_h^2 + \sigma_e^2}$ given σ_h and σ_e. The cumulative distribution function (CDF) for (C-1) can be approximated by the following discrete integral:

$$\int_{\mu_e-\sigma_e}^{\mu_e+\sigma_e} \int_{\mu_h-\sigma_h}^{\mu_h+\sigma_h} p(h,e)\, dh\, de \simeq \sum_{\mu_e-\sigma_e}^{\mu_e+\sigma_e} \sum_{\mu_h-\sigma_h}^{\mu_h+\sigma_h} p(h,e)\, \Delta h\, \Delta e, \qquad \text{(C-2)}$$

where $\frac{(h-\mu_h)^2}{\sigma_h^2} + \frac{(e-\mu_e)^2}{\sigma_e^2} \le 1$, and Δh and Δe are step size of h and e, respectively, for the discrete integral.

All points on the circle in Figure C-1 have the same magnitude of pointing error even though they have different values of σ_h and σ_e. The CDF for (C-1) in the

range of $\mu_h - r \le h \le \mu_h + r$, $\mu_e - r \le e \le \mu_e + r$, and $(h-\mu_h)^2 + (e-\mu_e)^2 \le r^2$ where $r = \sqrt{\sigma_h^2 + \sigma_e^2}$ can be approximated by the following:

$$\int_{\mu_e - r}^{\mu_e + r} \int_{\mu_h - r}^{\mu_h + r} p(h,e)\, dh\, de \simeq \sum_{\mu_e - r}^{\mu_e + r} \sum_{\mu_h - r}^{\mu_h + r} p(h,e)\, \Delta h\, \Delta e, \qquad \text{(C-3)}$$

where $(h-\mu_h)^2 + (e-\mu_e)^2 \le r^2$, and Δh and Δe are step size of h and e, respectively, for the discrete integral.

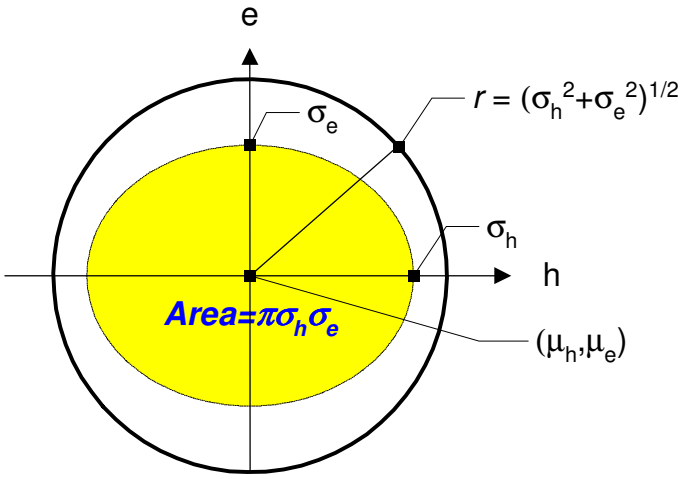

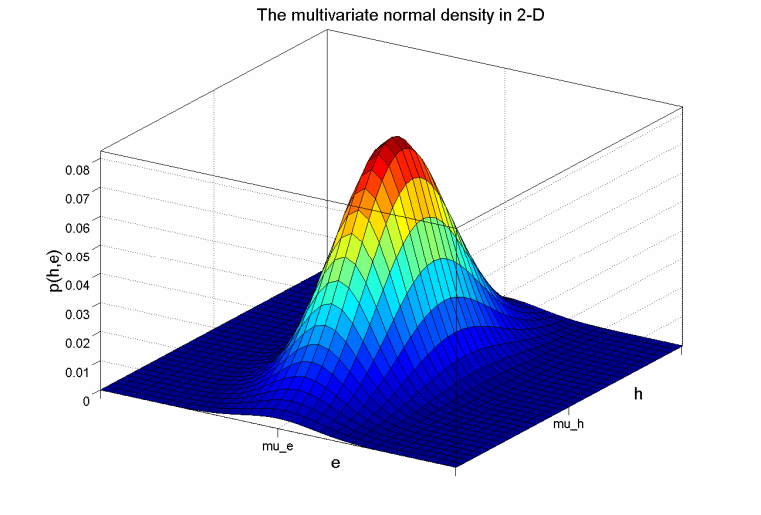

Figure C-1. A plot of 2-dimensional multivariate normal density

For the mean values of σ_h and σ_e in Columns E and F of Tables C-1~C-7, the discrete CDF value of (C-2) was approximately 39 %; the one of (C-3) was in the range of between 63 % and 68 %. Figure C-2 shows the CDF values of (C-2) for each set of (σ_h, σ_e) in Columns E and F of Tables C-1~C-7; Figure C-3 shows the CDF values of (C-3) for each set of (σ_h, σ_e) in Columns E and F of Tables C-1~C-7. Δh and Δe were set by $\Delta h = \sigma_h / 100$ and $\Delta e = \sigma_e / 100$ for the discrete integral in (C-2) and $\Delta h = \Delta e = r / 100$ for the one in (C-3).

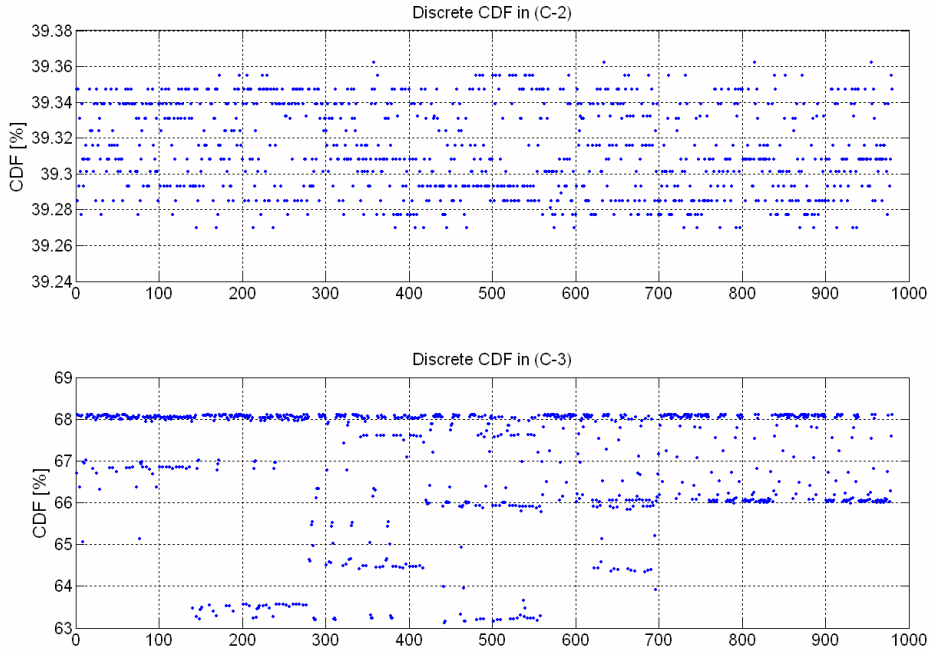

Figure C-2. CDF values for the discrete integral in (C-2) and (C-3)

Table C-1. $\left|\overrightarrow{AB}\right| = 7.5$ m

A	B	C					D	E		F	
Distance A to B (m) = length of pointing vector	Distance A to C (m) = link distance	Measurement Errors					sigma_psi (mrad)	sigma_h		sigma_e	
		RTK			Local Angular Sensor			mean (mrad)	stdev (mrad)	mean (mrad)	stdev (mrad)
		sigma_E (cm)	sigma_N (cm)	sigma_U (cm)	sigma_phi (mrad)	sigma_theta (mrad)					
7.5	39	0.5	0.5	1	0.0873	0.0873	0.9430	0.8282	0.0962	0.3777	0.0100
	264	0.5	0.5	1	0.0873	0.0873	0.9430	0.8075	0.0987	0.1290	0.0316
	1000	0.5	0.5	1	0.0873	0.0873	0.9430	0.8070	0.0988	0.1178	0.0341
	10000	0.5	0.5	1	0.0873	0.0873	0.9430	0.8070	0.0988	0.1170	0.0344
	100000	0.5	0.5	1	0.0873	0.0873	0.9430	0.8070	0.0988	0.1170	0.0344
	39	0.5	0.5	1	0.1745	0.1745	0.9430	0.8287	0.0961	0.4050	0.0089
	264	0.5	0.5	1	0.1745	0.1745	0.9430	0.8080	0.0986	0.1963	0.0203
	1000	0.5	0.5	1	0.1745	0.1745	0.9430	0.8076	0.0987	0.1895	0.0211
	10000	0.5	0.5	1	0.1745	0.1745	0.9430	0.8076	0.0987	0.1890	0.0211
	100000	0.5	0.5	1	0.1745	0.1745	0.9430	0.8076	0.0987	0.1890	0.0211
	39	0.5	0.5	1	0.3491	0.3491	0.9430	0.8309	0.0960	0.4991	0.0081
	264	0.5	0.5	1	0.3491	0.3491	0.9430	0.8102	0.0984	0.3521	0.0101
	1000	0.5	0.5	1	0.3491	0.3491	0.9430	0.8099	0.0985	0.3484	0.0103
	10000	0.5	0.5	1	0.3491	0.3491	0.9430	0.8098	0.0985	0.3482	0.0102
	100000	0.5	0.5	1	0.3491	0.3491	0.9430	0.8098	0.0985	0.3481	0.0102
	39	0.5	0.5	1	17.4533	17.4533	0.9430	3.1638	1.5923	16.8440	0.5236
	264	0.5	0.5	1	17.4533	17.4533	0.9430	3.1563	1.5966	16.8400	0.5236
	1000	0.5	0.5	1	17.4533	17.4533	0.9430	3.1562	1.5966	16.8400	0.5236
	10000	0.5	0.5	1	17.4533	17.4533	0.9430	3.1562	1.5967	16.8400	0.5236
	100000	0.5	0.5	1	17.4533	17.4533	0.9430	3.1562	1.5967	16.8400	0.5236
	39	0.5	0.5	1	34.9066	34.9066	0.9430	6.0685	3.3569	33.6820	1.0476
	264	0.5	0.5	1	34.9066	34.9066	0.9430	6.0636	3.3608	33.6800	1.0477
	1000	0.5	0.5	1	34.9066	34.9066	0.9430	6.0635	3.3608	33.6800	1.0477
	10000	0.5	0.5	1	34.9066	34.9066	0.9430	6.0635	3.3608	33.6800	1.0477
	100000	0.5	0.5	1	34.9066	34.9066	0.9430	6.0635	3.3608	33.6800	1.0477
	39	1	1	2	0.0873	0.0873	1.8860	1.6561	0.1925	0.7412	0.0208
	264	1	1	2	0.0873	0.0873	1.8860	1.6146	0.1975	0.2085	0.0765
	1000	1	1	2	0.0873	0.0873	1.8860	1.6138	0.1976	0.1771	0.0873
	10000	1	1	2	0.0873	0.0873	1.8860	1.6138	0.1976	0.1743	0.0884
	100000	1	1	2	0.0873	0.0873	1.8860	1.6138	0.1976	0.1743	0.0884
	39	1	1	2	0.1745	0.1745	1.8860	1.6564	0.1925	0.7554	0.0201
	264	1	1	2	0.1745	0.1745	1.8860	1.6150	0.1975	0.2583	0.0632
	1000	1	1	2	0.1745	0.1745	1.8860	1.6141	0.1976	0.2358	0.0682
	10000	1	1	2	0.1745	0.1745	1.8860	1.6140	0.1976	0.2341	0.0686
	100000	1	1	2	0.1745	0.1745	1.8860	1.6140	0.1976	0.2340	0.0686
	39	1	1	2	0.3491	0.3491	1.8860	1.6575	0.1924	0.8099	0.0179
	264	1	1	2	0.3491	0.3491	1.8860	1.6161	0.1973	0.3926	0.0408
	1000	1	1	2	0.3491	0.3491	1.8860	1.6152	0.1974	0.3790	0.0423
	10000	1	1	2	0.3491	0.3491	1.8860	1.6152	0.1974	0.3780	0.0424
	100000	1	1	2	0.3491	0.3491	1.8860	1.6152	0.1974	0.3780	0.0424
	39	1	1	2	17.4533	17.4533	1.8860	3.5551	1.4109	16.8560	0.5229
	264	1	1	2	17.4533	17.4533	1.8860	3.5329	1.4195	16.8410	0.5232
	1000	1	1	2	17.4533	17.4533	1.8860	3.5324	1.4196	16.8410	0.5230
	10000	1	1	2	17.4533	17.4533	1.8860	3.5323	1.4196	16.8410	0.5230
	100000	1	1	2	17.4533	17.4533	1.8860	3.5323	1.4196	16.8410	0.5230
	39	1	1	2	34.9066	34.9066	1.8860	6.3276	3.1845	33.6880	1.0473
	264	1	1	2	34.9066	34.9066	1.8860	6.3126	3.1931	33.6810	1.0474
	1000	1	1	2	34.9066	34.9066	1.8860	6.3124	3.1933	33.6800	1.0474
	10000	1	1	2	34.9066	34.9066	1.8860	6.3124	3.1933	33.6800	1.0473
	100000	1	1	2	34.9066	34.9066	1.8860	6.3124	3.1933	33.6800	1.0473
	39	2	2	4	0.0873	0.0873	3.7710	3.3121	0.3850	1.4751	0.0420
	264	2	2	4	0.0873	0.0873	3.7710	3.2292	0.3950	0.3866	0.1633
	1000	2	2	4	0.0873	0.0873	3.7710	3.2274	0.3951	0.3107	0.1950
	10000	2	2	4	0.0873	0.0873	3.7710	3.2273	0.3952	0.3029	0.1994
	100000	2	2	4	0.0873	0.0873	3.7710	3.2273	0.3952	0.3028	0.1994
	39	2	2	4	0.1745	0.1745	3.7710	3.3123	0.3849	1.4824	0.0416
	264	2	2	4	0.1745	0.1745	3.7710	3.2293	0.3950	0.4172	0.1530
	1000	2	2	4	0.1745	0.1745	3.7710	3.2276	0.3951	0.3541	0.1747
	10000	2	2	4	0.1745	0.1745	3.7710	3.2274	0.3952	0.3487	0.1768
	100000	2	2	4	0.1745	0.1745	3.7710	3.2274	0.3952	0.3486	0.1768
	39	2	2	4	0.3491	0.3491	3.7710	3.3127	0.3849	1.5109	0.0402
	264	2	2	4	0.3491	0.3491	3.7710	3.2298	0.3949	0.5164	0.1262
	1000	2	2	4	0.3491	0.3491	3.7710	3.2282	0.3951	0.4717	0.1364
	10000	2	2	4	0.3491	0.3491	3.7710	3.2279	0.3951	0.4681	0.1373
	100000	2	2	4	0.3491	0.3491	3.7710	3.2279	0.3951	0.4681	0.1373
	39	2	2	4	17.4533	17.4533	3.7710	4.6583	1.1261	16.9040	0.5202
	264	2	2	4	17.4533	17.4533	3.7710	4.5973	1.1392	16.8450	0.5207
	1000	2	2	4	17.4533	17.4533	3.7710	4.5961	1.1394	16.8440	0.5206
	10000	2	2	4	17.4533	17.4533	3.7710	4.5960	1.1394	16.8440	0.5206
	100000	2	2	4	17.4533	17.4533	3.7710	4.5960	1.1394	16.8440	0.5206
	39	2	2	4	34.9066	34.9066	3.7710	7.1103	2.8217	33.7120	1.0460
	264	2	2	4	34.9066	34.9066	3.7710	7.0657	2.8389	33.6820	1.0461
	1000	2	2	4	34.9066	34.9066	3.7710	7.0648	2.8392	33.6820	1.0462
	10000	2	2	4	34.9066	34.9066	3.7710	7.0647	2.8392	33.6820	1.0462
	100000	2	2	4	34.9066	34.9066	3.7710	7.0647	2.8392	33.6820	1.0462
	39	50	50	100	0.0873	0.0873	94.2820	82.8010	9.6244	36.8190	1.0528
	264	50	50	100	0.0873	0.0873	94.2820	80.7280	9.8744	9.3901	4.1823
	1000	50	50	100	0.0873	0.0873	94.2820	80.6850	9.8798	7.2738	5.1758
	10000	50	50	100	0.0873	0.0873	94.2820	80.6820	9.8802	6.9419	5.4389
	100000	50	50	100	0.0873	0.0873	94.2820	80.6820	9.8802	6.9312	5.4507
	39	50	50	100	0.1745	0.1745	94.2820	82.8010	9.6244	36.8200	1.0528
	264	50	50	100	0.1745	0.1745	94.2820	80.7280	9.8744	9.3914	4.1818
	1000	50	50	100	0.1745	0.1745	94.2820	80.6850	9.8798	7.2767	5.1739
	10000	50	50	100	0.1745	0.1745	94.2820	80.6820	9.8802	6.9508	5.4294
	100000	50	50	100	0.1745	0.1745	94.2820	80.6820	9.8802	6.9431	5.4375

A	B	C					D	E		F	
Distance A to B (m) = length of pointing vector	Distance A to C (m) = link distance	Measurement Errors					sigma_psi (mrad)	sigma_h		sigma_e	
		RTK			Local Angular Sensor			mean	stdev	mean	stdev
		sigma_E (cm)	sigma_N (cm)	sigma_U (cm)	sigma_phi (mrad)	sigma_theta (mrad)		(mrad)	(mrad)	(mrad)	(mrad)
7.5	39	50	50	100	0.3491	0.3491	94.2820	82.8010	9.6244	36.8210	1.0527
	264	50	50	100	0.3491	0.3491	94.2820	80.7280	9.8744	9.3968	4.1798
	1000	50	50	100	0.3491	0.3491	94.2820	80.6850	9.8798	7.2880	5.1662
	10000	50	50	100	0.3491	0.3491	94.2820	80.6820	9.8802	6.9774	5.4030
	100000	50	50	100	0.3491	0.3491	94.2820	80.6820	9.8802	6.9721	5.4081
	39	50	50	100	17.4533	17.4533	94.2820	82.8740	9.6166	40.4950	0.8936
	264	50	50	100	17.4533	17.4533	94.2820	80.8030	9.8654	19.6310	2.0384
	1000	50	50	100	17.4533	17.4533	94.2820	80.7590	9.8708	18.9500	2.1114
	10000	50	50	100	17.4533	17.4533	94.2820	80.7560	9.8712	18.8980	2.1169
	100000	50	50	100	17.4533	17.4533	94.2820	80.7560	9.8712	18.8980	2.1171
	39	50	50	100	34.9066	34.9066	94.2820	83.0900	9.5961	49.9160	0.8036
	264	50	50	100	34.9066	34.9066	94.2820	81.0260	9.8415	35.2140	1.0152
	1000	50	50	100	34.9066	34.9066	94.2820	80.9820	9.8469	34.8440	1.0251
	10000	50	50	100	34.9066	34.9066	94.2820	80.9790	9.8472	34.8160	1.0259
	100000	50	50	100	34.9066	34.9066	94.2820	80.9790	9.8473	34.8160	1.0259
	39	100	100	200	0.0873	0.0873	188.5700	165.6000	19.2490	73.6390	2.1056
	264	100	100	200	0.0873	0.0873	188.5700	161.4600	19.7490	18.7790	8.3648
	1000	100	100	200	0.0873	0.0873	188.5700	161.3700	19.7600	14.5460	10.3530
	10000	100	100	200	0.0873	0.0873	188.5700	161.3600	19.7600	13.8790	10.8830
	100000	100	100	200	0.0873	0.0873	188.5700	161.3600	19.7600	13.8520	10.9130
	39	100	100	200	0.1745	0.1745	188.5700	165.6000	19.2490	73.6390	2.1056
	264	100	100	200	0.1745	0.1745	188.5700	161.4600	19.7490	18.7800	8.3646
	1000	100	100	200	0.1745	0.1745	188.5700	161.3700	19.7600	14.5480	10.3520
	10000	100	100	200	0.1745	0.1745	188.5700	161.3600	19.7600	13.8840	10.8780
	100000	100	100	200	0.1745	0.1745	188.5700	161.3600	19.7600	13.8620	10.9010
	39	100	100	200	0.3491	0.3491	188.5700	165.6000	19.2490	73.6400	2.1055
	264	100	100	200	0.3491	0.3491	188.5700	161.4600	19.7490	18.7830	8.3636
	1000	100	100	200	0.3491	0.3491	188.5700	161.3700	19.7600	14.5530	10.3480
	10000	100	100	200	0.3491	0.3491	188.5700	161.3600	19.7600	13.9020	10.8590
	100000	100	100	200	0.3491	0.3491	188.5700	161.3600	19.7600	13.8860	10.8750
	39	100	100	200	17.4533	17.4533	188.5700	165.6400	19.2450	75.5440	2.0101
	264	100	100	200	17.4533	17.4533	188.5700	161.4900	19.7440	25.8180	6.3162
	1000	100	100	200	17.4533	17.4533	188.5700	161.4100	19.7550	23.5810	6.8224
	10000	100	100	200	17.4533	17.4533	188.5700	161.4000	19.7560	23.4050	6.8655
	100000	100	100	200	17.4533	17.4533	188.5700	161.4000	19.7560	23.4030	6.8660
	39	100	100	200	34.9066	34.9066	188.5700	165.7500	19.2330	80.9900	1.7873
	264	100	100	200	34.9066	34.9066	188.5700	161.6100	19.7310	39.2610	4.0768
	1000	100	100	200	34.9066	34.9066	188.5700	161.5200	19.7420	37.8990	4.2227
	10000	100	100	200	34.9066	34.9066	188.5700	161.5100	19.7420	37.7960	4.2341
	100000	100	100	200	34.9066	34.9066	188.5700	161.5100	19.7420	37.7950	4.2341
	39	500	500	1000	0.0873	0.0873	942.8200	828.0100	96.2440	368.1900	10.5280
	264	500	500	1000	0.0873	0.0873	942.8200	807.2800	98.7440	93.8960	41.8250
	1000	500	500	1000	0.0873	0.0873	942.8200	806.8500	98.7980	72.7280	51.7650
	10000	500	500	1000	0.0873	0.0873	942.8200	806.8200	98.8020	69.3840	54.4270
	100000	500	500	1000	0.0873	0.0873	942.8200	806.8200	98.8020	69.2290	54.6050
	39	500	500	1000	0.1745	0.1745	942.8200	828.0100	96.2440	368.1900	10.5280
	264	500	500	1000	0.1745	0.1745	942.8200	807.2800	98.7440	93.8960	41.8240
	1000	500	500	1000	0.1745	0.1745	942.8200	806.8500	98.7980	72.7290	51.7640
	10000	500	500	1000	0.1745	0.1745	942.8200	806.8200	98.8020	69.3850	54.4250
	100000	500	500	1000	0.1745	0.1745	942.8200	806.8200	98.8020	69.2350	54.5980
	39	500	500	1000	0.3491	0.3491	942.8200	828.0100	96.2440	368.1900	10.5280
	264	500	500	1000	0.3491	0.3491	942.8200	807.2800	98.7440	93.8960	41.8240
	1000	500	500	1000	0.3491	0.3491	942.8200	806.8500	98.7980	72.7300	51.7640
	10000	500	500	1000	0.3491	0.3491	942.8200	806.8200	98.8020	69.3900	54.4200
	100000	500	500	1000	0.3491	0.3491	942.8200	806.8200	98.8020	69.2520	54.5780
	39	500	500	1000	17.4533	17.4533	942.8200	828.0200	96.2430	368.5800	10.5080
	264	500	500	1000	17.4533	17.4533	942.8200	807.2900	98.7430	95.6820	41.1640
	1000	500	500	1000	17.4533	17.4533	942.8200	806.8600	98.7970	76.0560	49.6820
	10000	500	500	1000	17.4533	17.4533	942.8200	806.8200	98.8010	73.9230	50.9480
	100000	500	500	1000	17.4533	17.4533	942.8200	806.8200	98.8010	73.9000	50.9620
	39	500	500	1000	34.9066	34.9066	942.8200	828.0400	96.2410	369.7400	10.4480
	264	500	500	1000	34.9066	34.9066	942.8200	807.3100	98.7400	100.7400	39.3990
	1000	500	500	1000	34.9066	34.9066	942.8200	806.8800	98.7940	83.7380	45.7430
	10000	500	500	1000	34.9066	34.9066	942.8200	806.8500	98.7980	82.1860	46.4470
	100000	500	500	1000	34.9066	34.9066	942.8200	806.8500	98.7980	82.1700	46.4540
	39	1000	1000	2000	0.0873	0.0873	1885.6000	1656.0000	192.4900	736.3900	21.0560
	264	1000	1000	2000	0.0873	0.0873	1885.6000	1614.6000	197.4900	187.7900	83.6490
	1000	1000	1000	2000	0.0873	0.0873	1885.6000	1613.7000	197.6000	145.4600	103.5300
	10000	1000	1000	2000	0.0873	0.0873	1885.6000	1613.6000	197.6000	138.7700	108.8500
	100000	1000	1000	2000	0.0873	0.0873	1885.6000	1613.6000	197.6000	138.4600	109.2200
	39	1000	1000	2000	0.1745	0.1745	1885.6000	1656.0000	192.4900	736.3900	21.0560
	264	1000	1000	2000	0.1745	0.1745	1885.6000	1614.6000	197.4900	187.7900	83.6490
	1000	1000	1000	2000	0.1745	0.1745	1885.6000	1613.7000	197.6000	145.4600	103.5300
	10000	1000	1000	2000	0.1745	0.1745	1885.6000	1613.6000	197.6000	138.7700	108.8500
	100000	1000	1000	2000	0.1745	0.1745	1885.6000	1613.6000	197.6000	138.4600	109.2100
	39	1000	1000	2000	0.3491	0.3491	1885.6000	1656.0000	192.4900	736.3900	21.0560
	264	1000	1000	2000	0.3491	0.3491	1885.6000	1614.6000	197.4900	187.7900	83.6490
	1000	1000	1000	2000	0.3491	0.3491	1885.6000	1613.7000	197.6000	145.4600	103.5300
	10000	1000	1000	2000	0.3491	0.3491	1885.6000	1613.6000	197.6000	138.7700	108.8500
	100000	1000	1000	2000	0.3491	0.3491	1885.6000	1613.6000	197.6000	138.4700	109.2000
	39	1000	1000	2000	17.4533	17.4533	1885.6000	1656.0000	192.4900	736.5800	21.0460
	264	1000	1000	2000	17.4533	17.4533	1885.6000	1614.6000	197.4900	188.7000	83.3110
	1000	1000	1000	2000	17.4533	17.4533	1885.6000	1613.7000	197.6000	147.2800	102.3200
	10000	1000	1000	2000	17.4533	17.4533	1885.6000	1613.6000	197.6000	141.9500	106.0100
	100000	1000	1000	2000	17.4533	17.4533	1885.6000	1613.6000	197.6000	141.8900	106.0600
	39	1000	1000	2000	34.9066	34.9066	1885.6000	1656.0000	192.4900	737.1600	21.0160
	264	1000	1000	2000	34.9066	34.9066	1885.6000	1614.6000	197.4900	191.3600	82.3280
	1000	1000	1000	2000	34.9066	34.9066	1885.6000	1613.7000	197.5900	152.1100	99.3640
	10000	1000	1000	2000	34.9066	34.9066	1885.6000	1613.6000	197.6000	147.8500	101.9000
	100000	1000	1000	2000	34.9066	34.9066	1885.6000	1613.6000	197.6000	147.8000	101.9200

Table C-2. $\left|\overrightarrow{AB}\right| = 15$ m

A	B	C					D	E		F	
Distance A to B (m) = length of pointing vector	Distance A to C (m) = link distance	Measurement Errors					sigma_psi (mrad)	sigma_h		sigma_e	
		RTK			Local Angular Sensor			mean	stdev	mean	stdev
		sigma_E (cm)	sigma_N (cm)	sigma_U (cm)	sigma_phi (mrad)	sigma_theta (mrad)		(mrad)	(mrad)	(mrad)	(mrad)
15	39	0.5	0.5	1	0.0873	0.0873	0.4710	0.4445	0.0449	0.3701	0.0036
	264	0.5	0.5	1	0.0873	0.0873	0.4710	0.4047	0.0492	0.1083	0.0092
	1000	0.5	0.5	1	0.0873	0.0873	0.4710	0.4038	0.0494	0.0955	0.0106
	10000	0.5	0.5	1	0.0873	0.0873	0.4710	0.4038	0.0493	0.0944	0.0106
	100000	0.5	0.5	1	0.0873	0.0873	0.4710	0.4038	0.0493	0.0944	0.0106
	39	0.5	0.5	1	0.1745	0.1745	0.4710	0.4455	0.0448	0.3977	0.0046
	264	0.5	0.5	1	0.1745	0.1745	0.4710	0.4058	0.0492	0.1820	0.0049
	1000	0.5	0.5	1	0.1745	0.1745	0.4710	0.4049	0.0493	0.1746	0.0051
	10000	0.5	0.5	1	0.1745	0.1745	0.4710	0.4049	0.0493	0.1741	0.0052
	100000	0.5	0.5	1	0.1745	0.1745	0.4710	0.4049	0.0493	0.1741	0.0052
	39	0.5	0.5	1	0.3491	0.3491	0.4710	0.4495	0.0447	0.4932	0.0087
	264	0.5	0.5	1	0.3491	0.3491	0.4710	0.4102	0.0489	0.3438	0.0083
	1000	0.5	0.5	1	0.3491	0.3491	0.4710	0.4093	0.0490	0.3400	0.0083
	10000	0.5	0.5	1	0.3491	0.3491	0.4710	0.4093	0.0490	0.3397	0.0084
	100000	0.5	0.5	1	0.3491	0.3491	0.4710	0.4093	0.0490	0.3397	0.0084
	39	0.5	0.5	1	17.4533	17.4533	0.4710	3.0416	1.6728	16.8440	0.5238
	264	0.5	0.5	1	17.4533	17.4533	0.4710	3.0320	1.6803	16.8400	0.5238
	1000	0.5	0.5	1	17.4533	17.4533	0.4710	3.0317	1.6805	16.8400	0.5238
	10000	0.5	0.5	1	17.4533	17.4533	0.4710	3.0317	1.6805	16.8400	0.5238
	100000	0.5	0.5	1	17.4533	17.4533	0.4710	3.0317	1.6805	16.8400	0.5238
	39	0.5	0.5	1	34.9066	34.9066	0.4710	5.9871	3.4285	33.6820	1.0476
	264	0.5	0.5	1	34.9066	34.9066	0.4710	5.9805	3.4352	33.6800	1.0477
	1000	0.5	0.5	1	34.9066	34.9066	0.4710	5.9803	3.4353	33.6800	1.0477
	10000	0.5	0.5	1	34.9066	34.9066	0.4710	5.9803	3.4353	33.6800	1.0477
	100000	0.5	0.5	1	34.9066	34.9066	0.4710	5.9803	3.4353	33.6800	1.0477
	39	1	1	2	0.0873	0.0873	0.9430	0.8886	0.0896	0.7255	0.0066
	264	1	1	2	0.0873	0.0873	0.9430	0.8089	0.0986	0.1591	0.0262
	1000	1	1	2	0.0873	0.0873	0.9430	0.8071	0.0988	0.1206	0.0335
	10000	1	1	2	0.0873	0.0873	0.9430	0.8070	0.0988	0.1171	0.0344
	100000	1	1	2	0.0873	0.0873	0.9430	0.8070	0.0988	0.1170	0.0344
	39	1	1	2	0.1745	0.1745	0.9430	0.8891	0.0896	0.7401	0.0071
	264	1	1	2	0.1745	0.1745	0.9430	0.8094	0.0985	0.2168	0.0184
	1000	1	1	2	0.1745	0.1745	0.9430	0.8077	0.0987	0.1911	0.0209
	10000	1	1	2	0.1745	0.1745	0.9430	0.8076	0.0987	0.1891	0.0211
	100000	1	1	2	0.1745	0.1745	0.9430	0.8076	0.0987	0.1890	0.0211
	39	1	1	2	0.3491	0.3491	0.9430	0.8911	0.0895	0.7955	0.0093
	264	1	1	2	0.3491	0.3491	0.9430	0.8117	0.0982	0.3639	0.0099
	1000	1	1	2	0.3491	0.3491	0.9430	0.8099	0.0985	0.3492	0.0102
	10000	1	1	2	0.3491	0.3491	0.9430	0.8098	0.0985	0.3482	0.0102
	100000	1	1	2	0.3491	0.3491	0.9430	0.8098	0.0985	0.3481	0.0102
	39	1	1	2	17.4533	17.4533	0.9430	3.1863	1.5797	16.8550	0.5235
	264	1	1	2	17.4533	17.4533	0.9430	3.1568	1.5963	16.8410	0.5238
	1000	1	1	2	17.4533	17.4533	0.9430	3.1562	1.5966	16.8400	0.5236
	10000	1	1	2	17.4533	17.4533	0.9430	3.1562	1.5967	16.8400	0.5236
	100000	1	1	2	17.4533	17.4533	0.9430	3.1562	1.5967	16.8400	0.5236
	39	1	1	2	34.9066	34.9066	0.9430	6.0831	3.3457	33.6880	1.0476
	264	1	1	2	34.9066	34.9066	0.9430	6.0639	3.3605	33.6800	1.0477
	1000	1	1	2	34.9066	34.9066	0.9430	6.0635	3.3608	33.6800	1.0477
	10000	1	1	2	34.9066	34.9066	0.9430	6.0635	3.3608	33.6800	1.0477
	100000	1	1	2	34.9066	34.9066	0.9430	6.0635	3.3608	33.6800	1.0477
	39	2	2	4	0.0873	0.0873	1.8860	1.7770	0.1793	1.4438	0.0129
	264	2	2	4	0.0873	0.0873	1.8860	1.6175	0.1971	0.2816	0.0593
	1000	2	2	4	0.0873	0.0873	1.8860	1.6140	0.1976	0.1849	0.0843
	10000	2	2	4	0.0873	0.0873	1.8860	1.6138	0.1976	0.1743	0.0884
	100000	2	2	4	0.0873	0.0873	1.8860	1.6138	0.1976	0.1743	0.0884
	39	2	2	4	0.1745	0.1745	1.8860	1.7772	0.1794	1.4511	0.0132
	264	2	2	4	0.1745	0.1745	1.8860	1.6178	0.1971	0.3184	0.0524
	1000	2	2	4	0.1745	0.1745	1.8860	1.6143	0.1975	0.2409	0.0670
	10000	2	2	4	0.1745	0.1745	1.8860	1.6140	0.1976	0.2341	0.0686
	100000	2	2	4	0.1745	0.1745	1.8860	1.6140	0.1976	0.2340	0.0686
	39	2	2	4	0.3491	0.3491	1.8860	1.7782	0.1793	1.4802	0.0142
	264	2	2	4	0.3491	0.3491	1.8860	1.6189	0.1969	0.4335	0.0368
	1000	2	2	4	0.3491	0.3491	1.8860	1.6154	0.1974	0.3821	0.0419
	10000	2	2	4	0.3491	0.3491	1.8860	1.6152	0.1974	0.3780	0.0424
	100000	2	2	4	0.3491	0.3491	1.8860	1.6152	0.1974	0.3780	0.0424
	39	2	2	4	17.4533	17.4533	1.8860	3.6219	1.3860	16.9020	0.5226
	264	2	2	4	17.4533	17.4533	1.8860	3.5344	1.4188	16.8420	0.5231
	1000	2	2	4	17.4533	17.4533	1.8860	3.5325	1.4196	16.8410	0.5230
	10000	2	2	4	17.4533	17.4533	1.8860	3.5323	1.4196	16.8410	0.5230
	100000	2	2	4	17.4533	17.4533	1.8860	3.5323	1.4196	16.8410	0.5230
	39	2	2	4	34.9066	34.9066	1.8860	6.3725	3.1593	33.7110	1.0471
	264	2	2	4	34.9066	34.9066	1.8860	6.3137	3.1925	33.6810	1.0473
	1000	2	2	4	34.9066	34.9066	1.8860	6.3125	3.1932	33.6800	1.0474
	10000	2	2	4	34.9066	34.9066	1.8860	6.3124	3.1933	33.6800	1.0473
	100000	2	2	4	34.9066	34.9066	1.8860	6.3124	3.1933	33.6800	1.0473
	39	50	50	100	0.0873	0.0873	47.1410	44.4210	4.4837	36.0330	0.3221
	264	50	50	100	0.0873	0.0873	47.1410	40.4350	4.9285	6.7037	1.5545
	1000	50	50	100	0.0873	0.0873	47.1410	40.3470	4.9392	3.9486	2.4077
	10000	50	50	100	0.0873	0.0873	47.1410	40.3410	4.9401	3.4847	2.7055
	100000	50	50	100	0.0873	0.0873	47.1410	40.3410	4.9401	3.4716	2.7187
	39	50	50	100	0.1745	0.1745	47.1410	44.4210	4.4837	36.0330	0.3221
	264	50	50	100	0.1745	0.1745	47.1410	40.4350	4.9285	6.7054	1.5541
	1000	50	50	100	0.1745	0.1745	47.1410	40.3470	4.9392	3.9526	2.4056
	10000	50	50	100	0.1745	0.1745	47.1410	40.3410	4.9401	3.4960	2.6948
	100000	50	50	100	0.1745	0.1745	47.1410	40.3410	4.9401	3.4861	2.7039

A	B	C					D	E		F	
Distance A to B (m) = length of pointing vector	Distance A to C (m) = link distance	Measurement Errors					sigma_psi (mrad)	sigma_h		sigma_e	
		RTK			Local Angular Sensor			mean (mrad)	stdev (mrad)	mean (mrad)	stdev (mrad)
		sigma_E (cm)	sigma_N (cm)	sigma_U (cm)	sigma_phi (mrad)	sigma_theta (mrad)					
15	39	50	50	100	0.3491	0.3491	47.1410	44.4210	4.4837	36.0340	0.3222
	264	50	50	100	0.3491	0.3491	47.1410	40.4350	4.9285	6.7120	1.5527
	1000	50	50	100	0.3491	0.3491	47.1410	40.3470	4.9392	3.9684	2.3974
	10000	50	50	100	0.3491	0.3491	47.1410	40.3410	4.9401	3.5314	2.6643
	100000	50	50	100	0.3491	0.3491	47.1410	40.3410	4.9401	3.5242	2.6701
	39	50	50	100	17.4533	17.4533	47.1410	44.5550	4.4753	39.7760	0.4654
	264	50	50	100	17.4533	17.4533	47.1410	40.5830	4.9123	18.1920	0.4930
	1000	50	50	100	17.4533	17.4533	47.1410	40.4960	4.9229	17.4640	0.5115
	10000	50	50	100	17.4533	17.4533	47.1410	40.4900	4.9236	17.4080	0.5129
	100000	50	50	100	17.4533	17.4533	47.1410	40.4890	4.9236	17.4080	0.5130
	39	50	50	100	34.9066	34.9066	47.1410	44.9530	4.4701	49.3270	0.8827
	264	50	50	100	34.9066	34.9066	47.1410	41.0210	4.8866	34.3810	0.8388
	1000	50	50	100	34.9066	34.9066	47.1410	40.9360	4.8966	34.0020	0.8394
	10000	50	50	100	34.9066	34.9066	47.1410	40.9290	4.8974	33.9730	0.8394
	100000	50	50	100	34.9066	34.9066	47.1410	40.9290	4.8974	33.9730	0.8395
	39	100	100	200	0.0873	0.0873	94.2820	88.8410	8.9673	72.0660	0.6441
	264	100	100	200	0.0873	0.0873	94.2820	80.8690	9.8569	13.4070	3.1093
	1000	100	100	200	0.0873	0.0873	94.2820	80.6950	9.8786	7.8953	4.8164
	10000	100	100	200	0.0873	0.0873	94.2820	80.6820	9.8802	6.9629	5.4173
	100000	100	100	200	0.0873	0.0873	94.2820	80.6820	9.8802	6.9317	5.4501
	39	100	100	200	0.1745	0.1745	94.2820	88.8410	8.9673	72.0660	0.6441
	264	100	100	200	0.1745	0.1745	94.2820	80.8690	9.8569	13.4070	3.1090
	1000	100	100	200	0.1745	0.1745	94.2820	80.6950	9.8786	7.8973	4.8154
	10000	100	100	200	0.1745	0.1745	94.2820	80.6820	9.8802	6.9694	5.4109
	100000	100	100	200	0.1745	0.1745	94.2820	80.6820	9.8802	6.9434	5.4372
	39	100	100	200	0.3491	0.3491	94.2820	88.8410	8.9673	72.0670	0.6442
	264	100	100	200	0.3491	0.3491	94.2820	80.8690	9.8569	13.4110	3.1082
	1000	100	100	200	0.3491	0.3491	94.2820	80.6950	9.8786	7.9052	4.8112
	10000	100	100	200	0.3491	0.3491	94.2820	80.6820	9.8802	6.9920	5.3896
	100000	100	100	200	0.3491	0.3491	94.2820	80.6820	9.8802	6.9723	5.4079
	39	100	100	200	17.4533	17.4533	94.2820	88.9090	8.9625	74.0080	0.7092
	264	100	100	200	17.4533	17.4533	94.2820	80.9430	9.8481	21.6760	1.8422
	1000	100	100	200	17.4533	17.4533	94.2820	80.7690	9.8696	19.1050	2.0943
	10000	100	100	200	17.4533	17.4533	94.2820	80.7560	9.8712	18.9000	2.1169
	100000	100	100	200	17.4533	17.4533	94.2820	80.7560	9.8712	18.8980	2.1171
	39	100	100	200	34.9066	34.9066	94.2820	89.1090	8.9506	79.5510	0.9308
	264	100	100	200	34.9066	34.9066	94.2820	81.1650	9.8245	36.3850	0.9859
	1000	100	100	200	34.9066	34.9066	94.2820	80.9920	9.8457	34.9270	1.0229
	10000	100	100	200	34.9066	34.9066	94.2820	80.9790	9.8472	34.8170	1.0259
	100000	100	100	200	34.9066	34.9066	94.2820	80.9790	9.8472	34.8160	1.0259
	39	500	500	1000	0.0873	0.0873	471.4100	444.2100	44.8370	360.3300	3.2205
	264	500	500	1000	0.0873	0.0873	471.4100	404.3400	49.2850	67.0310	15.5460
	1000	500	500	1000	0.0873	0.0873	471.4100	403.4700	49.3930	39.4730	24.0840
	10000	500	500	1000	0.0873	0.0873	471.4100	403.4100	49.4010	34.8040	27.0970
	100000	500	500	1000	0.0873	0.0873	471.4100	403.4100	49.4010	34.6240	27.2920
	39	500	500	1000	0.1745	0.1745	471.4100	444.2100	44.8370	360.3300	3.2205
	264	500	500	1000	0.1745	0.1745	471.4100	404.3400	49.2850	67.0320	15.5460
	1000	500	500	1000	0.1745	0.1745	471.4100	403.4700	49.3930	39.4740	24.0830
	10000	500	500	1000	0.1745	0.1745	471.4100	403.4100	49.4010	34.8050	27.0960
	100000	500	500	1000	0.1745	0.1745	471.4100	403.4100	49.4010	34.6300	27.2840
	39	500	500	1000	0.3491	0.3491	471.4100	444.2100	44.8370	360.3300	3.2205
	264	500	500	1000	0.3491	0.3491	471.4100	404.3400	49.2850	67.0320	15.5460
	1000	500	500	1000	0.3491	0.3491	471.4100	403.4700	49.3930	39.4750	24.0830
	10000	500	500	1000	0.3491	0.3491	471.4100	403.4100	49.4010	34.8110	27.0900
	100000	500	500	1000	0.3491	0.3491	471.4100	403.4100	49.4010	34.6480	27.2630
	39	500	500	1000	17.4533	17.4533	471.4100	444.2200	44.8360	360.7200	3.2327
	264	500	500	1000	17.4533	17.4533	471.4100	404.3600	49.2830	69.2210	15.0720
	1000	500	500	1000	17.4533	17.4533	471.4100	403.4900	49.3910	44.0470	21.9510
	10000	500	500	1000	17.4533	17.4533	471.4100	403.4200	49.3990	41.1170	23.2120
	100000	500	500	1000	17.4533	17.4533	471.4100	403.4200	49.3990	41.0850	23.2270
	39	500	500	1000	34.9066	34.9066	471.4100	444.2600	44.8330	361.9000	3.2697
	264	500	500	1000	34.9066	34.9066	471.4100	404.4000	49.2780	75.3550	13.8540
	1000	500	500	1000	34.9066	34.9066	471.4100	403.5300	49.3850	54.1730	18.4090
	10000	500	500	1000	34.9066	34.9066	471.4100	403.4700	49.3940	52.1570	18.9890
	100000	500	500	1000	34.9066	34.9066	471.4100	403.4700	49.3940	52.1370	18.9950
	39	1000	1000	2000	0.0873	0.0873	942.8200	888.4100	89.6730	720.6600	6.4411
	264	1000	1000	2000	0.0873	0.0873	942.8200	808.6900	98.5700	134.0600	31.0930
	1000	1000	1000	2000	0.0873	0.0873	942.8200	806.9500	98.7860	78.9460	48.1670
	10000	1000	1000	2000	0.0873	0.0873	942.8200	806.8200	98.8020	69.6070	54.1950
	100000	1000	1000	2000	0.0873	0.0873	942.8200	806.8200	98.8020	69.2430	54.5880
	39	1000	1000	2000	0.1745	0.1745	942.8200	888.4100	89.6730	720.6600	6.4411
	264	1000	1000	2000	0.1745	0.1745	942.8200	808.6900	98.5700	134.0600	31.0930
	1000	1000	1000	2000	0.1745	0.1745	942.8200	806.9500	98.7860	78.9460	48.1670
	10000	1000	1000	2000	0.1745	0.1745	942.8200	806.8200	98.8020	69.6070	54.1950
	100000	1000	1000	2000	0.1745	0.1745	942.8200	806.8200	98.8020	69.2470	54.5840
	39	1000	1000	2000	0.3491	0.3491	942.8200	888.4100	89.6730	720.6600	6.4410
	264	1000	1000	2000	0.3491	0.3491	942.8200	808.6900	98.5700	134.0600	31.0930
	1000	1000	1000	2000	0.3491	0.3491	942.8200	806.9500	98.7860	78.9470	48.1670
	10000	1000	1000	2000	0.3491	0.3491	942.8200	806.8200	98.8020	69.6100	54.1920
	100000	1000	1000	2000	0.3491	0.3491	942.8200	806.8200	98.8020	69.2600	54.5680
	39	1000	1000	2000	17.4533	17.4533	942.8200	888.4200	89.6730	720.8500	6.4471
	264	1000	1000	2000	17.4533	17.4533	942.8200	808.7000	98.5690	135.1700	30.8480
	1000	1000	1000	2000	17.4533	17.4533	942.8200	806.9500	98.7850	81.4750	46.8860
	10000	1000	1000	2000	17.4533	17.4533	942.8200	806.8200	98.8010	73.9920	50.9050
	100000	1000	1000	2000	17.4533	17.4533	942.8200	806.8200	98.8010	73.9010	50.9620
	39	1000	1000	2000	34.9066	34.9066	942.8200	888.4400	89.6710	721.4400	6.4654
	264	1000	1000	2000	34.9066	34.9066	942.8200	808.7200	98.5660	138.4400	30.1440
	1000	1000	1000	2000	34.9066	34.9066	942.8200	806.9800	98.7820	88.0940	43.9020
	10000	1000	1000	2000	34.9066	34.9066	942.8200	806.8500	98.7980	82.2340	46.4250
	100000	1000	1000	2000	34.9066	34.9066	942.8200	806.8500	98.7980	82.1700	46.4540

Table C-3. $\left|\overrightarrow{AB}\right| = 40$ m

A	B	C					D	E		F	
Distance A to B (m) = length of pointing vector	Distance A to C (m) = link distance	Measurement Errors					sigma_psi (mrad)	sigma_h		sigma_e	
		RTK			Local Angular Sensor			mean	stdev	mean	stdev
		sigma_E (cm)	sigma_N (cm)	sigma_U (cm)	sigma_phi (mrad)	sigma_theta (mrad)		(mrad)	(mrad)	(mrad)	(mrad)
40	39	0.5	0.5	1	0.0873	0.0873	0.1770	0.2399	0.0120	0.3677	0.0045
	264	0.5	0.5	1	0.0873	0.0873	0.1770	0.1548	0.0182	0.1007	0.0018
	1000	0.5	0.5	1	0.0873	0.0873	0.1770	0.1525	0.0185	0.0868	0.0019
	10000	0.5	0.5	1	0.0873	0.0873	0.1770	0.1523	0.0185	0.0858	0.0019
	100000	0.5	0.5	1	0.0873	0.0873	0.1770	0.1523	0.0185	0.0857	0.0019
	39	0.5	0.5	1	0.1745	0.1745	0.1770	0.2417	0.0124	0.3957	0.0059
	264	0.5	0.5	1	0.1745	0.1745	0.1770	0.1576	0.0182	0.1773	0.0046
	1000	0.5	0.5	1	0.1745	0.1745	0.1770	0.1554	0.0184	0.1698	0.0046
	10000	0.5	0.5	1	0.1745	0.1745	0.1770	0.1552	0.0184	0.1693	0.0047
	100000	0.5	0.5	1	0.1745	0.1745	0.1770	0.1552	0.0184	0.1693	0.0047
	39	0.5	0.5	1	0.3491	0.3491	0.1770	0.2488	0.0155	0.4914	0.0101
	264	0.5	0.5	1	0.3491	0.3491	0.1770	0.1682	0.0209	0.3413	0.0101
	1000	0.5	0.5	1	0.3491	0.3491	0.1770	0.1661	0.0212	0.3375	0.0100
	10000	0.5	0.5	1	0.3491	0.3491	0.1770	0.1659	0.0212	0.3372	0.0102
	100000	0.5	0.5	1	0.3491	0.3491	0.1770	0.1659	0.0212	0.3372	0.0102
	39	0.5	0.5	1	17.4533	17.4533	0.1770	2.9963	1.7116	16.8440	0.5238
	264	0.5	0.5	1	17.4533	17.4533	0.1770	2.9825	1.7259	16.8400	0.5238
	1000	0.5	0.5	1	17.4533	17.4533	0.1770	2.9822	1.7263	16.8400	0.5238
	10000	0.5	0.5	1	17.4533	17.4533	0.1770	2.9821	1.7263	16.8400	0.5238
	100000	0.5	0.5	1	17.4533	17.4533	0.1770	2.9821	1.7263	16.8400	0.5238
	39	0.5	0.5	1	34.9066	34.9066	0.1770	5.9548	3.4638	33.6820	1.0476
	264	0.5	0.5	1	34.9066	34.9066	0.1770	5.9442	3.4773	33.6800	1.0477
	1000	0.5	0.5	1	34.9066	34.9066	0.1770	5.9439	3.4776	33.6800	1.0477
	10000	0.5	0.5	1	34.9066	34.9066	0.1770	5.9438	3.4777	33.6800	1.0477
	100000	0.5	0.5	1	34.9066	34.9066	0.1770	5.9438	3.4777	33.6800	1.0477
	39	1	1	2	0.0873	0.0873	0.3540	0.4788	0.0239	0.7208	0.0083
	264	1	1	2	0.0873	0.0873	0.3540	0.3080	0.0364	0.1391	0.0037
	1000	1	1	2	0.0873	0.0873	0.3540	0.3034	0.0369	0.0946	0.0056
	10000	1	1	2	0.0873	0.0873	0.3540	0.3031	0.0370	0.0903	0.0060
	100000	1	1	2	0.0873	0.0873	0.3540	0.3031	0.0370	0.0903	0.0060
	39	1	1	2	0.1745	0.1745	0.3540	0.4797	0.0240	0.7356	0.0091
	264	1	1	2	0.1745	0.1745	0.3540	0.3095	0.0363	0.2016	0.0038
	1000	1	1	2	0.1745	0.1745	0.3540	0.3049	0.0368	0.1739	0.0039
	10000	1	1	2	0.1745	0.1745	0.3540	0.3045	0.0369	0.1717	0.0039
	100000	1	1	2	0.1745	0.1745	0.3540	0.3045	0.0369	0.1717	0.0039
	39	1	1	2	0.3491	0.3491	0.3540	0.4833	0.0248	0.7912	0.0117
	264	1	1	2	0.3491	0.3491	0.3540	0.3151	0.0362	0.3546	0.0091
	1000	1	1	2	0.3491	0.3491	0.3540	0.3107	0.0367	0.3396	0.0091
	10000	1	1	2	0.3491	0.3491	0.3540	0.3104	0.0368	0.3385	0.0092
	100000	1	1	2	0.3491	0.3491	0.3540	0.3104	0.0368	0.3385	0.0092
	39	1	1	2	17.4533	17.4533	0.3540	3.0496	1.6671	16.8550	0.5238
	264	1	1	2	17.4533	17.4533	0.3540	3.0100	1.6986	16.8400	0.5239
	1000	1	1	2	17.4533	17.4533	0.3540	3.0091	1.6995	16.8400	0.5238
	10000	1	1	2	17.4533	17.4533	0.3540	3.0091	1.6995	16.8400	0.5238
	100000	1	1	2	17.4533	17.4533	0.3540	3.0091	1.6995	16.8400	0.5238
	39	1	1	2	34.9066	34.9066	0.3540	5.9926	3.4232	33.6880	1.0477
	264	1	1	2	34.9066	34.9066	0.3540	5.9650	3.4519	33.6800	1.0478
	1000	1	1	2	34.9066	34.9066	0.3540	5.9643	3.4526	33.6800	1.0477
	10000	1	1	2	34.9066	34.9066	0.3540	5.9643	3.4526	33.6800	1.0477
	100000	1	1	2	34.9066	34.9066	0.3540	5.9643	3.4526	33.6800	1.0477
	39	2	2	4	0.0873	0.0873	0.7070	0.9572	0.0478	1.4344	0.0163
	264	2	2	4	0.0873	0.0873	0.7070	0.6153	0.0729	0.2367	0.0093
	1000	2	2	4	0.0873	0.0873	0.7070	0.6061	0.0740	0.1192	0.0194
	10000	2	2	4	0.0873	0.0873	0.7070	0.6054	0.0741	0.1050	0.0218
	100000	2	2	4	0.0873	0.0873	0.7070	0.6054	0.0741	0.1048	0.0218
	39	2	2	4	0.1745	0.1745	0.7070	0.9575	0.0478	1.4419	0.0167
	264	2	2	4	0.1745	0.1745	0.7070	0.6160	0.0727	0.2781	0.0072
	1000	2	2	4	0.1745	0.1745	0.7070	0.6068	0.0739	0.1890	0.0113
	10000	2	2	4	0.1745	0.1745	0.7070	0.6061	0.0740	0.1807	0.0118
	100000	2	2	4	0.1745	0.1745	0.7070	0.6061	0.0740	0.1806	0.0118
	39	2	2	4	0.3491	0.3491	0.7070	0.9595	0.0481	1.4711	0.0182
	264	2	2	4	0.3491	0.3491	0.7070	0.6189	0.0726	0.4031	0.0074
	1000	2	2	4	0.3491	0.3491	0.7070	0.6097	0.0736	0.3479	0.0077
	10000	2	2	4	0.3491	0.3491	0.7070	0.6091	0.0737	0.3434	0.0077
	100000	2	2	4	0.3491	0.3491	0.7070	0.6091	0.0737	0.3433	0.0077
	39	2	2	4	17.4533	17.4533	0.7070	3.2114	1.5669	16.9010	0.5233
	264	2	2	4	17.4533	17.4533	0.7070	3.0905	1.6378	16.8410	0.5237
	1000	2	2	4	17.4533	17.4533	0.7070	3.0877	1.6396	16.8400	0.5237
	10000	2	2	4	17.4533	17.4533	0.7070	3.0876	1.6398	16.8400	0.5237
	100000	2	2	4	17.4533	17.4533	0.7070	3.0876	1.6398	16.8400	0.5237
	39	2	2	4	34.9066	34.9066	0.7070	6.0993	3.3342	33.7100	1.0474
	264	2	2	4	34.9066	34.9066	0.7070	6.0201	3.3973	33.6810	1.0477
	1000	2	2	4	34.9066	34.9066	0.7070	6.0183	3.3989	33.6800	1.0477
	10000	2	2	4	34.9066	34.9066	0.7070	6.0182	3.3991	33.6800	1.0477
	100000	2	2	4	34.9066	34.9066	0.7070	6.0182	3.3991	33.6800	1.0477
	39	50	50	100	0.0873	0.0873	17.6780	23.9240	1.1928	35.7990	0.4052
	264	50	50	100	0.0873	0.0873	17.6780	15.3760	1.8222	5.5304	0.2609
	1000	50	50	100	0.0873	0.0873	17.6780	15.1450	1.8504	2.0509	0.6926
	10000	50	50	100	0.0873	0.0873	17.6780	15.1280	1.8525	1.3313	0.9937
	100000	50	50	100	0.0873	0.0873	17.6780	15.1280	1.8525	1.3118	1.0098
	39	50	50	100	0.1745	0.1745	17.6780	23.9240	1.1928	35.8000	0.4052
	264	50	50	100	0.1745	0.1745	17.6780	15.3760	1.8222	5.5323	0.2608
	1000	50	50	100	0.1745	0.1745	17.6780	15.1450	1.8504	2.0566	0.6909
	10000	50	50	100	0.1745	0.1745	17.6780	15.1280	1.8525	1.3490	0.9804
	100000	50	50	100	0.1745	0.1745	17.6780	15.1280	1.8525	1.3335	0.9918

A	B	C					D	E		F	
Distance A to B (m) = length of pointing vector	Distance A to C (m) = link distance	Measurement Errors					sigma_psi (mrad)	sigma_h		sigma_e	
		RTK			Local Angular Sensor			mean	stdev	mean	stdev
		sigma_E (cm)	sigma_N (cm)	sigma_U (cm)	sigma_phi (mrad)	sigma_theta (mrad)		(mrad)	(mrad)	(mrad)	(mrad)
40	39	50	50	100	0.3491	0.3491	17.6780	23.9250	1.1928	35.8010	0.4053
	264	50	50	100	0.3491	0.3491	17.6780	15.3760	1.8223	5.5400	0.2603
	1000	50	50	100	0.3491	0.3491	17.6780	15.1450	1.8504	2.0794	0.6842
	10000	50	50	100	0.3491	0.3491	17.6780	15.1280	1.8525	1.4061	0.9430
	100000	50	50	100	0.3491	0.3491	17.6780	15.1280	1.8525	1.3944	0.9500
	39	50	50	100	17.4533	17.4533	17.6780	24.1680	1.2429	39.5640	0.5885
	264	50	50	100	17.4533	17.4533	17.6780	15.7580	1.8122	17.7280	0.4568
	1000	50	50	100	17.4533	17.4533	17.6780	15.5330	1.8373	16.9800	0.4585
	10000	50	50	100	17.4533	17.4533	17.6780	15.5160	1.8393	16.9230	0.4588
	100000	50	50	100	17.4533	17.4533	17.6780	15.5160	1.8392	16.9230	0.4587
	39	50	50	100	34.9066	34.9066	17.6780	24.8760	1.5521	49.1550	1.0110
	264	50	50	100	34.9066	34.9066	17.6780	16.8150	2.0931	34.1330	1.0102
	1000	50	50	100	34.9066	34.9066	17.6780	16.6050	2.1162	33.7500	1.0123
	10000	50	50	100	34.9066	34.9066	17.6780	16.5890	2.1180	33.7220	1.0126
	100000	50	50	100	34.9066	34.9066	17.6780	16.5890	2.1180	33.7220	1.0126
	39	100	100	200	0.0873	0.0873	35.3560	47.8490	2.3857	71.5990	0.8104
	264	100	100	200	0.0873	0.0873	35.3560	30.7520	3.6446	11.0600	0.5220
	1000	100	100	200	0.0873	0.0873	35.3560	30.2900	3.7008	4.0988	1.3861
	10000	100	100	200	0.0873	0.0873	35.3560	30.2560	3.7050	2.6528	1.9952
	100000	100	100	200	0.0873	0.0873	35.3560	30.2560	3.7051	2.6077	2.0348
	39	100	100	200	0.1745	0.1745	35.3560	47.8490	2.3857	71.5990	0.8104
	264	100	100	200	0.1745	0.1745	35.3560	30.7520	3.6446	11.0610	0.5219
	1000	100	100	200	0.1745	0.1745	35.3560	30.2910	3.7008	4.1017	1.3852
	10000	100	100	200	0.1745	0.1745	35.3560	30.2560	3.7050	2.6626	1.9873
	100000	100	100	200	0.1745	0.1745	35.3560	30.2560	3.7051	2.6237	2.0195
	39	100	100	200	0.3491	0.3491	35.3560	47.8490	2.3856	71.6000	0.8105
	264	100	100	200	0.3491	0.3491	35.3560	30.7520	3.6446	11.0650	0.5216
	1000	100	100	200	0.3491	0.3491	35.3560	30.2910	3.7008	4.1132	1.3818
	10000	100	100	200	0.3491	0.3491	35.3560	30.2560	3.7050	2.6981	1.9608
	100000	100	100	200	0.3491	0.3491	35.3560	30.2560	3.7051	2.6670	1.9836
	39	100	100	200	17.4533	17.4533	35.3560	47.9720	2.4040	73.5530	0.9080
	264	100	100	200	17.4533	17.4533	35.3560	30.9460	3.6266	20.1570	0.3733
	1000	100	100	200	17.4533	17.4533	35.3560	30.4880	3.6810	17.3900	0.3827
	10000	100	100	200	17.4533	17.4533	35.3560	30.4540	3.6851	17.1680	0.3842
	100000	100	100	200	17.4533	17.4533	35.3560	30.4530	3.6851	17.1650	0.3841
	39	100	100	200	34.9066	34.9066	35.3560	48.3370	2.4858	79.1270	1.1770
	264	100	100	200	34.9066	34.9066	35.3560	31.5150	3.6243	35.4570	0.9135
	1000	100	100	200	34.9066	34.9066	35.3560	31.0660	3.6746	33.9600	0.9172
	10000	100	100	200	34.9066	34.9066	35.3560	31.0330	3.6785	33.8470	0.9175
	100000	100	100	200	34.9066	34.9066	35.3560	31.0320	3.6785	33.8460	0.9176
	39	500	500	1000	0.0873	0.0873	176.7800	239.2400	11.9280	357.9900	4.0519
	264	500	500	1000	0.0873	0.0873	176.7800	153.7600	18.2230	55.2970	2.6099
	1000	500	500	1000	0.0873	0.0873	176.7800	151.4500	18.5040	20.4890	6.9318
	10000	500	500	1000	0.0873	0.0873	176.7800	151.2800	18.5250	13.2470	9.9893
	100000	500	500	1000	0.0873	0.0873	176.7800	151.2800	18.5250	12.9960	10.2200
	39	500	500	1000	0.1745	0.1745	176.7800	239.2400	11.9280	357.9900	4.0519
	264	500	500	1000	0.1745	0.1745	176.7800	153.7600	18.2230	55.2980	2.6099
	1000	500	500	1000	0.1745	0.1745	176.7800	151.4500	18.5040	20.4900	6.9317
	10000	500	500	1000	0.1745	0.1745	176.7800	151.2800	18.5250	13.2490	9.9875
	100000	500	500	1000	0.1745	0.1745	176.7800	151.2800	18.5250	13.0040	10.2110
	39	500	500	1000	0.3491	0.3491	176.7800	239.2400	11.9280	358.0000	4.0518
	264	500	500	1000	0.3491	0.3491	176.7800	153.7600	18.2230	55.2980	2.6098
	1000	500	500	1000	0.3491	0.3491	176.7800	151.4500	18.5040	20.4920	6.9310
	10000	500	500	1000	0.3491	0.3491	176.7800	151.2800	18.5250	13.2580	9.9808
	100000	500	500	1000	0.3491	0.3491	176.7800	151.2800	18.5250	13.0260	10.1870
	39	500	500	1000	17.4533	17.4533	176.7800	239.2700	11.9310	358.3900	4.0719
	264	500	500	1000	17.4533	17.4533	176.7800	153.8000	18.2180	57.8150	2.4294
	1000	500	500	1000	17.4533	17.4533	176.7800	151.4900	18.4990	26.8830	5.3881
	10000	500	500	1000	17.4533	17.4533	176.7800	151.3200	18.5200	22.8150	6.2140
	100000	500	500	1000	17.4533	17.4533	176.7800	151.3200	18.5200	22.7700	6.2244
	39	500	500	1000	34.9066	34.9066	176.7800	239.3400	11.9410	359.5800	4.1314
	264	500	500	1000	34.9066	34.9066	176.7800	153.9100	18.2050	64.7760	2.0217
	1000	500	500	1000	34.9066	34.9066	176.7800	151.6100	18.4850	39.8890	3.4927
	10000	500	500	1000	34.9066	34.9066	176.7800	151.4400	18.5060	37.3730	3.7326
	100000	500	500	1000	34.9066	34.9066	176.7800	151.4400	18.5060	37.3470	3.7352
	39	1000	1000	2000	0.0873	0.0873	353.5600	478.4900	23.8560	715.9900	8.1037
	264	1000	1000	2000	0.0873	0.0873	353.5600	307.5200	36.4460	110.5900	5.2198
	1000	1000	1000	2000	0.0873	0.0873	353.5600	302.9000	37.0070	40.9790	13.8640
	10000	1000	1000	2000	0.0873	0.0873	353.5600	302.5600	37.0500	26.4930	19.9790
	100000	1000	1000	2000	0.0873	0.0873	353.5600	302.5600	37.0510	25.9880	20.4450
	39	1000	1000	2000	0.1745	0.1745	353.5600	478.4900	23.8560	715.9900	8.1037
	264	1000	1000	2000	0.1745	0.1745	353.5600	307.5200	36.4460	110.5900	5.2198
	1000	1000	1000	2000	0.1745	0.1745	353.5600	302.9000	37.0070	40.9790	13.8640
	10000	1000	1000	2000	0.1745	0.1745	353.5600	302.5600	37.0500	26.4940	19.9780
	100000	1000	1000	2000	0.1745	0.1745	353.5600	302.5600	37.0510	25.9920	20.4400
	39	1000	1000	2000	0.3491	0.3491	353.5600	478.4900	23.8560	715.9900	8.1037
	264	1000	1000	2000	0.3491	0.3491	353.5600	307.5200	36.4460	110.6000	5.2198
	1000	1000	1000	2000	0.3491	0.3491	353.5600	302.9000	37.0070	40.9800	13.8630
	10000	1000	1000	2000	0.3491	0.3491	353.5600	302.5600	37.0500	26.4990	19.9750
	100000	1000	1000	2000	0.3491	0.3491	353.5600	302.5600	37.0510	26.0080	20.4230
	39	1000	1000	2000	17.4533	17.4533	353.5600	478.5000	23.8580	716.1900	8.1137
	264	1000	1000	2000	17.4533	17.4533	353.5600	307.5400	36.4440	111.8700	5.1246
	1000	1000	1000	2000	17.4533	17.4533	353.5600	302.9200	37.0050	44.6100	12.8530
	10000	1000	1000	2000	17.4533	17.4533	353.5600	302.5800	37.0480	33.4790	16.2510
	100000	1000	1000	2000	17.4533	17.4533	353.5600	302.5800	37.0480	33.3360	16.3070
	39	1000	1000	2000	34.9066	34.9066	353.5600	478.5400	23.8630	716.7800	8.1436
	264	1000	1000	2000	34.9066	34.9066	353.5600	307.5900	36.4370	115.6300	4.8588
	1000	1000	1000	2000	34.9066	34.9066	353.5600	302.9800	36.9980	53.7660	10.7760
	10000	1000	1000	2000	34.9066	34.9066	353.5600	302.6400	37.0400	45.6290	12.4280
	100000	1000	1000	2000	34.9066	34.9066	353.5600	302.6400	37.0410	45.5390	12.4490

Table C-4. $\left|\overrightarrow{AB}\right| = 150$ m

A	B	C					D	E		F	
Distance A to B (m) = length of pointing vector	Distance A to C (m) = link distance	Measurement Errors					sigma_psi (mrad)	sigma_h		sigma_e	
		RTK			Local Angular Sensor			mean	stdev	mean	stdev
		sigma_E (cm)	sigma_N (cm)	sigma_U (cm)	sigma_phi (mrad)	sigma_theta (mrad)		(mrad)	(mrad)	(mrad)	(mrad)
150	39	0.5	0.5	1	0.0873	0.0873	0.0470	0.1900	0.0038	0.3674	0.0049
	264	0.5	0.5	1	0.0873	0.0873	0.0470	0.0518	0.0047	0.0995	0.0024
	1000	0.5	0.5	1	0.0873	0.0873	0.0470	0.0446	0.0053	0.0855	0.0025
	10000	0.5	0.5	1	0.0873	0.0873	0.0470	0.0439	0.0054	0.0843	0.0026
	100000	0.5	0.5	1	0.0873	0.0873	0.0470	0.0439	0.0054	0.0843	0.0026
	39	0.5	0.5	1	0.1745	0.1745	0.0470	0.1923	0.0058	0.3953	0.0061
	264	0.5	0.5	1	0.1745	0.1745	0.0470	0.0592	0.0095	0.1766	0.0052
	1000	0.5	0.5	1	0.1745	0.1745	0.0470	0.0529	0.0104	0.1689	0.0052
	10000	0.5	0.5	1	0.1745	0.1745	0.0470	0.0523	0.0105	0.1686	0.0052
	100000	0.5	0.5	1	0.1745	0.1745	0.0470	0.0523	0.0105	0.1686	0.0052
	39	0.5	0.5	1	0.3491	0.3491	0.0470	0.2010	0.0132	0.4912	0.0103
	264	0.5	0.5	1	0.3491	0.3491	0.0470	0.0807	0.0251	0.3411	0.0104
	1000	0.5	0.5	1	0.3491	0.3491	0.0470	0.0758	0.0265	0.3372	0.0103
	10000	0.5	0.5	1	0.3491	0.3491	0.0470	0.0755	0.0267	0.3369	0.0106
	100000	0.5	0.5	1	0.3491	0.3491	0.0470	0.0755	0.0267	0.3369	0.0106
	39	0.5	0.5	1	17.4533	17.4533	0.0470	2.9876	1.7205	16.8440	0.5238
	264	0.5	0.5	1	17.4533	17.4533	0.0470	2.9688	1.7431	16.8400	0.5238
	1000	0.5	0.5	1	17.4533	17.4533	0.0470	2.9680	1.7444	16.8400	0.5238
	10000	0.5	0.5	1	17.4533	17.4533	0.0470	2.9679	1.7445	16.8400	0.5238
	100000	0.5	0.5	1	17.4533	17.4533	0.0470	2.9679	1.7445	16.8400	0.5238
	39	0.5	0.5	1	34.9066	34.9066	0.0470	5.9482	3.4722	33.6820	1.0476
	264	0.5	0.5	1	34.9066	34.9066	0.0470	5.9324	3.4939	33.6800	1.0477
	1000	0.5	0.5	1	34.9066	34.9066	0.0470	5.9317	3.4950	33.6800	1.0477
	10000	0.5	0.5	1	34.9066	34.9066	0.0470	5.9317	3.4951	33.6800	1.0477
	100000	0.5	0.5	1	34.9066	34.9066	0.0470	5.9317	3.4951	33.6800	1.0477
	39	1	1	2	0.0873	0.0873	0.0940	0.3788	0.0067	0.7200	0.0088
	264	1	1	2	0.0873	0.0873	0.0940	0.0994	0.0081	0.1354	0.0024
	1000	1	1	2	0.0873	0.0873	0.0940	0.0841	0.0096	0.0891	0.0023
	10000	1	1	2	0.0873	0.0873	0.0940	0.0829	0.0096	0.0846	0.0022
	100000	1	1	2	0.0873	0.0873	0.0940	0.0829	0.0096	0.0846	0.0022
	39	1	1	2	0.1745	0.1745	0.0940	0.3800	0.0077	0.7349	0.0096
	264	1	1	2	0.1745	0.1745	0.0940	0.1036	0.0094	0.1989	0.0050
	1000	1	1	2	0.1745	0.1745	0.0940	0.0892	0.0107	0.1708	0.0050
	10000	1	1	2	0.1745	0.1745	0.0940	0.0880	0.0108	0.1687	0.0051
	100000	1	1	2	0.1745	0.1745	0.0940	0.0880	0.0108	0.1687	0.0051
	39	1	1	2	0.3491	0.3491	0.0940	0.3845	0.0115	0.7906	0.0123
	264	1	1	2	0.3491	0.3491	0.0940	0.1184	0.0190	0.3532	0.0103
	1000	1	1	2	0.3491	0.3491	0.0940	0.1058	0.0208	0.3381	0.0103
	10000	1	1	2	0.3491	0.3491	0.0940	0.1047	0.0209	0.3370	0.0104
	100000	1	1	2	0.3491	0.3491	0.0940	0.1047	0.0210	0.3370	0.0104
	39	1	1	2	17.4533	17.4533	0.0940	3.0245	1.6869	16.8550	0.5238
	264	1	1	2	17.4533	17.4533	0.0940	2.9746	1.7352	16.8400	0.5239
	1000	1	1	2	17.4533	17.4533	0.0940	2.9727	1.7377	16.8400	0.5238
	10000	1	1	2	17.4533	17.4533	0.0940	2.9726	1.7379	16.8400	0.5238
	100000	1	1	2	17.4533	17.4533	0.0940	2.9726	1.7379	16.8400	0.5238
	39	1	1	2	34.9066	34.9066	0.0940	5.9753	3.4411	33.6870	1.0479
	264	1	1	2	34.9066	34.9066	0.0940	5.9377	3.4862	33.6800	1.0477
	1000	1	1	2	34.9066	34.9066	0.0940	5.9361	3.4887	33.6800	1.0477
	10000	1	1	2	34.9066	34.9066	0.0940	5.9359	3.4889	33.6800	1.0477
	100000	1	1	2	34.9066	34.9066	0.0940	5.9359	3.4889	33.6800	1.0477
	39	2	2	4	0.0873	0.0873	0.1890	0.7571	0.0129	1.4331	0.0175
	264	2	2	4	0.0873	0.0873	0.1890	0.1966	0.0161	0.2281	0.0028
	1000	2	2	4	0.0873	0.0873	0.1890	0.1656	0.0191	0.1026	0.0020
	10000	2	2	4	0.0873	0.0873	0.1890	0.1631	0.0194	0.0861	0.0019
	100000	2	2	4	0.0873	0.0873	0.1890	0.1631	0.0194	0.0859	0.0020
	39	2	2	4	0.1745	0.1745	0.1890	0.7577	0.0133	1.4404	0.0179
	264	2	2	4	0.1745	0.1745	0.1890	0.1987	0.0163	0.2708	0.0048
	1000	2	2	4	0.1745	0.1745	0.1890	0.1683	0.0191	0.1783	0.0045
	10000	2	2	4	0.1745	0.1745	0.1890	0.1658	0.0193	0.1695	0.0046
	100000	2	2	4	0.1745	0.1745	0.1890	0.1658	0.0194	0.1694	0.0046
	39	2	2	4	0.3491	0.3491	0.1890	0.7600	0.0153	1.4697	0.0195
	264	2	2	4	0.3491	0.3491	0.1890	0.2073	0.0189	0.3980	0.0099
	1000	2	2	4	0.3491	0.3491	0.1890	0.1783	0.0214	0.3418	0.0101
	10000	2	2	4	0.3491	0.3491	0.1890	0.1759	0.0216	0.3373	0.0101
	100000	2	2	4	0.3491	0.3491	0.1890	0.1759	0.0217	0.3373	0.0101
	39	2	2	4	17.4533	17.4533	0.1890	3.1346	1.6117	16.9010	0.5235
	264	2	2	4	17.4533	17.4533	0.1890	2.9890	1.7190	16.8410	0.5239
	1000	2	2	4	17.4533	17.4533	0.1890	2.9841	1.7241	16.8400	0.5238
	10000	2	2	4	17.4533	17.4533	0.1890	2.9838	1.7245	16.8400	0.5238
	100000	2	2	4	17.4533	17.4533	0.1890	2.9838	1.7245	16.8400	0.5238
	39	2	2	4	34.9066	34.9066	0.1890	6.0489	3.3739	33.7100	1.0474
	264	2	2	4	34.9066	34.9066	0.1890	5.9493	3.4706	33.6800	1.0479
	1000	2	2	4	34.9066	34.9066	0.1890	5.9455	3.4755	33.6800	1.0477
	10000	2	2	4	34.9066	34.9066	0.1890	5.9452	3.4759	33.6800	1.0477
	100000	2	2	4	34.9066	34.9066	0.1890	5.9452	3.4759	33.6800	1.0477
	39	50	50	100	0.0873	0.0873	4.7140	18.9230	0.3171	35.7640	0.4342
	264	50	50	100	0.0873	0.0873	4.7140	4.8947	0.4030	5.3016	0.0520
	1000	50	50	100	0.0873	0.0873	4.7140	4.1179	0.4791	1.4619	0.0689
	10000	50	50	100	0.0873	0.0873	4.7140	4.0541	0.4868	0.4027	0.2317
	100000	50	50	100	0.0873	0.0873	4.7140	4.0534	0.4868	0.3649	0.2518
	39	50	50	100	0.1745	0.1745	4.7140	18.9230	0.3171	35.7640	0.4342
	264	50	50	100	0.1745	0.1745	4.7140	4.8948	0.4030	5.3036	0.0521
	1000	50	50	100	0.1745	0.1745	4.7140	4.1180	0.4790	1.4692	0.0684
	10000	50	50	100	0.1745	0.1745	4.7140	4.0543	0.4868	0.4361	0.2167
	100000	50	50	100	0.1745	0.1745	4.7140	4.0536	0.4868	0.4065	0.2294

A	B	C					D	E		F	
Distance A to B (m) = length of pointing vector	Distance A to C (m) = link distance	Measurement Errors					sigma_psi (mrad)	sigma_h		sigma_e	
		RTK			Local Angular Sensor			mean (mrad)	stdev (mrad)	mean (mrad)	stdev (mrad)
		sigma_E (cm)	sigma_N (cm)	sigma_U (cm)	sigma_phi (mrad)	sigma_theta (mrad)					
150	39	50	50	100	0.3491	0.3491	4.7140	18.9230	0.3171	35.7650	0.4343
	264	50	50	100	0.3491	0.3491	4.7140	4.8952	0.4030	5.3116	0.0524
	1000	50	50	100	0.3491	0.3491	4.7140	4.1185	0.4790	1.4980	0.0663
	10000	50	50	100	0.3491	0.3491	4.7140	4.0548	0.4867	0.5380	0.1815
	100000	50	50	100	0.3491	0.3491	4.7140	4.0540	0.4868	0.5176	0.1873
	39	50	50	100	17.4533	17.4533	4.7140	19.2280	0.5751	39.5310	0.6155
	264	50	50	100	17.4533	17.4533	4.7140	5.9222	0.9477	17.6550	0.5143
	1000	50	50	100	17.4533	17.4533	4.7140	5.2871	1.0411	16.9030	0.5185
	10000	50	50	100	17.4533	17.4533	4.7140	5.2365	1.0497	16.8460	0.5190
	100000	50	50	100	17.4533	17.4533	4.7140	5.2359	1.0498	16.8460	0.5189
	39	50	50	100	34.9066	34.9066	4.7140	20.0960	1.3145	49.1280	1.0333
	264	50	50	100	34.9066	34.9066	4.7140	8.0758	2.5102	34.0950	1.0426
	1000	50	50	100	34.9066	34.9066	4.7140	7.5847	2.6570	33.7120	1.0451
	10000	50	50	100	34.9066	34.9066	4.7140	7.5463	2.6695	33.6830	1.0454
	100000	50	50	100	34.9066	34.9066	4.7140	7.5458	2.6696	33.6830	1.0453
	39	100	100	200	0.0873	0.0873	9.4280	37.8460	0.6341	71.5270	0.8684
	264	100	100	200	0.0873	0.0873	9.4280	9.7894	0.8060	10.6020	0.1038
	1000	100	100	200	0.0873	0.0873	9.4280	8.2358	0.9581	2.9201	0.1381
	10000	100	100	200	0.0873	0.0873	9.4280	8.1081	0.9735	0.7865	0.4727
	100000	100	100	200	0.0873	0.0873	9.4280	8.1069	0.9736	0.7005	0.5239
	39	100	100	200	0.1745	0.1745	9.4280	37.8460	0.6341	71.5270	0.8684
	264	100	100	200	0.1745	0.1745	9.4280	9.7894	0.8060	10.6030	0.1038
	1000	100	100	200	0.1745	0.1745	9.4280	8.2359	0.9581	2.9238	0.1378
	10000	100	100	200	0.1745	0.1745	9.4280	8.1082	0.9735	0.8054	0.4633
	100000	100	100	200	0.1745	0.1745	9.4280	8.1069	0.9736	0.7299	0.5036
	39	100	100	200	0.3491	0.3491	9.4280	37.8460	0.6341	71.5280	0.8685
	264	100	100	200	0.3491	0.3491	9.4280	9.7896	0.8060	10.6070	0.1041
	1000	100	100	200	0.3491	0.3491	9.4280	8.2362	0.9581	2.9383	0.1367
	10000	100	100	200	0.3491	0.3491	9.4280	8.1084	0.9734	0.8721	0.4336
	100000	100	100	200	0.3491	0.3491	9.4280	8.1072	0.9736	0.8130	0.4588
	39	100	100	200	17.4533	17.4533	9.4280	38.0000	0.7628	73.4830	0.9650
	264	100	100	200	17.4533	17.4533	9.4280	10.3660	0.9413	19.9000	0.4955
	1000	100	100	200	17.4533	17.4533	9.4280	8.9138	1.0684	17.0920	0.5032
	10000	100	100	200	17.4533	17.4533	9.4280	8.7961	1.0810	16.8650	0.5045
	100000	100	100	200	17.4533	17.4533	9.4280	8.7949	1.0811	16.8630	0.5043
	39	100	100	200	34.9066	34.9066	9.4280	38.4550	1.1503	79.0620	1.2309
	264	100	100	200	34.9066	34.9066	9.4280	11.8440	1.8954	35.3100	1.0287
	1000	100	100	200	34.9066	34.9066	9.4280	10.5740	2.0821	33.8070	1.0371
	10000	100	100	200	34.9066	34.9066	9.4280	10.4730	2.0993	33.6930	1.0379
	100000	100	100	200	34.9066	34.9066	9.4280	10.4720	2.0995	33.6920	1.0380
	39	500	500	1000	0.0873	0.0873	47.1410	189.2300	3.1707	357.6400	4.3420
	264	500	500	1000	0.0873	0.0873	47.1410	48.9470	4.0298	53.0090	0.5192
	1000	500	500	1000	0.0873	0.0873	47.1410	41.1790	4.7906	14.5950	0.6909
	10000	500	500	1000	0.0873	0.0873	47.1410	40.5410	4.8673	3.9010	2.3800
	100000	500	500	1000	0.0873	0.0873	47.1410	40.5340	4.8681	3.4326	2.6784
	39	500	500	1000	0.1745	0.1745	47.1410	189.2300	3.1707	357.6400	4.3420
	264	500	500	1000	0.1745	0.1745	47.1410	48.9470	4.0298	53.0090	0.5192
	1000	500	500	1000	0.1745	0.1745	47.1410	41.1790	4.7906	14.5950	0.6908
	10000	500	500	1000	0.1745	0.1745	47.1410	40.5410	4.8673	3.9050	2.3780
	100000	500	500	1000	0.1745	0.1745	47.1410	40.5340	4.8681	3.4441	2.6677
	39	500	500	1000	0.3491	0.3491	47.1410	189.2300	3.1707	357.6400	4.3420
	264	500	500	1000	0.3491	0.3491	47.1410	48.9470	4.0298	53.0100	0.5192
	1000	500	500	1000	0.3491	0.3491	47.1410	41.1790	4.7906	14.5980	0.6907
	10000	500	500	1000	0.3491	0.3491	47.1410	40.5410	4.8673	3.9209	2.3698
	100000	500	500	1000	0.3491	0.3491	47.1410	40.5340	4.8681	3.4798	2.6371
	39	500	500	1000	17.4533	17.4533	47.1410	189.2600	3.1963	358.0300	4.3618
	264	500	500	1000	17.4533	17.4533	47.1410	49.0680	4.0283	55.6210	0.6464
	1000	500	500	1000	17.4533	17.4533	47.1410	41.3240	4.7758	22.2970	0.4217
	10000	500	500	1000	17.4533	17.4533	47.1410	40.6890	4.8512	17.4490	0.5069
	100000	500	500	1000	17.4533	17.4533	47.1410	40.6820	4.8520	17.3940	0.5084
	39	500	500	1000	34.9066	34.9066	47.1410	189.3500	3.2732	359.2200	4.4208
	264	500	500	1000	34.9066	34.9066	47.1410	49.4280	4.0410	62.8070	0.9854
	1000	500	500	1000	34.9066	34.9066	47.1410	41.7550	4.7543	36.7180	0.8425
	10000	500	500	1000	34.9066	34.9066	47.1410	41.1260	4.8260	33.9940	0.8446
	100000	500	500	1000	34.9066	34.9066	47.1410	41.1200	4.8267	33.9660	0.8446
	39	1000	1000	2000	0.0873	0.0873	94.2820	378.4600	6.3413	715.2700	8.6841
	264	1000	1000	2000	0.0873	0.0873	94.2820	97.8940	8.0597	106.0200	1.0382
	1000	1000	1000	2000	0.0873	0.0873	94.2820	82.3580	9.5812	29.1890	1.3818
	10000	1000	1000	2000	0.0873	0.0873	94.2820	81.0810	9.7347	7.8001	4.7611
	100000	1000	1000	2000	0.0873	0.0873	94.2820	81.0680	9.7362	6.8588	5.3631
	39	1000	1000	2000	0.1745	0.1745	94.2820	378.4600	6.3413	715.2700	8.6841
	264	1000	1000	2000	0.1745	0.1745	94.2820	97.8940	8.0597	106.0200	1.0383
	1000	1000	1000	2000	0.1745	0.1745	94.2820	82.3580	9.5812	29.1890	1.3817
	10000	1000	1000	2000	0.1745	0.1745	94.2820	81.0810	9.7347	7.8021	4.7601
	100000	1000	1000	2000	0.1745	0.1745	94.2820	81.0680	9.7362	6.8653	5.3567
	39	1000	1000	2000	0.3491	0.3491	94.2820	378.4600	6.3413	715.2700	8.6841
	264	1000	1000	2000	0.3491	0.3491	94.2820	97.8940	8.0597	106.0200	1.0383
	1000	1000	1000	2000	0.3491	0.3491	94.2820	82.3580	9.5812	29.1900	1.3817
	10000	1000	1000	2000	0.3491	0.3491	94.2820	81.0810	9.7347	7.8101	4.7559
	100000	1000	1000	2000	0.3491	0.3491	94.2820	81.0690	9.7362	6.8881	5.3353
	39	1000	1000	2000	17.4533	17.4533	94.2820	378.4800	6.3542	715.4700	8.6940
	264	1000	1000	2000	17.4533	17.4533	94.2820	97.9540	8.0583	107.3500	1.1033
	1000	1000	1000	2000	17.4533	17.4533	94.2820	82.4310	9.5731	33.7130	1.0970
	10000	1000	1000	2000	17.4533	17.4533	94.2820	81.1550	9.7258	19.0560	2.0585
	100000	1000	1000	2000	17.4533	17.4533	94.2820	81.1430	9.7274	18.8500	2.0808
	39	1000	1000	2000	34.9066	34.9066	94.2820	378.5200	6.3925	716.0600	8.7236
	264	1000	1000	2000	34.9066	34.9066	94.2820	98.1360	8.0566	111.2400	1.2929
	1000	1000	1000	2000	34.9066	34.9066	94.2820	82.6490	9.5517	44.5940	0.8433
	10000	1000	1000	2000	34.9066	34.9066	94.2820	81.3770	9.7024	34.8990	1.0139
	100000	1000	1000	2000	34.9066	34.9066	94.2820	81.3640	9.7039	34.7880	1.0168

Table C-5. $\left|\overrightarrow{AB}\right| = 1$ km

A	B	C					D	E		F	
Distance A to B (m) = length of pointing vector	Distance A to C (m) = link distance	Measurement Errors					sigma_psi (mrad)	sigma_h		sigma_e	
		RTK			Local Angular Sensor			mean	stdev	mean	stdev
		sigma_E (cm)	sigma_N (cm)	sigma_U (cm)	sigma_phi (mrad)	sigma_theta (mrad)		(mrad)	(mrad)	(mrad)	(mrad)
1000	39	0.5	0.5	1	0.0873	0.0873	0.0070	0.1855	0.0038	0.3674	0.0049
	264	0.5	0.5	1	0.0873	0.0873	0.0070	0.0326	0.0044	0.0995	0.0025
	1000	0.5	0.5	1	0.0873	0.0873	0.0070	0.0185	0.0069	0.0853	0.0026
	10000	0.5	0.5	1	0.0873	0.0873	0.0070	0.0167	0.0075	0.0841	0.0026
	100000	0.5	0.5	1	0.0873	0.0873	0.0070	0.0167	0.0075	0.0841	0.0026
	39	0.5	0.5	1	0.1745	0.1745	0.0070	0.1879	0.0059	0.3953	0.0061
	264	0.5	0.5	1	0.1745	0.1745	0.0070	0.0428	0.0121	0.1766	0.0052
	1000	0.5	0.5	1	0.1745	0.1745	0.0070	0.0321	0.0157	0.1686	0.0052
	10000	0.5	0.5	1	0.1745	0.1745	0.0070	0.0309	0.0164	0.1686	0.0052
	100000	0.5	0.5	1	0.1745	0.1745	0.0070	0.0309	0.0164	0.1686	0.0052
	39	0.5	0.5	1	0.3491	0.3491	0.0070	0.1968	0.0133	0.4912	0.0103
	264	0.5	0.5	1	0.3491	0.3491	0.0070	0.0682	0.0295	0.3410	0.0104
	1000	0.5	0.5	1	0.3491	0.3491	0.0070	0.0611	0.0335	0.3372	0.0103
	10000	0.5	0.5	1	0.3491	0.3491	0.0070	0.0601	0.0339	0.3368	0.0107
	100000	0.5	0.5	1	0.3491	0.3491	0.0070	0.0601	0.0339	0.3368	0.0107
	39	0.5	0.5	1	17.4533	17.4533	0.0070	2.9868	1.7214	16.8440	0.5238
	264	0.5	0.5	1	17.4533	17.4533	0.0070	2.9665	1.7463	16.8400	0.5238
	1000	0.5	0.5	1	17.4533	17.4533	0.0070	2.9647	1.7492	16.8400	0.5238
	10000	0.5	0.5	1	17.4533	17.4533	0.0070	2.9644	1.7497	16.8400	0.5238
	100000	0.5	0.5	1	17.4533	17.4533	0.0070	2.9644	1.7497	16.8400	0.5238
	39	0.5	0.5	1	34.9066	34.9066	0.0070	5.9475	3.4727	33.6820	1.0476
	264	0.5	0.5	1	34.9066	34.9066	0.0070	5.9305	3.4971	33.6800	1.0477
	1000	0.5	0.5	1	34.9066	34.9066	0.0070	5.9287	3.5001	33.6800	1.0477
	10000	0.5	0.5	1	34.9066	34.9066	0.0070	5.9284	3.5006	33.6800	1.0477
	100000	0.5	0.5	1	34.9066	34.9066	0.0070	5.9284	3.5006	33.6800	1.0477
	39	1	1	2	0.0873	0.0873	0.0140	0.3702	0.0064	0.7200	0.0088
	264	1	1	2	0.0873	0.0873	0.0140	0.0585	0.0031	0.1351	0.0026
	1000	1	1	2	0.0873	0.0873	0.0140	0.0250	0.0053	0.0885	0.0026
	10000	1	1	2	0.0873	0.0873	0.0140	0.0202	0.0063	0.0841	0.0026
	100000	1	1	2	0.0873	0.0873	0.0140	0.0202	0.0063	0.0841	0.0026
	39	1	1	2	0.1745	0.1745	0.0140	0.3713	0.0074	0.7349	0.0096
	264	1	1	2	0.1745	0.1745	0.0140	0.0651	0.0086	0.1986	0.0052
	1000	1	1	2	0.1745	0.1745	0.0140	0.0368	0.0137	0.1706	0.0052
	10000	1	1	2	0.1745	0.1745	0.0140	0.0333	0.0150	0.1686	0.0052
	100000	1	1	2	0.1745	0.1745	0.0140	0.0333	0.0150	0.1686	0.0052
	39	1	1	2	0.3491	0.3491	0.0140	0.3761	0.0117	0.7906	0.0123
	264	1	1	2	0.3491	0.3491	0.0140	0.0854	0.0240	0.3532	0.0103
	1000	1	1	2	0.3491	0.3491	0.0140	0.0641	0.0314	0.3380	0.0104
	10000	1	1	2	0.3491	0.3491	0.0140	0.0618	0.0328	0.3368	0.0107
	100000	1	1	2	0.3491	0.3491	0.0140	0.0618	0.0328	0.3368	0.0107
	39	1	1	2	17.4533	17.4533	0.0140	3.0225	1.6888	16.8550	0.5238
	264	1	1	2	17.4533	17.4533	0.0140	2.9695	1.7422	16.8400	0.5239
	1000	1	1	2	17.4533	17.4533	0.0140	2.9655	1.7477	16.8400	0.5238
	10000	1	1	2	17.4533	17.4533	0.0140	2.9649	1.7487	16.8400	0.5238
	100000	1	1	2	17.4533	17.4533	0.0140	2.9649	1.7487	16.8400	0.5238
	39	1	1	2	34.9066	34.9066	0.0140	5.9737	3.4424	33.6870	1.0479
	264	1	1	2	34.9066	34.9066	0.0140	5.9330	3.4929	33.6800	1.0477
	1000	1	1	2	34.9066	34.9066	0.0140	5.9295	3.4987	33.6800	1.0477
	10000	1	1	2	34.9066	34.9066	0.0140	5.9289	3.4997	33.6800	1.0477
	100000	1	1	2	34.9066	34.9066	0.0140	5.9289	3.4997	33.6800	1.0477
	39	2	2	4	0.0873	0.0873	0.0280	0.7396	0.0125	1.4330	0.0177
	264	2	2	4	0.0873	0.0873	0.0280	0.1132	0.0030	0.2276	0.0033
	1000	2	2	4	0.0873	0.0873	0.0280	0.0413	0.0038	0.1011	0.0026
	10000	2	2	4	0.0873	0.0873	0.0280	0.0297	0.0050	0.0845	0.0025
	100000	2	2	4	0.0873	0.0873	0.0280	0.0296	0.0050	0.0841	0.0026
	39	2	2	4	0.1745	0.1745	0.0280	0.7403	0.0128	1.4403	0.0180
	264	2	2	4	0.1745	0.1745	0.0280	0.1169	0.0062	0.2702	0.0055
	1000	2	2	4	0.1745	0.1745	0.0280	0.0500	0.0105	0.1776	0.0051
	10000	2	2	4	0.1745	0.1745	0.0280	0.0404	0.0126	0.1686	0.0052
	100000	2	2	4	0.1745	0.1745	0.0280	0.0403	0.0126	0.1686	0.0052
	39	2	2	4	0.3491	0.3491	0.0280	0.7426	0.0150	1.4696	0.0195
	264	2	2	4	0.3491	0.3491	0.0280	0.1302	0.0172	0.3976	0.0102
	1000	2	2	4	0.3491	0.3491	0.0280	0.0736	0.0273	0.3413	0.0104
	10000	2	2	4	0.3491	0.3491	0.0280	0.0666	0.0301	0.3369	0.0106
	100000	2	2	4	0.3491	0.3491	0.0280	0.0665	0.0301	0.3368	0.0107
	39	2	2	4	17.4533	17.4533	0.0280	3.1285	1.6155	16.9000	0.5235
	264	2	2	4	17.4533	17.4533	0.0280	2.9764	1.7335	16.8410	0.5239
	1000	2	2	4	17.4533	17.4533	0.0280	2.9676	1.7450	16.8400	0.5238
	10000	2	2	4	17.4533	17.4533	0.0280	2.9662	1.7468	16.8400	0.5238
	100000	2	2	4	17.4533	17.4533	0.0280	2.9661	1.7468	16.8400	0.5238
	39	2	2	4	34.9066	34.9066	0.0280	6.0449	3.3771	33.7100	1.0474
	264	2	2	4	34.9066	34.9066	0.0280	5.9389	3.4843	33.6800	1.0479
	1000	2	2	4	34.9066	34.9066	0.0280	5.9314	3.4956	33.6800	1.0477
	10000	2	2	4	34.9066	34.9066	0.0280	5.9301	3.4978	33.6800	1.0477
	100000	2	2	4	34.9066	34.9066	0.0280	5.9301	3.4978	33.6800	1.0477
	39	50	50	100	0.0873	0.0873	0.7070	18.4880	0.3066	35.7610	0.4362
	264	50	50	100	0.0873	0.0873	0.7070	2.7975	0.0470	5.2840	0.0642
	1000	50	50	100	0.0873	0.0873	0.7070	0.9447	0.0477	1.3988	0.0159
	10000	50	50	100	0.0873	0.0873	0.7070	0.6126	0.0725	0.1750	0.0130
	100000	50	50	100	0.0873	0.0873	0.7070	0.6083	0.0730	0.1053	0.0213
	39	50	50	100	0.1745	0.1745	0.7070	18.4880	0.3066	35.7610	0.4365
	264	50	50	100	0.1745	0.1745	0.7070	2.7977	0.0472	5.2860	0.0643
	1000	50	50	100	0.1745	0.1745	0.7070	0.9452	0.0478	1.4064	0.0163
	10000	50	50	100	0.1745	0.1745	0.7070	0.6133	0.0724	0.2281	0.0090
	100000	50	50	100	0.1745	0.1745	0.7070	0.6090	0.0729	0.1809	0.0116

A	B	C					D	E		F	
Distance A to B (m) = length of pointing vector	Distance A to C (m) = link distance	Measurement Errors					sigma_psi (mrad)	sigma_h		sigma_e	
		RTK			Local Angular Sensor			mean	stdev	mean	stdev
		sigma_E (cm)	sigma_N (cm)	sigma_U (cm)	sigma_phi (mrad)	sigma_theta (mrad)		(mrad)	(mrad)	(mrad)	(mrad)
1000	39	50	50	100	0.3491	0.3491	0.7070	18.4880	0.3066	35.7630	0.4366
	264	50	50	100	0.3491	0.3491	0.7070	2.7983	0.0476	5.2941	0.0647
	1000	50	50	100	0.3491	0.3491	0.7070	0.9471	0.0481	1.4364	0.0178
	10000	50	50	100	0.3491	0.3491	0.7070	0.6163	0.0722	0.3704	0.0076
	100000	50	50	100	0.3491	0.3491	0.7070	0.6120	0.0726	0.3434	0.0076
	39	50	50	100	17.4533	17.4533	0.7070	18.7990	0.5786	39.5290	0.6174
	264	50	50	100	17.4533	17.4533	0.7070	4.2704	1.2011	17.6490	0.5188
	1000	50	50	100	17.4533	17.4533	0.7070	3.2064	1.5696	16.8980	0.5233
	10000	50	50	100	17.4533	17.4533	0.7070	3.0897	1.6383	16.8410	0.5238
	100000	50	50	100	17.4533	17.4533	0.7070	3.0884	1.6391	16.8400	0.5237
	39	50	50	100	34.9066	34.9066	0.7070	19.6850	1.3373	49.1260	1.0350
	264	50	50	100	34.9066	34.9066	0.7070	6.8222	2.9472	34.0920	1.0450
	1000	50	50	100	34.9066	34.9066	0.7070	6.0960	3.3366	33.7090	1.0476
	10000	50	50	100	34.9066	34.9066	0.7070	6.0196	3.3977	33.6800	1.0479
	100000	50	50	100	34.9066	34.9066	0.7070	6.0188	3.3985	33.6800	1.0477
	39	100	100	200	0.0873	0.0873	1.4140	36.9760	0.6132	71.5220	0.8728
	264	100	100	200	0.0873	0.0873	1.4140	5.5950	0.0940	10.5670	0.1283
	1000	100	100	200	0.0873	0.0873	1.4140	1.8892	0.0955	2.7937	0.0317
	10000	100	100	200	0.0873	0.0873	1.4140	1.2248	0.1449	0.3180	0.0294
	100000	100	100	200	0.0873	0.0873	1.4140	1.2162	0.1460	0.1464	0.0592
	39	100	100	200	0.1745	0.1745	1.4140	36.9760	0.6132	71.5220	0.8729
	264	100	100	200	0.1745	0.1745	1.4140	5.5951	0.0940	10.5680	0.1283
	1000	100	100	200	0.1745	0.1745	1.4140	1.8895	0.0955	2.7975	0.0318
	10000	100	100	200	0.1745	0.1745	1.4140	1.2251	0.1450	0.3500	0.0259
	100000	100	100	200	0.1745	0.1745	1.4140	1.2166	0.1460	0.2106	0.0426
	39	100	100	200	0.3491	0.3491	1.4140	36.9760	0.6132	71.5230	0.8729
	264	100	100	200	0.3491	0.3491	1.4140	5.5954	0.0943	10.5720	0.1285
	1000	100	100	200	0.3491	0.3491	1.4140	1.8903	0.0956	2.8127	0.0326
	10000	100	100	200	0.3491	0.3491	1.4140	1.2266	0.1448	0.4561	0.0180
	100000	100	100	200	0.3491	0.3491	1.4140	1.2181	0.1458	0.3617	0.0232
	39	100	100	200	17.4533	17.4533	1.4140	37.1330	0.7512	73.4780	0.9693
	264	100	100	200	17.4533	17.4533	1.4140	6.5133	0.8594	19.8810	0.5115
	1000	100	100	200	17.4533	17.4533	1.4140	3.6828	1.3656	17.0700	0.5220
	10000	100	100	200	17.4533	17.4533	1.4140	3.3329	1.5043	16.8430	0.5235
	100000	100	100	200	17.4533	17.4533	1.4140	3.3290	1.5061	16.8400	0.5234
	39	100	100	200	34.9066	34.9066	1.4140	37.5980	1.1572	79.0570	1.2350
	264	100	100	200	34.9066	34.9066	1.4140	8.5406	2.4021	35.2990	1.0379
	1000	100	100	200	34.9066	34.9066	1.4140	6.4128	3.1391	33.7950	1.0468
	10000	100	100	200	34.9066	34.9066	1.4140	6.1795	3.2765	33.6810	1.0476
	100000	100	100	200	34.9066	34.9066	1.4140	6.1769	3.2782	33.6800	1.0476
	39	500	500	1000	0.0873	0.0873	7.0710	184.8800	3.0657	357.6100	4.3642
	264	500	500	1000	0.0873	0.0873	7.0710	27.9750	0.4696	52.8330	0.6414
	1000	500	500	1000	0.0873	0.0873	7.0710	9.4456	0.4772	13.9620	0.1578
	10000	500	500	1000	0.0873	0.0873	7.0710	6.1234	0.7250	1.5346	0.1535
	100000	500	500	1000	0.0873	0.0873	7.0710	6.0806	0.7302	0.5624	0.3690
	39	500	500	1000	0.1745	0.1745	7.0710	184.8800	3.0657	357.6100	4.3642
	264	500	500	1000	0.1745	0.1745	7.0710	27.9750	0.4696	52.8330	0.6414
	1000	500	500	1000	0.1745	0.1745	7.0710	9.4457	0.4772	13.9630	0.1578
	10000	500	500	1000	0.1745	0.1745	7.0710	6.1234	0.7250	1.5416	0.1526
	100000	500	500	1000	0.1745	0.1745	7.0710	6.0806	0.7301	0.5904	0.3539
	39	500	500	1000	0.3491	0.3491	7.0710	184.8800	3.0657	357.6100	4.3642
	264	500	500	1000	0.3491	0.3491	7.0710	27.9750	0.4697	52.8340	0.6414
	1000	500	500	1000	0.3491	0.3491	7.0710	9.4458	0.4773	13.9660	0.1579
	10000	500	500	1000	0.3491	0.3491	7.0710	6.1238	0.7250	1.5693	0.1493
	100000	500	500	1000	0.3491	0.3491	7.0710	6.0810	0.7301	0.6779	0.3152
	39	500	500	1000	17.4533	17.4533	7.0710	184.9100	3.0935	358.0100	4.3840
	264	500	500	1000	17.4533	17.4533	7.0710	28.1820	0.6437	55.4520	0.7696
	1000	500	500	1000	17.4533	17.4533	7.0710	10.0370	0.7485	21.8760	0.5032
	10000	500	500	1000	17.4533	17.4533	7.0710	6.9932	0.9825	16.9110	0.5124
	100000	500	500	1000	17.4533	17.4533	7.0710	6.9557	0.9871	16.8530	0.5128
	39	500	500	1000	34.9066	34.9066	7.0710	185.0000	3.1767	359.1900	4.4429
	264	500	500	1000	34.9066	34.9066	7.0710	28.7900	1.1623	62.6570	1.1028
	1000	500	500	1000	34.9066	34.9066	7.0710	11.5460	1.8793	36.4600	1.0277
	10000	500	500	1000	34.9066	34.9066	7.0710	8.9466	2.3191	33.7150	1.0419
	100000	500	500	1000	34.9066	34.9066	7.0710	8.9160	2.3261	33.6870	1.0422
	39	1000	1000	2000	0.0873	0.0873	14.1420	369.7600	6.1314	715.2200	8.7285
	264	1000	1000	2000	0.0873	0.0873	14.1420	55.9500	0.9393	105.6700	1.2826
	1000	1000	1000	2000	0.0873	0.0873	14.1420	18.8910	0.9544	27.9240	0.3155
	10000	1000	1000	2000	0.0873	0.0873	14.1420	12.2470	1.4499	3.0657	0.3073
	100000	1000	1000	2000	0.0873	0.0873	14.1420	12.1610	1.4603	1.1090	0.7473
	39	1000	1000	2000	0.1745	0.1745	14.1420	369.7600	6.1314	715.2200	8.7285
	264	1000	1000	2000	0.1745	0.1745	14.1420	55.9500	0.9393	105.6700	1.2827
	1000	1000	1000	2000	0.1745	0.1745	14.1420	18.8910	0.9544	27.9250	0.3155
	10000	1000	1000	2000	0.1745	0.1745	14.1420	12.2470	1.4499	3.0692	0.3069
	100000	1000	1000	2000	0.1745	0.1745	14.1420	12.1610	1.4604	1.1248	0.7381
	39	1000	1000	2000	0.3491	0.3491	14.1420	369.7600	6.1315	715.2200	8.7284
	264	1000	1000	2000	0.3491	0.3491	14.1420	55.9500	0.9393	105.6700	1.2827
	1000	1000	1000	2000	0.3491	0.3491	14.1420	18.8910	0.9545	27.9260	0.3156
	10000	1000	1000	2000	0.3491	0.3491	14.1420	12.2470	1.4499	3.0832	0.3051
	100000	1000	1000	2000	0.3491	0.3491	14.1420	12.1610	1.4603	1.1807	0.7078
	39	1000	1000	2000	17.4533	17.4533	14.1420	369.7700	6.1453	715.4200	8.7384
	264	1000	1000	2000	17.4533	17.4533	14.1420	56.0540	1.0258	107.0000	1.3489
	1000	1000	1000	2000	17.4533	17.4533	14.1420	19.1980	1.0276	32.6100	0.5395
	10000	1000	1000	2000	17.4533	17.4533	14.1420	12.7200	1.4588	17.1210	0.4806
	100000	1000	1000	2000	17.4533	17.4533	14.1420	12.6380	1.4677	16.8940	0.4816
	39	1000	1000	2000	34.9066	34.9066	14.1420	369.8200	6.1869	716.0100	8.7680
	264	1000	1000	2000	34.9066	34.9066	14.1420	56.3650	1.2875	110.9000	1.5394
	1000	1000	1000	2000	34.9066	34.9066	14.1420	20.0730	1.4971	43.7530	1.0061
	10000	1000	1000	2000	34.9066	34.9066	14.1420	13.9860	1.9650	33.8210	1.0249
	100000	1000	1000	2000	34.9066	34.9066	14.1420	13.9110	1.9741	33.7070	1.0257

Table C-6. $\left|\overrightarrow{AB}\right| = 1000$ km

A	B	C					D	E		F	
Distance A to B (m) = length of pointing vector	Distance A to C (m) = link distance	Measurement Errors					sigma_psi (mrad)	sigma_h		sigma_e	
		RTK			Local Angular Sensor			mean	stdev	mean	stdev
		sigma_E (cm)	sigma_N (cm)	sigma_U (cm)	sigma_phi (mrad)	sigma_theta (mrad)		(mrad)	(mrad)	(mrad)	(mrad)
1.00E+06	39	0.5	0.5	1	0.0873	0.0873	0.0000	0.1855	0.0038	0.3674	0.0049
	264	0.5	0.5	1	0.0873	0.0873	0.0000	0.0319	0.0044	0.0995	0.0025
	1000	0.5	0.5	1	0.0873	0.0873	0.0000	0.0172	0.0072	0.0853	0.0026
	10000	0.5	0.5	1	0.0873	0.0873	0.0000	0.0148	0.0086	0.0841	0.0026
	100000	0.5	0.5	1	0.0873	0.0873	0.0000	0.0147	0.0088	0.0841	0.0026
	39	0.5	0.5	1	0.1745	0.1745	0.0000	0.1879	0.0059	0.3953	0.0061
	264	0.5	0.5	1	0.1745	0.1745	0.0000	0.0423	0.0120	0.1766	0.0052
	1000	0.5	0.5	1	0.1745	0.1745	0.0000	0.0312	0.0161	0.1686	0.0052
	10000	0.5	0.5	1	0.1745	0.1745	0.0000	0.0299	0.0174	0.1686	0.0052
	100000	0.5	0.5	1	0.1745	0.1745	0.0000	0.0298	0.0176	0.1686	0.0052
	39	0.5	0.5	1	0.3491	0.3491	0.0000	0.1968	0.0133	0.4912	0.0103
	264	0.5	0.5	1	0.3491	0.3491	0.0000	0.0677	0.0297	0.3410	0.0104
	1000	0.5	0.5	1	0.3491	0.3491	0.0000	0.0605	0.0338	0.3372	0.0103
	10000	0.5	0.5	1	0.3491	0.3491	0.0000	0.0594	0.0347	0.3368	0.0107
	100000	0.5	0.5	1	0.3491	0.3491	0.0000	0.0593	0.0349	0.3368	0.0107
	39	0.5	0.5	1	17.4533	17.4533	0.0000	2.9868	1.7214	16.8440	0.5238
	264	0.5	0.5	1	17.4533	17.4533	0.0000	2.9665	1.7464	16.8400	0.5238
	1000	0.5	0.5	1	17.4533	17.4533	0.0000	2.9645	1.7495	16.8400	0.5238
	10000	0.5	0.5	1	17.4533	17.4533	0.0000	2.9639	1.7504	16.8400	0.5238
	100000	0.5	0.5	1	17.4533	17.4533	0.0000	2.9638	1.7506	16.8400	0.5238
	39	0.5	0.5	1	34.9066	34.9066	0.0000	5.9475	3.4727	33.6820	1.0476
	264	0.5	0.5	1	34.9066	34.9066	0.0000	5.9305	3.4972	33.6800	1.0477
	1000	0.5	0.5	1	34.9066	34.9066	0.0000	5.9285	3.5005	33.6800	1.0477
	10000	0.5	0.5	1	34.9066	34.9066	0.0000	5.9279	3.5014	33.6800	1.0477
	100000	0.5	0.5	1	34.9066	34.9066	0.0000	5.9278	3.5016	33.6800	1.0477
	39	1	1	2	0.0873	0.0873	0.0000	0.3699	0.0064	0.7200	0.0088
	264	1	1	2	0.0873	0.0873	0.0000	0.0571	0.0029	0.1351	0.0026
	1000	1	1	2	0.0873	0.0873	0.0000	0.0216	0.0059	0.0885	0.0026
	10000	1	1	2	0.0873	0.0873	0.0000	0.0150	0.0084	0.0841	0.0026
	100000	1	1	2	0.0873	0.0873	0.0000	0.0147	0.0088	0.0841	0.0026
	39	1	1	2	0.1745	0.1745	0.0000	0.3710	0.0076	0.7349	0.0096
	264	1	1	2	0.1745	0.1745	0.0000	0.0638	0.0085	0.1986	0.0052
	1000	1	1	2	0.1745	0.1745	0.0000	0.0345	0.0147	0.1706	0.0052
	10000	1	1	2	0.1745	0.1745	0.0000	0.0301	0.0175	0.1686	0.0052
	100000	1	1	2	0.1745	0.1745	0.0000	0.0298	0.0176	0.1686	0.0052
	39	1	1	2	0.3491	0.3491	0.0000	0.3759	0.0114	0.7906	0.0123
	264	1	1	2	0.3491	0.3491	0.0000	0.0845	0.0242	0.3532	0.0103
	1000	1	1	2	0.3491	0.3491	0.0000	0.0624	0.0323	0.3380	0.0104
	10000	1	1	2	0.3491	0.3491	0.0000	0.0594	0.0347	0.3368	0.0107
	100000	1	1	2	0.3491	0.3491	0.0000	0.0593	0.0349	0.3368	0.0107
	39	1	1	2	17.4533	17.4533	0.0000	3.0225	1.6888	16.8550	0.5238
	264	1	1	2	17.4533	17.4533	0.0000	2.9695	1.7423	16.8400	0.5239
	1000	1	1	2	17.4533	17.4533	0.0000	2.9651	1.7484	16.8400	0.5238
	10000	1	1	2	17.4533	17.4533	0.0000	2.9639	1.7504	16.8400	0.5238
	100000	1	1	2	17.4533	17.4533	0.0000	2.9638	1.7506	16.8400	0.5238
	39	1	1	2	34.9066	34.9066	0.0000	5.9737	3.4424	33.6870	1.0479
	264	1	1	2	34.9066	34.9066	0.0000	5.9329	3.4931	33.6800	1.0477
	1000	1	1	2	34.9066	34.9066	0.0000	5.9291	3.4994	33.6800	1.0477
	10000	1	1	2	34.9066	34.9066	0.0000	5.9279	3.5014	33.6800	1.0477
	100000	1	1	2	34.9066	34.9066	0.0000	5.9278	3.5016	33.6800	1.0477
	39	2	2	4	0.0873	0.0873	0.0000	0.7394	0.0123	1.4330	0.0177
	264	2	2	4	0.0873	0.0873	0.0000	0.1105	0.0033	0.2276	0.0033
	1000	2	2	4	0.0873	0.0873	0.0000	0.0331	0.0042	0.1011	0.0026
	10000	2	2	4	0.0873	0.0873	0.0000	0.0152	0.0081	0.0845	0.0025
	100000	2	2	4	0.0873	0.0873	0.0000	0.0147	0.0088	0.0841	0.0026
	39	2	2	4	0.1745	0.1745	0.0000	0.7399	0.0130	1.4403	0.0180
	264	2	2	4	0.1745	0.1745	0.0000	0.1145	0.0063	0.2702	0.0055
	1000	2	2	4	0.1745	0.1745	0.0000	0.0431	0.0119	0.1776	0.0051
	10000	2	2	4	0.1745	0.1745	0.0000	0.0303	0.0172	0.1686	0.0052
	100000	2	2	4	0.1745	0.1745	0.0000	0.0298	0.0176	0.1686	0.0052
	39	2	2	4	0.3491	0.3491	0.0000	0.7423	0.0151	1.4696	0.0195
	264	2	2	4	0.3491	0.3491	0.0000	0.1279	0.0178	0.3976	0.0102
	1000	2	2	4	0.3491	0.3491	0.0000	0.0687	0.0292	0.3413	0.0104
	10000	2	2	4	0.3491	0.3491	0.0000	0.0595	0.0344	0.3368	0.0107
	100000	2	2	4	0.3491	0.3491	0.0000	0.0593	0.0349	0.3368	0.0107
	39	2	2	4	17.4533	17.4533	0.0000	3.1285	1.6156	16.9000	0.5235
	264	2	2	4	17.4533	17.4533	0.0000	2.9761	1.7339	16.8410	0.5239
	1000	2	2	4	17.4533	17.4533	0.0000	2.9667	1.7465	16.8400	0.5238
	10000	2	2	4	17.4533	17.4533	0.0000	2.9641	1.7501	16.8400	0.5238
	100000	2	2	4	17.4533	17.4533	0.0000	2.9638	1.7506	16.8400	0.5238
	39	2	2	4	34.9066	34.9066	0.0000	6.0448	3.3772	33.7100	1.0474
	264	2	2	4	34.9066	34.9066	0.0000	5.9386	3.4847	33.6800	1.0479
	1000	2	2	4	34.9066	34.9066	0.0000	5.9305	3.4971	33.6800	1.0477
	10000	2	2	4	34.9066	34.9066	0.0000	5.9281	3.5011	33.6800	1.0477
	100000	2	2	4	34.9066	34.9066	0.0000	5.9278	3.5016	33.6800	1.0477
	39	50	50	100	0.0873	0.0873	0.0010	18.4780	0.3069	35.7610	0.4362
	264	50	50	100	0.0873	0.0873	0.0010	2.7296	0.0453	5.2836	0.0645
	1000	50	50	100	0.0873	0.0873	0.0010	0.7206	0.0120	1.3972	0.0174
	10000	50	50	100	0.0873	0.0873	0.0010	0.0741	0.0029	0.1629	0.0029
	100000	50	50	100	0.0873	0.0873	0.0010	0.0172	0.0072	0.0853	0.0026
	39	50	50	100	0.1745	0.1745	0.0010	18.4780	0.3069	35.7610	0.4365
	264	50	50	100	0.1745	0.1745	0.0010	2.7300	0.0454	5.2856	0.0645
	1000	50	50	100	0.1745	0.1745	0.0010	0.7215	0.0126	1.4050	0.0177
	10000	50	50	100	0.1745	0.1745	0.0010	0.0795	0.0075	0.2186	0.0052
	100000	50	50	100	0.1745	0.1745	0.0010	0.0312	0.0161	0.1686	0.0052

A	B	C					D	E		F	
Distance A to B (m) = length of pointing vector	Distance A to C (m) = link distance	Measurement Errors					sigma_psi (mrad)	sigma_h		sigma_e	
		RTK			Local Angular Sensor			mean	stdev	mean	stdev
		sigma_E (cm)	sigma_N (cm)	sigma_U (cm)	sigma_phi (mrad)	sigma_theta (mrad)		(mrad)	(mrad)	(mrad)	(mrad)
1.00E+06	39	50	50	100	0.3491	0.3491	0.0010	18.4780	0.3068	35.7630	0.4366
	264	50	50	100	0.3491	0.3491	0.0010	2.7305	0.0462	5.2936	0.0652
	1000	50	50	100	0.3491	0.3491	0.0010	0.7239	0.0148	1.4350	0.0189
	10000	50	50	100	0.3491	0.3491	0.0010	0.0972	0.0215	0.3643	0.0104
	100000	50	50	100	0.3491	0.3491	0.0010	0.0605	0.0338	0.3372	0.0103
	39	50	50	100	17.4533	17.4533	0.0010	18.7890	0.5791	39.5290	0.6174
	264	50	50	100	17.4533	17.4533	0.0010	4.2224	1.2141	17.6490	0.5190
	1000	50	50	100	17.4533	17.4533	0.0010	3.1221	1.6193	16.8980	0.5235
	10000	50	50	100	17.4533	17.4533	0.0010	2.9715	1.7396	16.8410	0.5241
	100000	50	50	100	17.4533	17.4533	0.0010	2.9645	1.7495	16.8400	0.5238
	39	50	50	100	34.9066	34.9066	0.0010	19.6760	1.3378	49.1260	1.0350
	264	50	50	100	34.9066	34.9066	0.0010	6.7878	2.9628	34.0920	1.0450
	1000	50	50	100	34.9066	34.9066	0.0010	6.0408	3.3808	33.7090	1.0476
	10000	50	50	100	34.9066	34.9066	0.0010	5.9346	3.4906	33.6800	1.0479
	100000	50	50	100	34.9066	34.9066	0.0010	5.9285	3.5005	33.6800	1.0477
	39	100	100	200	0.0873	0.0873	0.0010	36.9550	0.6134	71.5220	0.8730
	264	100	100	200	0.0873	0.0873	0.0010	5.4594	0.0905	10.5660	0.1290
	1000	100	100	200	0.0873	0.0873	0.0010	1.4415	0.0240	2.7907	0.0343
	10000	100	100	200	0.0873	0.0873	0.0010	0.1452	0.0033	0.2916	0.0039
	100000	100	100	200	0.0873	0.0873	0.0010	0.0216	0.0059	0.0885	0.0026
	39	100	100	200	0.1745	0.1745	0.0010	36.9550	0.6134	71.5220	0.8732
	264	100	100	200	0.1745	0.1745	0.0010	5.4595	0.0908	10.5670	0.1290
	1000	100	100	200	0.1745	0.1745	0.0010	1.4416	0.0243	2.7947	0.0343
	10000	100	100	200	0.1745	0.1745	0.0010	0.1479	0.0059	0.3258	0.0058
	100000	100	100	200	0.1745	0.1745	0.0010	0.0345	0.0147	0.1706	0.0052
	39	100	100	200	0.3491	0.3491	0.0010	36.9550	0.6134	71.5230	0.8729
	264	100	100	200	0.3491	0.3491	0.0010	5.4595	0.0908	10.5710	0.1292
	1000	100	100	200	0.3491	0.3491	0.0010	1.4429	0.0253	2.8096	0.0350
	10000	100	100	200	0.3491	0.3491	0.0010	0.1590	0.0152	0.4372	0.0103
	100000	100	100	200	0.3491	0.3491	0.0010	0.0624	0.0323	0.3380	0.0104
	39	100	100	200	17.4533	17.4533	0.0010	37.1130	0.7516	73.4780	0.9696
	264	100	100	200	17.4533	17.4533	0.0010	6.3954	0.8742	19.8810	0.5117
	1000	100	100	200	17.4533	17.4533	0.0010	3.4324	1.4652	17.0700	0.5224
	10000	100	100	200	17.4533	17.4533	0.0010	2.9806	1.7281	16.8420	0.5239
	100000	100	100	200	17.4533	17.4533	0.0010	2.9651	1.7484	16.8400	0.5238
	39	100	100	200	34.9066	34.9066	0.0010	37.5790	1.1577	79.0570	1.2350
	264	100	100	200	34.9066	34.9066	0.0010	8.4450	2.4280	35.2990	1.0382
	1000	100	100	200	34.9066	34.9066	0.0010	6.2438	3.2390	33.7950	1.0472
	10000	100	100	200	34.9066	34.9066	0.0010	5.9426	3.4793	33.6810	1.0477
	100000	100	100	200	34.9066	34.9066	0.0010	5.9291	3.4994	33.6800	1.0477
	39	500	500	1000	0.0873	0.0873	0.0070	184.7800	3.0672	357.6100	4.3647
	264	500	500	1000	0.0873	0.0873	0.0070	27.2970	0.4533	52.8290	0.6446
	1000	500	500	1000	0.0873	0.0873	0.0070	7.2065	0.1196	13.9470	0.1700
	10000	500	500	1000	0.0873	0.0873	0.0070	0.7208	0.0120	1.3972	0.0174
	100000	500	500	1000	0.0873	0.0873	0.0070	0.0741	0.0029	0.1629	0.0029
	39	500	500	1000	0.1745	0.1745	0.0070	184.7800	3.0672	357.6100	4.3647
	264	500	500	1000	0.1745	0.1745	0.0070	27.2970	0.4532	52.8290	0.6448
	1000	500	500	1000	0.1745	0.1745	0.0070	7.2066	0.1197	13.9480	0.1704
	10000	500	500	1000	0.1745	0.1745	0.0070	0.7215	0.0126	1.4050	0.0177
	100000	500	500	1000	0.1745	0.1745	0.0070	0.0797	0.0074	0.2186	0.0052
	39	500	500	1000	0.3491	0.3491	0.0070	184.7800	3.0672	357.6100	4.3648
	264	500	500	1000	0.3491	0.3491	0.0070	27.2970	0.4532	52.8300	0.6446
	1000	500	500	1000	0.3491	0.3491	0.0070	7.2066	0.1197	13.9510	0.1704
	10000	500	500	1000	0.3491	0.3491	0.0070	0.7239	0.0148	1.4350	0.0189
	100000	500	500	1000	0.3491	0.3491	0.0070	0.0975	0.0216	0.3643	0.0104
	39	500	500	1000	17.4533	17.4533	0.0070	184.8100	3.0951	358.0100	4.3844
	264	500	500	1000	17.4533	17.4533	0.0070	27.5090	0.6393	55.4490	0.7731
	1000	500	500	1000	17.4533	17.4533	0.0070	7.9514	0.7541	21.8670	0.5117
	10000	500	500	1000	17.4533	17.4533	0.0070	3.1221	1.6193	16.8980	0.5235
	100000	500	500	1000	17.4533	17.4533	0.0070	2.9715	1.7396	16.8410	0.5241
	39	500	500	1000	34.9066	34.9066	0.0070	184.9000	3.1781	359.1900	4.4436
	264	500	500	1000	34.9066	34.9066	0.0070	28.1300	1.1783	62.6540	1.1056
	1000	500	500	1000	34.9066	34.9066	0.0070	9.7310	2.1575	36.4540	1.0329
	10000	500	500	1000	34.9066	34.9066	0.0070	6.0408	3.3808	33.7090	1.0476
	100000	500	500	1000	34.9066	34.9066	0.0070	5.9348	3.4904	33.6800	1.0479
	39	1000	1000	2000	0.0873	0.0873	0.0140	369.5500	6.1345	715.2200	8.7295
	264	1000	1000	2000	0.0873	0.0873	0.0140	54.5930	0.9063	105.6600	1.2897
	1000	1000	1000	2000	0.0873	0.0873	0.0140	14.4130	0.2392	27.8940	0.3403
	10000	1000	1000	2000	0.0873	0.0873	0.0140	1.4415	0.0240	2.7907	0.0343
	100000	1000	1000	2000	0.0873	0.0873	0.0140	0.1455	0.0033	0.2916	0.0039
	39	1000	1000	2000	0.1745	0.1745	0.0140	369.5500	6.1345	715.2200	8.7295
	264	1000	1000	2000	0.1745	0.1745	0.0140	54.5930	0.9063	105.6600	1.2898
	1000	1000	1000	2000	0.1745	0.1745	0.0140	14.4130	0.2392	27.8940	0.3404
	10000	1000	1000	2000	0.1745	0.1745	0.0140	1.4416	0.0243	2.7947	0.0343
	100000	1000	1000	2000	0.1745	0.1745	0.0140	0.1487	0.0058	0.3258	0.0058
	39	1000	1000	2000	0.3491	0.3491	0.0140	369.5500	6.1345	715.2200	8.7294
	264	1000	1000	2000	0.3491	0.3491	0.0140	54.5930	0.9063	105.6600	1.2894
	1000	1000	1000	2000	0.3491	0.3491	0.0140	14.4130	0.2395	27.8960	0.3403
	10000	1000	1000	2000	0.3491	0.3491	0.0140	1.4429	0.0253	2.8096	0.0350
	100000	1000	1000	2000	0.3491	0.3491	0.0140	0.1594	0.0150	0.4372	0.0103
	39	1000	1000	2000	17.4533	17.4533	0.0140	369.5700	6.1486	715.4200	8.7393
	264	1000	1000	2000	17.4533	17.4533	0.0140	54.7000	0.9999	106.9900	1.3558
	1000	1000	1000	2000	17.4533	17.4533	0.0140	14.8080	0.5839	32.5840	0.5617
	10000	1000	1000	2000	17.4533	17.4533	0.0140	3.4324	1.4652	17.0700	0.5224
	100000	1000	1000	2000	17.4533	17.4533	0.0140	2.9807	1.7279	16.8420	0.5239
	39	1000	1000	2000	34.9066	34.9066	0.0140	369.6200	6.1902	716.0100	8.7689
	264	1000	1000	2000	34.9066	34.9066	0.0140	55.0180	1.2786	110.9000	1.5459
	1000	1000	1000	2000	34.9066	34.9066	0.0140	15.9030	1.5085	43.7330	1.0231
	10000	1000	1000	2000	34.9066	34.9066	0.0140	6.2438	3.2390	33.7950	1.0472
	100000	1000	1000	2000	34.9066	34.9066	0.0140	5.9427	3.4792	33.6810	1.0477

Table C-7. $\left|\overrightarrow{AB}\right| = 1.5\text{E+}08$ km (Approximate distance to Sun)

A	B	C					D	E		F	
Distance A to B (m) = length of pointing vector	Distance A to C (m) = link distance	Measurement Errors					sigma_psi (mrad)	sigma_h		sigma_e	
		RTK			Local Angular Sensor						
		sigma_E (cm)	sigma_N (cm)	sigma_U (cm)	sigma_phi (mrad)	sigma_theta (mrad)		mean (mrad)	stdev (mrad)	mean (mrad)	stdev (mrad)
1.50E+11	39	0.5	0.5	1	0.0873	0.0873	0.0000	0.1855	0.0038	0.3674	0.0049
	264	0.5	0.5	1	0.0873	0.0873	0.0000	0.0319	0.0044	0.0995	0.0025
	1000	0.5	0.5	1	0.0873	0.0873	0.0000	0.0172	0.0072	0.0853	0.0026
	10000	0.5	0.5	1	0.0873	0.0873	0.0000	0.0148	0.0086	0.0841	0.0026
	100000	0.5	0.5	1	0.0873	0.0873	0.0000	0.0147	0.0088	0.0841	0.0026
	39	0.5	0.5	1	0.1745	0.1745	0.0000	0.1879	0.0059	0.3953	0.0061
	264	0.5	0.5	1	0.1745	0.1745	0.0000	0.0423	0.0120	0.1766	0.0052
	1000	0.5	0.5	1	0.1745	0.1745	0.0000	0.0312	0.0161	0.1686	0.0052
	10000	0.5	0.5	1	0.1745	0.1745	0.0000	0.0299	0.0174	0.1686	0.0052
	100000	0.5	0.5	1	0.1745	0.1745	0.0000	0.0298	0.0176	0.1686	0.0052
	39	0.5	0.5	1	0.3491	0.3491	0.0000	0.1968	0.0133	0.4912	0.0103
	264	0.5	0.5	1	0.3491	0.3491	0.0000	0.0677	0.0297	0.3410	0.0104
	1000	0.5	0.5	1	0.3491	0.3491	0.0000	0.0605	0.0338	0.3372	0.0103
	10000	0.5	0.5	1	0.3491	0.3491	0.0000	0.0594	0.0347	0.3368	0.0107
	100000	0.5	0.5	1	0.3491	0.3491	0.0000	0.0593	0.0349	0.3368	0.0107
	39	0.5	0.5	1	17.4533	17.4533	0.0000	2.9868	1.7214	16.8440	0.5238
	264	0.5	0.5	1	17.4533	17.4533	0.0000	2.9665	1.7464	16.8400	0.5238
	1000	0.5	0.5	1	17.4533	17.4533	0.0000	2.9645	1.7495	16.8400	0.5238
	10000	0.5	0.5	1	17.4533	17.4533	0.0000	2.9639	1.7504	16.8400	0.5238
	100000	0.5	0.5	1	17.4533	17.4533	0.0000	2.9638	1.7506	16.8400	0.5238
	39	0.5	0.5	1	34.9066	34.9066	0.0000	5.9475	3.4727	33.6820	1.0476
	264	0.5	0.5	1	34.9066	34.9066	0.0000	5.9305	3.4972	33.6800	1.0477
	1000	0.5	0.5	1	34.9066	34.9066	0.0000	5.9285	3.5005	33.6800	1.0477
	10000	0.5	0.5	1	34.9066	34.9066	0.0000	5.9279	3.5014	33.6800	1.0477
	100000	0.5	0.5	1	34.9066	34.9066	0.0000	5.9278	3.5016	33.6800	1.0477
	39	1	1	2	0.0873	0.0873	0.0000	0.3699	0.0064	0.7200	0.0088
	264	1	1	2	0.0873	0.0873	0.0000	0.0571	0.0029	0.1351	0.0026
	1000	1	1	2	0.0873	0.0873	0.0000	0.0216	0.0059	0.0885	0.0026
	10000	1	1	2	0.0873	0.0873	0.0000	0.0150	0.0084	0.0841	0.0026
	100000	1	1	2	0.0873	0.0873	0.0000	0.0147	0.0088	0.0841	0.0026
	39	1	1	2	0.1745	0.1745	0.0000	0.3710	0.0076	0.7349	0.0096
	264	1	1	2	0.1745	0.1745	0.0000	0.0638	0.0085	0.1986	0.0052
	1000	1	1	2	0.1745	0.1745	0.0000	0.0345	0.0147	0.1706	0.0052
	10000	1	1	2	0.1745	0.1745	0.0000	0.0301	0.0175	0.1686	0.0052
	100000	1	1	2	0.1745	0.1745	0.0000	0.0298	0.0176	0.1686	0.0052
	39	1	1	2	0.3491	0.3491	0.0000	0.3759	0.0114	0.7906	0.0123
	264	1	1	2	0.3491	0.3491	0.0000	0.0845	0.0242	0.3532	0.0103
	1000	1	1	2	0.3491	0.3491	0.0000	0.0624	0.0323	0.3380	0.0104
	10000	1	1	2	0.3491	0.3491	0.0000	0.0594	0.0347	0.3368	0.0107
	100000	1	1	2	0.3491	0.3491	0.0000	0.0593	0.0349	0.3368	0.0107
	39	1	1	2	17.4533	17.4533	0.0000	3.0225	1.6888	16.8550	0.5238
	264	1	1	2	17.4533	17.4533	0.0000	2.9695	1.7423	16.8400	0.5239
	1000	1	1	2	17.4533	17.4533	0.0000	2.9651	1.7484	16.8400	0.5238
	10000	1	1	2	17.4533	17.4533	0.0000	2.9639	1.7504	16.8400	0.5238
	100000	1	1	2	17.4533	17.4533	0.0000	2.9638	1.7506	16.8400	0.5238
	39	1	1	2	34.9066	34.9066	0.0000	5.9737	3.4424	33.6870	1.0479
	264	1	1	2	34.9066	34.9066	0.0000	5.9329	3.4931	33.6800	1.0477
	1000	1	1	2	34.9066	34.9066	0.0000	5.9291	3.4994	33.6800	1.0477
	10000	1	1	2	34.9066	34.9066	0.0000	5.9279	3.5014	33.6800	1.0477
	100000	1	1	2	34.9066	34.9066	0.0000	5.9278	3.5016	33.6800	1.0477
	39	2	2	4	0.0873	0.0873	0.0000	0.7394	0.0123	1.4330	0.0177
	264	2	2	4	0.0873	0.0873	0.0000	0.1105	0.0033	0.2276	0.0033
	1000	2	2	4	0.0873	0.0873	0.0000	0.0331	0.0042	0.1011	0.0026
	10000	2	2	4	0.0873	0.0873	0.0000	0.0152	0.0081	0.0845	0.0025
	100000	2	2	4	0.0873	0.0873	0.0000	0.0147	0.0088	0.0841	0.0026
	39	2	2	4	0.1745	0.1745	0.0000	0.7399	0.0130	1.4403	0.0180
	264	2	2	4	0.1745	0.1745	0.0000	0.1145	0.0063	0.2702	0.0055
	1000	2	2	4	0.1745	0.1745	0.0000	0.0431	0.0119	0.1776	0.0051
	10000	2	2	4	0.1745	0.1745	0.0000	0.0303	0.0172	0.1686	0.0052
	100000	2	2	4	0.1745	0.1745	0.0000	0.0298	0.0176	0.1686	0.0052
	39	2	2	4	0.3491	0.3491	0.0000	0.7423	0.0151	1.4696	0.0195
	264	2	2	4	0.3491	0.3491	0.0000	0.1279	0.0178	0.3976	0.0102
	1000	2	2	4	0.3491	0.3491	0.0000	0.0687	0.0292	0.3413	0.0104
	10000	2	2	4	0.3491	0.3491	0.0000	0.0595	0.0344	0.3368	0.0107
	100000	2	2	4	0.3491	0.3491	0.0000	0.0593	0.0349	0.3368	0.0107
	39	2	2	4	17.4533	17.4533	0.0000	3.1285	1.6156	16.9000	0.5235
	264	2	2	4	17.4533	17.4533	0.0000	2.9761	1.7339	16.8410	0.5239
	1000	2	2	4	17.4533	17.4533	0.0000	2.9667	1.7465	16.8400	0.5238
	10000	2	2	4	17.4533	17.4533	0.0000	2.9641	1.7501	16.8400	0.5238
	100000	2	2	4	17.4533	17.4533	0.0000	2.9638	1.7506	16.8400	0.5238
	39	2	2	4	34.9066	34.9066	0.0000	6.0448	3.3772	33.7100	1.0474
	264	2	2	4	34.9066	34.9066	0.0000	5.9386	3.4847	33.6800	1.0479
	1000	2	2	4	34.9066	34.9066	0.0000	5.9305	3.4971	33.6800	1.0477
	10000	2	2	4	34.9066	34.9066	0.0000	5.9281	3.5011	33.6800	1.0477
	100000	2	2	4	34.9066	34.9066	0.0000	5.9278	3.5016	33.6800	1.0477
	39	50	50	100	0.0873	0.0873	0.0000	18.4780	0.3069	35.7610	0.4362
	264	50	50	100	0.0873	0.0873	0.0000	2.7296	0.0453	5.2836	0.0645
	1000	50	50	100	0.0873	0.0873	0.0000	0.7206	0.0120	1.3972	0.0174
	10000	50	50	100	0.0873	0.0873	0.0000	0.0741	0.0029	0.1629	0.0029
	100000	50	50	100	0.0873	0.0873	0.0000	0.0172	0.0072	0.0853	0.0026
	39	50	50	100	0.1745	0.1745	0.0000	18.4780	0.3069	35.7610	0.4365
	264	50	50	100	0.1745	0.1745	0.0000	2.7300	0.0454	5.2856	0.0645
	1000	50	50	100	0.1745	0.1745	0.0000	0.7215	0.0126	1.4050	0.0177
	10000	50	50	100	0.1745	0.1745	0.0000	0.0795	0.0075	0.2186	0.0052
	100000	50	50	100	0.1745	0.1745	0.0000	0.0312	0.0161	0.1686	0.0052

A	B	C					D	E		F	
Distance A to B (m) = length of pointing vector	Distance A to C (m) = link distance	Measurement Errors					sigma_psi (mrad)	sigma_h		sigma_e	
		RTK			Local Angular Sensor			mean	stdev	mean	stdev
		sigma_E (cm)	sigma_N (cm)	sigma_U (cm)	sigma_phi (mrad)	sigma_theta (mrad)		(mrad)	(mrad)	(mrad)	(mrad)
1.50E+11	39	50	50	100	0.3491	0.3491	0.0000	18.4780	0.3068	35.7630	0.4366
	264	50	50	100	0.3491	0.3491	0.0000	2.7305	0.0462	5.2936	0.0652
	1000	50	50	100	0.3491	0.3491	0.0000	0.7239	0.0148	1.4350	0.0189
	10000	50	50	100	0.3491	0.3491	0.0000	0.0972	0.0215	0.3643	0.0104
	100000	50	50	100	0.3491	0.3491	0.0000	0.0605	0.0338	0.3372	0.0103
	39	50	50	100	17.4533	17.4533	0.0000	18.7890	0.5791	39.5290	0.6174
	264	50	50	100	17.4533	17.4533	0.0000	4.2224	1.2141	17.6490	0.5190
	1000	50	50	100	17.4533	17.4533	0.0000	3.1221	1.6193	16.8980	0.5235
	10000	50	50	100	17.4533	17.4533	0.0000	2.9715	1.7396	16.8410	0.5241
	100000	50	50	100	17.4533	17.4533	0.0000	2.9645	1.7495	16.8400	0.5238
	39	50	50	100	34.9066	34.9066	0.0000	19.6760	1.3378	49.1260	1.0350
	264	50	50	100	34.9066	34.9066	0.0000	6.7878	2.9628	34.0920	1.0450
	1000	50	50	100	34.9066	34.9066	0.0000	6.0408	3.3808	33.7090	1.0476
	10000	50	50	100	34.9066	34.9066	0.0000	5.9346	3.4906	33.6800	1.0479
	100000	50	50	100	34.9066	34.9066	0.0000	5.9285	3.5005	33.6800	1.0477
	39	100	100	200	0.0873	0.0873	0.0000	36.9550	0.6134	71.5220	0.8730
	264	100	100	200	0.0873	0.0873	0.0000	5.4594	0.0905	10.5660	0.1290
	1000	100	100	200	0.0873	0.0873	0.0000	1.4415	0.0240	2.7907	0.0343
	10000	100	100	200	0.0873	0.0873	0.0000	0.1452	0.0033	0.2916	0.0039
	100000	100	100	200	0.0873	0.0873	0.0000	0.0216	0.0059	0.0885	0.0026
	39	100	100	200	0.1745	0.1745	0.0000	36.9550	0.6134	71.5220	0.8732
	264	100	100	200	0.1745	0.1745	0.0000	5.4595	0.0908	10.5670	0.1290
	1000	100	100	200	0.1745	0.1745	0.0000	1.4416	0.0243	2.7947	0.0343
	10000	100	100	200	0.1745	0.1745	0.0000	0.1479	0.0059	0.3258	0.0058
	100000	100	100	200	0.1745	0.1745	0.0000	0.0345	0.0147	0.1706	0.0052
	39	100	100	200	0.3491	0.3491	0.0000	36.9550	0.6134	71.5230	0.8729
	264	100	100	200	0.3491	0.3491	0.0000	5.4595	0.0908	10.5710	0.1292
	1000	100	100	200	0.3491	0.3491	0.0000	1.4429	0.0253	2.8096	0.0350
	10000	100	100	200	0.3491	0.3491	0.0000	0.1590	0.0152	0.4372	0.0103
	100000	100	100	200	0.3491	0.3491	0.0000	0.0624	0.0323	0.3380	0.0104
	39	100	100	200	17.4533	17.4533	0.0000	37.1130	0.7516	73.4780	0.9696
	264	100	100	200	17.4533	17.4533	0.0000	6.3954	0.8742	19.8810	0.5117
	1000	100	100	200	17.4533	17.4533	0.0000	3.4324	1.4652	17.0700	0.5224
	10000	100	100	200	17.4533	17.4533	0.0000	2.9806	1.7281	16.8420	0.5239
	100000	100	100	200	17.4533	17.4533	0.0000	2.9651	1.7484	16.8400	0.5238
	39	100	100	200	34.9066	34.9066	0.0000	37.5790	1.1577	79.0570	1.2350
	264	100	100	200	34.9066	34.9066	0.0000	8.4450	2.4280	35.2990	1.0382
	1000	100	100	200	34.9066	34.9066	0.0000	6.2438	3.2390	33.7950	1.0472
	10000	100	100	200	34.9066	34.9066	0.0000	5.9426	3.4793	33.6810	1.0477
	100000	100	100	200	34.9066	34.9066	0.0000	5.9291	3.4994	33.6800	1.0477
	39	500	500	1000	0.0873	0.0873	0.0000	184.7800	3.0672	357.6100	4.3647
	264	500	500	1000	0.0873	0.0873	0.0000	27.2970	0.4533	52.8290	0.6446
	1000	500	500	1000	0.0873	0.0873	0.0000	7.2065	0.1196	13.9470	0.1700
	10000	500	500	1000	0.0873	0.0873	0.0000	0.7206	0.0120	1.3972	0.0174
	100000	500	500	1000	0.0873	0.0873	0.0000	0.0741	0.0029	0.1629	0.0029
	39	500	500	1000	0.1745	0.1745	0.0000	184.7800	3.0672	357.6100	4.3647
	264	500	500	1000	0.1745	0.1745	0.0000	27.2970	0.4532	52.8290	0.6448
	1000	500	500	1000	0.1745	0.1745	0.0000	7.2066	0.1197	13.9480	0.1704
	10000	500	500	1000	0.1745	0.1745	0.0000	0.7215	0.0126	1.4050	0.0177
	100000	500	500	1000	0.1745	0.1745	0.0000	0.0795	0.0075	0.2186	0.0052
	39	500	500	1000	0.3491	0.3491	0.0000	184.7800	3.0672	357.6100	4.3648
	264	500	500	1000	0.3491	0.3491	0.0000	27.2970	0.4532	52.8300	0.6446
	1000	500	500	1000	0.3491	0.3491	0.0000	7.2066	0.1197	13.9510	0.1704
	10000	500	500	1000	0.3491	0.3491	0.0000	0.7239	0.0148	1.4350	0.0189
	100000	500	500	1000	0.3491	0.3491	0.0000	0.0972	0.0215	0.3643	0.0104
	39	500	500	1000	17.4533	17.4533	0.0000	184.8100	3.0951	358.0100	4.3844
	264	500	500	1000	17.4533	17.4533	0.0000	27.5090	0.6393	55.4490	0.7731
	1000	500	500	1000	17.4533	17.4533	0.0000	7.9514	0.7541	21.8670	0.5117
	10000	500	500	1000	17.4533	17.4533	0.0000	3.1221	1.6193	16.8980	0.5235
	100000	500	500	1000	17.4533	17.4533	0.0000	2.9715	1.7396	16.8410	0.5241
	39	500	500	1000	34.9066	34.9066	0.0000	184.9000	3.1781	359.1900	4.4436
	264	500	500	1000	34.9066	34.9066	0.0000	28.1300	1.1783	62.6540	1.1056
	1000	500	500	1000	34.9066	34.9066	0.0000	9.7310	2.1575	36.4540	1.0329
	10000	500	500	1000	34.9066	34.9066	0.0000	6.0408	3.3808	33.7090	1.0476
	100000	500	500	1000	34.9066	34.9066	0.0000	5.9346	3.4906	33.6800	1.0479
	39	1000	1000	2000	0.0873	0.0873	0.0000	369.5500	6.1345	715.2200	8.7295
	264	1000	1000	2000	0.0873	0.0873	0.0000	54.5930	0.9063	105.6600	1.2897
	1000	1000	1000	2000	0.0873	0.0873	0.0000	14.4130	0.2392	27.8940	0.3403
	10000	1000	1000	2000	0.0873	0.0873	0.0000	1.4415	0.0240	2.7907	0.0343
	100000	1000	1000	2000	0.0873	0.0873	0.0000	0.1452	0.0033	0.2916	0.0039
	39	1000	1000	2000	0.1745	0.1745	0.0000	369.5500	6.1345	715.2200	8.7295
	264	1000	1000	2000	0.1745	0.1745	0.0000	54.5930	0.9063	105.6600	1.2898
	1000	1000	1000	2000	0.1745	0.1745	0.0000	14.4130	0.2392	27.8940	0.3404
	10000	1000	1000	2000	0.1745	0.1745	0.0000	1.4416	0.0243	2.7947	0.0343
	100000	1000	1000	2000	0.1745	0.1745	0.0000	0.1479	0.0059	0.3258	0.0058
	39	1000	1000	2000	0.3491	0.3491	0.0000	369.5500	6.1345	715.2200	8.7294
	264	1000	1000	2000	0.3491	0.3491	0.0000	54.5930	0.9063	105.6600	1.2894
	1000	1000	1000	2000	0.3491	0.3491	0.0000	14.4130	0.2395	27.8960	0.3403
	10000	1000	1000	2000	0.3491	0.3491	0.0000	1.4429	0.0253	2.8096	0.0350
	100000	1000	1000	2000	0.3491	0.3491	0.0000	0.1590	0.0152	0.4372	0.0103
	39	1000	1000	2000	17.4533	17.4533	0.0000	369.5700	6.1486	715.4200	8.7393
	264	1000	1000	2000	17.4533	17.4533	0.0000	54.7000	0.9999	106.9900	1.3558
	1000	1000	1000	2000	17.4533	17.4533	0.0000	14.8080	0.5839	32.5840	0.5617
	10000	1000	1000	2000	17.4533	17.4533	0.0000	3.4324	1.4652	17.0700	0.5224
	100000	1000	1000	2000	17.4533	17.4533	0.0000	2.9806	1.7281	16.8420	0.5239
	39	1000	1000	2000	34.9066	34.9066	0.0000	369.6200	6.1902	716.0100	8.7689
	264	1000	1000	2000	34.9066	34.9066	0.0000	55.0180	1.2786	110.9000	1.5459
	1000	1000	1000	2000	34.9066	34.9066	0.0000	15.9030	1.5085	43.7330	1.0231
	10000	1000	1000	2000	34.9066	34.9066	0.0000	6.2438	3.2390	33.7950	1.0472
	100000	1000	1000	2000	34.9066	34.9066	0.0000	5.9426	3.4793	33.6810	1.0477

D. MATLAB code for computing *LTC*

Inputs:
(a) *R*: Input traffic matrix
(b) *NODE_ARRAY*: The order of nodes in a bi-connected ring network topology

Outputs:
(a) *maxTrafficOnLink*: The maximum load in the given ring topology
(b) *(link_node_i,link_node_j)*: The link (i,j) which bears the maximum load

```
function [link_node_i,link_node_j,maxTrafficOnLink] = measureMaxTrafficOnLink(R,NODE_ARRAY)

[row,n]   = size(NODE_ARRAY);

for loop=0:n-1
   k          = 0;
   node_array  = transpose(circshift(NODE_ARRAY',-loop));

   for i=1:floor(n/2)+1,
      if node_array(1)~=node_array(i)
         k   = k+1;
         OD_set(k,1:2,loop+1)    = [node_array(1),node_array(i)];
      end
   end
   for i=2:floor(n/2),
      for j=2:i,
         if node_array(floor(n/2)+1+i)~=node_array(j)
            k   = k+1;
            OD_set(k,1:2,loop+1)    = [node_array(floor(n/2)+1+i),node_array(j)];
         end
      end
   end
end

k   = 0;
for loop=n:2*n-1
   k       = k+1;
   temp1   = OD_set(:,1,k);
   temp2   = OD_set(:,2,k);
   OD_set(:,1,loop+1)  = temp2;
   OD_set(:,2,loop+1)  = temp1;
end


[row,col,depth] = size(OD_set);
for loop=1:2*n
   link_congestion = 0;
   for i=1:row
      link_congestion = link_congestion + R(OD_set(i,1,loop),OD_set(i,2,loop));
   end
   link_congestion_set(loop,:) = [OD_set(1,1:2,loop),link_congestion];
end

link_congestion_set1         = link_congestion_set;
[val,ind]   = max(link_congestion_set(:,3));
link_node_i = link_congestion_set(ind,1);
link_node_j = link_congestion_set(ind,2);
maxTrafficOnLink    = link_congestion_set(ind,3);
```

Bibliography

Arras KO (1998). An Introduction to Error Propagation: Derivation, Meaning and Examples of Equation $C_Y = F_X C_X F_X^T$. Technical Report (N^{o} EPFL-ASL-TR-98-01 R3). Swiss Federal Institute of Technology Lausanne.

Banerjee N, Mehta V and Pandey S (2004). A Genetic Algorithm Approach for Solving the Routing and Wavelength Assignment Problem in WDM Networks. In 3rd IEEE/IEE International Conference on Networking, ICN 2004, Paris, Feb-March, pp 70-78.

Bannister JA, Fratta L and Gelra M (1990). Topological Design of the Wavelength-Division Optical Network. in Proc. IEEE INFOCOM '90. Ninth Annual Joint Conference of the IEEE Computer and Communication Societies, San Francisco, CA, June, pp 1005-1013

Berman Z and Powell JD (1998). The Role of Dead Reckoning and Inertial Sensors in Future General Aviation Navigation. Position Location and Navigation Symposium, IEEE. Palm Springs, CA. 20-23 April: 510-517

Bertsimas D and Tsitsiklis J (1993). Simulated Annealing. *Statiscal Science* 8(1). Report from the Committee on Applied and Theoretical Statistics of the National Research Council on Probability and Algorithms: 10-15.

Bevly DM, Gerdes JC, Wilson C and Zhang G (2000). The Use of GPS Based Velocity Measurements for Improved Vehicle State Estimation. Proceedings of the American Control Conference 4. Chicago, Il. 28-30 June: 2538-2542.

Black PE (2005). Dictionary of Algorithms and Data Structures (online: http://www.nist.gov/dads). U.S. National Institute of Standards and Technology (NIST).

Breipohl AM (1970). Probabilistic Systems Analysis: An Introduction to Probabilistic Models, Decisions, and Applications of Random Processes. John Wiley & Sons, Inc.

Brooks SP and Morgan BJT (1995). Optimization using Simulated Annealing. *The Statistician* 44(2): 241-257.

Buick R (2006). White Paper: RTK base station networks driving adoption of GPS +1/-1 inch automated steering among crop growers. Trimble Navigation Limited.

Davis CC, Smolyaninov II and Milner SD (2003). Flexible optical high data rate wireless links and networks, *IEEE Communications Magazine*, March.

Chlamtac I, Ganz A and Karmi G (1993). Lightnets: Topologies for High-Speed Optical Networks. *Journal of Lightwave Technology* 11(5/6): 951-961.

Connolly D (1992). General Purpose Simulated Annealing. *The Journal of the Operational Research Society* 43(5): 495-505.

Cohen C, McNally BD and Parkinson BW (1993). Flight Tests of Attitude Determination using GPS compared against an Inertial Navigation Unit. Presented at the ION National Technical Meeting, San Francisco, California.

Cohon J (2003). Multiobjective Programming and Planning. Dover Publications, inc., Mineola, New York. ISBN 0-486-43263-7.

Davis CC, Smolyaninov II and Milner SD (2003). Flexible optical high data rate wireless links and networks, *IEEE Communications Magazine*, March.

Desai A and Milner S (2005). Autonomous Reconfiguration in Free-Space Optical Sensor Networks. *IEEE Journal on Selected Areas in Communications* 23(8): 1556-1563.

Dowsland KA (1996). Genetic Algorithms-A Tool for OR? *The Journal of the Operational Research Society* 47(4): 550-561.

Enge P (2003). GPS Modernization: New Capabilities of the New Civil Signals. Invited Paper for the Australian International Aerospace Congress Brisbane, 29 July – 1 August 2003.

Epple B (2006). Using a GPS-aided Inertial System for Coarse-Pointing of Free-Space Optical Communication Terminals. Proceedings of SPIE 2006, San Diego

Farrell JA, Givargis TD and Barth MJ (2000). Real-Time Differential Carrier Phase GPS-Aided INS. IEEE Transactions on Control Systems Technology 8(4). July: 709-721.

Federal Aviation Administration (2007). Wide-Area Augmentation System Performance Analysis Report (Report #21).

Freisleben B and Merz P (1996). A Genetic Local Search Algorithm for solving Symmetric and Asymmetric Traveling Salesman Problems. Proceedings of IEEE International Conference on Evolutionary Computation, 1996. Nagoya, Japan: 616-621.

Gabriel SA, Sahakij P, Ramirez M and Peot C (2006). A Multiobjective Optimization Model for Processing and Distributing Biosolids to Reuse Fields. *Journal of the Operational Research Society*. DOI 10.1057/palgrave.jors.2602201.

Gabriel SA, Shim Y, Llorca J and Milner S (2006). A Multiobjective Optimization Model for Dynamic Reconfiguration of Ring Topologies with Stochastic Load. *Networks and Spatial Economics*. advance online publication 20 July 2007; doi: 10.1007/s11067-007-9025-8.

Gela M, Leonardi E, Neri F and Palnati P (2001). Routing in the Bidirectional Shufflenet. *IEEE/ACM Transactions on Networking* 9(1): 91-102.

Gebre-Egziabher D, Hayward RC and Powell JD (1998). A Low-Cost GPS/Inertial Attitude Heading Reference System (AHRS) for General Aviation Applications. Position Location and Navigation Symposium, IEEE. Palm Springs, CA. 20-23 April: 518-525.

Gendreau M, Hertz A and Laporte G (1992). New Insertion and Postoptimization Procedures for the Traveling Salesman Problem. *Operations Research* 40(6) (Nov. - Dec., 1992): 1086-1094.

Glover F (2007). Tabu Search--Uncharted Domains. *Annals of Operations Research* 149(1): 89-98(10)

Glover F (1996). Tabu search and Adaptive Memory Programming: Advances, Applications and Challenges. Interfaces in Computer Science and Operations Research. Barr, Helgason andKennington, eds., Kluwer Academic Publishers.

Glover F (1995). Tabu Search Fundamentals and Uses. University of Colorado, Boulder: http://spot.colorado.edu/~glover/Recentpapers.html

Glover F (1991). Multilevel Tabu Search and Embedded Search Neighborhoods for the Traveling Salesman Problem. University of Colorado, Boulder: http://spot.colorado.edu/~glover/Recentpapers.html

Goldberg DE (1990). A Note on Boltzmann Tournament Selection for Genetic Algorithms and Population-Oriented Simulated Annealing. in: Complex Systems 4. Complex Systems Publications, Inc.: 445-460.

Hayward R, Marchick A and Powell JD (1999). Single Baseline GPS Based Attitude Heading Reference System (AHRS) for Aircraft Applications. Proceedings of the American Control Conference 5. San Diego, CA. 2-4 June: 3655-3659

Ho TH and Davis C (2006). Three-dimensional Optical Pointing System Encoded by Radial Trifocal Tensor. Proceedings of SPIE 2006, San Diego.

Ho TH, Trisno S, Smolyaninov II, Milner SD and Davis CC (2004). Studies of Pointing. Acquisition, and Tracking of Agile Optical Wireless Transceivers for Free Space Optical Communication Networks. Optics in Atmospheric Propoagation and Adaptive Systems VI, Proceedings of SPIE, 5237, 137-158.

Hong S, Harashima F. Kwon SH, Choi SB, Lee MH and Lee H (2001). Estimation of Errors in Inertial Navigation Systems with GPS Measurements. Estimation of errors

in inertial navigation systems with GPSmeasurements. IEEE International Symposium on Industrial Electronics 3. Pusan, South Korea. 12-16 June: 1477-1483.

Jin GG (2002). Genetic Algorithms and Their Applications. KYOWOO Publishing Co.,Ltd (http://www.kyowoo.co.kr/). ISBN 89-8172-191-2.

Johnson DS, Aragon CR, McGeoch LA and Schevon C (1991). Optimization by Simulated Annealing: An Experimental Evaluation; Part II, Graph Coloring and Number Partitioning. *Operations Research* 39(3): 378-406.

Krishnaswamy RM and Sivarajan KN (2001). Design of Logical Topologies: A Linear Formulation for Wavelength-Routed Optical Networks with No Wavelength Changers. *IEEE/ACM Transactions of Networking* 9(2): 186-198.

Labourdette JP and Acampora AS (1991). Logically Rearrangeable Multihop Lightwave Networks. *IEEE Transactions on Communications* 39(8): 1223-1230.

Lachapelle G, Cannon ME, Lu G and Loncarevic B (1996). Shipborne GPS Attitude Determination During MMST-93. *IEEE Journal of Oceanic Engineering* 21(1).

Larrañaga P, Kuijpers CMH, Murga RH, Inza I and Dizdarevi S (1999). Genetic Algorithms for the Travelling Salesman Problem: A Review of Representations and Operators. *Artificial Intelligence Review* 13(2): 129-170

Lee S, Yoo C, Shim Y and Kim J (2001). Performance Testing of Integrated Strapdown INS and GPS. *KSAS International Journal* 2(1).

Lee S, Shim Y, Kim D, Kang C, Yoo C, Tunik AA and Kim J (1998). RDGPS-based Automatic Landing System for Light and Commuter Aircraft. The 14th IFAC Symposium on Automatic Control in Aerospace.

Lee YC (1992). Receiver autonomous integrity monitoring (RAIM) capability for sole-means GPS navigation in the oceanic phase of flight*, IEEE Aerospace and Electronic Systems Magazine* 7(5): 29 - 36

Leick A (1995). GPS Satellite Surveying, 2nd ed. Wiley-Interscience, John Wiley & Sons, New York.

Llorca J, Desai A, Milner S (2004a). Obscuration Minimization In Dynamic Free Space Optical Networks Through Topology Control. Proc. IEEE MILCOM.

Llorca J, Desai A, Vishkin U, Davis CC, Milner SD (2004b). Reconfigurable optical wireless sensor networks, Optics in Atmospheric Propagation and Adaptive Systems VI, J.D. Gonglewski and K. Stein, eds., Proc. SPIE 5237, 136-146.

Luxner L (1997). The Manhattan Project: AT&T Wireless invades the Big Apple with microcells. *Telephony Magazine* 232(8).

Marler RT and Arora JS (2004). Survey of Multi-objective Optimization Methods for Engineering. *Structural and Multidisciplinary Optimization* 26: 369-395. DOI 10.1007/s00158-003-0368-6.

Meister O, Mönikes R, Wendel J, Frietsch N, Schlaile C and Trommer GF (2007). Development of a GPS/INS/MAG navigation system and waypoint navigator for a VTOL UAV. Unmanned Systems Technology IX. Edited by Gerhart, Grant R.; Gage, Douglas W.; Shoemaker, Charles M.. Proceedings of the SPIE 6561: 65611D

Merz P and Freisleben B (1997). Genetic local search for the TSP: new results. IEEE International Conference on Evolutionary Computation, 1997. Indianapolis, IN, USA: 159-164.

Meyer C (2000). Matrix Analysis and Applied Linear Algebra. SIAM. ISBN 0-89871-454-0. pp.273.

Michalewicz Z (1999). Genetic Algorithms + Data Structures = Evolution Programs, Third, Revised, and Extended Edition. Springer: 209-237. ISBN 3-540-60676-9.

Miettinen KM (1999). Nonlinear Multiobjective Optimization. Kluwer's International Series: 79-85. ISBN 0-7923-8278-1.

Pióro M and Medhi D (2004). Routing, Flow, and Capacity Design in Communication and Computer Networks. Elsevier. ISBN 0-12-557189-5: 105.

Michalson WR (1995). Ensuring GPS navigation integrity using receiver autonomousintegrity monitoring. *IEEE Aerospace and Electronic Systems Magazine* 10(10): 31-34.

Milner SD, Thakkar S, Chandrashekar K and Chen W (2003). Performance and Scalability of Wireless Base-Station-Oriented Networks. Invited paper, *Mobile Computing and Communications Review*.

Mukherjee B, Banerjee D, Ramamurthy S and Mukherjee A (1996). Some Principles for Designing a Wide-Area WDM Optical Network. *IEEE/ACM Transactions on Networking* 4(5): 684-696

Narula-Tam A and Modiano E (2000). Dynamic Load Balancing in WDM Packet Networks With and Without Wavelength Constraints. *IEEE Journal on Selected Areas in Communications* 18(10): 1972-1979.

Nebot E (1999). Sensors used for autonomous navigation. Advances in Intelligent Autonomous Systems, Chapter 7, 135-156, ISBN 0-7923-5580-6.

Park C and Kim I (1998). Integer ambiguity resolution for GPS based attitude determination system. SICE '98. Proceedings of the 37th SICE Annual Conference. International Session Papers: 1115-1120.

Park C, Kim I, Lee JG and Jee GI (1997). Efficient technique to fix GPS carrier phase integer ambiguity on-the-fly. EE Proceedings - Radar, Sonar and Navigation 144(3): 148-155

Pflimlin JM, Soueres P and Hamel T (2006). Waypoint Navigation Control of a VTOL UAV Amidst Obstacles. Proceedings of the 2006 IEEE/RSJ International Conference on Intelligent Robots and Systems. Beijing, China. 9-15 October: 3544-3549.

Potts JC, Giddens TD and Yadav SB (1994). The Development and Evaluation of an Improved Genetic Algorithm based on Migration and Artificial Selection. *IEEE Transactions on Systems, Man and Cybernetics* 24(1): 73-86

Ramaswami R and Sivarajan KN (1996). Design of Logical Topologies for Wavelength-Routed Optical Networks. *IEEE Journal of Selected Areas in Communications* 14(5): 840-851.

Redmill KA, Kitajima T and Ozguner U (2001). DGPS/INS Integrated Positioning for Control of Automated Vehicle. IEEE Intelligent Transportation Systems Conference Proceedings. Oakland, CA. 25-29 August: 172-178.

Shim Y, Gabriel SA, Desai A, Sahakij P, Milner S (2005). A Fast Heuristic Method for Minimizing Traffic Congestion on Reconfigurable Ring Topologies. *Journal of the Operational Research Society (JORS)* advance online publication 7 February 2007; doi: 10.1057/palgrave.jors.2602360

Sinclair M (1999). Evolutionary Telecommunications: A Summary. In A. Wu, editor, Proceedings 1999 Generic and Evolutionary Computation Conference. Morgan Kaufmann Publishers.

Steuer RE (2004). Multiple Criteria Optimization and Computation. Class material in ENCE723, University of Maryland at College Park.

West WJ and White MG (2000). A Reconfigurable Navigation Test Bed. Position Location and Navigation Symposium, IEEE. San Diego, CA. 13-16 March: 494-501

Wilkerson BL, Giggenbach D and Epple B (2006). Concepts for Fast Acquisition in Optical Communications Systems. Proceedings of SPIE 2006, San Diego

Winston (2003). Introduction to Mathematical Programming, Fourth Edition: 800-822. ISBN 0-471-28366-5.

Wolf PR and Ghilani CD (1997). Adjustment Computations: Statistics and Least Squares in Surveying and GIS. Wiley-Interscience. ISBN 0-471-16833-5.

Yee R and Robbins F (1998). Inertial Pointing and Positioning System. US Patent 5809457.

Zhang Z and Acampora AS (1995). A Heuristic Wavelength Assignment Algorithm for Multihop WDM Networks with Wavelength Routing and Wavelength Re-Use. *IEEE/ACM Transactions on Networking* 3(3): 281-288.